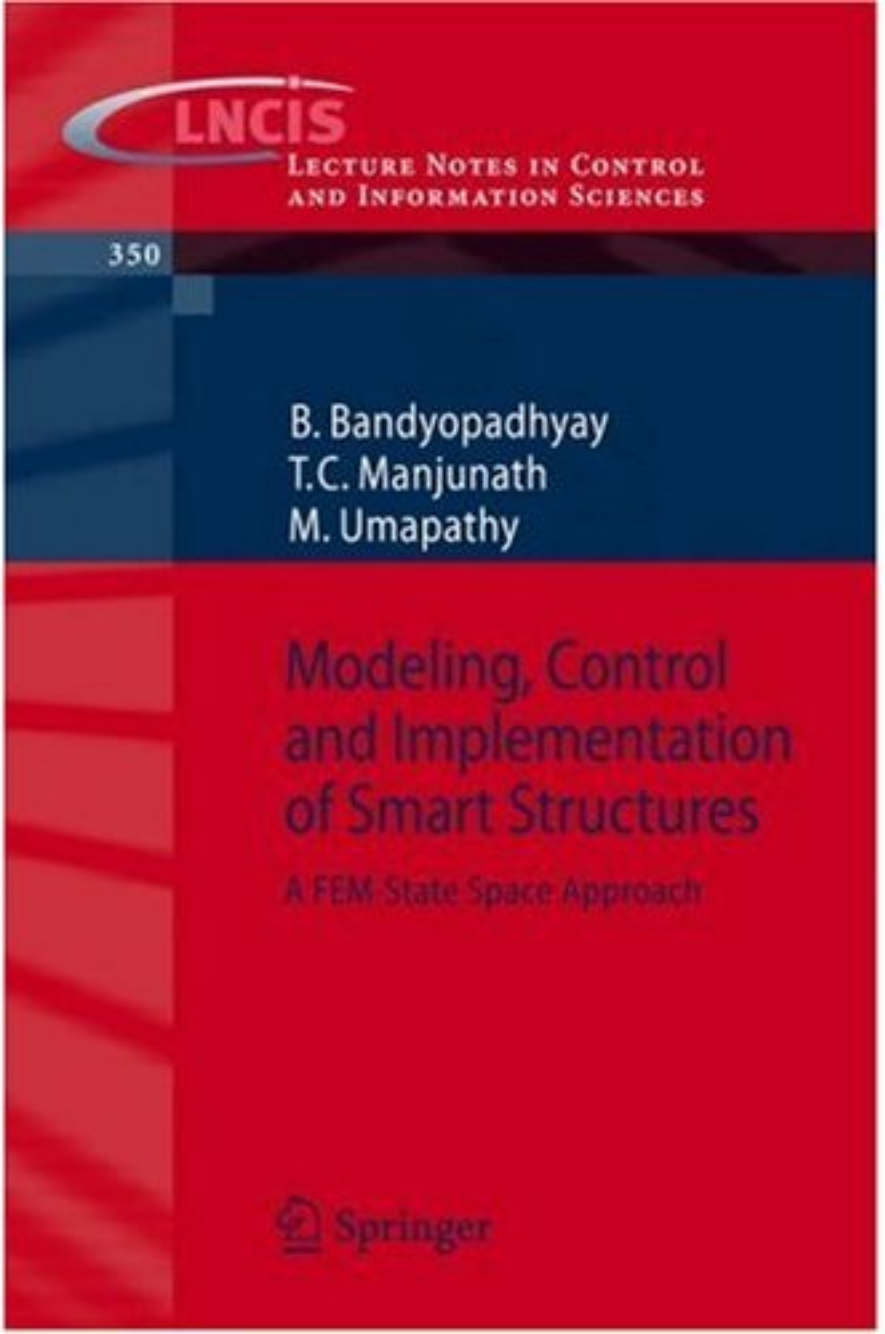
LNCIS
Lecture Notes in Control and Information Sciences
350
B. Bandyopadhyay
T.C. Manjunath
M. Umapathy
Modeling, Control and Implementation of Smart Structures
A FEM-State Space Approach
Springer

Lecture Notes
in Control and Information Sciences 350

Editors: M. Thoma · M. Morari

B. Bandyopadhyay · T.C. Manjunath · M. Umapathy

Modeling, Control and Implementation of Smart Structures

A FEM-State Space Approach

With 142 Figures

Springer

Series Advisory Board

F. Allgöwer · P. Fleming · P. Kokotovic · A.B. Kurzhanski ·
H. Kwakernaak · A. Rantzer · J.N. Tsitsiklis

Authors

Prof. B. Bandyopadhyay
Dr. T.C. Manjunath
IIT Bombay
Systems and Control Engineering
400076 Powai, Mumbai
Maharashtra, India
bijnan@ee.iitb.ac.in
tcmanju@sc.iitb.ac.in

Prof. M. Umapathy
NIT Trichy
Department of Instrumentation
and Control Engineering
Tanjore Road
620015 Trichy, Tamilnadu
India
umapathy@nitt.edu

ISSN 0170-8643

ISBN-10 3-540-48393-4 **Springer Berlin Heidelberg New York**
ISBN-13 978-3-540-48393-9 **Springer Berlin Heidelberg New York**

Library of Congress Control Number: 2006936727

Springer is a part of Springer Science+Business Media

springer.com

Printed in Germany

Typesetting: Data conversion by authors.
Final processing by PTP-Berlin Protago-TEX-Production GmbH, Germany (www.ptp-berlin.com)
Cover-Design: WMXDesign GmbH, Heidelberg
Printed on acid-free paper 89/3141/Yu - 5 4 3 2 1 0

"Where the mind is without fear and the head is held high;
Where knowledge is free;
Where the world has not been broken up into fragments by narrow domestic walls;
Where words come out from the depth of truth;
Where tireless striving stretches its arms towards perfection;
Where the clear stream of reason has not lost its way into the dreary desert sand of dead habit;
Where the mind is led forward by thee into ever-widening thought and action
- - -
Into that heaven of freedom, my Father, let my country awake."

..... *Rabindranath Tagore*

Dedicated to our Wives

Tamisra, Uma, Sujatha

and
Children

Trisha, Nidhisha and Nikhitha, Rahul

Preface

Smart materials and smart structures, often called as the intelligent structures forms a new rapidly growing interdisciplinary technology in the modern day world embracing the fields of materials, structures, mechatronics, sensor - actuator systems, information and signal processing, electronics, mathematics, control and are basically distributed parameter systems.

A common feature in majority of the structures is the active vibration control problem, which has to be dealt with as it would lead to the degradation of the structural performance if left uncontrolled. A modest attempt is made to reduce the structural vibrations in smart cantilever beam using various control strategies and is presented in this monograph, which is entirely based on the authors work. Some of the developed control techniques are also experimentally verified.

Much of the research work done in the area of smart structures so far is mainly concentrated in the modeling and control techniques, static and dynamic analysis which make use of state feedback, output feedback principles, linear quadratic regulator, optimal control and PID based techniques, etc.,. Since most of these types of control techniques needs all the system states for feedback, which may not be available for measurement, they may suffer from the problem of real time implementation and some times need a state observer for control purposes. These drawbacks could be overcome by the use of multirate output feedback techniques (MROF).

With the increasing use of computers and discrete-time samplers in controller implementation in the recent past, discrete-time systems and computer based control have become the topics that have a lot of potential in them. An MROF based control technique can be applied to almost all the systems which are controllable and observable, while at the same time being simple enough as not to tax the computers too much.

State feedback algorithms can be converted into output feedback algorithms by the use of multirate output feedback sampling technique. Consequently, the MROF based control strategies has the advantages of both the state feedback and output feedback control philosophies. This has further opened up the field of multirate output feedback based discrete time sliding mode control of smart structures.

The authors would like to express their deep sense of gratitude to their parents and teachers who have made them capable enough to write this book.

The authors wish to place on record their hearty thanks to many of the individuals who had helped them directly or indirectly in completing this monograph. Notable among them being Prof. P. Seshu of Mechanical Engineering Department, IIT Bombay, who had helped the authors by giving constructive suggestions in the preparation of some part of this monograph. The authors would like to thank Prof. P.S.V. Nataraj of Systems and Control Engg. Dept. for his cooperation during the preparation of this monograph.

The authors would also like to thank a large number of people of various departments of Indian Institute of Technology Bombay, National Institute of Technology Tiruchirapalli, Indian Institute of Science Bangalore and various other organizations for their critical comments and stimulating technical discussions which the authors had with them during the preparation of this monograph and to bring out their work in a fine form. To name a few of them, Ezhil Arasi, G.Uma, Juhi, Dhuri and S.Janardhanan.

Finally, the authors like to thank the entire team of springer publications for their cooperation and encouragement in bringing out the authors work in the form of a monograph in such a short span of time.

Mumbai-400076,
Maharashtra, India,
August 2006.

Bijnan Bandyopadhyay
Tadaga Channaveerappa Manjunath
Managalanathan Umapathy

Contents

List of Figures

List of Tables

Nomenclature

List of Roman symbols:

a_1 to a_4	Constants used in the solution of the displacement function
a_c	Actuator constant
A	Area ($m^2,\ mm^2$)
A_{11}	Extensional coefficient
A_{55}	Transverse shear stiffness coefficient
A_b	Area of the beam element
$\hat{A}$	Diagonalized A matrix consisting of eigen values
A_p	Area of the beam piezoelectric element ($m^2,\ mm^2$)
$A,\ \mathbf{A}$	State matrix in continuous-time model of LTI system,
b	Width of the beam or piezoelectric sensor or actuator (m, cm, mm)
B	Spatial derivative of the vector of inertial forces $\mathbb{N}$
$B,\ \mathbf{B}$	Input matrix in continuous-time model of LTI system
B_{11}	Bending-extensional coefficient
c	Constant which is given by $\sqrt{\frac{EI}{\rho A}}$, width of the beam
$C,\ \mathbf{C}$	Output matrix in continuous-time model of LTI system
$\mathbf{C}_0,\ \mathbf{D}_0$	Fictitious matrices or the matrices of the lifted system
$\mathbf{C}(F, N)$	Fictitious measurement matrix
$\mathbf{C}^*$	Generalized structural modal damping matrix
$d_{15},\ d_{31}$	Piezoelectric constants
$d(k),\ \tilde{d}(k)$	Bounded disturbance
$d_l,\ d_u$	Known lower and upper bounds on the disturbance
dA	Elemental area ($m^2,\ mm^2$)
dx	Elemental length along the x-axis ($m,\ mm$)
$D,\ \mathbf{D}$	Transmission matrix in continuous-time model of LTI system
D_z	Electric displacement

D_{11}	Bending coefficient
e	Permittivity of the medium (dielectric constant)
$e(k)$	Variable resulting due to effect of disturbance on sampled output
$e_l,\ e_u$	Lower and upper bounds of $e(k)$
e_0	Mean (average value) of the function of uncertainty
e_{31}	Piezoelectric stress/charge constant
e_{15}	Piezoelectric constant
E_{11}	Actuator induced piezoelectric axial force
E_b	Young's modulus of the beam, modulus of elasticity (GPa)
E_p	Young's modulus of the piezo patch or modulus of elasticity (GPa)
E_f	Electric field (V)
$E,\ \mathbf{E}$	External load matrix which couples disturbance to the system
E	Young's modulus or modulus of elasticity (GPa)
EI	Flexural rigidity
f	Frequency (Hertz)
$\mathbf{f}_{ext}$	External force, i.e., disturbance applied to the beam (N)
$\mathbf{f}^*_{ext}$	Generalized external force vector
$\mathbf{f}_{ctrl\ i}$	Control force coefficient vector
$\mathbf{f}^*_{ctrl\ i}$	Generalized control force coefficient vector
$\mathbf{f}^{\ t}$	Total force coefficient vector
$\mathbf{f}^*_t$	Generalized total force coefficient vector
$f_i(x)$	Shape functions of the beam
$F_1,\ F_2$	Forces acting at the nodes 1 and 2 (N)
F	State feedback gain
F_{11}	Actuator induced bending moment
g_{31}	PZT stress constant (VmN^{-1})
$\mathbf{g}$	Generalized coordinates
G_c	Signal conditioning device gain
G_{55}	Actuator induced shear force
G_i	Output injection gain
$\mathbf{h}$	Constant vector which depends on actuator characteristics
h	Height of the beam + 2 piezo patches, i.e., the thickness of total structure ($m,\ mm$)
$i(t)$	Sensor current ($Amps$)
$i,\ j$	Variables, i.e., 1, 2, 3,....
I_b	Moment of inertia of the beam
I_p	Moment of inertia of the piezoelectric patch
I	Identity matrix
$I_1,\ I_2,\ I_3$	Mass inertias of the cross-section of the beam
k^*	Positive integer chosen by the designer
k	Discrete samples

K^b	Stiffness matrix of the regular beam element, i.e., local stiffness matrix
K^p	Stiffness matrix of the piezoelectric element, i.e., local stiffness matrix
K_c	Controller gain
K	Stiffness matrix of the piezoelectric beam element
$\mathbf{K}$	Assembled stiffness matrix of the beam, i.e., global stiffness matrix Periodic output feedback gain matrix
$\mathbf{K}^*$	Generalized stiffness matrix of the beam
l_p	Length of piezo patch (either sensor/actuator) (m or cm or mm)
l_b	Length of the beam element (m or cm or mm)
$\mathbf{L}$	Fast output sampling feedback gain matrix
L_b	Total length of the beam (m or cm or mm)
L_j	Matrix blocks represent the output feedback gains
m	Moment along the length of the beam
M_1, M_2	Bending moments acting at node 1 and 2
M^b	Mass of the regular beam element, i.e., local mass matrix
M_a	Resultant moment acting on the structure
M^p	Mass matrix of the piezoelectric element
M	Mass matrix of the piezoelectric beam element
$\mathbf{M}$	Assembled mass matrix of the beam, i.e., global mass matrix
$M_{\rho_b A_b}$	Mass matrix of the beam associated with the translational inertia
$M_{\rho_p A_p}$	Mass matrix of piezoelectric element associated with translational inertia
$M_{\rho_b I_b}$	Mass matrix of the beam associated with the rotary inertia
$M_{\rho_p I_p}$	Mass matrix of the piezoelectric element associated with the rotary inertia
$\mathbf{M}^*$	Generalized mass matrix of the beam
M_x	Bending moment
$\mathbf{n}_i^T$	Spatial derivative of the shape functions
N_w^T	Mode shape functions for displacement taking shear into consideration
N_θ^T	Mode shape functions for velocity taking shear into consideration

N_a^T	Mode shape functions for acceleration taking shear into consideration
N_x	Internal forces acting on the cross section of the beam, i.e., axial force
N_a	Number of actuators
N	Number of layers of the beam, Number of sub-intervals
$\mathbf{p}$	Constant vector which depends on sensor characteristics
P	Transformation matrix
$P_{11},\ P_{21}$	$(r \times r)$ and $(n-r)\ \times\ r$ sub-matrices obtained by partitioning of P matrix
$q(x,t)$	Externally applied pressure loading at the tip of the beam
$q(t)$	Charge accumulated on the sensor surfaces
$\mathbf{q}$	Vector of displacements and slopes, i.e., nodal displacement vector Principal coordinates
$\dot{\mathbf{q}}$	Velocity vector
$\ddot{\mathbf{q}}$	Acceleration vector
q_d	Distributed force along the length of the beam
q_0	Transverse distributed loading
$Q(t)$	Total charge developed on sensor surface (Coloumbs)
Q_{xz}	Shear force
$\overline{Q}_{11},\ \overline{Q}_{55}$	Constants of the composite beam
$r(t)$	Reference input to the beam, i.e., impulse or sinusoidal disturbance
$s(k)$	Switching function or the sliding function or the switching surface
sgn	Signum function
s^σ	Compliance of the medium
$s_d(k)$	apriori known function
S_c	Sensor constant
t_b	Thickness of the beam (m or cm or mm)
t_a	Thickness of the actuator (m or cm or mm)
t_s	Thickness of the sensor (m or cm or mm)
t	Time (sec)
$\mathbf{T}$	Modal matrix containing eigenvectors representing desired number of modes
T	Transpose, Kinetic energy
u_0	Initial control
$u_0(x)$	Axial displacement of a point on the composite beam
$\hat{u}$	Stabilizing control for the reduced order model
u	Control input applied to actuator from controller (V) Axial displacement along the x-axis (mm)

$\mathbf{u}(t)$	Input vector
U	Strain energy
v	Lateral displacement along the y-axis
$V^s(t)$	Sensor voltage (V)
$V^a(t)$	Actuator voltage (V)
$V^k(x,t)$	Applied voltage to k^{th} actuator having a thickness of $\left(z^a_{k+} - z^a_{k-}\right)$
$w_0(x)$	Lateral displacement of a point on the composite beam
$w(x,t)$	Displacement function
$w'(x,t)$	First spatial derivative of the displacement function
$w'(x,t)$	Second spatial derivative of the displacement function
w_i, θ_i	Degrees of freedom at the nodes
$\dot{w}(x,t)$	Time derivative of the displacement function
w	Transverse displacement (mm)
W	External work done
x	Distance of the local coordinate from the fixed end State variable or axis
x_0	Initial state
$\mathbf{x}(t)$	State vector in CT consisting of state variables $x_1,\ x_2, ...$
$\mathbf{x}(k)$	State vector in DT consisting of samples at $k\ =\ 0, 1, 2, 3, ..$
$y(t),\ y_i$	System output, i.e., sensor o/p of the CT system (volts)
y_τ	Output sampled at τ
$y(k)$	System output, i.e., sensor o/p of the DT system (Volts)
y	Axis
z_k	Distance of the k^{th} layer from the x-axis
$z_1,\ z_2$	r and $(n-r)$ dimensional state vectors corresponding to the original state variables
z	Distance from the center of the beam to the piezo patch, i.e., $\left(t_a + \frac{t_b}{2}\right)$ (mm) Axis Depth of the material point measured from beam reference plane along vertical axis (mm)
$\bar{z},\ \bar{h}$	Distance between neutral axis of the beam and the PE layer $\left(\frac{t_a+t_b}{2}\right)$ (mm)
Z_i	Vector of forces and moments

List of Greek symbols:

α	Frictional damping constant
β	Structural damping constant
δ_e	Variation (maximum deviation) of the function of the uncertainty
$\delta\Pi$	Change in energy
δ	Half the quasi sliding mode band width
δU	Variation in the strain energy
δT	Variation in the kinetic energy
δW_e	Variation in the work done due to the external forces
ϵ	Belongs to
ε	Strain
ε_{xx}, ε_{yy}, ε_{zz}	Longitudinal strains or the tensile strains in the x, y and z directions
ε_x	Mechanical normal strain
ε_z	Transverse shear strain
ϕ	Ratio of the beam bending stiffness to shear stiffness
$\phi(x)$	Bending slope
$(\Phi_\tau, \Gamma_\tau, C)$	DT system obtained by sampling CT system with sampling interval of τ sec.
	Tau system
(Φ, Γ, C)	DT obtained by sampling CT system with sampling interval of Δ sec.
	Delta system
$\tilde{\Phi}, \tilde{\Gamma}, \tilde{C}^T$	Augmented DT system
γ	Shear strain
	Controllability index of the system
γ_{xz}, γ_{yz}, γ_{xy}	Shear strains in the 3 directions
$\gamma(x)$	Additional shear deformation angle
$\mathbb{K}$	Shear coefficient
$\mathbb{G}$	Shear modulus or modulus of rigidity
λ	Angle between the fiber direction and the longitudinal axis of the beam
	Eigen values of the system
υ	Poisson's ratio
	Observability index of the system

$\mathbb{N}$	Vector of inertia forces
π	$\frac{22}{7}$
θ	Time dependent rotation of the beam cross section about the y-axis
	Angle of rotation or slope in EB beam($rads$ or $degs$)
ρ_b	Density of the beam (Kg/m^3)
ρ_p	Density of the piezoelectric patch (Kg/m^3)
ρA	Mass / unit length
$\rho(\cdot)$	Spectral radius
ρ_1, ρ_2, ρ_3	LMI norms
$\Re^n$	n-dimensional real space
$\Re^m$	m-dimensional real space
$\Re^p$	p-dimensional real space
σ_a	Stress in the actuator
σ	Stress
σ_{xz}	Shear stress
σ_x	Normal shear stress
σ_{xx}	Tensile stress
τ	Sampling interval ($secs$)
τ_{xz}	Shear stress
ω	Natural frequency ($rads/sec$)
ξ	Damping ratio

List of Acronyms/Abbreviations:

ADC	Analog to Digital Converter
AVC	Active Vibration Control
CC	Clamped Clamped
CF	Clamped Free
CL	Closed Loop
CT	Continuous Time
DAC	Digital to Analog Converter
DOF	Degree Of Freedom
DSM	Discrete Sliding Mode
DSMC	Discrete Sliding Mode Control
DT	Discrete Time
DTQSMC	Discrete Time Quasi Sliding Mode Control
DTSMC	Discrete Time Sliding Mode Control
EB	Euler-Bernoulli
ER	Electro Rheological
FE	Finite Element

FEM	Finite Element Method
FFT	Fast Fourier Transform
FOS	Fast Output Sampling
FOSSMC	Fast Output Sampling based Sliding Mode Control
HOBT	Higher Order Beam Theory
IEEE	Institute of Electrical and Electronics Engineers
IOP	Institute of Physics
ISSS	Institute of Smart Structures and Systems
LHS	Left Hand Side
LMI	Linear Matrix Inequalities
LTI	Linear Time Invariant
LTI	Linear Time Invariant
MATLAB	MATrix LABoratory
MEMS	Micro Electronic Mechanical Systems
MIMO	Multiple Input Multiple Output
MR	Magneto Rheological
MROF	Multi-Rate Output Feedback
NEMS	Nano Electronic Mechanical Systems
OL	Open Loop
PC	Personal Computer
PCI	Personal Computer Interface
PE	Piezo Electric
POF	Periodic Output Feedback
PVC	Poly Vinyl Chloride
PVDF	Poly Vinylidene Fluoride
PZT	Lead Zirconate Titanate
QSM	Quasi Sliding Mode
QSMC	Quasi Sliding Mode Control
RDFOS	Robust Decentralized Fast Output Sampling
RDPOF	Robust Decentralized Periodic Output Feedback
RHS	Right Hand Side
RTI	Real Time Interface
RTW	Real Time Workshop
SFB	State Feedback Gain
SISO	Single Input Single Output
SMA	Shape Memory Alloys
SMC	Sliding Mode Control
SPIE	Society of Photonics and Instrumentation Engineers
SS	State Space
TLC	Target Language Compiler

1

Introduction to Smart Structures

The first Chapter of this monograph deals with a brief introduction to the theory and concepts of smart materials and structures, mathematical modeling and the active vibration control of smart structures. Some of the application fields of this emerging topic in the modern day world are also mentioned. Various types of control strategies are also presented in this context, which are used to suppress the vibrations of flexible beams and to make the structures safe, reliable and from further damage. A brief survey on the research on smart structures done so far is also presented along with the authors contributions. Finally, the motivation that made us to venture into this smart structures field is presented at the end.

1.1 Smart Materials and Structures – Theory and Concepts

Smart materials and smart structures, often called as the intelligent structures forms a new rapidly growing interdisciplinary technology in the modern day world embracing the fields of materials, structures, sensor - actuator systems, information and signal processing, electronics and control [1]. These structures involve the synergism of intelligent materials with embedded or surface mounted sensors whose information is collected, processed and controlled by a sophisticated controller, which controls the actuator to perform the corrective action.

A smart structure is basically a distributed parameter system that employs sensors and actuators at different finite element locations on the beam and makes use of one or more microprocessors that analyze the responses obtained from the sensors and use different control logics to command the actuators to apply localized strains to the plant to respond in a desired fashion and bring the system to equilibrium. It has also got the capability to respond to the changes in the environment on the plant, whether internal or external such as load changes, temperature changes. Smart actuators are used to alter system

characteristics (such as stiffness or damping) as well as of the system response (such as strain or shape) in a controlled manner.

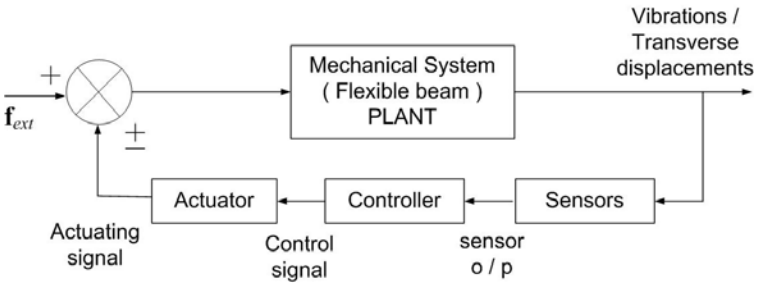

Fig. 1.1. Block-diagrammatic view of a smart structure system

One way of interpreting a smart structure system is as follows: It is a combination of sensing, processing, actuating, feedback, self-diagnosing and self-recovering sub-systems as shown in the Fig. 1.1. Sensors and actuators together integrated into the structure is what is called a "Smart Structure". The smart system uses the functional properties of advanced materials to achieve high performances with capabilities of recognition, discrimination and adjustification in response to a change of its environment. These structures are made up of sensors - which describe the physical state of their environment; actuators - which adapt to their environment ; a system or network - which handles the transfer of information and real-time computation. Each component of this system has certain functionality, and the entire sub-systems are integrated to perform a self-controlled smart action, similar to a living creature who can "think", make judgement and take actions on its own at the appropriate time.

Thus, a smart structure [2] can be considered as a design philosophy that emphasizes predictivity, adaptivity and repetivity and are composed of materials called as "smart materials" that can determine the present state of their structure, decide what is the most desirable state, and carry out an appropriate response in a controlled manner, thus saving the structure from damage. Thus, these smart materials have become an integral part or a subset of the smart structure. A couple of months back, scientists and researchers had demonstrated the further development of smart technology concept into the microscopic and nanoscopic levels by developing smart adaptive and intelligent systems such as the microbots, nanobots, micro-cantilevers, micro motors etc.,.

The development of smart materials will undoubtedly be an essential task in many fields of science and technology such as information science, microelectronics, computer science, medical treatment, life science, energy, transportation, safety engineering and military technologies. Advances in the

smart structure technology in the current scenario has thus provided a means for integrating sensors and actuators into the structure and make them self-adapting and self-controlling in various types of mechanical, flexible and rigid engineering structures such as in aerospace applications, civil engineering applications, robotics, bio-technology, MEMS and NEMS.

1.2 Active Vibration Control (AVC)

Active vibration control is an important problem in structures. One of the ways to tackle this problem is to make the structure smart, intelligent, adaptive and self-controlling by making use of one type of materials called as smart materials. The main objective of active vibration control is to reduce the vibration of a system by automatic modification of the system's structural response and this process is shown in Fig. 1.2. In many situations, it is important to minimize these structural vibrations, as they may affect the stability and performance of the structures. This obviates the need to strengthen the structure from dynamic forces and disturbances in order to minimize the effect of vibrations and enables the development of lighter, often-cheaper structures exhibiting superior performance. Thus, the vibration control of any system is always a formidable challenge for any control system designer. Any AVC system consists of a plant, actuator, sensor and a controller.

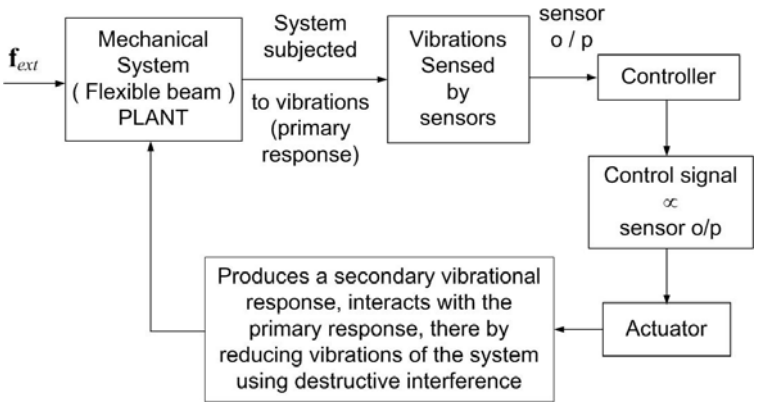

Fig. 1.2. Concept of reduction of vibrations using AVC

The need for such intelligent structures called as smart structures [3] arises because of their high performances in numerous structural applications. Such intelligent structures incorporate smart materials called as actuators and sensors (based on Piezoelectrics, Magneto-Rheological Fluids, Piezo-ceramics, Electro-Rheological Fluids, Shape Memory Alloys, PVDF, Optical fibers, etc.)

that are integrated into the structure and have structural functionality, as well as highly integrated control logic, signal conditioning and power amplification electronics. These materials can be used to generate a secondary vibrational response in a mechanical system which has the potential to reduce the overall response of the system plant by the destructive interference with the original response of the system, caused by the primary source of vibration [4].

Piezoelectric materials can be used as sensors to detect the vibrations occurring because of the external disturbances on the system and actuators to suppress them and hence increase the reliability and longevity of the structure. These materials possesses the property of piezoelectricity, which describes the phenomenon of generating an electric charge in a material when subjected to a mechanical stress (direct effect) and conversely, generating a mechanical strain in response to an applied electric field. This property prepares the piezo materials to function as both sensors and actuators. The advantages of these materials include high efficiency, no moving parts, fast response and compact size. A commonly used piezoelectric is the lead zirconate titanate (PZT), which has a strong piezo-effect. PZT's can be fabricated into different shapes to meet specific geometric requirements and are often integrated into the structures. The actuation strains can be of the order of 1000μ strain. With the linear range piezos, actuators can produce strains that are proportional to the applied electric field. These added features make them attractive for structural control applications like the active vibration control in beams.

Active control of vibrations in flexible structures through the smart structure concept is a developing area of research and has numerous applications, especially in the vibration control of structures (such as beams, plates, shells), in aerospace engineering, flexible robot manipulators, antennas, active noise control, shape control and in earthquakes [5]. AVC is critical especially in the field of aerospace applications because the flexible structures can undergo high-amplitude oscillations near their lower natural frequencies, thus damaging the structures. Research on smart structures is interdisciplinary because it involves materials, structural mechanics, electronics, signal processing, communication, mathematics and control. The goal of this multi-disciplinary research is to develop techniques to design, control, analyze and visualize optimal or near optimal smart and adaptive structures using smart materials. A specific area discussed in this monograph is particularly pertinent to the recent new research developments carried out by the authors in the field of modeling, new control techniques and implementation of smart structures (flexible beams with integrated sensors and actuators) in the institute.

1.3 A Brief Survey on Smart Structures Research

Considerable interest is focused on the modeling, control and implementation of smart structures using Euler-Bernoulli beam theory and Timoshenko Beam theory with integrated piezoelectric layers in the recent past. The following

few paragraphs gives a deep insight into the research work done on the intelligent structures so far. Culshaw [3] discussed the concept of smart structure, its benefits and applications. Rao and Sunar explained the use of piezo materials as sensors and actuators in sensing vibrations in their survey paper [6]. Hubbard and Baily [7] have studied the application of piezoelectric materials as sensor / actuator for flexible structures. Hanagud *et.al.* [8] developed a Finite Element Model (FEM) for a beam with many distributed piezoceramic sensors / actuators.

Fanson *et.al.* [9] performed some experiments on a beam with piezoelectrics using positive position feedback. Balas [10] did extensive work on the feedback control of flexible structures. Experimental evaluation of piezoelectric actuation for the control of vibrations in a cantilever beam was presented by Burdess and Fawcett [11]. Brenan *et. al.* [12] performed some experiments on the beam for different actuator technologies. Yang and Lee [13] studied the optimization of feedback gain in control system design for structures. They developed an analytical model for structural control in which both non-collocated sensor/actuator placement and feedback control gain were considered as independent variables. Crawley and Luis [14] presented the development of piezoelectric sensor / actuator as elements of intelligent structures.

Hwang and Park [15] presented a new finite element (FE) modeling technique for flexible beams. Continuous time and discrete time algorithms were proposed to control a thin piezoelectric structure by Bona, *et.al.* [16]. Schiehlen and Schonerstedt [17] reported the optimal control designs for the first few vibration modes of a cantilever beam using piezoelectric sensors / actuators. S. B. Choi *et.al.* [18] have shown a design of position tracking sliding mode control for a smart structure. Distributed controllers for flexible structures can be seen in Forouza Pourki [19]. A higher order sliding mode control technique for vibration suppression in flexible beams was presented by Bandyopadhyay and Axay [20]. Shiang Lee [21] devised a new form of control strategy for vibration control of smart structures using neural networks.

A passivity-based control for smart structures was designed by Gosavi and Kelkar [22]. A self tuning active vibration control scheme in flexible beam structures was carried out by Tokhi [23]. Active control of adaptive laminated structures with bonded piezoelectric sensors and actuators was investigated by Moita *et. al.* [24]. Ulrich *et. al.* [25] devised a optimal LQG control scheme to suppress the vibrations of a cantilever beam. Finite element simulation of smart structures using an optimal output feedback controller for vibration and noise control was performed by Young *et. al.* [26]. Work on vibration suppression of flexible beams with bonded piezo-transducers using wave-absorbing controllers was done by Vukowich and Koma [27]. Apart from piezoelectric as sensor/actuator, Anjanappa [28] developed an integrated model to analyze the vibration control of cantilever beams using magnetostrictive mini-actuators.

Aldraihem *et. al.* [29] have developed a laminated beam model using two theories; namely, Euler-Bernoulli beam theory and Timoshenko beam theory. Abramovich [30] has presented analytical formulation and closed form solu-

tions of composite beams with piezoelectric actuators, which was based on Timoshenko beam theory. He also studied the effects of actuator location and number of patches on the actuator's performance for various configurations of the piezo patches and boundary conditions under mechanical and / or electric loads. Using a higher-order shear deformation theory, Chandrashekhara and Varadarajan [31] presented a finite element model of a composite beam to produce a desired deflection in beams with clamped-free, clamped-clamped and simply supported ends.

Sun and Zhang [32] suggested the idea of exploiting the shear mode to create transverse deflection in sandwich structures. Here, he proved that embedded shear actuators offer many advantages over surface mounted extension actuators. Aldraihem and Khdeir [33] proposed analytical models and exact solutions for beams with shear and extension piezoelectric actuators and the models were based on Timoshenko beam theory and higher-order beam theory. Exact solutions were obtained by using the state-space approach. Doschner and Enzmann [34] designed a model-based controller for smart structures. Robust multivariable control of a double beam cantilever smart structure was implemented by Robin Scott *et. al.* [35].

In a more recent work, Zhang and Sun [36] formulated an analytical model of a sandwich beam with shear piezoelectric actuator that occupies the entire core. The model derivation was simplified by assuming that the face layers follow Euler-Bernoulli beam theory, whereas the core layer obeys Timoshenko beam theory. Furthermore, a closed form solution of the static deflection was presented for a cantilever beam. A new method of modeling and shape control of composite beams with embedded piezoelectric actuators was proposed by Donthireddy and Chandrashekara [37]. A model reference method of controlling the vibrations in flexible smart structures was shown by Murali *et. al.* [38]. Thomas and Abbas [39] explained some techniques of performing finite element methods for dynamic analysis of Timoshenko beams.

A FEM approach was used by Benjeddou *et. al.* [40] to model a sandwich beam with shear and extension piezoelectric elements. The finite element model employed the displacement field of Zhang and Sun [36]. It was shown that the finite element results agree quite well with the analytical results. Raja *et. al.* [41] extended the finite element model of Benjeddou's research team to include a vibration control scheme. An improved 2-node Timoshenko beam model was presented by Kosmataka and Friedman [42]. Azulay and Abramovich [43] have presented analytical formulation and closed form solutions of composite beams with piezoelectric actuators. Stiffening effects of smart composite piezo-laminated beams was studied by Waisman and Abramovich [44]. Abramovich and Lishvits [45] did extensive work on cross-ply beams to control the free vibrations.

1.4 Review of Beam Theories

The study of physical systems such as beams frequently results in partial differential equations, which either cannot be solved analytically, or lack an exact analytic solution due to the complexity of the boundary conditions. For a realistic and detailed study, a numerical method must be used to solve the problem. The finite element method is often found to be the most adequate. Over the years, with the development of modern computers, the finite element method [46] has become one of the most important analysis tools in engineering. A number of finite element tools such ANSYS, NASTRAN, FEMLAB are used to obtain the finite element model of a structure. Basically, the finite element method consists of a piecewise application of classical variational methods to smaller and simpler sub-domains called finite elements connected to each other in a finite number of points called nodes. A precise mathematical model is required for the controller design for vibration control to predict the structure's response. Two beam models [29] in common use in the structural mechanics are the Euler-Bernoulli beam model and the Timoshenko beam model, which are considered here below.

1.4.1 Euler-Bernoulli Beam Theory

The Euler-Bernoulli beam model often called as the classical beam model for plane beams rests on the following assumptions.

(a) *Planar symmetry* : The longitudinal axis is straight and the cross section of the beam has a longitudinal plane of symmetry. The resultant of the transverse loads acting on each section lies on that plane. The support conditions are also symmetric about this plane.
(b) *Cross section variation* : The cross section is either constant or varies smoothly.
(c) *Normality* : The Euler-Bernoulli beam equation is based on the assumption that the plane cross section normal to the neutral axis before deformation remains normal to the neutral axis after deformation or bending. This assumption is valid if length to thickness ratio is large and for small deflection of beam. The total rotation will be due to the bending stress alone. This rotation θ occurs about the y-axis and is the slope of the beam as shown in Fig. 1.3 and is the first derivative of deflection given by $\theta = \frac{dw}{dx}$. However, if the length to thickness ratio is small, the plane cross section of the beam will not remain normal to the neutral axis after bending.
(d) *Strain energy* : The internal strain energy of the member accounts only for the bending deformations and all other contributions such as the transverse shear and the axial forces are ignored.
(e) *Linearization* : Transverse deflections, rotations and deformations are considered so small that the assumptions of the infinitesimal deformations apply.

(f) *Material model* : The material is assumed to be elastic, slender thin and long.

Crawley and Luis [14] have developed analytical models of beams with piezoelectric actuators. These models illustrate the mechanics of Euler - Bernoulli beams with surface mounted actuators and the analytical results have been verified by carrying out experiments. In practical situations, a large number of modes of vibrations contribute to the structure's performance. Since the shear forces, axial displacement are neglected in Euler-Bernoulli theory, slightly inaccurate results may be obtained.

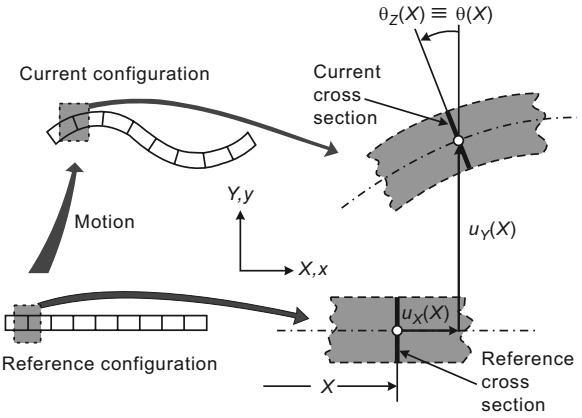

Fig. 1.3. Euler-Bernoulli beam model

1.4.2 Timoshenko Beam Theory

The Timoshenko beam model corrects the classical beam model by considering the effects of the first-order transverse shear deformation and the axial displacements. Thus, the Timoshenko beam theory overcomes the drawbacks of the Euler-Bernoulli beam theory and the mathematical model obtained can be closer to an exact one. For isotropic beams, the next logical step beyond Euler-Bernoulli beam theory is the Timoshenko beam theory, in which there are 6 fundamental global deformations (bending and transverse shear in two directions, extension, and twist).

In this model, a plane cross section of the beam normal to the beam axis before deformation does not remain normal to the beam axis any longer after deformation because of the shear as shown in the Fig. 1.4. The deviation from normality is produced by a transverse shear that is assumed to be constant over the cross section. Thus, the Timoshenko beam model is superior to Euler-Bernoulli model in precisely predicting the beam response and assumes additional importance in beam dynamics and in controlling the vibrations.

The total slope of the beam $\phi(x)$ consists of two parts, viz., one due to the bending rotation $\frac{dw}{dx}$ and other due to the shear γ. The two generalized displacements are the transverse displacement w and the axial displacement u. Because of the transverse shear deformation, the total slope of the beam in the Timoshenko model is different from the slope $\frac{dw}{dx}$ in the EB model. Instead, it is equal to $\frac{dw}{dx} - \gamma$, where γ is the transverse shear strain.

Extensive research in modeling of piezoelectric materials in building actuators and sensors for smart structures using Timoshenko theory was reported in the literature survey in the previous section. A new concept of finite element modeling of the flexible structures using Timoshenko beam theory with the inclusion of the shear related terms both in the piezo-patches as well as in the host structure is proposed for the first time and is being reported in this monograph.

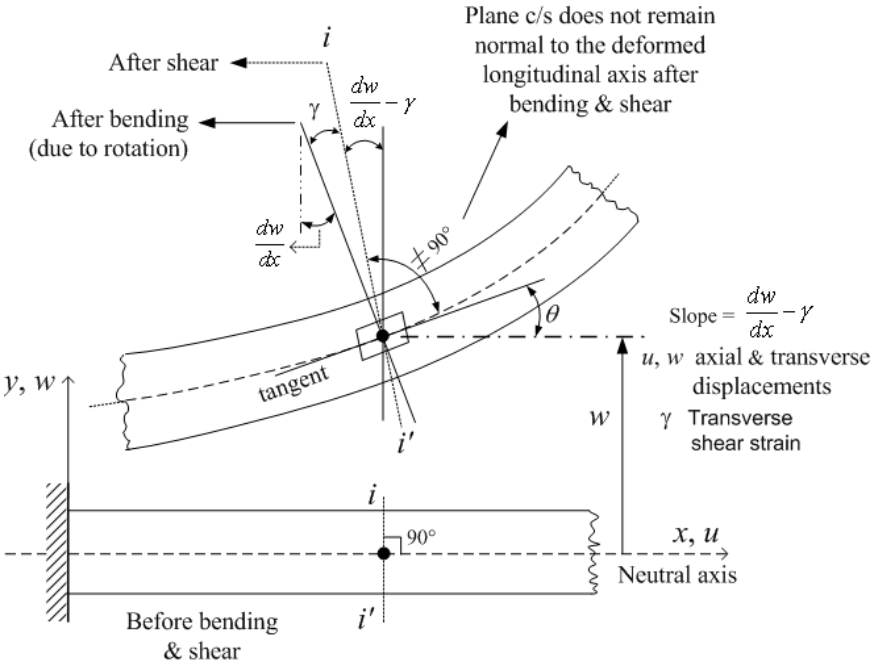

Fig. 1.4. Timoshenko beam model

1.5 Mathematical Models for Smart Structures

Mathematical modeling of any system is the art and craft of building a system of equations that is both sufficiently complex and simple to give real insight

into the situation. It brings together mathematicians and specialists in other fields to improve existing system, develop better ones or predict the behavior of a certain system and how the things will be in the future. With the advent of more powerful computers, modeling teams have been able to tackle more complex problems, develop more accurate models, get answers in less time, and reduce research and development costs. Finally, it is the process of creating a mathematical representation of some phenomenon in order to gain a better understanding of that phenomenon.

It is a process that attempts to match observations with symbolic statements. During the process of building a mathematical model, the modeller will decide what factors are relevant to the problem and what factors can be de-emphasized. Once a model has been developed and used to answer questions, it should be critically examined and often modified to obtain a more accurate reflection of the observed reality of that phenomenon. Mathematical models of time dependent processes (dynamical systems) can be split into 2 categories depending on how the time variable is to be treated. A continuous time mathematical model is based on a set of equations that are valid for any value of the time variable. A discrete time mathematical model is designed to provide information about the state of the physical system only at a selected set of distinct times.

The solution of a CT mathematical model provides information about the physical phenomenon in the system at every time value, i.e., gives information about the parameters for a continuum of the values of the independent variable, whereas the solution of a DT mathematical model provides information about the physical system only at discrete instants of time. CT models have 2 advantages over DT models - they provide information at all times and more clearly show the qualitative effects that can be expected when a parameter or an input variable is changed. On the other hand, DT models have 2 advantages over CT models - they are less demanding with respect to skill level in algebra, trigonometry, calculus, differential equations, etc. and are better suited for digital implementation on a computer. The main advantage of mathematical modeling of systems (say, a structure) is, simulating the system off-line, observing its behavioral response and then using it to control in real time.

For the control of these structures, a precise mathematical model is required to start with. These mathematical models are further used to design a controller and put it in the feedback loop with the plant for its overall satisfactory performance. It is common to assume the availability of a model of the plant to be controlled, especially in the form of a differential equation or a system of differential equations (i.e., an input-output relation or the transfer function model or the state space model). The number of inputs and outputs or the number of states of a system can be regarded as parameters that are used to control the system. This approach works well for mechanical systems with a few DOF, keeping in mind that each DOF gives rise to 2 state variables, viz., displacement and velocity. A structural dynamic model or a finite ele-

ment model is obtained by the finite element discretization of a structure and then using the modern control theory, a state-space model of the structural system can be obtained.

In this monograph, a precise finite element model of the flexible structure is obtained starting from the fundamental equations governing the system and this finite element model is further used to obtain a state-space model (CT and DT) by retaining the first few vibratory modes. Further, these continuous and the discrete state space models are used for the controller design for vibration suppression of flexible cantilever beams.

1.6 Review of Control Techniques

A brief review of various control techniques used for the active vibration control (AVC) presented in this monograph is as follows.

1.6.1 Multirate Output Feedback

Much of the research work done in the area of smart structures is mainly concentrated in the field of modeling and control techniques such as state feedback, static output feedback with too many design restrictions have been used for controller design. The problem with these control techniques is that the state feedback controller needs the availability of the entire state vector or needs an estimator. The problem with the observer-based controllers is that the state feedback and state estimation cannot be separated in the face of uncertainty represented by a whole family of systems.

However, it is known that though most of the practical systems are observable, all the system states are seldom measurable. Therefore, the above mentioned control algorithms may not be implementable in many cases as some states are not available. Hence, it is desirable to go for an output feedback design. The output of the system, however, is always a measurable quantity. Therefore, output feedback based control [47] algorithms are more practical compared to state feedback-based algorithms. Considerable amount of research has been performed in the field of developing control laws using output feedback techniques (static and dynamic output feedback), which requires only the measurement of the system output.

The static output feedback problem [48] is one of the most investigated problems in control theory and applications. One reason why the static output feedback has received so much attention is that it represents the simplest closed loop control that can be realized in practice. Another reason is that many problems consisting of synthesizing the dynamic controllers can be formulated as static output feedback problems involving augmented plants.

In a recent survey by Syrmos *et.al.* [48], the authors say that the problem of static output feedback is still open and that the output feedback problem may be NP-hard. The complete pole assignment and guaranteed closed

loop stability is still not obtained by using static output feedback. Hence, the desired control law should incorporate the simplicity of a static output feedback [49], while at the same time assuring the stability [50] and performance obtained by a state feedback.

So, if for an example, smart cantilever beam, in this case, has to be stabilized using only the output feedback (states may not be available for measurement), one can resort to multirate output feedback technique which is static in nature as well as guarantees the closed loop stability. It has been shown that closed loop stability and performance can be guaranteed by multirate output feedback technique if the system output or the control input is sampled at a rate faster than the other, a feature not assured by the static output feedback while retaining the structural simplicity of static output feedback.

The former method of control being called as the fast output sampling (FOS) [51], [52] and the latter being called as the periodic output feedback (POF) [53], [54], [55]. A control can thus, be designed based on this multirate technique. This technique of designing the controller is termed as 'Multirate Output Feedback (MROF) Technique', which is nothing but sampling the control input and sensor output at different sampling rates. Further, this technique can also be combined with discrete sliding mode control to evolve a new type of control strategy called as the multirate output feedback based discrete-time sliding mode [56].

Hence, it can be found here that the state feedback based control laws of any structure may be realized by the use of multirate output feedback by representing the system states in terms of the past control inputs and multirate output samples. Another advantage of the MROF control technique is that it does not need all the system states for control and feedback purposes. One main feature of the MROF control technique that makes it attractive for robust controller design is the fact that a result similar to the above can be shown to hold good when the state feedback is applied simultaneously to a family of models representing different operating conditions of the plant.

The multirate concept is also being extended to the design of controllers for active vibration control of flexible structures using discrete sliding mode control algorithms. A multirate output feedback (POF and FOS) and multirate output feedback based sliding mode control philosophy can thus be applied to almost all the controllable and observable systems, while at the same time being simple enough as not to tax the computer too much.

1.6.2 Periodic Output Feedback

One of the effective methods of performing the multirate output feedback [57] is the periodic output feedback (POF). The problem of pole assignment by piecewise constant output feedback was studied by Chammas and Leondes [53], [54] for LTI systems with infrequent observations. They have shown that by the use of a periodically time-varying piecewise constant output feedback, the poles of the discrete time control system could be assigned arbitrarily

(within the natural restriction that they should be located symmetrically with respect to the real axis).

Here, the value of the input at a particular moment depends on the output value at a time prior to this moment (namely at the beginning of the period). Since the feedback gains are piecewise constants, their method could easily be implemented and guarantees the closed loop stability. Such a control law can stabilize a much larger class of systems than the static output feedback. Werner and his co-workers have successfully applied the periodic output feedback control method for the robust multivariable control of a turbogenerator [55]. In this monograph, the problem of POF control design and its numerous applications to active vibration control of smart structures is presented.

1.6.3 Fast Output Sampling Feedback

Another method of multirate output feedback (MROF) [57] is the fast output sampling feedback technique. The problem of fast output sampling was studied by Werner and Furuta [51], [52] for linear time invariant systems. They have shown that the poles of the discrete time control system could be assigned arbitrarily (within the natural restriction that they should be located symmetrically with respect to the real axis) using the fast output sampling technique provided the number of gain changes is not less than the system's observability index. Since the feedback gains are piecewise constants, their method could easily be implemented. Such a control law can also stabilize a much larger class of systems. The problem is to find a FOS feedback gain that realizes the state feedback gain. In this monograph, the problem of FOS control design and its numerous applications to active vibration control of smart structures is also presented.

1.6.4 Robust Decentralized Multirate Output Feedback

The multirate output feedback (POF / FOS) concept is being extended to design a robust decentralized controller. In multirate output feedback, say, for the multimodel synthesis, the gain matrix is generally full. This results in the control input of each plant being a function of the output of all the plants. Robust decentralized multirate output feedback control can be achieved by making the off-diagonal elements of POF or the FOS gain matrices zero. So, the structure of this gain matrix is assumed as a diagonal one. With this structure of the robust decentralized gain matrix, the problem can be formulated in the framework of LMI and the desired matrices can be obtained. Now, it is evident that the control input of each model of the plant is a function of the output of that plant only and this makes the smart structure controller design using multirate output feedback method a robust decentralized one. In the context of smart structures, this robust decentralized controller concept is being presented in this monograph for the first time and is used for the

design of a fault tolerant controller and for a multimodel representation of multivariable systems.

1.6.5 Model Order Reduction

Smart structure systems are distributed parameter systems and in general these models are of higher order as it requires a large number of vibratory modes for its satisfactory performance. As a result of which the cost, size and complexity involved in controller design is also high. It is a common procedure to model it as a higher order system, then reduce it to a lower order by using model order reduction techniques, design a controller for the reduced order and then apply it to the higher order. A number of model order reduction techniques have been proposed by many researchers. To name a few, Marshall [58], Chidambara [59] and Mahapatra [60], Vittal Rao [61], Davison [62], etc.,.

The principle of the model order reduction method is to neglect the eigen values of the original system that are farthest from the origin and retain only the dominant eigenvalues and hence dominant time constants of the original system in the reduced order model. This implies that the overall behaviour of the approximate system will be very similar to that of the original system. Many different methods have been developed to accomplish the purpose by estimating the 'dominant' part of the large system and finding a simpler (or reduced order) system representation that has its behaviour akin to the original system.

One of the well-known techniques is based on dominant eigenvalue retention method based on the Davison technique [61], [62]. By this method, a system of higher order can be numerically approximated to one of smaller order. The method suggests that a large $(n \times n)$ system can be reduced to a simpler $(r \times r)$ model by considering the effects of the r most dominant (dominant in the sense of being closest to the instability) eigenvalues alone where r being $\leq n$.

In this monograph, a higher order state space model is developed by considering more number of vibratory modes for the smart beam and a reduced order model is obtained using the method of Davison. These developed reduced order models are used for the design of robust decentralized controller for the multimodel representation of the multivariable systems of the smart structure using MROF via reduced order model in order to suppress the transverse vibrations in the smart structure.

1.6.6 Sliding Mode Control

Discrete-time multirate output feedback based sliding mode control proposed in [56] can be used as one of the efficient methods of controlling the vibrations of flexible structures. Here, follows a small insight into the design problem. The theory of sliding model control (SMC) is based on the concept of varying

the structure of the controller by changing the state of the system in order to obtain a desired response [63]. Generally, a switching control action is used to switch between different structures and the system state is forced to move along the chosen manifold, called the switching manifold [64] which determines the closed loop system behavior [65], [66].

With the increasing use of computers and discrete-time samplers in the design and implementation of controllers now-a-days, the discrete-time systems and the computer based control have become current topics of research. In the recent past, considerable efforts have been put into studying the concepts of Digital Sliding Mode (DSM) controller design [67], [68], [69]. In the case of DSM design, the control input is applicable only at certain sampling instants and the control effort remains constant over the entire sampling period. Moreover, when the states reach the switching surface, the subsequent control would be unable to keep the states confined to the surface.

As a result, DSM can undergo only quasi-sliding mode, i.e., the system states would approach the sliding surface but would generally be unable to stay on it. Thus, in general, DSM does not possess the invariance property found in continuous-time sliding mode. Gao [69] has introduced a new "reaching law approach" to design the controller for a discrete-time system using state feedback. This reaching law ensures that the system trajectory will hit the switching manifold and thereafter will undergo a zigzag motion about the switching manifold. The magnitude of each successive zigzagging step decreases so that the trajectory stays within a specified band called the quasi-sliding mode band (QSMB).

However, many of the sliding mode control strategies require full-state feedback. But, in practice, all the states of the system are not always available for measurement. But, it is of common knowledge that only the system output is available. More often than not, the system output is not coincident with the system state. Since the system output is always available for measurement, output feedback [47] can be used for controller design and this lead us to the requirement of the output feedback based sliding mode control strategy.

In this context, two discrete time sliding mode control strategies [56], [70] is explored in this monograph.

- Bandyopadhyay *et. al.* [70] proposed a discrete time sliding mode control strategy that makes the use of a switching function in the control, resulting in a quasi sliding mode. This DTSM control concept is used to control the vibrations of the smart structures.
- The multirate discrete-time output feedback sliding mode control algorithm proposed in [56] and based on Bartoszewicz's control law [71] and MROF technique [52] is also used to control the flexural vibrations of the smart structure. Moreover, this law avoids the switching function present in other sliding mode control algorithms and thus avoids chatter [69].

Here, the disturbance is the external force signal, which is applied to the cantilever beam at its free end. The above two algorithms has the advantage

that it does not require the state information for control purposes as it makes use of only the output samples for designing the controller. The control input is deduced using past output samples and the immediate past input signal alone instead of the system states. Hence, it is more practical and easy to implement.

1.7 Contributions of the Monograph

A brief look into the smart structures, its concepts, its active involvement in the vibration control, its applications and the extensive research work done on it so far was provided in the previous sections. The contributory chapters of the research monograph presented by the authors are summarized in the following manner as 5 chapters.

1.7.1 Modeling of Smart Structures

The modeling of flexible beams using two types of beam theories, viz., the Euler-Bernoulli theory and the Timoshenko beam theory is presented in the second chapter of this monograph.

Using the FEM and state space techniques, the finite element model and the state space model of the beam is arrived at, which is used for the controller design. The sensor-actuator dynamics is also included in this context while obtaining the model. Two separate cases are dealt with. One is the SISO case and the other is the MIMO case. In both the cases, the piezoelectric patches are bonded to the master structure as surface mounted sensor / actuators (beam is sandwiched between top and bottom piezoelectric layers) or as embedded sensor / actuators (piezoelectric patches, i.e., shear sensors / actuators are sandwiched in between two beam layers) at different finite element locations along the length of the beam.

Either one sensor-actuator pair at a time or multiple sensor-actuator pairs being active at a time has been considered. The piezos are bonded to the beam either as collocated pairs or as non-collocated pairs (only for embedded case). The first few dominant vibratory modes are considered in the design (say, 2, 3, 4, 5 or 6).

In the SISO case,

(a) The entire structure is modeled in state space form by dividing the structure into 3, 4, 5 finite elements, thus giving rise to three types of systems, viz., system 1 (beam divided into 3 finite elements), system 2 (4 finite elements) and system 3 (5 finite elements). A pair of piezo-patch is bonded to the beam only at one finite element location as surface mounted sensor-actuator pair, thus giving rise to one sensor output and one actuator input. The sensor actuator pair is moved from the fixed end to the free end, thus

giving rise to many SISO models of the same smart structure plant and which is being proposed in [72], [73]. The importance in considering such models are that, it allows to have redundancy in sensor / actuator locations on the smart structure systems. It allows to study the role of sensor / actuator mass and stiffness in the system characteristics and the position of the piezo pair in the beam dynamics.

(b) State space models are also developed for various aspect ratios of the beam by dividing it into 4 finite elements and placing the piezo pair at the nearby fixed end. [74].

(c) Single input single output state space models are also obtained for the embedded case by dividing the beam into 5 finite elements. The actuator is placed at the first location and the sensor is moved from the second position to the free end, thus giving rise to 4 SISO models [75], [76].

In the MIMO case,

(d) The cantilever beam is divided into a number of finite elements viz., 4. The piezoelectric sensor / actuator is bonded to the smart structure at finite element positions numbering 2 and 4. Thus, a multivariable system with 2 actuator inputs and 2 sensor outputs is obtained. By making two piezoelectric elements as active sensor / actuator at a time and by making other elements as regular beam elements, state space model of the MIMO system is obtained and is proposed in [77], [78].

(e) For the above case, 5 such multivariable models are obtained by varying the thickness parameter of the aluminum beam, thus giving rise to a multimodel smart structure system by retaining the first 6 modes of vibration. Using model order reduction technique, the reduced order model of the higher order system is obtained based on the dominant eigen value retention and the method of Davison [79], [80].

(f) The entire structure is modeled in state space form by dividing the master structure into 8 finite elements and placing the piezoelectric sensor / actuator as collocated pairs at finite element positions 2, 4, 6 and 8. Thus, a MIMO model with 4 actuator inputs and 4 sensor outputs is obtained and proposed in [81], [82], [83], [84].

(g) For the embedded case, the state space model is obtained by dividing the composite beam into 8 finite elements and placing the sensors at positions 6 and 8, actuators at 2 and 4. Thus, a multivariable system with 2 actuator inputs and 2 sensor outputs is obtained [85].

The multirate output feedback based control design techniques (the periodic output feedback, fast output sampling feedback, multirate output feedback based discrete sliding mode control) have been applied for the first time in several smart structure models discussed in (a)-(g) and is presented in the subsequent chapters of this monograph.

1.7.2 Design of POF Controllers

The third Chapter deals with the design of the periodic output feedback control system for smart structure systems.

When an external force input (impulse disturbance or sinusoidal disturbance) is applied to the free end of the beam, it is subjected to vibrations. These vibrations should be suppressed quickly. Periodic output feedback controllers are designed [72], [75], [86], [87] and applied to control the first few vibration modes of the smart cantilever beam for the various developed SISO state space models (a)-(c) in Chapter 2. Simulations are performed in Matlab. The open loop responses, closed loop responses with the output injection gain, closed loop responses with the POF gain, the control effort required to suppress the vibrations and the tip displacements are observed.

The performance of the smart system is evaluated for active vibration control. Responses of the system are also observed without the controller and are compared with the controller to show the control effect. The effect of placing the sensor / actuator at various locations along the length of the beam for all the types of systems shown in (a)-(c) in Chapter 2 is observed. The conclusions are drawn for the best performance (best model) and for the smallest magnitude of the control input required to control the vibrations of the beam. Through the simulation results, it is shown that when the plant is placed with this designed POF controller, the plant performs well and the vibrations are damped out quickly with the introduction of the controller.

POF controllers are also designed [77], [78], [85] for the multivariable models shown in (d) and (g) of Chapter 2. It is observed that modeling a smart structure by including the sensor / actuator mass and stiffness and by placing the sensor / actuator at 2 different positions introduces a considerable change in the structural vibration characteristics than placing the sensor / actuator pair at only one location. MIMO dynamic analysis is able to identify pairs of modes that occur at nearly identical frequencies. There is multiple interactions of the input and the output which will make the vibrations to be damped out faster.

For the multivariable case, it is observed that when the pair is kept at 2 different locations, the closed loop responses of the MIMO system is less oscillatory compared to the single input single output case. MIMO excitation is better than SISO excitation as only exciting at a single point may cause poor distribution of input energy throughout the structure and may result in somewhat slightly disturbed frequency responses. A multi input test provides better energy distribution and even better actuation forces.

Further, the design of a robust decentralized controller for the beam model (f) in Chapter 2 using POF control technique when there is a failure of a system component to function (say, an actuator) is discussed. 4 multivariable models of the same plant are obtained by considering one actuator failure at a time. The effect of failure of one of the piezo patches on the system is observed. In the designed control law, the control inputs to each actuator of

the multimodel system is a function of the output of the corresponding sensor only and the gain matrix has got all off-diagonal terms zero. This makes the POF control technique a robust decentralized one.

It is also observed that when any one of the actuators fails to function, even then the controller stabilizes all the 4 models. [81], [82]. This Chapter also gives an insight into the design of a Robust Decentralized Periodic Output Feedback (RDPOF) controller for the multivariable smart structure using the various models of the single plant (shown in (e) in Chapter 2) via the reduced order modeling [88], [89]. Simulations are done in Matlab and the various responses are obtained for the designed state space based FE model of the smart flexible cantilever beam. In the control law, the control input to each actuator of the multivariable plant is a function of the output of the corresponding sensor only and the gain matrix has got all off-diagonal elements zero. This makes the POF control technique a robust decentralized one. This would render better control and is more feasible.

The robust decentralized POF controller designed by the above method requires only constant gains. The computation of the output injection gain, which is needed to obtain the decentralized POF based smart structure system, becomes very tedious when the number of modes, especially greater than 5 are considered. Here, a output injection gain is computed from the reduced order model of the smart system and using the aggregation techniques, a output injection gain can be obtained for the higher order (actual) model. The RDPOF feedback gain, which realizes this output injection gain, can be obtained for the actual model. It is found that the designed robust controller via the reduced order model provides good damping enhancement for the models of the smart structure system.

1.7.3 Design of FOS Controllers

The design of the FOS controllers for active vibration control is presented in the fourth chapter. Fast output sampling feedback controllers are designed [76], [90], [91], [92] and applied to control the first few vibration modes of the smart cantilever beam for the various developed SISO state space models (a) - (c) of Chapter 2. Simulations are performed in Matlab. The open loop responses, closed loop responses with the state feedback gain, closed loop responses with the FOS gain, the control effort required to suppress the vibrations and the tip displacements are also observed.

The performance of the smart system is evaluated for active vibration control. Responses of the system are also observed without the controller and are compared with the controller to show the control effect. The effect of placing the sensor / actuator at various locations along the length of the beam for all the types of systems shown in (a) - (c) in Chapter 2 is observed. The conclusions are drawn for the best performance (best model) and for the smallest magnitude of the control input required to control the vibrations of the beam. Through the simulation results, it is shown that when the plant

is placed with this designed FOS controller, the plant performs well and the vibrations are damped out quickly with the introduction of the FOS controller.

FOS controllers are also designed and proposed in [93] for the multivariable models shown in (d) and (g) in Chapter 2. It is observed that modeling a smart structure by including the sensor / actuator mass and stiffness and by placing the sensor / actuator at two different positions introduces a considerable change in the structural vibration characteristics than placing the sensor / actuator pair at only one location.

As in the case of POF, the FOS feedback control technique is also used to design a robust decentralized fault tolerant controller [83], [84] for the multimodel system (f) in the event of an actuator failure. Further, the decentralized FOS feedback controller concept is extended to design a robust controller for a multimodel representation of a family of multivariable plants in (e) using the model order reduction techniques [79], [88], [89].

1.7.4 Design of DSM Controllers

Design of Discrete Sliding Mode controllers using multirate output feedback technique [56], [70] is presented in the fifth Chapter of this monograph. Two different methods of DTSMC have been used in this application. One which does not use the switching function and the other which uses a switching function. Discrete sliding mode control algorithm using multirate output feedback which used switching function in the control law is designed [94], [95] for SISO state space models in (a) and MIMO models [96] shown in (d) of Chapter 2. An external force input is applied at the free end of the beams. There are two inputs to the plant. One is the external force input, which is considered as the disturbance. The other input is the control input to the actuator from the controller. The performance of the system is evaluated with the controller in the feedback loop.

In the work considered, the plot of the time derivative of the displacement, i.e., the sensor outputs as a function of time, the magnitude of the control inputs w.r.t. time and the sliding function w.r.t. time are observed. It is observed that modeling a smart structure by including the sensor / actuator mass and stiffness and by placing the sensor / actuator at different positions along the length of the beam introduces a considerable change in the structural vibration characteristics both for SISO as well as for MIMO systems. Another application of the discrete sliding mode control using output samples [91] which does not make use of a switching function in the control law is designed for a flexible structure for a SISO case [97] in (a) and for a MIMO case in (d). The conclusions are finally drawn.

1.7.5 Implementation of the Designed Controllers

The last Chapter of this monograph depicts the experimental evaluation (implementation) of some of the developed control algorithms using dSPACE

and Real Time Workshop. A flexible aluminum beam of suitable dimensions is considered. POF and FOS simulations are performed for this experimental beam considered starting from the first principles in the subsequent Chapters. At the end, the experimental evaluation is performed. A system identification of the experimental beam is performed first. The experimental state space model is obtained next which is used for the controller design.

The beam is excited at its natural frequency using a disturbing piezo-actuator placed at the free end of the beam. Two piezo-patches are bonded as surface mounted sensor / actuator nearby the root of the beam. The bottom one acts as the sensor, while the top one acts as the actuator. The sensor output is given as input to the piezo sensing system, which consists of high quality charge to voltage converting signal conditioning amplifier with variable gain. The conditioned sensor output signal is given as analog input to dSPACE 1104 controller board through its ADC channel. The sensor output is sampled at a particular sampling rate and given as input to the POF / FOS controller.

The output of the controller, i.e., the control signal is updated and applied to the control actuator at a particular sampling interval through the DAC port of dSPACE 1104 system and the piezo actuation system. The control algorithm is developed using simulink software of MATLAB and implemented in real time on dSPACE 1104 system using RTW and dSPACE real time interface tools. The simulink software is used to build control block diagrams and real time workshop is used to generate C code from the simulink model. The C code is then converted to target specific code by RTI and target language compiler supported by dSPACE 1104.

This target code is then deployed on to the rapid prototype hardware system to run the Hardware In Loop Simulation (HILS). The excitation signal, open loop response, closed loop response with POF / FOS control and control signal acquired from dSPACE control desk are observed in real time. The control is switched on after a certain time and the decay of vibrations is observed. Their FFT's are also observed using a Tektronix oscilloscope from which the reduction in the vibrations can be observed. The results of the simulations and the experimental results are compared. The experimental study demonstrated good closed loop performance and the simplicity of the multirate output feedback controllers.

1.8 Motivation for Modeling and Control of Smart Structures

The advent of computers and sophisticated signal processing electronics in the modern day world has made the use of DT system representation of the plant more suitable for design of controllers than its CT counterpart. Much of the research work done in the area of smart structures so far is mainly concentrated in the modeling and control techniques, static and dynamic analysis which

make use of state feedback, output feedback principles, linear quadratic regulator, optimal feedback and PID based techniques, etc.,. Since most of these type of control techniques may need all the states for feedback, which may not be available for measurement, they may suffer from the problem of real time implementation and some times need a state observer for control purposes. These drawbacks could be rectified by the use of MROF.

An MROF based control technique can be applied to almost all the systems which are controllable and observable, while at the same time being simple enough as not to tax the computers too much. State feedback algorithms can be converted into output feedback algorithms by the use of multirate output feedback sampling. Consequently, the MROF based control strategies has the advantages of both the state feedback and output feedback control philosophies. In MROF based DSMC, the main motivation for carrying out the work was to develop control strategies for vibration suppression of flexible structures with and without the use of switching function in the control law. We found the answer in the synergy of the multirate output sampling concept and hence, the end result, "*Modeling, Control and Implementation of Smart Structures*", which was the motivation of this monograph.

This monograph is based on the authors work on the multirate output sampling techniques (FOS and POF) and the multirate output feedback based discrete-time sliding mode control of cantilever beams. The resultant controllers would be output feedback based, thus being more practical than the more prevalent state feedback based approaches of controls.

2

Modeling of Smart Structures

The modeling of smart cantilever beams using two types of beam theories, viz., the Euler-Bernoulli beam theory and the Timoshenko beam theory is presented in this chapter. While the former method is discussed in Section 2.1, the latter method is discussed in Section 2.2.

2.1 Modeling of Smart Structures Using Euler–Bernoulli Beam Theory

Low frequency structural noise and vibration is a persistent problem in a variety of light weight flexible structures such as flexible manipulators, flexible cantilever beams, aircrafts and space structures. These structures are, in general, distributed and flexible in nature. Attractive fields of application are slender structures with low natural damping like the beams. Beam structures form a basis for lot of mechanical structures. The use of the active vibration suppression can improve the dynamic performance of these structures like the wings of an airplane or the blades of turbine or helicopter or a jet engine.

Structures with integrated self-monitoring and control capabilities to suppress unwanted vibrations are becoming increasingly practical due to the rapid development of one type of materials called as *smart materials* (PZT, ER Fluids, MR Fluids, SMA, PVDF, optic fibres). Such structures incorporating these smart materials for intelligent control purposes are called as *smart structures*. For the control of these structures, a precise mathematical model is required to start with. These mathematical models are further used to design a controller and put it in the feedback loop with the plant for its overall satisfactory performance.

In this Section, the mathematical modeling of beams as SISO and MIMO systems based on Euler-Bernoulli beam theory is presented. The first few vibratory modes are retained (say, 2 or 3 ... or 6) in modeling the beam. The concepts of finite element theory, state space techniques and the piezoelectric theory are used in this context. This is followed by the multi-model concepts

and the modeling of the Euler-Bernoulli beams by considering more number of modes, thus obtaining a higher order system. The higher order model is then reduced to a lower order one by retaining the dominant modes of vibration and neglecting the fast modes. Conclusions are finally drawn regarding the proposed models.

2.1.1 Modeling of Smart Beams as SISO Systems for 2 and 3 Vibratory Modes

Consider a flexible aluminium cantilever beam as shown in Fig. 2.1(a) bonded with surface mounted piezoelectric sensor and actuator at a discrete location along the length of the beam (say, at the fixed end) as shown in Fig. 2.1(b). The physical properties of the flexible cantilever beam element and the piezoelectric element are given in Table 2.1, where L_b represents the length of the beam as shown in Fig. 2.2, l_b represents the length of the beam element which is also equal to l_p and l_p represents the length of the piezoelectric patch (sensor or actuator).

Table 2.1. Properties of the flexible cantilever (aluminium beam) and the piezoelectric element when beam is divided into 4 finite elements

Physical parameters	**Cantilever beam**	**Piezoelectric (PZT) sensor / actuator**
Length	$L_b = 0.3$ m	$l_p = 0.075$ m
Width	$b = 0.03$ m	$b = 0.03$ m
Thickness	$t_b = 0.5$ mm	$t_a = t_s = 0.35$mm
Density	$\rho_b = 8030\, Kg/m^3$	$\rho_p = 7700\, Kg/m^3$
Young's Modulus	$E_b = 193.06\, GPa$	$E_p = 68\, GPa$
Damping Constants used in $\mathbf{C}^*$	$\alpha = 0.001$, $\beta = 0.0001$	
PZT Strain Constant		$d_{31} = 125 \times 10^{-12} m/V$
PZT Stress Constant		$g_{31} = 10.5 \times 10^{-3} V m N^{-1}$

An external force input $\mathbf{f}_{ext}$ (impulse or sinusoidal disturbance) is applied at the free end of the smart beam as shown in Fig. 2.1(a). The beam is thus subjected to vibrations. These vibrations which are suppressed quickly in no time by the closed loop action of the sensor, controller and the actuator, would have taken a longer time to damp out without the controller. Thus, there are two inputs to the plant. One is the external force input $\mathbf{f}_{ext}$ and other is the control input u to the actuator from the controller [98].

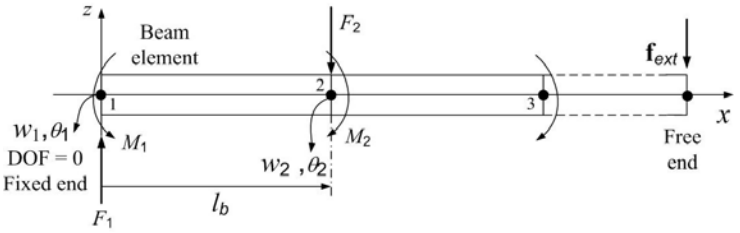

(a) A aluminum beam element

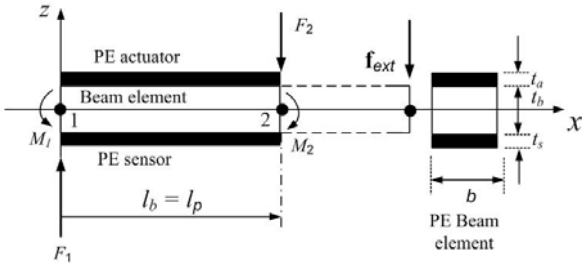

(b) A piezoelectric beam element

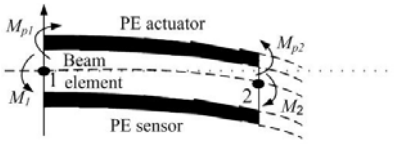

(c) PE beam element subjected to bending moments due to the application of external force at free end

Fig. 2.1. A flexible aluminum cantilever beam element and a smart beam element

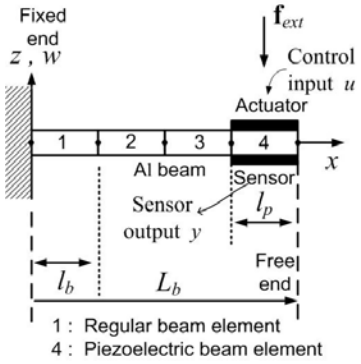

Fig. 2.2. A flexible beam divided into 4 finite elements

In order to develop the mathematical model of the smart beam, we first start with the modelling of the regular beam element and the piezoelectric beam element for a 2 node finite beam element as shown in Figs. 2.1(a) or (b) and in Fig. 2.2. The flexible beam is divided into a number of finite elements (say, 4) as shown in Fig. 2.2. The piezoelectric element is bonded on one of the section of the host surface as shown in Fig. 2.2, thus giving rise to a smart beam. The smart cantilever beam model is then developed using a piezoelectric beam element, which includes sensor and actuator dynamics and a regular beam element which is modeled using Euler-Bernoulli theory and the Finite Element Method (FEM). The piezoelectric beam element is used to model the regions where the piezoelectric is bonded as sensor/actuator and the rest of the structure is modeled by the regular beam elements. In modeling and analysis of cantilever beams, the following assumptions are made.

- The mass and stiffness of the bonding or the adhesive between the master structure and the sensor / actuator pair is neglected, i.e., the adhesive used in between the beam and the sensor/actuator has been assumed to add no mass or stiffness to the structure.
- The signal conditioning device gain G_c is assumed as 100.
- The cable capacitance between the sensor / actuator and the signal conditioning device have been considered negligible and temperature effects have been neglected.
- The beam element is supposed to have 2 degrees of freedom (DOF) at each node, viz., a transverse deflection w at the node and an angle of rotation or slope θ at the node, which are called as the nodal variables.
- Corresponding to the two DOF, a bending moment acts at each nodal point.
- The beam element has constant moment of inertia, modulus of elasticity, mass density and length.

2.1.1.1 Displacement Function $w(x,t)$

When an external force acts on the beam as shown in Figs. 2.1(a) or in 2.2, there is a transverse displacement w as well as bending moments M_1, M_2 occurring at the node 1 (fixed end) and node 2 of the beam element respectively as shown in Fig. 2.1(b). The displacement function $w(x,t)$ is used to study the deflection behavior of the flexible cantilever beam element. The forced vibration characteristics of a flexible beam element [99] is governed by the following fourth order partial differential equation

$$c^2 \frac{\partial^4 w(x,t)}{\partial x^4} + \frac{\partial^2 w(x,t)}{\partial t^2} = \mathbf{f}_{ext}, \tag{2.1}$$

where w is the transverse displacement of the beam and is a function of x and t, x being the distance of the local coordinate from the fixed end, t being the time and c is a constant which is given by $\sqrt{\frac{EI}{\rho A}}$. E, I, ρ, A, $\mathbf{f}_{ext}$ are the

young's modulus, moment of inertia, mass density, area of the beam element and the externally applied pressure loading at the tip of the beam respectively. Note that for free vibrations, $\mathbf{f}_{ext} = 0$.

When the beam vibrates by the application of an external force (impulse or sinusoidal force) as shown in Fig. 2.2, it undergoes to and fro motions. It has transverse displacements and so all positions vary with time and therefore, the system has velocities and accelerations. The first term in the governing differential equation of the beam in Eq. (2.1) refers to the rate of loading, where as the second term refers to the inertia force, which is nothing but mass times acceleration, i.e., the equation of motion involves a fourth order derivative of $w(x,t)$ w.r.t. x and a second order derivative of $w(x,t)$ w.r.t. time (acceleration). The solution of the Eq. (2.1) is assumed as a cubic polynomial function of x and is given by

$$w(x,t) = a_1 + a_2 x + a_3 x^2 + a_4 x^3, \tag{2.2}$$

where $w(x,t)$ is the displacement function which satisfies the fourth order partial differential equation (2.1). The constants a_1 to a_4 are obtained by using the boundary conditions given below at both the nodal points (node 1 and node 2 of the beam element). The Euler-Bernoulli beam equation is based on the assumption that the plane normal to the neutral axis before deformation remains normal to the neutral axis after the deformation. This assumption denotes that the slope $\theta = \frac{dw}{dx}$ is the first spatial derivative of the deflection w w.r.t x. Because there are 4 nodal variables for each beam element, we have assumed a cubic polynomial for $w(x,t)$ as shown in Eq. (2.2). At $x = 0$ (fixed end),

$$w(x,t) = w_1 = a_1 \text{ and } w'(x,t) = \frac{\partial w}{\partial x} = a_2 = \theta_1 \tag{2.3}$$

and at $x = l_b$ (free end),

$$w(x,t) = w_2 \text{ and } w'(x,t) = \frac{\partial w}{\partial x} = \theta_2, \tag{2.4}$$

where w_1, θ_1 and w_2, θ_2 are the degrees of freedom at node 1 and node 2 respectively and l_b is the length of the regular beam element. Note that the degrees of freedom at the fixed end of any beam is zero (say, Fig. 2.1(a) or Fig. 2.2). Application of the boundary conditions from Eqs. (2.3) and (2.4) in Eq. (2.2) yields

$$\begin{bmatrix} a_1 \\ a_2 \\ a_3 \\ a_4 \end{bmatrix} = \frac{1}{l_b^3} \begin{bmatrix} l_b^3 & 0 & 0 & 0 \\ 0 & l_b^3 & 0 & 0 \\ -3l_b & -2l_b^2 & 3l_b & -l_b^2 \\ 2 & l_b & -2 & l_b \end{bmatrix} \begin{bmatrix} w_1 \\ \theta_1 \\ w_2 \\ \theta_2 \end{bmatrix}. \tag{2.5}$$

Substituting the constants obtained from Eq. (2.5) into Eq. (2.2) and by rearranging the terms, the final form of $w(x,t)$ is obtained as

$$[w(x,t)] = \begin{bmatrix} f_1(x) & f_2(x) & f_3(x) & f_4(x) \end{bmatrix} \begin{bmatrix} w_1 \\ \theta_1 \\ w_2 \\ \theta_2 \end{bmatrix} = \left[\mathbf{n}^T\right][\mathbf{q}], \tag{2.6}$$

where $[\mathbf{n}]$ gives the shape functions $f_1(x)$ to $f_4(x)$ of the beam element as

$$[\mathbf{n}] = \begin{bmatrix} f_1(x) \\ f_2(x) \\ f_3(x) \\ f_4(x) \end{bmatrix} = \begin{bmatrix} 1 - 3\frac{x^2}{l_b^2} + 2\frac{x^3}{l_b^3} \\ x - 2\frac{x^2}{l_b} + \frac{x^3}{l_b^2} \\ 3\frac{x^2}{l_b^2} - 2\frac{x^3}{l_b^3} \\ -\frac{x^2}{l_b} + \frac{x^3}{l_b^2} \end{bmatrix}. \tag{2.7}$$

The first, second spatial derivative of $[\mathbf{n}]$ and its time derivative is given in Appendix IV. The vector $\mathbf{q}$ is called as the vector of displacements and slopes (nodal displacement vector) and is given by

$$\begin{bmatrix} w_1 \\ \theta_1 \\ w_2 \\ \theta_2 \end{bmatrix}. \tag{2.8}$$

The first, second spatial derivatives and the time derivative of the displacement function in (2.2) are given by the equations

$$[w'(x,t)] = \frac{\partial w}{\partial x} = \begin{bmatrix} f_1'(x) & f_2'(x) & f_3'(x) & f_4'(x) \end{bmatrix} \begin{bmatrix} w_1 \\ \theta_1 \\ w_2 \\ \theta_2 \end{bmatrix} = \left[\mathbf{n}_2^T\right][\mathbf{q}], \tag{2.9}$$

$$[w''(x,t)] = \frac{\partial^2 w}{\partial x^2} = \begin{bmatrix} f_1''(x) & f_2''(x) & f_3''(x) & f_4''(x) \end{bmatrix} \begin{bmatrix} w_1 \\ \theta_1 \\ w_2 \\ \theta_2 \end{bmatrix} = \left[\mathbf{n}_1^T\right][\mathbf{q}], \tag{2.10}$$

$$[\dot{w}(x,t)] = \frac{\partial w}{\partial t} = \begin{bmatrix} f_1(x) & f_2(x) & f_3(x) & f_4(x) \end{bmatrix} \begin{bmatrix} \dot{w}_1 \\ \dot{\theta}_1 \\ \dot{w}_2 \\ \dot{\theta}_2 \end{bmatrix} = \left[\mathbf{n}_3^T\right][\dot{\mathbf{q}}]. \tag{2.11}$$

2.1.1.2 Regular Beam Element

The strain energy (U) and the kinetic energy (T) of the beam element with uniform cross section in bending is obtained as

$$U = \frac{E_b I_b}{2} \int_{l_b} \left[\frac{\partial^2 w}{\partial x^2}\right]^2 dx = \frac{E_b I_b}{2} \int_{l_b} \left[w''(x,t)\right]^T \left[w''(x,t)\right] dx, \tag{2.12}$$

$$T = \frac{\rho_b A_b}{2} \int_{l_b} \left[\frac{\partial^2 w}{\partial t^2}\right]^2 dt = \frac{\rho_b A_b}{2} \int_{l_b} \left[\dot{w}(x,t)\right]^T \left[\dot{w}(x,t)\right] dt, \tag{2.13}$$

where ρ_b is the mass density of the beam material, A_b is the cross sectional area of the beam element, I_b is the moment of inertia of the beam element, l_b is the length of the beam element and E_b is the modulus of elasticity (Young's moudulus) of the beam material. The equation of motion of a regular 2 node beam element is obtained by using Eqs. (2.12) and (2.13) in the Lagrange's equation

$$\frac{d}{dt}\left[\frac{\partial T}{\partial \dot{q}_i}\right] + \left[\frac{\partial U}{\partial q_i}\right] = [Z_i], \tag{2.14}$$

as

$$M^b \ddot{\mathbf{q}} + K^b \mathbf{q} = \mathbf{f}^b(t), \tag{2.15}$$

where $\ddot{\mathbf{q}}$ is the acceleration vector, Z_i is the vector of forces and moments, M^b, K^b and $\mathbf{f}^b$ are the elemental mass matrix and stiffness matrix of size (4×4) and the force vector of size (4×1) respectively. The elemental mass and stiffness matrices are obtained as

$$\left[M^b\right] = \rho_b A_b \int_{l_b} \left[\mathbf{n}_3^T\right]^T \left[\mathbf{n}_3^T\right] dx, \tag{2.16}$$

$$\left[M_{ij}^b\right] = \rho_b A_b \int_{l_b} f_i(x) f_j(x) dx, \tag{2.17}$$

$$\left[K^b\right] = E_b I_b \int_{l_b} \left[\mathbf{n}_1^T\right]^T \left[\mathbf{n}_1^T\right] dx, \tag{2.18}$$

$$\left[K_{ij}^b\right] = E_b I_b \int_{l_b} f_i''(x) f_j''(x) dx, \tag{2.19}$$

where i, $j = 1$ to 4. The resulting equation of motion for the regular beam element in its explicit form is obtained after simplifying the Eq. (2.15) further as

$$\frac{\rho_b A_b l_b}{420} \begin{bmatrix} 156 & 22l_b & 54 & -13l_b \\ 22l_b & 4l_b^2 & 13l_b & -3l_b^2 \\ 54 & 13l_b & 156 & -22l_b \\ -13l_b & -3l_b^2 & -22l_b & 4l_b^2 \end{bmatrix} \begin{bmatrix} \ddot{w}_1 \\ \ddot{\theta}_1 \\ \ddot{w}_2 \\ \ddot{\theta}_2 \end{bmatrix}$$
$$+ \frac{E_b I_b}{l_b} \begin{bmatrix} 12/l_b^2 & 6/l_b & -12/l_b^2 & 6/l_b \\ 6/l_b & 4 & -6/l_b & 2 \\ -12/l_b^2 & -6/l_b & 12/l_b^2 & -6/l_b \\ 6/l_b & 2 & -6/l_b & 4 \end{bmatrix} \begin{bmatrix} w_1 \\ \theta_1 \\ w_2 \\ \theta_2 \end{bmatrix} = \begin{bmatrix} F_1 \\ M_1 \\ F_2 \\ M_2 \end{bmatrix}, \tag{2.20}$$

where F_1, F_2 and M_1, M_2 are the forces and bending moments acting at the nodes 1 and node 2 of the beam element in Fig. 2.1(b).

2.1.1.3 Piezoelectric Element and Piezoelectric Beam Element

Piezoelectric elements can be used as sensors and actuators in flexible structures for sensing and actuating purposes on the host structure. The dimensions of the piezoelectric patch are given in Table 2.1. The element is assumed to have 2 structural DOF at each nodal point which are, a transverse deflection, an angle of rotation or slope and an electrical Degree of Freedom (DOF) as the voltage. Since the voltage is constant over the electrode, the number of electrical DOF is one for each piezoelectric element. The electrical DOF is used as a sensor voltage or actuator voltage when the piezoelectric material bonded on the structure behaves as sensor or actuator.

When voltage (control input) is applied to the actuator, counteracting moments will be induced by the piezoelectric actuators at each nodal point as shown in Fig. 2.1(c). The bending moment resulting from the applied voltage to the actuator adds a positive bending moment $+M_{p2}$ at node 2 and a negative bending moment $-M_{p1}$ at node 1, which are approximately equal and opposite to the moments induced by the disturbance on the beam. The displacement functions of the PZT will remain the same as that of the regular beam element. Similar to the Eq. (2.15) obtained for a regular beam element, the Lagrange's equation of motion of the piezoelectric element can be obtained as

$$M^p\,\ddot{\mathbf{q}} + K^p\,\mathbf{q} = \mathbf{f}^p(t), \tag{2.21}$$

where M^p, K^p are the mass, stiffness matrices of size (4×4) and $\mathbf{f}^p$ is the force coefficient vector of the piezoelectric element of size (4×1). The elemental mass and stiffness matrices of the piezoelectric element M^p and K^p are obtained on the similar lines given in the regular beam element as

$$M^p = \frac{\rho_p A_p l_p}{420}\begin{bmatrix} 156 & 22l_p & 54 & -13l_p \\ 22l_p & 4l_p^2 & 13l_p & -3l_p^2 \\ 54 & 13l_p & 156 & -22l_p \\ -13l_p & -3l_p^2 & -22l_p & 4l_p^2 \end{bmatrix} \tag{2.22}$$

and

$$K^p = \frac{E_p I_p}{l_p}\begin{bmatrix} 12/l_p^2 & 6/l_p & -12/l_p^2 & 6/l_p \\ 6/l_p & 4 & -6/l_p & 2 \\ -12/l_p^2 & -6/l_p & 12/l_p^2 & -6/l_p \\ 6/l_p & 2 & -6/l_p & 4 \end{bmatrix}, \tag{2.23}$$

where

ρ_p is the mass density of piezoelectric material,

A_p is the area of the piezoelectric patches $= 2t_a b$, i.e., the area of the sensor as well as actuator,

l_p is the length of the piezoelectric element,

b is the width of the piezoelectric patches as well as that of the beam,

E_p is the modulus of elasticity (Young's modulus) of the piezoelectric material,

I_p is the moment of inertia of piezoelectric layer with respect to the neutral axis of the beam and is given by $I_p = \frac{1}{12} b t_a^3 + b t_a \left(\frac{t_a + t_b}{2}\right)^2$,

t_a is the thickness of the actuators,

t_b is the thickness of the beam element or the beam.

The elemental mass and stiffness matrices of the piezoelectric patches are obtained by assuming sensor and actuator of same thickness, same width and are collocated in nature. The piezo mass and stiffness matrices M^p, K^p are obtained by evaluating the equations

$$[M^p] = \rho_p A_p \int_{l_p} \left[\mathbf{n}_3^T\right]^T \left[\mathbf{n}_3^T\right] dx, \tag{2.24}$$

$$\left[M_{ij}^p\right] = \rho_p A_p \int_{l_p} f_i(x) f_j(x) dx, \tag{2.25}$$

$$[K^p] = E_p I_p \int_{l_p} \left[\mathbf{n}_1^T\right]^T \left[\mathbf{n}_1^T\right] dx \tag{2.26}$$

and

$$\left[K_{ij}^p\right] = E_p I_p \int_{l_p} f_i^{''}(x) f_j^{''}(x) dx, \tag{2.27}$$

where $i, j = 1$ to n (n finite elements).

The piezoelectric beam element (top piezo patch + middle beam element + bottom piezo patch) is obtained by sandwiching the regular beam element in between a layer of 2 thin piezoelectric patches of thickness t_a or t_s as shown in Fig. 2.1(b) or in Fig. 2.2 (finite element 4), i.e., as surface mounted piezo-patches on the master structure. The bottom layer acts as a piezoelectric sensor and the upper layer acts as an piezoelectric actuator. The mass and stiffness of the piezoelectric beam element is obtained by using the equations

$$[M] = \rho\ A \int_{l_p} \left[\mathbf{n}_3^T\right]^T \left[\mathbf{n}_3^T\right] dx \quad \text{and} \quad [K] = E\ I \int_{l_p} \left[\mathbf{n}_1^T\right]^T \left[\mathbf{n}_1^T\right] dx, \tag{2.28}$$

where $EI = E_b I_b + 2E_p I_p$ is the flexural rigidity of the piezoelectric beam element, $\rho A = b(\rho_b t_b + 2\rho_p t_p)$ is the mass per unit length, t_p is the thickness

of the piezo patch, which is also equal to the thickness of the actuator t_a or the thickness of the sensor t_s.

2.1.1.4 Piezoelectric Strain Rate Sensors and Actuators

A piezoelectric material can act both as a sensor and an actuator. When used as an actuator, it produces mechanical strain as the output, whereas voltage will be the input. When used as a sensor, it converts the mechanical stress induced in the material into output voltage. This voltage after appropriate signal conditioning is applied as input to the controller. The output of the controller is applied as a control signal to the actuator. The actuator produces the mechanical strain and this is further used to suppress the vibrations using destructive interference. The linear piezoelectric coupling between the elastic field and electric field can be expressed by the direct and the converse piezoelectric constitutive equations [100], [101] as

$$D_z = d_{31}\ \sigma + e^{\sigma} E_f, \quad \varepsilon = d_{31} E_f + s^E \sigma, \tag{2.29}$$

where D_z is the electric displacement, d_{31} is the piezoelectric constant, σ is the stress, e is the permittivity of the medium (dielectric constant), E_f is the electric field, ε is the strain and s^E is the compliance of the piezoelectric medium [6].

Sensor equation

The sensor equation is derived from the direct piezoelectric equation which is used to calculate the total charge created by the strain in the structure. Since no external field is applied to the sensor layer, the electric displacement developed on the sensor surface is directly proportional to the strain acting on it. If the poling is done along the thickness direction of the sensors with the electrodes on the upper and lower surfaces, then the electric displacement D_z is given as

$$D_z \propto \varepsilon_x = e_{31}\ \varepsilon_x, \tag{2.30}$$

where e_{31} is the piezoelectric stress/charge constant, ε_x is the strain of the testing structure at a point. The total charge $Q(t)$ developed on the sensor surface (due to the strain) is the spatial summation of all the point charges developed on the sensor layer and is given by

$$Q(t) = \int_A D_z\ dA. \tag{2.31}$$

Piezoelectric materials can be used as strain rate sensors . When used so, the output charge can be transformed into the sensor current

$$i(t) = \frac{dQ(t)}{dt} = \frac{d}{dt}\int_A D_z\ dA = \frac{d}{dt}\int_A e_{31}\varepsilon_x\ dA. \tag{2.32}$$

Since the strain ε_x of the testing structure at a point can be expressed in terms of the second spatial derivative of the displacement function $w''(x,t)$ as $\varepsilon_x = z\ \frac{d^2w}{dx^2}$, where z is a coordinate of the point on the beam w.r.t. the neutral axis of the beam, the Eq. (2.32) can be written as

$$i(t) = \frac{d}{dt}\int\limits_A e_{31}\ z\ \mathbf{n}_1^T\mathbf{q}\ dA \quad = \quad \int\limits_A e_{31}\ z\ \mathbf{n}_1^T\ \frac{d}{dt}(\mathbf{q})\ dA, \tag{2.33}$$

$$i(t) = z\ e_{31}b\int\limits_0^{l_p} \mathbf{n}_1^T\ \dot{\mathbf{q}}\ dx, \tag{2.34}$$

where $z = \left(\frac{t_b}{2} + t_a\right)$, $\mathbf{n}_1^T$ is the second spatial derivative of the shape function of the beam as given in Appendix IV and $\dot{\mathbf{q}}$ is the time derivative of the nodal coordinate vector $\mathbf{q}$.

The output current of the piezo sensor measures the moment rate of the flexible beam. This current is converted into the open circuit sensor voltage V^s using a signal conditioning device with the gain G_c and applied to an actuator with a suitable controller gain. Thus, the sensor output voltage $V^s(t)$ is obtained as

$$V^s(t) = G_c e_{31} z b \int_0^{l_p} \mathbf{n}_1^T \dot{\mathbf{q}}\, dx, \tag{2.35}$$

which is nothing but the signal conditioning gain G_c multiplied by the closed circuit current $i(t)$ generated by the piezoelectric lamina, i.e., $V^s(t) = G_c\, i(t)$. The vectors $\mathbf{n}_1^T$ and $\mathbf{q}$ are of size (1×4) and (4×1) respectively. Substituting for $\mathbf{n}_1^T$ from Eq. (2.10) and further simplifying, we get the sensor voltage for a two node finite element of the beam as

$$V^s(t) = \begin{bmatrix} 0 & -G_c e_{31} z b & 0 & G_c e_{31} z b \end{bmatrix} \begin{bmatrix} \dot{w}_1 \\ \dot{\theta}_1 \\ \dot{w}_2 \\ \dot{\theta}_2 \end{bmatrix} = G_c e_{31} z b \begin{bmatrix} 0 & -1 & 0 & 1 \end{bmatrix} \begin{bmatrix} \dot{w}_1 \\ \dot{\theta}_1 \\ \dot{w}_2 \\ \dot{\theta}_2 \end{bmatrix}, \tag{2.36}$$

i.e.,

$$V^s(t) = S_c\ \dot{\mathbf{q}}, \tag{2.37}$$

where $G_c e_{31} z b = S_c$ is the sensor constant. Note that the sensor output voltage is a function of the second spatial derivative of the mode shape. The above Eq. (2.37) can be re-written as a scalar of vector product

$$V^s(t) = \mathbf{p}^T \dot{\mathbf{q}}, \tag{2.38}$$

where $\mathbf{p}$ is a constant vector of size (4×1) and depends on the type of sensor, its characteristics and its location on the beam.

This sensor voltage is given as input to the controller and the output of the controller is the controller gain multiplied by the sensor voltage $V^s(t)$. Thus, the input voltage to the actuator $V^a(t)$, i.e., the control input u is given by

$$V^a(t) = u = \text{Controller gain} \times V^s(t). \tag{2.39}$$

Actuator equation

The actuator equation is derived from the converse piezoelectric equation. The strain developed ε_a by the electric field E_f on the actuator layer is given by

$$\varepsilon_a = d_{31}\ E_f, \tag{2.40}$$

where d_{31} is the piezoelectric constant. When the input voltage $V^a(t)$ is applied to the piezoelectric actuator in the thickness direction t_a, the electric field E_f and the stress σ_a developed by the actuator is given by

$$E_f = \frac{V^a(t)}{t_a} \text{ and } \sigma_a = E_p\, d_{31}\, \frac{V^a(t)}{t_a}, \tag{2.41}$$

where E_p is the young's modulus of the piezoelectric layer. Because of this stress in the structure, bending moments acts at nodes 1 and 2. In general, the expression for the bending moment in a small cross section of the piezoelectric element is given by

$$\mathrm{d}M_a = E_p I_p \frac{d^2 w}{dx^2}. \tag{2.42}$$

Since the strain $\varepsilon_a = z\frac{d^2w}{dx^2}$ which is also equal to $\frac{\sigma_a}{E_p}$, the bending moment in the small cross section can be finally obtained as $\mathrm{d}M_a = \sigma_a\ z$. The resultant moment M_a acting on the beam element due to the applied voltage V^a is determined by integrating the stress in Eq. (2.41) throughout the structure thickness as

$$M_a = \int\limits_{thickness} z\ \sigma_a\ dz, \tag{2.43}$$

which after simplifying becomes

$$M_a = E_p\ d_{31}\ \bar{z}\ V^a(t), \tag{2.44}$$

where $\bar{z} = \left(\frac{t_a + t_b}{2}\right)$ is the distance between neutral axis of the beam and the piezoelectric layer.

The control force $\mathbf{f}_{ctrl}$ produced by the actuator that is applied on the beam element is obtained using the Eq. (2.44) as

$$\mathbf{f}_{ctrl} = E_p\, d_{31}\, b\bar{z} \int\limits_{l_p} \mathbf{n}_2\, dx\, V^a(t) \tag{2.45}$$

or can be expressed as

$$\mathbf{f}_{ctrl} = \mathbf{h}\ V^a(t) = \mathbf{h}\ \mathbf{u}(t), \tag{2.46}$$

where $\mathbf{n}_2^T$ is the first spatial derivative of shape function of the flexible beam, $\mathbf{u}(t)$ is nothing but the control input to the actuator, i.e., $V^a(t)$ from the controller and $\mathbf{h}$ is a constant vector of size (4×1) which depends on the type of actuator, its location on the beam, its characteristic properties and is given by

$$\mathbf{h}^T = \begin{bmatrix} -E_p d_{31} b\bar{z} & 0 & E_p d_{31} b\bar{z} & 0 \end{bmatrix} = E_p d_{31} b\bar{z} \begin{bmatrix} -1 & 0 & 1 & 0 \end{bmatrix}, \tag{2.47}$$

i.e.,

$$\mathbf{h}^T = a_c \begin{bmatrix} -1 & 0 & -1 & 0 \end{bmatrix}, \tag{2.48}$$

where $E_p d_{31} b\bar{z} = a_c$ is the actuator constant.

If any external forces $\mathbf{f}_{ext}$ are acting on the beam, then the total force vector becomes

$$\mathbf{f}^{\,t} = \mathbf{f}_{ext} + \mathbf{f}_{ctrl}.$$

2.1.1.5 Dynamic Equation of the Smart Structure

Consider Fig. 2.2 in which the beam is divided into 4 FE and the PZT's placed as collocated sensor / actuator pair at FE position numbering 4. Let M^{bi}, M^{pi} and K^{bi}, K^{pi} $(i, j = 1$ to $4)$ be the individual mass and stiffness matrices of the regular beam elements and the piezoelectric beam elements respectively and are of sizes (4×4). Consider 2 vibratory modes. The dynamic equation of the smart structure is obtained by using both the equations of regular beam elements in Eq. (2.15) and the piezoelectric beam elements given in Eq. (2.28).

Here, in Eqs. (2.15) and (2.28), the mass and stiffness matrices of the regular beam element and the piezoelectric beam element are called as the local mass and stiffness matrices and they give only the mass and stiffness of one of the finite elements of the smart beam in Fig. 2.2. The mass and stiffness matrices of the entire beam, which is divided into 4 finite elements are obtained by assembling the local mass and stiffness matrices using the FEM technique and the assembled matrices (global mass matrix $\mathbf{M}$ and global stiffness matrix $\mathbf{K}$) are given in Appendix IV.

The mass and stiffness matrices $\mathbf{M}$ (8×8) and $\mathbf{K}$ (8×8) of the dynamic equation of the smart structure includes the sensor / actuator mass and stiffness. The equation of motion of the smart structure and the sensor output is finally given by

$$\mathbf{M}\,\ddot{\mathbf{q}} + \mathbf{K}\,\mathbf{q} = \mathbf{f}_{ext} + \mathbf{f}_{ctrl} = \mathbf{f}^{\,t} \tag{2.49}$$

and

$$y(t) = V^s(t) = \mathbf{p}^T \dot{\mathbf{q}}, \tag{2.50}$$

where $\mathbf{q}$, $\ddot{\mathbf{q}}$, $\mathbf{f}_{ext}$, $\mathbf{f}_{ctrl}$, $\mathbf{f}^{\,t}$ and $\mathbf{p}$ are the vector of displacements and slopes (nodal variable vector), the acceleration vector, the external force vector, the controlling force vector, the total force vector and a constant vector of the beam which are of sizes (8×1) respectively.

The mass and stiffness matrices $\mathbf{M}$ and $\mathbf{K}$ of the beam in the system equation (2.49) can be varied by changing the position or location of the piezo patches on the beam and by varying the number of regular and piezoelectric beam elements. The generalized coordinates are introduced into Eq. (2.49) using a transformation $\mathbf{q} = \mathbf{Tg}$ in order to reduce it further such that the resultant equation represents the dynamics of the first few dominant vibratory modes of the smart flexible cantilever beam.

Here, $\mathbf{T}$ is the modal matrix (8×2) containing the eigenvectors representing the desired number of modes of vibration of the cantilever beam as shown in the Appendix VI. This method is used to derive the uncoupled equations governing the motion of the forced vibrations of the smart beam in terms of principal coordinates by introducing a linear transformation between the generalized coordinates $\mathbf{q}$ and the principal coordinates $\mathbf{g}$ and thus decouples into the equations corresponding to each individual mode. Using the transformation $\mathbf{q} = \mathbf{Tg}$, Eqs. (2.49) and (2.50) becomes

$$\mathbf{MT}\ddot{\mathbf{g}} + \mathbf{KTg} = \mathbf{f}_{ext} + \mathbf{f}_{ctrl} = \mathbf{f}^{\,t} \tag{2.51}$$

and

$$y(t) = V^s(t) = \mathbf{p}^T\dot{\mathbf{q}} = \mathbf{p}^T\mathbf{T}\dot{\mathbf{g}}. \tag{2.52}$$

Pre-multiplying Eq. (2.51) by $\mathbf{T}^T$, we get

$$\mathbf{T}^T\mathbf{MT}\ddot{\mathbf{g}} + \mathbf{T}^T\mathbf{K}\ \mathbf{T}\ \mathbf{g} = \mathbf{T}^T\mathbf{f}_{ext} + \mathbf{T}^T\mathbf{f}_{ctrl} = \mathbf{T}^T\mathbf{f}^{\,t}, \tag{2.53}$$

which can be rewritten as

$$\mathbf{M}^*\ddot{\mathbf{g}} + \mathbf{K}^*\mathbf{g} = \mathbf{f}^*_{ext} + \mathbf{f}^*_{ctrl}, \tag{2.54}$$

where the matrices $\mathbf{M}^*$ and $\mathbf{K}^*$ given by $\mathbf{M}^* = \mathbf{T}^T\mathbf{MT}$ and $\mathbf{K}^* = \mathbf{K}^T\mathbf{MT}$ are called as the generalized mass and stiffness matrices and are of size (2×2). The generalized external force vector $\mathbf{f}^*_{ext}$ is given by

$$\mathbf{f}^*_{ext} = \mathbf{T}^T\mathbf{f}_{ext} = \mathbf{T}^T\ \mathbf{f}\ r(t), \tag{2.55}$$

where $r(t)$ is the external force input to the smart beam. The generalized control force vector $\mathbf{f}^*_{ctrl}$ is given by

$$\mathbf{f}^*_{ctrl} = \mathbf{T}^T\mathbf{f}_{ctrl} = \mathbf{T}^T\mathbf{h}V^a(t) = \mathbf{T}^T\mathbf{h}\ \mathbf{u}(t). \tag{2.56}$$

Note that the generalized force vectors for the 2 node beam element considered is of size (2×1). The structural modal damping matrix $\mathbf{C}^*_{(2\times 2)}$ is introduced into Eq. (2.54) by using Raleigh's proportional damping as

$$\mathbf{C}^* = \alpha\mathbf{M}^* + \beta\mathbf{K}^*, \tag{2.57}$$

where α and β are the frictional damping constant and the structural damping constant used in $\mathbf{C}^*$.

The dynamic equation and the sensor output of the smart structure finally is given by

$$\mathbf{M}^*\ddot{\mathbf{g}} + \mathbf{C}^*\dot{\mathbf{g}} + \mathbf{K}^*\mathbf{g} = \mathbf{f}^*_{ext} + \mathbf{f}^*_{ctrl} \tag{2.58}$$

and

$$y(t) = V^s(t) = \mathbf{p}^T\dot{\mathbf{q}} = \mathbf{p}^T\mathbf{T}\dot{\mathbf{g}}. \tag{2.59}$$

Note that this dynamic equation of the smart beam decouples into the equations corresponding to each individual mode, provided the damping is represented as described by Eq. (2.57).

2.1.1.6 State Space Model of the Smart Structure for 2, 3 Modes

I. SS Model for 2 vibratory modes : The governing equation of the smart structure obtained in the previous subsection 2.1.1:5 using the generalized coordinates as shown in Eq. (2.58) is often written in the state space form and is obtained as follows. Let the vector $\mathbf{g} = \mathbf{x}$, i.e.,

$$\mathbf{g} = \begin{bmatrix} g_1 \\ g_2 \end{bmatrix} = \begin{bmatrix} x_1 \\ x_2 \end{bmatrix}_{(2\times 1)} = x. \tag{2.60}$$

$\therefore$,

$$\dot{\mathbf{g}} = \dot{\mathbf{x}} = \begin{bmatrix} \dot{x}_1 \\ \dot{x}_2 \end{bmatrix} = \begin{bmatrix} x_3 \\ x_4 \end{bmatrix}_{(2\times 1)} \text{ and } \ddot{\mathbf{g}} = \ddot{\mathbf{x}} = \begin{bmatrix} \dot{x}_3 \\ \dot{x}_4 \end{bmatrix}_{(2\times 1)}. \tag{2.61}$$

Thus, $\dot{x}_1 = x_3$ and $\dot{x}_2 = x_4$. Using the Eqs. (2.55), (2.56), (2.60), (2.61) in Eq. (2.58), Eq. (2.58) now becomes

$$\mathbf{M}^* \begin{bmatrix} \dot{x}_3 \\ \dot{x}_4 \end{bmatrix} + \mathbf{C}^* \begin{bmatrix} x_3 \\ x_4 \end{bmatrix} + \mathbf{K}^* \begin{bmatrix} x_1 \\ x_2 \end{bmatrix} = \mathbf{f}^*_{ext} + \mathbf{f}^*_{ctrl}, \tag{2.62}$$

which can be further simplified as

$$\begin{bmatrix} \dot{x}_3 \\ \dot{x}_4 \end{bmatrix} = -\mathbf{M}^{*^{-1}}\mathbf{K}^* \begin{bmatrix} x_1 \\ x_2 \end{bmatrix} - \mathbf{M}^{*^{-1}}\mathbf{C}^* \begin{bmatrix} x_3 \\ x_4 \end{bmatrix} + \mathbf{M}^{*^{-1}}\mathbf{f}^*_{ext} + \mathbf{M}^{*^{-1}}\mathbf{f}^*_{ctrl}. \tag{2.63}$$

Eq. (2.63) is written in the state equation form as

$$\begin{bmatrix} \dot{x}_1 \\ \dot{x}_2 \\ \dot{x}_3 \\ \dot{x}_4 \end{bmatrix} = \begin{bmatrix} 0 & I \\ -\mathbf{M}^{*^{-1}}\mathbf{K}^* & -\mathbf{M}^{*^{-1}}\mathbf{C}^* \end{bmatrix} \begin{bmatrix} x_1 \\ x_2 \\ x_3 \\ x_4 \end{bmatrix} + \begin{bmatrix} 0 \\ \mathbf{M}^{*^{-1}}\mathbf{T}^T\mathbf{h} \end{bmatrix} \mathbf{u}(t) + \begin{bmatrix} 0 \\ \mathbf{M}^{*^{-1}}\mathbf{T}^T\mathbf{f} \end{bmatrix} r(t) \tag{2.64}$$

for 2 vibratory modes.

The sensor voltage is taken as the output of the smart beam. The output of the plant is given by

$$y(t) = \mathbf{p}^T\,\mathbf{T}\,\dot{\mathbf{g}} = \begin{bmatrix} \mathbf{p}^T\,\mathbf{T} \end{bmatrix} \begin{bmatrix} x_3 \\ x_4 \end{bmatrix}, \tag{2.65}$$

which can be written in the output equation form as

$$y(t) = \begin{bmatrix} 0 & \mathbf{p}^T\,\mathbf{T} \end{bmatrix} \begin{bmatrix} x_1 \\ x_2 \\ x_3 \\ x_4 \end{bmatrix}. \tag{2.66}$$

The constant vectors $\mathbf{h}$ and $\mathbf{p}$ in Eq. (2.64) and (2.66) for a 2 node beam element is given by

$$\mathbf{p}^T = S_c \begin{bmatrix} 0 & 0 & 0 & 0 & 0 & -1 & 0 & 1 \end{bmatrix}_{(1\times 8)} \tag{2.67}$$

and

$$\mathbf{h}^T = a_c \begin{bmatrix} 0 & 0 & 0 & 0 & -1 & 0 & 1 & 0 \end{bmatrix}_{(1\times 8)}. \tag{2.68}$$

Similarly, the force vector in Eq. (2.64) is given by

$$\mathbf{f} = \begin{bmatrix} 0 \\ 0 \\ 0 \\ 0 \\ 0 \\ 0 \\ 0 \\ 1 \end{bmatrix}_{(8\times 1)}. \tag{2.69}$$

The SISO state space model [state equation (2.64) and output equation (2.66)] of the smart flexible cantilever beam for the first 2 vibratory modes of the Fig. 2.2 is thus given by

$$\dot{\mathbf{x}} = \mathbf{A}\,\mathbf{x}(t) + \mathbf{B}\,\mathbf{u}(t) + \mathbf{E}\,r(t) \text{ and } y(t) = \mathbf{C}^T\,\mathbf{x}(t) + \mathbf{D}\,\mathbf{u}(t) \tag{2.70}$$

with

$$\mathbf{A} = \begin{bmatrix} 0 & I \\ -\mathbf{M}^{*^{-1}}\mathbf{K}^* & -\mathbf{M}^{*^{-1}}\mathbf{C}^* \end{bmatrix}_{(4\times 4)}, \quad \mathbf{B} = \begin{bmatrix} 0 \\ \mathbf{M}^{*^{-1}}\mathbf{T}^T\mathbf{h} \end{bmatrix}_{(4\times 1)}, \tag{2.71}$$

$$\mathbf{C}^T = \begin{bmatrix} 0 & \mathbf{p}^T\mathbf{T} \end{bmatrix}_{(1\times 4)},\ \mathbf{D} = 0 \text{ and } \mathbf{E} = \begin{bmatrix} 0 \\ \mathbf{M}^{*^{-1}}\mathbf{T}^T\mathbf{f} \end{bmatrix}_{(4\times 1)}, \tag{2.72}$$

where $r(t)$, $\mathbf{u}(t)$, **A, B, C, D, E,** $\mathbf{x}(t)$ and $y(t)$ represent the external force input, the control input, system matrix, input matrix, output matrix, transmission matrix, external load matrix, state vector, system output (sensor output) respectively. **E** is the external disturbance matrix which couples the disturbance to the system.

(i) Cantilever beam divided into 3 FE (system 1), 4 FE (system 2) and 5 FE (system 3)

The flexible cantilever beam as shown in Fig. 2.1(a) is divided into a number of finite elements [72], [87], [91], [92] as shown in Fig. 2.3, thus, giving rise to 3 types of systems, viz., *system 1* : three FE, Fig. 2.3(a), *system 2* : four FE, Fig. 2.3(b), *system 3* : five FE, Fig. 2.3(c). The piezoelectric sensor / actuator is bonded to the master structure at only one finite element, say at the fixed end.

By placing a piezoelectric element as sensor - actuator at one finite element of the cantilever beam and making other elements as regular beam elements and by varying the position of the piezoelectric sensor / actuator from the fixed end to the free end, various models of the 3 systems are obtained as shown in Appendix V in Fig. A.1. These models also include mass and stiffness of sensor and actuator. In Figs. 2.3(a)-(c), placement of the piezoelectric element only at the fixed end are shown here for convenience. In other words, the state space model in Eq. (2.70) is obtained for various sensor / actuator locations on the cantilever beam by using

- 2 regular beam elements and 1 piezoelectric element as shown in Fig. 2.3(a) - giving rise to 3 models of system 1.
- 3 regular beam elements and 1 piezoelectric element as shown in Fig. 2.3(b) - giving rise to 4 models of system 2.
- 4 regular beam elements and 1 piezoelectric element as shown in Fig. 2.3(c) - giving rise to 5 models of system 3.

Then, the control of these developed state space models is obtained using the various types of control techniques which are discussed in the subsequent Chapters. Here, for the sake of convenience, only the state space models of the 3 types of systems for the piezo patch placed at the fixed end is given below.

$$\mathbf{A}_{11} = 10^4 \begin{bmatrix} 0 & 0 & 0.0001 & 0 \\ 0 & 0 & 0 & 0.0001 \\ -5.0976 & -0.0000 & -0.0005 & -0.0000 \\ -0.0000 & -0.2266 & -0.0000 & -0.0000 \end{bmatrix}, \ \mathbf{B}_{11} = \begin{bmatrix} 0 \\ 0 \\ -0.1175 \\ -0.0093 \end{bmatrix},$$

$$\mathbf{E}_{11} = 10^3 \begin{bmatrix} 0 & 0 & 2.2114 & -1.0906 \end{bmatrix}, \ \mathbf{C}_{11}^T = \begin{bmatrix} 0 & 0 & -0.0050 & -0.0028 \end{bmatrix}, \quad (2.73)$$

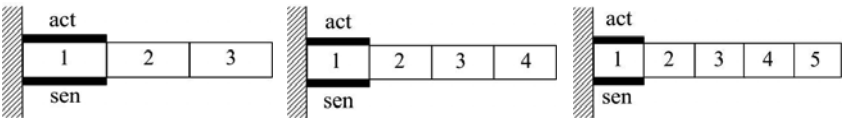

(a) Model 1 of system 1 (b) Model 1 of system 2 (c) Model 1 of system 3

Fig. 2.3. A flexible aluminum cantilever beam divided into 3, 4, 5 FE with PZT's at fixed end

$$\mathbf{A}_{12} = 10^4 \begin{bmatrix} 0 & 0 & 0.0001 & 0 \\ 0 & 0 & 0 & 0.0001 \\ -5.2872 & -0.0000 & -0.0005 & -0.0000 \\ -0.0000 & -0.1752 & -0.0000 & -0.0000 \end{bmatrix}, \; \mathbf{B}_{12} = \begin{bmatrix} 0 \\ 0 \\ -0.0971 \\ -0.0046 \end{bmatrix},$$

$$\mathbf{E}_{12} = 10^3 \begin{bmatrix} 0 \; 0 \; 2.7116 \; -1.1669 \end{bmatrix}, \; \mathbf{C}_{12}^T = \begin{bmatrix} 0 \; 0 \; -0.0038 \; -0.0016 \end{bmatrix}, \quad (2.74)$$

$$\mathbf{A}_{13} = 10^4 \begin{bmatrix} 0 & 0 & 0.0001 & 0 \\ 0 & 0 & 0 & 0.0001 \\ -5.0516 & 0.0000 & -0.0005 & 0.0000 \\ 0.0000 & -0.1488 & 0.0000 & -0.0000 \end{bmatrix}, \; \mathbf{B}_{13} = \begin{bmatrix} 0 \\ 0 \\ -0.0514 \\ -0.0027 \end{bmatrix},$$

$$\mathbf{E}_{13} = 10^3 \begin{bmatrix} 0 \; 0 \; 3.0567 \; -1.2241 \end{bmatrix}, \; \mathbf{C}_{13}^T = \begin{bmatrix} 0 \; 0 \; -0.0026 \; -0.0010 \end{bmatrix}. \quad (2.75)$$

In all the above state space models, $\mathbf{D}$ is a null matrix.

(ii) Beam divided into 4 FE with sensor-actuator position varying from free end to fixed end

Consider Fig. 2.4(a)-(d) in which the flexible beam is divided into 4 finite elements and the sensor-actuator pair is bonded to the master structure as a collocated pair at one position only, say fixed end. By varying the position of the sensor-actuator pair from the fixed end to the free end, 4 SISO state space models are obtained.

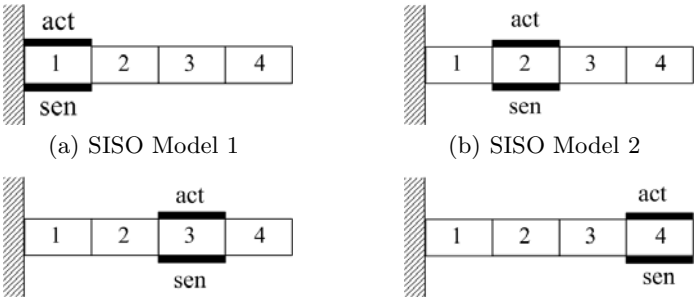

(a) SISO Model 1 (b) SISO Model 2

(c) SISO Model 3 (d) SISO Model 4

Fig. 2.4. A flexible aluminum cantilever beam divided into 4 FE with PZT's moved from fixed end to free end : 4 SISO models

State space model of the smart cantilever beam with sensor / actuator at FE position 1 (fixed end) as shown in Fig. 2.4(a) is given by

$$\dot{\mathbf{x}} = \mathbf{A}_{14}\,\mathbf{x}(t) + \mathbf{B}_{14}\,\mathbf{u}(t) + \mathbf{E}_{14}\,r(t) \;\text{ and }\; y(t) = \mathbf{C}_{14}^T\,\mathbf{x}(t) + \mathbf{D}_{14}\,\mathbf{u}(t) \quad (2.76)$$

with

$$\mathbf{A}_{14} = 10^4 \begin{bmatrix} 0 & 0 & 0.0001 & 0 \\ 0 & 0 & 0 & 0.0001 \\ -5.2872 & -0.0000 & -0.0005 & -0.0000 \\ -0.0000 & -0.1752 & -0.0000 & -0.0000 \end{bmatrix}, \; \mathbf{B}_{14} = \begin{bmatrix} 0 \\ 0 \\ -0.0791 \\ -0.0046 \end{bmatrix},$$

$$\mathbf{C}_{14}^T = \begin{bmatrix} 0 \; 0 \; 0.0038 \; -0.0016 \end{bmatrix}, \; \mathbf{D}_{14} = 0, \; \mathbf{E}_{14} = 10^3 \begin{bmatrix} 0 \\ 0 \\ 2.7116 \\ -1.1669 \end{bmatrix}.$$

State space model of the smart cantilever beam with sensor / actuator at FE position 2 (nearby fixed end) as shown in Fig. 2.4(b) is given by

$$\dot{\mathbf{x}} = \mathbf{A}_{24}\,\mathbf{x}(t) + \mathbf{B}_{24}\,\mathbf{u}(t) + \mathbf{E}_{24}\,r(t) \;\text{ and }\; y(t) = \mathbf{C}_{24}^T\,\mathbf{x}(t) + \mathbf{D}_{24}\,\mathbf{u}(t) \quad (2.77)$$

with

$$\mathbf{A}_{24} = 10^3 \begin{bmatrix} 0 & 0 & 0.0001 & 0 \\ 0 & 0 & 0 & 0.0001 \\ -2.9708 & -0.0000 & -0.0003 & -0.0000 \\ -0.0000 & -0.0886 & -0.0000 & -0.0000 \end{bmatrix}, \; \mathbf{B}_{24} = \begin{bmatrix} 0 \\ 0 \\ 0.0550 \\ -0.0204 \end{bmatrix},$$

$$\mathbf{C}_{24}^T = \begin{bmatrix} 0 \; 0 \; -0.0020 \; -0.0006 \end{bmatrix}, \; \mathbf{D}_{24} = 0, \; \mathbf{E}_{24} = 10^2 \begin{bmatrix} 0 \\ 0 \\ -2.5581 \\ -0.7451 \end{bmatrix}.$$

State space model of the smart cantilever beam with sensor / actuator at FE position 3 (middle) as shown in Fig. 2.4(c) is given by

$$\dot{\mathbf{x}} = \mathbf{A}_{34}\,\mathbf{x}(t) + \mathbf{B}_{34}\,\mathbf{u}(t) + \mathbf{E}_{34}\,r(t) \;\text{ and }\; y(t) = \mathbf{C}_{34}^T\,\mathbf{x}(t) + \mathbf{D}_{34}\,\mathbf{u}(t) \quad (2.78)$$

with

$$\mathbf{A}_{34} = 10^3 \begin{bmatrix} 0 & 0 & 0.0001 & 0 \\ 0 & 0 & 0 & 0.0001 \\ -3.6793 & -0.0000 & -0.0004 & -0.0000 \\ -0.0000 & -0.0587 & -0.0000 & -0.0000 \end{bmatrix}, \; \mathbf{B}_{34} = \begin{bmatrix} 0 \\ 0 \\ -0.1470 \\ -0.0207 \end{bmatrix},$$

$$\mathbf{C}_{34}^T = \begin{bmatrix} 0 \; 0 \; -0.0024 \; -0.0002 \end{bmatrix}, \; \mathbf{D}_{34} = 0, \; \mathbf{E}_{34} = 10^2 \begin{bmatrix} 0 \\ 0 \\ -2.1551 \\ -0.6092 \end{bmatrix}.$$

State space model of the smart cantilever beam with sensor / actuator at FE position 4 (free end) as shown in Fig. 2.4(d) is given by

$$\dot{\mathbf{x}} = \mathbf{A}_{44}\,\mathbf{x}(t) + \mathbf{B}_{44}\,\mathbf{u}(t) + \mathbf{E}_{44}\,r(t) \;\text{ and }\; y(t) = \mathbf{C}_{44}^{T}\,\mathbf{x}(t) + \mathbf{D}_{44}\,\mathbf{u}(t) \quad (2.79)$$

with

$$\mathbf{A}_{44} = 10^{3}\begin{bmatrix} 0 & 0 & 0.0001 & 0 \\ 0 & 0 & 0 & 0.0001 \\ 2.5356 & 0.0000 & 0.0003 & 0.0000 \\ -0.0000 & -0.0396 & -0.0000 & -0.0000 \end{bmatrix},\; \mathbf{B}_{44} = \begin{bmatrix} 0 \\ 0 \\ -0.1961 \\ -0.0172 \end{bmatrix},$$

$$\mathbf{C}_{44}^{T} = 10^{-4}\begin{bmatrix} 0\ 0\ -0.5091\ -0.0411 \end{bmatrix},\; \mathbf{D}_{44} = 0,\; \mathbf{E}_{44} = 10^{2}\begin{bmatrix} 0 \\ 0 \\ -1.2749 \\ -0.4607 \end{bmatrix}.$$

From Fig. A.1 shown in Appendix V, the state space models of the smart cantilever beam divided into 3 FE (system 1) with sensor / actuator pair at element 2, 3 (free end), 4 FE (system 2) with sensor / actuator pair at elements 2, 3, 4 (free end), 5 FE (system 3) with sensor / actuator pair at elements 2, 3, 4, 5 (free end) are obtained similarly as shown in [72], [87], [91], [92] as shown in Fig. 2.3. The characteristics of the smart cantilever beam with the piezo pair at various locations along the length of the beam for different models of the 3 systems shown in Figs. 2.3 and in A.1 are given in the Tables 2.2 - 2.4 respectively.

II. SS Model for 3 vibratory modes : The state space model (state equation and output equation) for the first 3 vibratory modes is obtained on the similar lines as shown in the previous sub-section 2.1.1:6(I) as follows. The governing equation is often written in state space form by using a vector $\mathbf{g} = \mathbf{x}$, where

$$\mathbf{g} = \begin{bmatrix} g_1 \\ g_2 \\ g_3 \end{bmatrix} = \begin{bmatrix} x_1 \\ x_2 \\ x_3 \end{bmatrix}_{(3\times 1)} = \mathbf{x}. \quad (2.80)$$

Now,

$$\dot{\mathbf{g}} = \dot{\mathbf{x}} = \begin{bmatrix} \dot{g}_1 \\ \dot{g}_2 \\ \dot{g}_3 \end{bmatrix} = \begin{bmatrix} \dot{x}_1 \\ \dot{x}_2 \\ \dot{x}_3 \end{bmatrix} = \begin{bmatrix} x_4 \\ x_5 \\ x_6 \end{bmatrix}_{(3\times 1)} \text{ and } \ddot{\mathbf{g}} = \ddot{\mathbf{x}} = \begin{bmatrix} \dot{x}_4 \\ \dot{x}_5 \\ \dot{x}_6 \end{bmatrix}_{(3\times 1)}. \quad (2.81)$$

Therefore, $\dot{x}_1 = x_4$, $\dot{x}_2 = x_5$, and $\dot{x}_3 = x_6$. Thus, using Eqs. (2.55), (2.56), (2.80) and (2.81) in Eq. (2.58), the dynamic equation of the smart structure for 3 vibratory modes becomes

$$\mathbf{M}^{*}\begin{bmatrix} \dot{x}_4 \\ \dot{x}_5 \\ \dot{x}_6 \end{bmatrix} + \mathbf{C}^{*}\begin{bmatrix} x_4 \\ x_5 \\ x_6 \end{bmatrix} + \mathbf{K}^{*}\begin{bmatrix} x_1 \\ x_2 \\ x_3 \end{bmatrix} = \mathbf{f}_{ext}^{*} + \mathbf{f}_{ctrl}^{*}, \quad (2.82)$$

Table 2.2. Characteristics of the smart beam for 2 modes, beam divided into 3 FE (system 1)

Position of sensor/actuator	**Eigen values**	**Natural frequency (Hz)**
Element 1 : Fixed end	$-2.55 \pm j225.76$	35.93
Model 1	$-0.11 \pm j47.61$	7.57
Element 2 : Fixed end	$-2.1 \pm j204.69$	32.57
Model 2	$-0.04 \pm j26.44$	4.21
Element 3 : Free end	$-1.72 \pm j211.35$	33.63
Model 3	$-0.02 \pm j19.16$	3.04

Table 2.3. Characteristics of the smart beam for 2 modes, beam divided into 4 FE (system 2)

Position of sensor/actuator	**Eigen values**	**Natural frequency (Hz)**
Element 1 : Fixed end	$-2.64 \pm j229.92$	36.89
Model 1	$-0.09 \pm j41.86$	6.66
Element 2	$-1.19 \pm j172.35$	27.43
Model 2	$-0.04 \pm j29.77$	4.73
Element 3	$-1.84 \pm j191.81$	30.52
Model 3	$-0.03 \pm j24.22$	3.85
Element 4 : Free end	$-1.27 \pm j159.23$	25.34
Model 4	$-0.02 \pm j19.89$	3.16

Table 2.4. Characteristics of the smart beam for 2 modes, beam divided into 5 FE (system 3)

Position of sensor/actuator	**Eigen values**	**Natural frequency (Hz)**
Element 1 : Fixed end	$-2.53 \pm j224.74$	35.76
Model 1	$-0.07 \pm j38.57$	6.14
Element 2	$-1.34 \pm j163.70$	26.05
Model 2	$-0.05 \pm j31.06$	4.94
Element 3	$-1.65 \pm j181.19$	28.88
Model 3	$-0.04 \pm j26.90$	4.28
Element 4	$-1.69 \pm j183.93$	29.27
Model 4	$-0.03 \pm j26.63$	3.76
Element 5 : Free end	$-1.24 \pm j157.68$	25.09
Model 5	$-0.02 \pm j20.57$	3.27

which can be further simplified as

$$\begin{bmatrix} \dot{x}_4 \\ \dot{x}_5 \\ \dot{x}_6 \end{bmatrix} = -\mathbf{M}^{*-1}\mathbf{K}^* \begin{bmatrix} x_4 \\ x_5 \\ x_6 \end{bmatrix} - \mathbf{M}^{*-1}\mathbf{C}^* \begin{bmatrix} x_1 \\ x_2 \\ x_3 \end{bmatrix} + \mathbf{M}^{*-1}\mathbf{f}^*_{ext} + \mathbf{M}^{*-1}\mathbf{f}^*_{ctrl} \quad (2.83)$$

and finally written in state space form

$$\dot{\mathbf{x}} = \mathbf{A}\,\mathbf{x}(t) + \mathbf{B}\,\mathbf{u}(t) + \mathbf{E}\,r(t) \text{ and } y(t) = \mathbf{C}^T\,\mathbf{x}(t) + \mathbf{D}\,\mathbf{u}(t) \quad (2.84)$$

as

$$\begin{bmatrix} \dot{x}_1 \\ \dot{x}_2 \\ \dot{x}_3 \\ \dot{x}_4 \\ \dot{x}_5 \\ \dot{x}_6 \end{bmatrix} = \begin{bmatrix} 0 & I \\ -\mathbf{M}^{*-1}\mathbf{K}^* & -\mathbf{M}^{*-1}\mathbf{C}^* \end{bmatrix} \begin{bmatrix} x_1 \\ x_2 \\ x_3 \\ x_4 \\ x_5 \\ x_6 \end{bmatrix} + \begin{bmatrix} 0 \\ \mathbf{M}^{*-1}\mathbf{T}^T\mathbf{h} \end{bmatrix} u(t) + \begin{bmatrix} 0 \\ \mathbf{M}^{*-1}\mathbf{T}^T\mathbf{f} \end{bmatrix} r(t), \quad (2.85)$$

and

$$y(t) = \begin{bmatrix} 0 & \mathbf{p}^T\,\mathbf{T} \end{bmatrix} \begin{bmatrix} x_1 \\ x_2 \\ x_3 \\ x_4 \\ x_5 \\ x_6 \end{bmatrix}, \quad (2.86)$$

where the size of the matrices $\mathbf{A}$, $\mathbf{B}$, $\mathbf{C}$, $\mathbf{E}$, $\mathbf{T}$ are (6×6), (6×1), (1×6), (6×1), (8×3) with $\mathbf{D}$ being a null matrix. The generalized matrices (mass, stiffness, structural damping) are of size (3×3). Here, in Eqs. (2.85) and (2.86), the constant vectors $\mathbf{p}^T$, $\mathbf{h}$ and $\mathbf{f}$ are of sizes (1×8), (8×1) and (8×1) respectively.

2.1.2 Modeling of Smart Beams as MIMO Systems for 2 and 3 Vibratory Modes

Consider the flexible aluminum cantilever beam [77], [93] as shown in Fig. 2.1(a). The beam has been divided into 4 finite elements as shown in Fig. 2.5. A collocated piezoelectric pair is bonded onto 2 discrete sections (two FE) on the surface of the beam as surface mounted sensor / actuators. Then, the smart cantilever beam model is developed using 2 piezoelectric beam elements (top actuator + middle beam element + bottom sensor), which includes sensor and actuator dynamics and remaining beam elements as regular beam elements based on Euler-Bernoulli beam theory assumptions. The dimensions and properties of the aluminum cantilever beam and piezoelectric sensor / actuator used are given in Table 2.1. The 2 piezo pairs are made up of the same material and type. The regular beam modeling and the piezoelectric beam modeling as a multivariable system is developed on the similar lines as that of the smart beam modelling for a SISO case as explained in Sections 2.1.1:1 to 2.1.1:4.

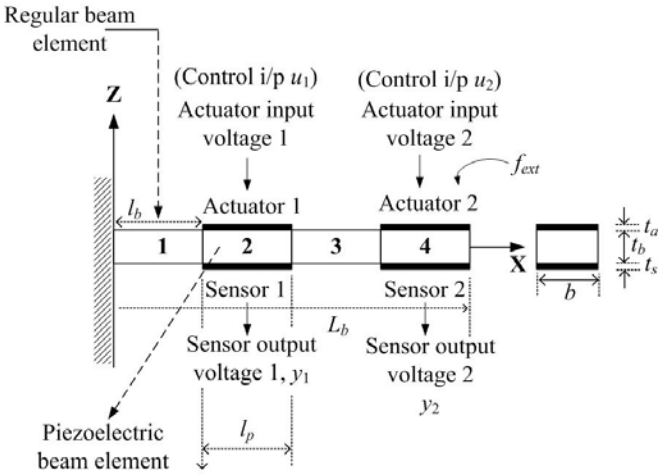

Fig. 2.5. A smart EB beam as a multivariable system with 2 inputs and 2 outputs

2.1.2.1 Dynamic Equation of the Smart Beam for a MIMO Case

The dynamic equation of the smart structure is obtained by using the mass and stiffness of both the equations of the regular beam elements and the piezoelectric beam elements given in Eqs. (2.15) and (2.28). Two vibratory modes are considered to start with in modelling the beam. The mass and stiffness matrices **M**, **K** of the entire beam divided into 4 finite elements with the piezo-patches placed at positions 2 and 4 are obtained by assembling the mass and stiffness matrices of the regular beam elements and the piezoelectric beam elements. The dynamic equation is finally given by

$$\mathbf{M}\,\ddot{\mathbf{q}} + \mathbf{K}\,\mathbf{q} = \mathbf{f}_{ext} + \mathbf{f}_{ctrl\,1} + \mathbf{f}_{ctrl\,2}, \tag{2.87}$$

where the mass and stiffness matrices **M**, **K** are of size (8×8) and the force vectors of size (8×1).

Using $\mathbf{q} = \mathbf{T}\ \mathbf{g}$, Eq. (2.87) becomes

$$\mathbf{MT}\ddot{\mathbf{g}} + \mathbf{KTg} = \mathbf{f}_{ext} + \mathbf{f}_{ctrl\,1} + \mathbf{f}_{ctrl\,2}. \tag{2.88}$$

Pre-multiplying Eq. (2.88) by $\mathbf{T}^T$, the following equation is obtained.

$$\mathbf{M}^*\ddot{\mathbf{g}} + \mathbf{K}^*\mathbf{g} = \mathbf{f}^*_{ext} + \mathbf{f}^*_{ctrl\,1} + \mathbf{f}^*_{ctrl\,2}, \tag{2.89}$$

where $\mathbf{f}_{ctrl\,1}$, $\mathbf{f}_{ctrl\,2}$ and $\mathbf{f}^*_{ctrl\,1}$ $\mathbf{f}^*_{ctrl\,2}$ are the control force vectors and the generalized control force vectors. Introducing the damping matrix $\mathbf{C}^*$ into the Eq. (2.89), we get the dynamic equation of the smart flexible cantilever beam as multivariable system (2 inputs, 2 outputs) which is given below.

$$\mathbf{M}^*\ddot{\mathbf{g}} + \mathbf{C}^*\dot{\mathbf{g}} + \mathbf{K}^*\mathbf{g} = \mathbf{f}^*_{ext} + \mathbf{f}^*_{ctrl\,1} + \mathbf{f}^*_{ctrl\,2} = \mathbf{f}^*_{ext} + \mathbf{f}^*_{ctrl\,i},\ \ i = 1, 2, \tag{2.90}$$

where the generalized matrices and the generalized force vectors are of size (2×2) and (2×1) respectively.

2.1.2.2 State Space Model of the Smart Beam for a MIMO Case

The state space model of the beam is obtained on the similar lines as explained in Section 2.1.1:6(I) and (II) for 2 and 3 vibratory modes. The governing equation Eq. (2.90) is written in state space form as

$$\mathbf{M}^* \begin{bmatrix} \dot{x}_3 \\ \dot{x}_4 \end{bmatrix} + \mathbf{C}^* \begin{bmatrix} x_3 \\ x_4 \end{bmatrix} + \mathbf{K}^* \begin{bmatrix} x_1 \\ x_2 \end{bmatrix} = \mathbf{f}^*_{ext} + \mathbf{f}^*_{ctrl\,i}, \tag{2.91}$$

which can be further simplified as

$$\begin{bmatrix} \dot{x}_3 \\ \dot{x}_4 \end{bmatrix} = -\mathbf{M}^{*-1}\mathbf{K}^* \begin{bmatrix} x_1 \\ x_2 \end{bmatrix} - \mathbf{M}^{*-1}\mathbf{C}^* \begin{bmatrix} x_3 \\ x_4 \end{bmatrix} + \mathbf{M}^{*-1}\mathbf{f}^*_{ext} + \mathbf{M}^{*-1}\mathbf{f}^*_{ctrl\,i} \tag{2.92}$$

and finally written in state equation form as

$$\begin{bmatrix} \dot{x}_1 \\ \dot{x}_2 \\ \dot{x}_3 \\ \dot{x}_4 \end{bmatrix} = \begin{bmatrix} 0 & I \\ -\mathbf{M}^{*-1}\mathbf{K}^* & -\mathbf{M}^{*-1}\mathbf{C}^* \end{bmatrix}_{(4\times4)} \begin{bmatrix} x_1 \\ x_2 \\ x_3 \\ x_4 \end{bmatrix}$$

$$+ \begin{bmatrix} 0 & 0 \\ \mathbf{M}^{*-1}\mathbf{T}^T\mathbf{h}_1 & \mathbf{M}^{*-1}\mathbf{T}^T\mathbf{h}_2 \end{bmatrix}_{(4\times2)} \begin{bmatrix} u_1 \\ u_2 \end{bmatrix} + \begin{bmatrix} 0 \\ \mathbf{M}^{*-1}\mathbf{T}^T\mathbf{f} \end{bmatrix}_{(4\times1)} r(t) \tag{2.93}$$

for 2 vibratory modes. The Eq. (2.93) can be written in compact form as

$$\dot{\mathbf{x}} = \mathbf{A}\,\mathbf{x}(t) + \mathbf{B}\,\mathbf{u}(t) + \mathbf{E}\,r(t). \tag{2.94}$$

The generalized control force vector is given by

$$\mathbf{f}^*_{ctrl\,i} = \mathbf{T}^T\mathbf{f}_{ctrl\,i} = \mathbf{T}^T\mathbf{h}_i V^a_i(t) = \mathbf{T}^T\mathbf{h}_i\mathbf{u}_i(t), \;\; i = 1, 2, \tag{2.95}$$

where the voltages $V^a_i(t)$ are the input voltages to the actuators 1 and 2 and are nothing but the control inputs $u_i(t)$ to the actuators. $\mathbf{T}$ is the modal matrix of size (8×2). $\mathbf{h}_i$ is a constant vector of size (8×1) which depends on the actuator type, its position on the beam, its characteristics and is given by

$$\mathbf{h}_1^T = E_{p_1}\, d_{31}\, b\, \bar{z} \begin{bmatrix} -1 & 0 & 1 & 0 & 0 & 0 & 0 & 0 \end{bmatrix}_{(1\times8)} = a_{c1} \begin{bmatrix} -1 & 0 & 1 & \cdots & 0 \end{bmatrix} \tag{2.96}$$

and

$$\mathbf{h}_2^T = E_{p_2}\, d_{31}\, b\, \bar{z} \begin{bmatrix} 0 & 0 & 0 & 0 & -1 & 0 & 1 & 0 \end{bmatrix}_{(1\times8)} = a_{c2} \begin{bmatrix} 0 & \cdots & -1 & 0 & 1 & 0 \end{bmatrix} \tag{2.97}$$

for the two piezoelectric actuator elements placed at the FE positions, numbering 2 and 4, where a_{c1} and a_{c2} are the actuator constants.

The sensor voltages y_1 and y_2 are taken as the outputs of the MIMO plant and the output equation is obtained as

$$y_i(t) = V^s_i(t) = \mathbf{p}_i^T\,\mathbf{T}\,\dot{\mathbf{g}} = \begin{bmatrix} \mathbf{p}_i^T\,\mathbf{T} \end{bmatrix} \begin{bmatrix} x_3 \\ x_4 \end{bmatrix}, \quad i = 1, 2, \tag{2.98}$$

where $\mathbf{p}_i^T$ is a constant vector of size (1×8) which depends on the piezoelectric sensor characteristics and on the position of the sensor location on the beam. The

constant vectors for the sensors placed at FE positions numbering 2 and 4 are given by

$$\mathbf{p}_1^T = G_c\, e_{31}\, b\, z \left[0\ -1\ 0\ 1\ 0\ 0\ 0\ 0\right]_{(1\times 8)} = S_{c1} \left[0\ -1\ \ 0\ \ \ 1\ \ \cdots 0\right] \tag{2.99}$$

and

$$\mathbf{p}_2^T = G_c\, e_{31}\, b\, z \left[0 \cdots -1\ \ 0\ \ \ 1\ \right]_{(1\times 8)} = S_{c2} \left[0 \cdots -1\ \ 0\ \ \ 1\ \right], \tag{2.100}$$

where S_{c1} and S_{c2} are the sensor constants. Eq. (2.98) can be further re-written as

$$\begin{bmatrix} y_1 \\ \\ y_2 \end{bmatrix} = \begin{bmatrix} 0 & & \mathbf{p}_1^T\,\mathbf{T} \\ \\ 0 & & \mathbf{p}_2^T\,\mathbf{T} \end{bmatrix}_{(2\times 4)} \begin{bmatrix} x_1 \\ x_2 \\ x_3 \\ x_4 \end{bmatrix}_{(4\times 1)} \tag{2.101}$$

and finally, the output equation becomes

$$y(t) = \mathbf{C}^T\,\mathbf{x}(t) \ + \ \mathbf{D}\,\mathbf{u}(t). \tag{2.102}$$

Similarly, the MIMO state space model for 3 vibratory modes is given by

$$\begin{bmatrix} \dot{x}_1 \\ \dot{x}_2 \\ \dot{x}_3 \\ \dot{x}_4 \\ \dot{x}_5 \\ \dot{x}_6 \end{bmatrix} = \begin{bmatrix} 0 & & I \\ -\mathbf{M}^{*-1}\mathbf{K}^* & & -\mathbf{M}^{*-1}\mathbf{C}^* \end{bmatrix}_{(6\times 6)} \begin{bmatrix} x_1 \\ x_2 \\ x_3 \\ x_4 \\ x_5 \\ x_6 \end{bmatrix}$$

$$+ \begin{bmatrix} 0 & & 0 \\ \mathbf{M}^{*-1}\mathbf{T}^T\mathbf{h}_1 & & \mathbf{M}^{*-1}\mathbf{T}^T\mathbf{h}_2 \end{bmatrix}_{(6\times 2)} \begin{bmatrix} u_1 \\ u_2 \end{bmatrix} + \begin{bmatrix} 0 \\ \mathbf{M}^{*-1}\mathbf{T}^T\mathbf{f} \end{bmatrix}_{(6\times 1)} r(t) \tag{2.103}$$

and

$$\begin{bmatrix} y_1 \\ \\ y_2 \end{bmatrix} = \begin{bmatrix} 0 & & \mathbf{p}_1^T\,\mathbf{T} \\ \\ 0 & & \mathbf{p}_2^T\,\mathbf{T} \end{bmatrix}_{(2\times 6)} \begin{bmatrix} x_1 \\ x_2 \\ x_3 \\ x_4 \\ x_5 \\ x_6 \end{bmatrix}_{(6\times 1)}, \tag{2.104}$$

where the generalized mass and stiffness matrices, the modal matrix $\mathbf{T}$ are of size (3×3) and (8×3) and the constant vectors $\mathbf{p}_i$, $\mathbf{h}_i$ and $\mathbf{f}$ are of sizes (8×1) respectively.

The MIMO state space model of the smart structure divided into 4 FE with sensor / actuator pair placed at FE positions 2 and 4 as shown in the Fig. 2.5 and for 2 vibratory modes is given by Eqs. (2.94) and (2.102) with

$$\mathbf{A} = 10^4 \begin{bmatrix} 0 & 0 & 0.0001 & 0 \\ 0 & 0 & 0 & 0.0001 \\ -4.6629 & -0.0000 & -0.0005 & -0.0000 \\ -0.0000 & -0.0434 & -0.0000 & -0.0000 \end{bmatrix},\ \mathbf{B} = \begin{bmatrix} 0 & 0 \\ 0 & 0 \\ 0.0618 & 0.0998 \\ -0.0102 & -0.0104 \end{bmatrix},$$

Table 2.5. Characteristics of the smart flexible beam for a MIMO case (2 modes)

Position of the piezoelectric sensor / actuator	Eigen values	Natural frequency (Hz)
2, 4	$-1.7188 \pm j\,211.3523$	33.6378
	$-0.0245 \pm j\,24.9096$	3.9645

$$\mathbf{C}^T = \begin{bmatrix} 0 & 0 & 0.0065 & -0.0003 \\ 0 & 0 & 0.0015 & -0.0000 \end{bmatrix}, \quad \mathbf{E} = \begin{bmatrix} 0 & 0 & 881.7568 & -322.3558 \end{bmatrix}^T,$$

$$\mathbf{D} = \text{a null matrix.} \tag{2.105}$$

Control of this developed MIMO smart structure state space model is obtained using the different control laws which are considered in the subsequent chapters. The characteristics of the MIMO state space model obtained by retaining the first 2 vibratory modes in Eq. (2.105) of the smart structure are given in the Table 2.5.

2.1.3 Modeling of the Smart Structure as Multimodel System Comprising of Multivariable Plants

The flexible aluminium cantilever beam as shown in the Fig. 2.1(a) is divided into a number of finite elements, viz., 8 as shown in Fig. 2.6. The dimensions and properties of the aluminum cantilever beam and piezoelectric sensor / actuator used are given in Table 2.1. The entire structure (cantilever beam with the surface mounted piezos) is modeled by dividing it into 8 finite elements and placing the sensor /actuator at finite element positions 2, 4, 6 an 8, thus giving rise to a single Multiple Input Multiple Output [MIMO] system with 4 actuator inputs u_1, u_2, u_3, u_4 and 4 sensor outputs, y_1, y_2, y_3, y_4 [81], [82], [83], [84].

Considering a failure of one of the 4 actuator pairs to function (may be due to mechanical / electrical / bonding failure or the connecting leads to the piezos

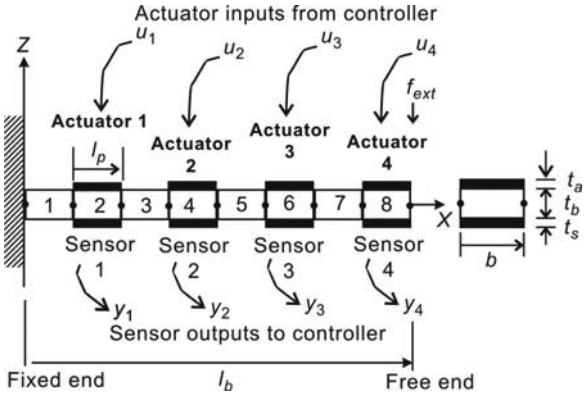

Fig. 2.6. A MIMO smart EB beam with 4 inputs and 4 outputs

coming out during vibrations) at any one of the finite elements, 4 multivariable state space models of the same smart structure plant can be obtained, thus giving rise to a multimodel system. The regular beam modeling and the piezoelectric beam modeling of the multivariable plant is developed on the similar lines as that of the SISO plant model as explained in Sections 2.1.1:1 to 2.1.1:4. In this type of modeling the beam, 4 piezoelectric elements are considered as active sensors and actuators and the other elements as regular beam elements. The **A** matrices of the multimodel system of the single plant remains the same, while **B** and **C** changes due to the consideration of the failure of one of the piezo patches.

2.1.3.1 Dynamic Equation of the Smart Beam for Multimodel Case

The dynamic equation of the smart structure is obtained by using the mass and stiffness of both the equations of the regular beam elements and the piezoelectric beam elements similar to the method given in Section 2.1.2:1. The mass and stiffness matrices **M**, **K** of the entire beam, which is divided into 8 finite elements with the piezo-patches placed at even FE positions are obtained by assembling the mass and stiffness matrices of each elements. The dynamic equation is finally given by [81] - [84]

$$\mathbf{M}\,\ddot{\mathbf{q}} + \mathbf{K}\,\mathbf{q} = \mathbf{f}_{ext} + \mathbf{f}_{ctrl\,1} + \mathbf{f}_{ctrl\,2} + \mathbf{f}_{ctrl\,3} + \mathbf{f}_{ctrl\,4}. \tag{2.106}$$

The Eq. (2.106) is written in the following form by using the relation $\mathbf{q} = \mathbf{T}\ \mathbf{g}$.

$$\mathbf{MT}\ddot{\mathbf{g}} + \mathbf{KTg} = \mathbf{f}_{ext} + \mathbf{f}_{ctrl\,1} + \mathbf{f}_{ctrl\,2} + \mathbf{f}_{ctrl\,3} + \mathbf{f}_{ctrl\,4}. \tag{2.107}$$

Pre-multiplying Eq. (2.107) by $\mathbf{T}^T$, the above equation takes the form as

$$\mathbf{M}^*\ddot{\mathbf{g}} + \mathbf{K}^*\mathbf{g} = \mathbf{f}^*_{ext} + \mathbf{f}^*_{ctrl\,1} + \mathbf{f}^*_{ctrl\,2} + \mathbf{f}^*_{ctrl\,3} + \mathbf{f}^*_{ctrl\,4}, \tag{2.108}$$

where the generalized mass and stiffness matrices $\mathbf{M}^*$ and $\mathbf{K}^*$ given by $\mathbf{M}^* = \mathbf{T}^T\mathbf{MT}$ and $\mathbf{K}^* = \mathbf{T}^T\mathbf{KT}$ are of size (2×2) and the generalized force vectors, viz., $\mathbf{f}^*_{ctrl\,i} = \mathbf{T}^T\ \mathbf{f}_{ctrl\ i}$ and $\mathbf{f}^*_{ext} = \mathbf{T}^T\ \mathbf{f}_{ext}$ are of size (2×1).

Introducing the damping matrix $\mathbf{C}^*$ into the Eq. (2.108), we get the dynamic equation of the smart flexible cantilever beam with 4 input-outputs as

$$\mathbf{M}^*\ddot{\mathbf{g}} + \mathbf{C}^*\dot{\mathbf{g}} + \mathbf{K}^*\mathbf{g} = \mathbf{f}^*_{ext} + \mathbf{f}^*_{ctrl\,1} + \mathbf{f}^*_{ctrl\,2} + \mathbf{f}^*_{ctrl\,3} + \mathbf{f}^*_{ctrl\,4} = \mathbf{f}^*_{ext} + \mathbf{f}^*_{ctrl\,i}, \tag{2.109}$$

where $i = 1, ..., 4$.

2.1.3.2 State Space Model of the Smart Beam for the Multimodel Case

The state space model of the beam with 4 inputs and 4 outputs is obtained on the similar lines as explained in Section 2.1.2:2. The governing equation Eq. (2.109) is written in state space form as

$$\mathbf{M}^*\begin{bmatrix}\dot{x}_3\\ \dot{x}_4\end{bmatrix} + \mathbf{C}^*\begin{bmatrix}x_3\\ x_4\end{bmatrix} + \mathbf{K}^*\begin{bmatrix}x_1\\ x_2\end{bmatrix} = \mathbf{f}^*_{ext} + \mathbf{f}^*_{ctrl\,i}, \tag{2.110}$$

which can be further simplified as

$$\begin{bmatrix}\dot{x}_3\\ \dot{x}_4\end{bmatrix} = -\mathbf{M}^{*-1}\mathbf{K}^* \begin{bmatrix}x_1\\ x_2\end{bmatrix} - \mathbf{M}^{*-1}\mathbf{C}^* \begin{bmatrix}x_3\\ x_4\end{bmatrix} + \mathbf{M}^{*-1}\mathbf{f}^*_{ext} + \mathbf{M}^{*-1}\mathbf{f}^*_{ctrl\,i} \tag{2.111}$$

and finally written in state equation form as

$$\begin{bmatrix}\dot{x}_1\\ \dot{x}_2\\ \dot{x}_3\\ \dot{x}_4\end{bmatrix} = \begin{bmatrix}0 & I\\ -\mathbf{M}^{*-1}\mathbf{K}^* & -\mathbf{M}^{*-1}\mathbf{C}^*\end{bmatrix}_{(4\times4)} \begin{bmatrix}x_1\\ x_2\\ x_3\\ x_4\end{bmatrix}$$

$$+\begin{bmatrix}0 & \cdots & 0\\ \mathbf{M}^{*-1}\mathbf{T}^T\mathbf{h}_1 & \cdots & \mathbf{M}^{*-1}\mathbf{T}^T\mathbf{h}_4\end{bmatrix}_{(4\times4)} \begin{bmatrix}u_1\\ u_2\\ u_3\\ u_4\end{bmatrix} + \begin{bmatrix}0\\ \mathbf{M}^{*-1}\mathbf{T}^T\mathbf{f}\end{bmatrix}_{(4\times1)} r(t), \tag{2.112}$$

where the generalized matrices (mass, stiffness, structural damping), the modal matrix $\mathbf{T}$ are of size (2×2) and (16×2), the constant vector $\mathbf{h}_i$ of size (16×1) and the force vector $\mathbf{f}$ of size (16×1).

The equation (2.112) can be written in compact form as

$$\dot{\mathbf{x}} = \mathbf{A}\,\mathbf{x}(t) + \mathbf{B}\,\mathbf{u}(t) + \mathbf{E}\,r(t). \tag{2.113}$$

The generalized control force vector of size (2×1) is given by

$$\mathbf{f}^*_{ctrl\,i} = \mathbf{T}^T\mathbf{f}_{ctrl\,i} = \mathbf{T}^T\mathbf{h}_i V_i^a(t) = \mathbf{T}^T\mathbf{h}_i\mathbf{u}_i(t), \;\; i = 1 \text{ to } 4, \tag{2.114}$$

where the voltages $V_i^a(t)$ are the input voltages to the actuators 1 to 4 and are nothing but the control inputs $\mathbf{u}_i(t)$ to the actuators, $\mathbf{h}_i$ is a constant vector which depends on the actuator type, its position on the beam, the actuator characteristics and is given by

$$\mathbf{h}^T = \begin{bmatrix}\mathbf{h}_1\\ \mathbf{h}_2\\ \mathbf{h}_3\\ \mathbf{h}_4\end{bmatrix}^T = E_p\,d_{31}\,b\,\bar{z} \begin{bmatrix}-1\,0\,1\,0 & 0\,0\,0\,0 & 0\,0\,0\,0 & 0\,0\,0\,0\\ 0\,0\,0\,0 & -1\,0\,1\,0 & 0\,0\,0\,0 & 0\,0\,0\,0\\ 0\,0\,0\,0 & 0\,0\,0\,0 & -1\,0\,1\,0 & 0\,0\,0\,0\\ 0\,0\,0\,0 & 0\,0\,0\,0 & 0\,0\,0\,0 & -1\,0\,1\,0\end{bmatrix}_{(4\times16)} \tag{2.115}$$

for the 4 piezoelectric actuator elements placed at FE positions 2, 4, 6 and 8 respectively, where $E_p\,d_{31}\,b\,\bar{z} = a_c$ being the actuator constants of the piezo actuators.

The sensor voltages are taken as the output of the multivariable plant and the output equation is obtained as

$$y_i(t) = V_i^s(t) = \mathbf{p}_i^T\,\mathbf{T}\,\dot{\mathbf{g}} = \begin{bmatrix}\mathbf{p}_i^T\,\mathbf{T}\end{bmatrix} \begin{bmatrix}x_3\\ x_4\end{bmatrix}, \qquad i = 1 \text{ to } 4, \tag{2.116}$$

where $\mathbf{p}_i^T$ is a constant vector of size (1×16), which depends on the piezoelectric sensor characteristics and on the position of the sensor location on the beam. The constant vectors for the sensors placed at even FE positions is given by

$$\mathbf{p}^T = \begin{bmatrix}\mathbf{p}_1\\ \mathbf{p}_2\\ \mathbf{p}_3\\ \mathbf{p}_4\end{bmatrix}^T = G_c\,e_{31}\,b\,z \begin{bmatrix}0 & -1\,0\,1\,0 & 0\,0\,0\,0 & 0\,0\,0\,0 & 0\,0\,0\\ 0 & 0\,0\,0\,0 & -1\,0\,1\,0 & 0\,0\,0\,0 & 0\,0\,0\\ 0 & 0\,0\,0\,0 & 0\,0\,0\,0 & -1\,0\,1\,0 & 0\,0\,0\\ 0 & 0\,0\,0\,0 & 0\,0\,0\,0 & 0\,0\,0\,0 & -1\,0\,1\end{bmatrix}_{(4\times16)}, \tag{2.117}$$

where $G_c\, e_{31}\, b\, z = S_c$ are the sensor constants of the sensors placed at even FE positions.

The Eq. (2.116) can be further re-written for a multivariable system with 4 inputs-outputs as

$$\begin{bmatrix} y_1 \\ y_2 \\ y_3 \\ y_4 \end{bmatrix}_{(4\times 1)} = \begin{bmatrix} 0 & \mathbf{p}_1^T\,\mathbf{T} \\ 0 & \mathbf{p}_2^T\,\mathbf{T} \\ 0 & \mathbf{p}_3^T\,\mathbf{T} \\ 0 & \mathbf{p}_4^T\,\mathbf{T} \end{bmatrix}_{(4\times 4)} \begin{bmatrix} x_1 \\ x_2 \\ x_3 \\ x_4 \end{bmatrix}_{(4\times 1)} \tag{2.118}$$

and in the compact form

$$y(t) = \mathbf{C}^T\,\mathbf{x}(t) + \mathbf{D}\,\mathbf{u}(t). \tag{2.119}$$

The multimodel system comprising of 4 multivariable SS models are obtained with the failure of one of the 4 actuators to function at any one of the finite elements. The $\mathbf{A}$ and $\mathbf{E}$ matrices of all the 4 models of the single plant remain the same, while $\mathbf{B}_i$ and $\mathbf{C}_i$ matrices changes due to the failure of one of the piezo pairs to function. Let $\mathbf{A}$, $\mathbf{B}_i$, $\mathbf{C}_i$, $\mathbf{E}$, where $i = 1, 2, 3, 4$ be the state space matrices of the 4 multivariable models of the single plant when one of the 4 actuators fails to function at the finite element position 2 or 4 or 6 or 8.

The input matrix $\mathbf{B}_i$ when the fault takes place at any one of the finite element positions is obtained by making the i^{th} column of $\mathbf{B}_i$ as zeroes, indicating that the i^{th} actuator on the beam has failed and this consideration leads us to the problem of finding a control law that stabilizes the plant in the event of the actuator failure. The modeling approach presented in this section is to model the flexible cantilever beam structure with piezoelectric sensor / actuator as collocated pairs by considering the first 2 vibration modes and to analyze the effect of the failure of one of the actuators in a MIMO system to function in the system dynamics.

The above analysis can also be performed by considering an sensor failure or both actuator and sensor failure at a time. Control of this 4 input-output multimodel smart structure is obtained when there is a failure of one of the actuators to function using the Robust Decentralized Periodic Output Feedback (RDPOF) technique [81], [82] or the Robust Decentralized Fast Output Sampling Feedback (RDFOS) technique [83], [84] which is considered in the latter chapters.

The multivariable state space model of the smart cantilever beam when the piezo patch fails to function at FE position numbering 8 is given by Eqs. (2.112) and (2.118) with

$$\mathbf{A} = 10^3 \begin{bmatrix} 0 & 0 & 0.0001 & 0 \\ 0 & 0 & 0 & 0.0001 \\ -3.7415 & 0 & -0.0004 & 0.000 \\ -0.00 & -0.1277 & -0.0000 & -0.000 \end{bmatrix}, \quad \mathbf{E} = 1e3 \begin{bmatrix} 0 \\ 0 \\ 1.0829 \\ -0.4486 \end{bmatrix} \tag{2.120}$$

$$\mathbf{B} = \begin{bmatrix} 0 & 0 & 0 & 0 \\ 0 & 0 & 0 & 0 \\ -0.0327 & 0.0057 & -0.0470 & 0 \\ -0.0034 & -0.0063 & -0.0082 & 0 \end{bmatrix}, \quad \mathbf{C}^T = 1e-3 * \begin{bmatrix} 0 & 0 & -0.2436 & -0.1598 \\ 0 & 0 & -0.0427 & -0.2989 \\ 0 & 0 & 0.3496 & -0.3879 \\ 0 & 0 & 0.5134 & -0.4091 \end{bmatrix}.$$

Similarly, the state space models of the single plant when piezo patch fails at FE positions 6, 4 and 2 are obtained respectively. The characteristics of the smart flexible cantilever beam when the actuator placed at FE position 8 fails is given in Table 2.6.

Table 2.6. Characteristics of the multimodel system when actuator fails at FE position 8

Failure of the sensor / actuator position	Eigen values	Natural frequency (Hz)
8	$-0.1876 \pm\ i\ 61.1677$	9.7351
(free end)	$-0.0069\ \pm i\ 11.3005$	1.7985

2.1.4 Modeling of Smart Beams for 6 Vibratory Modes (Higher Order)

In theory, flexible structures require an infinite number of elastic modes to completely describe their behavior and in practice, they are usually modeled by large finite dimensional systems. The fundamental problem of feedback control of these flexible structures is to precisely control a large dimensional system [102] with a smaller dimensional controller because of the on-board computer limitations and the cost and complexity involved in the controller design. This restricts the control to a few critical modes, viz., the first few vibratory modes in the flexible system.

In this section, we consider the MIMO modeling of the smart flexible aluminium beam {as shown in Fig. 2.1(a)} based on Euler-Bernoulli beam theory and by dividing the beam into 4 finite elements with placement of the sensor/actuator pair at finite element positions 2 and 4 (as shown in the Fig. 2.5). This gives rise to a multivariable system with 2 actuator inputs u_1, u_2 and 2 sensor outputs y_1, y_2 [79], [80].

The dimensions and properties of the flexible beam and that of the piezoelectric sensor/actuator are given in Table 2.1. The first 6 vibratory modes ω_1 to ω_6 are considered for obtaining a higher order model of the smart structure (say, a 12^{th} order model). Modeling of the multivariable system was discussed in the Section 2.1.2. On the similar lines, the state space model (state equation and the output equation) for 6 vibratory modes of the MIMO system is obtained as

$$\begin{bmatrix} \dot{x}_1 \\ \dot{x}_2 \\ \dot{x}_3 \\ \vdots \\ \dot{x}_{12} \end{bmatrix}_{(12\times 1)} = \begin{bmatrix} 0 & I \\ -\mathbf{M}^{*-1}\mathbf{K}^* & -\mathbf{M}^{*-1}\mathbf{C}^* \end{bmatrix}_{(12\times 12)} \begin{bmatrix} x_1 \\ x_2 \\ x_3 \\ \vdots \\ x_{12} \end{bmatrix}_{(12\times 1)}$$

$$+ \begin{bmatrix} 0 & 0 \\ \mathbf{M}^{*-1}\mathbf{T}^T\mathbf{h}_1 & \mathbf{M}^{*-1}\mathbf{T}^T\mathbf{h}_2 \end{bmatrix}_{(12\times 2)} \begin{bmatrix} u_1 \\ u_2 \end{bmatrix}_{(2\times 1)} + \begin{bmatrix} 0 \\ \mathbf{M}^{*-1}\mathbf{T}^T\mathbf{f} \end{bmatrix}_{(12\times 1)} r(t), \quad (2.121)$$

i.e.,

$$\dot{\mathbf{x}} = \mathbf{A}\,\mathbf{x}(t) + \mathbf{B}\,\mathbf{u}(t) + \mathbf{E}\,r(t)$$

and

$$\begin{bmatrix} y_1 \\ \\ y_2 \end{bmatrix}_{(2\times 1)} = \begin{bmatrix} 0 & \mathbf{p}_1^T\,\mathbf{T} \\ \\ 0 & \mathbf{p}_2^T\,\mathbf{T} \end{bmatrix}_{(2\times 12)} \begin{bmatrix} x_1 \\ x_2 \\ x_3 \\ \vdots \\ x_{12} \end{bmatrix}_{(12\times 1)}, \tag{2.122}$$

i.e.,

$$y(t) = \mathbf{C}^T\,\mathbf{x}(t) \;+\; \mathbf{D}\,\mathbf{u}(t),$$

where the generalized matrices (mass, stiffness, structural damping), the modal matrix $\mathbf{T}$ are of sizes (6×6) and (8×6), the constant vectors $\mathbf{h}_i$ and $\mathbf{p}_i^T$ of sizes (8×1) and (1×8) and the force vector $\mathbf{f}$ are of size (8×1) respectively.

5 multivariable state space models are obtained by varying the thickness parameter of the beam. The thickness parameter of the 5 MIMO models of the same smart structure plant shown in Eq. (2.121) and Eq. (2.122) are taken as 0.5 mm, 0.6 mm, 0.7 mm, 0.8 mm and 1 mm. Let $(\mathbf{A}_i, \mathbf{B}_i, \mathbf{C}_i, \mathbf{D}_i, \mathbf{E}_i,)$; $i = 1$ to 5 be the state space matrices of the multimodel system.

State space model of the smart cantilever beam with sensor / actuator pair at element 2 and 4 for the first 6 modes of the MIMO model 1 is represented by Eqs. (2.121) and (2.122) with

$$\mathbf{A}_1 = 10^6 \begin{bmatrix} a_{11} & a_{12} \\ a_{13} & a_{14} \end{bmatrix},\; a_{11} = \begin{bmatrix} 0&0&0&0&0&0 \\ 0&0&0&0&0&0 \\ 0&0&0&0&0&0 \\ 0&0&0&0&0&0 \\ 0&0&0&0&0&0 \\ 0&0&0&0&0&0 \end{bmatrix},\; a_{12} = \begin{bmatrix} 0&0&0&0&0&0 \\ 0&0&0&0&0&0 \\ 0&0&0&0&0&0 \\ 0&0&0&0&0&0 \\ 0&0&0&0&0&0 \\ 0&0&0&0&0&0 \end{bmatrix},$$

$$a_{13} = \begin{bmatrix} -2.992 & 0.000 & -0.000 & -0.000 & -0.000 & 0.000 \\ -0.000 & -1.0823 & 0.000 & 0.000 & -0.000 & -0.000 \\ -0.000 & -0.000 & -0.2836 & -0.000 & 0.000 & -0.000 \\ 0.000 & 0.000 & -0.000 & -0.0661 & 0.000 & 0.000 \\ -0.000 & -0.000 & -0.000 & -0.000 & -0.0080 & 0.000 \\ -0.000 & -0.000 & 0.000 & -0.000 & 0.000 & -0.001 \end{bmatrix},$$

$$a_{14} = \begin{bmatrix} -0.0004 & 0.000 & -0.000 & -0.000 & -0.000 & 0.000 \\ -0.000 & -0.0002 & 0.000 & 0.000 & -0.000 & -0.000 \\ -0.000 & -0.000 & -0.000 & -0.000 & 0.000 & -0.000 \\ 0.000 & 0.000 & -0.000 & -0.000 & 0.000 & 0.000 \\ -0.000 & -0.000 & -0.000 & -0.000 & -0.000 & 0.000 \\ -0.000 & -0.000 & 0.000 & -0.000 & 0.000 & -0.000 \end{bmatrix},$$

$$\mathbf{C}_1^T = \begin{bmatrix} 0&0&0&0&0&0 & -0.0404 & -0.0453 & 0.0415 & -0.0044 & -0.0212 & -0.0200 \\ 0&0&0&0&0&0 & 0.2084 & -0.1783 & -0.1050 & 0.0455 & 0.1427 & -0.1254 \end{bmatrix},$$

$$\mathbf{B}_1 = \begin{bmatrix} 0 & 0 \\ 0 & 0 \\ 0 & 0 \\ 0 & 0 \\ 0 & 0 \\ 0 & 0 \\ 16.5924 & -21.3687 \\ -7.1011 & 25.4467 \\ 13.5529 & 15.3619 \\ -6.5758 & 9.1164 \\ -0.4503 & 3.9458 \\ -0.3630 & -0.4057 \end{bmatrix}, \quad \mathbf{D}_1 = 0, \quad \mathbf{E}_1 = \begin{bmatrix} 0 \\ 0 \\ 0 \\ 0 \\ 0 \\ 0 \\ -2.4449 \\ 1.6580 \\ 0.7635 \\ 0.4944 \\ 0.3082 \\ -1110 \end{bmatrix}. \tag{2.123}$$

The state space matrices of the remaining 4 MIMO models are obtained similarly. Control of the multimodel system for the flexural vibrations is obtained using the robust decentralized technique [79], [80] via the reduced order modeling which is presented in the subsequent chapters. The characteristics of the smart flexible cantilever beam of the model 1 (with thickness of 0.5 mm) are given in Table 2.7. Similarly, the characteristics of the other 4 multivariable state space models of the smart structure are also obtained.

Table 2.7. Characteristics of the smart beam for the multivariable model 1

Eigen values (Model 1)	Natural frequency (Hertz)
$-0.0071 \pm j9.36$	1.4892
$-0.5975 \pm j\,89.2$	14.1995
$-4.96 \pm j\,257.1$	40.9239
$-21.3 \pm j\,532.1$	84.6910
$-81.2 \pm j\,1037.2$	165.0721
$-224.4 \pm j\,1715.1$	272.9711

2.1.5 Conclusions

Smart cantilever beam models bonded with surface mounted piezoelectric sensors and actuators at discrete locations on the flexible beam are presented using the concepts of piezoelectrics, Euler-Bernoulli beam theory, finite element method and the state space techniques. In the first case, the flexible beam is divided into 3, 4 and 5 finite elements with sensor-actuator pair placed at only one FE location. Different SISO models of the same smart structure plant are obtained by varying the sensor-actuator location from the fixed end to the free end with 1 input and 1 output. 2 and 3 vibratory modes was considered in these cases. The case of modeling a smart structure with more than one active piezo sensor/actuator as collocated pairs at

discrete locations on the structure as a multivariable system is also considered. Two situations are dealt in the modeling procedure.

One is the beam divided into 4 FE and the other is, the beam divided into 8 finite elements. In both the situations, the piezo sensor/actuators are placed as collocated pairs at even FE locations. State space models are also presented for the case when one of the 4 actuators in a multimodel system failed to function. In the modeling of the smart structure, the mass and stiffness of the adhesive which is used to bond the piezo patches to the structure is neglected. A higher order smart structure model is presented by considering the first 6 modes of vibration. To overcome the problems such as the order of the state space model and the numerical difficulties in processing the model data for higher order systems, a reduced order model is presented to represent the first few vibratory modes and this reduced order model is used for the controller design.

2.2 Modeling of Smart Structures Based on Timoshenko Beam Theory

In this following Sections, the mathematical modeling of smart beam modelled as SISO and MIMO systems with surface mounted shear sensors and actuators is presented. The first few vibratory modes are retained while modeling the beam. This is followed by the modeling of the Timoshenko cantilever beams with embedded shear sensors and actuators as SISO and MIMO systems. The effect of shear and axial displacement is considered in the modeling, which was neglected in the E-B beams. Finally, the state space models of the above mentioned two types of beams as SISO and MIMO systems is arrived at starting from the FE model of the Timoshenko beam. Conclusions are drawn at the end.

2.2.1 Modeling of SISO Structures with Surface Mounted Shear Sensors and Actuators

Few researchers have well established a mathematical finite element Euler-Bernoulli model. These models do not consider the shear effects, rotary inertia, axial displacements, etc.,. Modeling of smart structures by shear deformable (Timoshenko) theory is limited. Here, the effect of rotary inertia and the axial displacement along the x axis has been considered in modeling. Consider a thick aluminum prismatic isotropic cantilever beam as shown in Fig. (2.1)(a) divided into 4 finite elements as shown in Fig. 2.7.

The smart beam is obtained by sandwiching the regular beam element between 2 thin piezoelectric layers (as extension mode sensors and actuators, i.e., as surface mounted piezo pair) placed at only 1 FE location as a collocated pair (Fig. 2.7). The bottom layer is acting as a sensor and the top layer is acting as an actuator. The same assumptions made in deriving the E-B model is used here while deriving the Timoshenko beam model as shown at the end of the Section 2.1.1. An external force input $\mathbf{f}_{ext}$ (impulse disturbance) is applied at the free end of the smart beam.

The beam is thus subjected to vibrations and takes a certain amount of time for the vibrations to die out. These vibrations are suppressed quickly in no time by the feedback action of the sensor, controller and actuator, which would have taken

a longer time to damp out without the controller. Thus, there are 2 inputs to the plant. One is the external force input $\mathbf{f}_{ext}$ (impulse disturbance), which is taken as a load matrix of 1 unit in the simulation and the other input is the control input u to the actuator. The dimensions and properties of the aluminum cantilever beam and that of the piezoelectric sensor / actuator used are given in Table 2.8.

Table 2.8. Properties of the thick cantilever (aluminium beam) and the piezoelectric element when beam is divided into 4 finite elements

Physical parameters	**Cantilever beam**	**Piezoelectric (PZT) sensor / actuator**
Length	$L_b = 0.2$ m	$l_p = 0.05$ m
Width	$b = 0.03$ m	$b = 0.03$ m
Thickness	$t_b = 1$ mm	$t_a = t_s = 0.5$mm
Density	$\rho_b = 8030\, Kg/m^3$	$\rho_p = 7700\, Kg/m^3$
Young's Modulus	$E_b = 193.06\, GPa$	$E_p = 68\, GPa$
Damping Constants used in $\mathbf{C}^*$	$\alpha = 0.001$, $\beta = 0.0001$	
PZT Strain Constant		$d_{31} = 125 \times 10^{-12} m/V$
PZT Stress Constant		$g_{31} = 10.5 \times 10^{-3} V m N^{-1}$

2.2.1.1 Modeling of the Regular Beam Element

To start with, consider a regular beam element (say, FE position 1) as shown in Fig. 2.7. The displacement relation in the x, y and z directions of the beam [42] can be written as

$$u(x, y, z, t) = z\theta(x, t), \tag{2.124}$$

$$v(x, y, z, t) = 0, \qquad w(x, y, z, t) = w(x, t), \tag{2.125}$$

where w is the time dependent transverse displacement of the centroidal axis (along z-axis), θ is the time dependent rotation of the beam cross-section about y-axis, u is the axial displacement along the x-axis. We are restricting ourselves to the behavior of the beam in the $x - z$ plane only [103].

The axial displacement u of a point at a certain distance z from the center line is only due to the bending slope and the shear slope has no contribution to this. The centroidal axis of the beam is coincident with the elastic axis so that the bending-torsion coupling is negligible. The strain components of the beam are given as

$$\varepsilon_{xx} = \frac{\partial u}{\partial x} = \frac{\partial u}{\partial \theta}\frac{\partial \theta}{\partial x} = z\frac{\partial \theta}{\partial x}, \qquad \varepsilon_{yy} = \frac{\partial v}{\partial y} = 0, \qquad \varepsilon_{zz} = \frac{\partial w}{\partial z} = 0, \tag{2.126}$$

where ε_{xx}, ε_{yy}, ε_{zz} are the longitudinal strains or the tensile strains in the 3 directions, i.e., in the x, y and z directions. The shear strains γ induced in the beam along the 3 directions (viz., along x, y and z directions) are given by [104]

$$\gamma_{xz} = \left[\frac{\partial u}{\partial z} + \frac{\partial w}{\partial x}\right],\ \gamma_{yz} = \left[\frac{\partial v}{\partial z} + \frac{\partial w}{\partial y}\right],\ \gamma_{xy} = \left[\frac{\partial u}{\partial y} + \frac{\partial v}{\partial x}\right], \tag{2.127}$$

where $\frac{\partial u}{\partial z} = \theta$.

The effect of shear strains along y and z directions is equal to zero. Thus, the stresses in the beam element are given as

$$\sigma_{xx} = E_b\, \epsilon_{xx} = E_b\, z\, \frac{\partial \theta}{\partial x}, \tag{2.128}$$

$$\sigma_{xz} = \mathbb{G}\, \gamma_{xz} = \mathbb{G}\left[\frac{\partial w}{\partial x} + \theta\right], \tag{2.129}$$

where $\mathbb{G}$ is shear modulus (or modulus of rigidity) of the beam material given by $\mathbb{G} = \frac{E_b}{1+\nu}$, where ν is the poisons ratio, σ_{xz} is the shear stress and σ_{xx} is the tensile stress [105].

The strain energy U of the beam element depends upon the linear strain ε, the shear strain γ and is given by

$$U = \frac{1}{2} E_b I_b \left(\frac{\partial \theta}{\partial x}\right)^2 + \frac{1}{2}\, \mathbb{K}\mathbb{G} A_b \left(\frac{\partial w}{\partial x} + \theta\right)^2 \tag{2.130}$$

and the total strain energy is finally written as

$$U = \frac{1}{2} \int_0^{l_b} \begin{bmatrix} \frac{\partial \theta}{\partial x} \\ \frac{\partial w}{\partial x} + \theta \end{bmatrix}^T \begin{bmatrix} E_b I_b & 0 \\ 0 & \mathbb{K}\mathbb{G} A_b \end{bmatrix} \begin{bmatrix} \frac{\partial \theta}{\partial x} \\ \frac{\partial w}{\partial x} + \theta \end{bmatrix} dx, \tag{2.131}$$

where $\mathbb{K}$ is the shear coefficient [106] which depends on the material definition and on the cross sectional geometry, usually taken equal to $\frac{5}{6}$ or can be obtained from the poisson's ratio of the beam as

$$\mathbb{K} = \frac{10(1+v)}{12+11v}. \tag{2.132}$$

The kinetic energy T of the beam element depends on the sum of the kinetic energy due to the linear velocity and due to the angular twist θ and is given by

$$T = \frac{1}{2} \int_0^{l_b} \int_A \rho_b \left\{ \left(\frac{\partial u}{\partial t}\right)^2 + \left(\frac{\partial v}{\partial t}\right)^2 + \left(\frac{\partial w}{\partial t}\right)^2 \right\} dA\, dx, \tag{2.133}$$

which can be written using Eqs. (2.124) - (2.129) as

$$T = \frac{1}{2} \int_0^{l_b} \begin{bmatrix} \frac{\partial w}{\partial t} \\ \\ \frac{\partial \theta}{\partial t} \end{bmatrix}^T \begin{bmatrix} \rho_b\, A_b & 0 \\ 0 & \rho_b\, I_b \end{bmatrix} \begin{bmatrix} \frac{\partial w}{\partial t} \\ \\ \frac{\partial \theta}{\partial t} \end{bmatrix} dx. \tag{2.134}$$

The Eq. (2.134) can be further rewritten after simplifying as

$$T = \frac{1}{2} \rho_b\, A_b \left(\frac{\partial w}{\partial t}\right)^2 + \frac{1}{2} \rho_b\, I_b \left(\frac{\partial \theta}{\partial t}\right)^2. \tag{2.135}$$

The total work done W_e due to the external forces in the beam is given by

$$W_e = \int_0^{l_b} \begin{bmatrix} w \\ \theta \end{bmatrix}^T \begin{bmatrix} q_d \\ m \end{bmatrix} dx, \tag{2.136}$$

which can be written as

$$W_e = \int_0^{l_b} (w\ q_d + \theta\ m)\, dx, \tag{2.137}$$

where q_d represents distributed force along the length of the beam element and m represents the moment along the length of the beam element.

The equation of motion is derived from the concept of the total strain energy being equal to the sum of the change in the kinetic energy and the work done due to the external forces (Hamilton's principle) and is given by

$$\delta\Pi = \int_{t_1}^{t_2} (\delta U - \delta T - \delta W_e)\, dt = 0. \tag{2.138}$$

Here, δU, δT and δW_e are the variations of the strain energy, the kinetic energy, work done due to the external forces, t is the time and δ is the first variational operator.

Substituting the values of strain energy from Eq. (2.131), kinetic energy from Eq. (2.135) and external work done from Eq. (2.136) in Eq. (2.138) and integrating by parts, we get the differential equations of motion of a general shaped beam modeled with Timoshenko beam theory [42] as

$$\frac{\partial \left\{ \mathbb{K}\mathbb{G}A_b \left(\frac{\partial w}{\partial x} + \theta \right) \right\}}{\partial x} + q_d = \rho_b A_b \frac{\partial^2 w}{\partial t^2}, \tag{2.139}$$

$$\frac{\partial \left\{ E_b I_b \frac{\partial \theta}{\partial x} \right\}}{\partial x} - \mathbb{K}\mathbb{G}A_b \left(\frac{\partial w}{\partial x} + \theta \right) + m = \rho_b I_b \frac{\partial^2 \theta}{\partial t^2}. \tag{2.140}$$

The R.H.S. of Eq. (2.139) is the time derivative of the linear momentum, whereas the R.H.S. of Eq. (2.140) is the time derivative of the moment of momentum. For the static case with no external force acting on the beam, the differential equations of motion (Timoshenko beam equations) reduces to

$$\frac{\partial \left\{ \mathbb{K}\mathbb{G}A_b \left(\frac{\partial w}{\partial x} + \theta \right) \right\}}{\partial x} = 0 \tag{2.141}$$

and

$$\frac{\partial \left\{ E_b I_b \frac{\partial \theta}{\partial x} \right\}}{\partial x} - \mathbb{K}\mathbb{G}A_b \left(\frac{\partial w}{\partial x} + \theta \right) = 0. \tag{2.142}$$

.

From Eqs. (2.141) and (2.142), it can be seen that this governing equation of the beam based on Timoshenko beam theory can be satisfied only if the polynomial order for w is selected one order higher than the polynomial order for θ. Since there are 4 nodes for one beam element [45], [107], [108], [109], w, i.e., the transverse displacement is approximated by a cubic polynomial and θ is approximated by a quadratic polynomial as

$$w = a_1 + a_2 x + a_3 x^2 + a_4 x^3, \tag{2.143}$$

and

$$\theta = b_1 + b_2 x + b_3 x^2. \tag{2.144}$$

Here, in Eqs. (2.143) and (2.144), x is the distance of the finite element node from the fixed end of the beam, a_i and b_j, $(i = 1\,\text{to}\,4)$, $(j = 1\,\text{to}\,3)$ are the unknown coefficients and are found out using the boundary conditions at the ends of the beam element, i.e., $x = (0, l_b)$ as follows (Fig. 2.7).

$$\text{At}\;\; x = 0,\; w = w_1, w' = \theta_1 \quad \text{and} \quad \text{at}\;\; x = l_b,\; w = w_2, w' = \theta_2. \tag{2.145}$$

After applying the boundary conditions from Eq. (2.145) on Eqs. (2.143) and (2.144), the unknown coefficients a_i and b_j can be obtained. Substituting the obtained unknown coefficients a_i and b_j in Eqs. (2.143) and (2.144) and after rearranging and writing them in matrix form, we get the transverse displacement, first spatial derivative, the second spatial derivative and the time derivative of the transverse displacement $w(x,t)$ as

$$w(x,t) = [N_w]\,[\mathbf{q}]\,, \tag{2.146}$$

$$w^{'}(x,t) = [N_\theta]\,[\mathbf{q}]\,, \tag{2.147}$$

$$w^{''}(x,t) = [N_a]\,[\mathbf{q}]\,, \tag{2.148}$$

$$\dot{w}(x,t) = [N_w]\,[\dot{\mathbf{q}}]\,, \tag{2.149}$$

where $\mathbf{q}$ is the vector of displacements and slopes given by $\{w_1, \theta_1, w_2, \theta_2\}^T$, $\dot{\mathbf{q}}$ is the time derivative of the nodal coordinate vector $\mathbf{q}$, $[N_w]^T$, $[N_\theta]^T$ and $[N_a]^T$ are the mode shape functions (for displacement, rotations and accelerations) taking the beam bending stiffness and shear stiffness, i.e., the shear related terms into consideration and are given as [110], [111]

$$[N_w]^T = \begin{bmatrix} \frac{1}{1+\phi}\left\{2\left(\frac{x}{l_b}\right)^3 - 3\left(\frac{x}{l_b}\right)^2 - \phi\left(\frac{x}{l_b}\right) + (1+\phi)\right\} \\ \frac{l_b}{1+\phi}\left\{\left(\frac{x}{l_b}\right)^3 - \left(2+\frac{\phi}{2}\right)\left(\frac{x}{l_b}\right)^2 + \left(1+\frac{\phi}{2}\right)\left(\frac{x}{l_b}\right)\right\} \\ -\frac{1}{1+\phi}\left\{2\left(\frac{x}{l_b}\right)^3 - 2\left(\frac{x}{l_b}\right)^2 - \phi\left(\frac{x}{l_b}\right)\right\} \\ \frac{l_b}{1+\phi}\left\{\left(\frac{x}{l_b}\right)^3 - \left(1-\frac{\phi}{2}\right)\left(\frac{x}{l_b}\right)^2 - \frac{\phi}{2}\left(\frac{x}{l_b}\right)\right\} \end{bmatrix}, \tag{2.150}$$

$$[N_\theta]^T = \begin{bmatrix} \frac{6}{(1+\phi)l_b}\left\{\left(\frac{x}{l_b}\right)^2 - \left(\frac{x}{l_b}\right) - \phi\right\} \\ \frac{1}{1+\phi}\left\{3\left(\frac{x}{l_b}\right)^2 - (4+\phi)\left(\frac{x}{l_b}\right) + (1+\phi)\right\} \\ -\frac{6}{(1+\phi)l_b}\left\{\left(\frac{x}{l_b}\right)^2 - \left(\frac{x}{l_b}\right)\right\} \\ \frac{1}{(1+\phi)}\left\{3\left(\frac{x}{l_b}\right)^2 - (2-\phi)\left(\frac{x}{l_b}\right)\right\} \end{bmatrix}, \tag{2.151}$$

$$[N_a]^T = \begin{bmatrix} \frac{6}{(1+\phi)l_b}\left\{\frac{2x}{l_b^2} - \frac{1}{l_b}\right\} \\ \frac{1}{(1+\phi)l_b}\left\{\frac{6x}{l_b} - (4+\phi)\right\} \\ -\frac{6}{(1+\phi)l_b}\left\{\frac{6x}{l_b^2} - \frac{1}{l_b}\right\} \\ \frac{1}{(1+\phi)}\left\{\frac{6x}{l_b^2} - \frac{(2-\phi)}{l_b}\right\} \end{bmatrix}, \tag{2.152}$$

where $[N_\theta] = [N_w]^{'}$, $[N_a] = [N_w]^{''}$ and ϕ is the ratio of the beam bending stiffness to shear stiffness and is given by

$$\phi = \frac{12}{l_b^2}\left(\frac{E_b I_b}{\mathbb{K} G A_b}\right) = \frac{24}{l_b^2}\left(\frac{I_b}{\mathbb{K} A_b}\right)(1+\upsilon). \tag{2.153}$$

From the Eqs. (2.150)-(2.152), it is inferred that the shape function of the beam has strong dependence on ϕ. Also, it can be observed that when ϕ is set to zero, the shape function $[N_w]^T$ of the Timoshenko beam reduces to that of the EB beam as given in Eq. (2.7). The equation of motion of the beam element is developed by substituting the shape functions into the hamiltonian equation and integrating over the entire length of the beam element. Thus, we get,

$$M^b \ddot{\mathbf{q}} + K^b \mathbf{q} = \mathbf{f}^{\ b} \tag{2.154}$$

where M^b, K^b are the local mass, stiffness matrices of the regular beam element or the elemental mass and stiffness matrices of size (4×4) and $\mathbf{f}^{\ b}$ is the force vector of size (4×1).

The mass matrix of the regular beam element is the sum of the translational mass and the rotational mass and is given as

$$\left[M^b\right] = \int_0^{l_b} \begin{bmatrix} N_w \\ N_\theta \end{bmatrix}^T \begin{bmatrix} \rho_b A_b & 0 \\ 0 & \rho_b I_{yy} \end{bmatrix} \begin{bmatrix} N_w \\ N_\theta \end{bmatrix} dx. \tag{2.155}$$

Substituting the mode shape functions $[N_w]$, $[N_\theta]$ into Eq. (2.155) and integrating, we get the mass matrix of the regular beam element as

$$\left[M^b\right] = \left[M_{\rho_b A_b}\right] + \left[M_{\rho_b I_b}\right], \tag{2.156}$$

where the symmetric matrices $[M_{\rho_b A_b}]$ and $[M_{\rho_b I_b}]$ in Eq. (2.156) is associated with the translational inertia and rotary inertia as

$$[M_{\rho_b A_b}] = \frac{\rho_b A_b l_b}{210(1+\phi)^2} \begin{bmatrix} (70\phi^2+147\phi+78) & (35\phi^2+77\phi+44)\frac{l_b}{4} & (35\phi^2+63\phi+27) & -(35\phi^2+63\phi+26)\frac{l_b}{4} \\ (35\phi^2+77\phi+44)\frac{l_b}{4} & (7\phi^2+14\phi+8)\frac{l_b^2}{4} & (35\phi^2+63\phi+26)\frac{l_b}{4} & -(7\phi^2+14\phi+6)\frac{l_b^2}{4} \\ (35\phi^2+63\phi+27) & (35\phi^2+63\phi+26)\frac{l_b}{4} & (70\phi^2+147\phi+78) & -(35\phi^2+77\phi+44)\frac{l_b}{4} \\ -(35\phi^2+63\phi+26)\frac{l_b}{4} & -(7\phi^2+14\phi+6)\frac{l_b^2}{4} & -(35\phi^2+77\phi+44)\frac{l_b}{4} & (7\phi^2+14\phi+8)\frac{l_b^2}{4} \end{bmatrix}, \tag{2.157}$$

$$[M_{\rho_b I_b}] = \frac{\rho_b I_b}{30(1+\phi)^2 l_b} \begin{bmatrix} 36 & -(15\phi-3)l_b & -36 & -(15\phi-3)l_b \\ -(15\phi-3)l_b & (10\phi^2+5\phi+4)l_b^2 & (15\phi-3)l_b & (5\phi^2-5\phi-1)l_b^2 \\ -36 & (15\phi-3)l_b & 36 & (15\phi-3)l_b \\ -(15\phi-3)l_b & (5\phi^2-5\phi-1)l_b^2 & (15\phi-3)l_b & (10\phi^2+5\phi+4)l_b^2 \end{bmatrix} \text{ and} \tag{2.158}$$

The stiffness matrix $\left[K^b\right]$ of the regular beam element (also called as the local stiffness matrix) is the sum of the bending stiffness and the shear stiffness and is written in matrix form as

$$\left[K^b\right] = \int_0^{l_b} \begin{bmatrix} \frac{\partial}{\partial x} N_\theta \\ N_\theta + \frac{\partial}{\partial x} N_w \end{bmatrix}^T \begin{bmatrix} E_b I_b & 0 \\ 0 & \mathbb{K}\mathbb{G} A_b \end{bmatrix} \begin{bmatrix} \frac{\partial}{\partial x} N_\theta \\ N_\theta + \frac{\partial}{\partial x} N_w \end{bmatrix} dx. \tag{2.159}$$

Substituting the mode shape functions $[N_w]$, $[N_\theta]$ into Eq. (2.159) and integrating, we get the stiffness matrix $\left[K^b\right]$ of the regular beam element of size (4×4) as

$$\left[K^b\right] = \frac{E_b I_b}{(1+\phi) l_b^3} \begin{bmatrix} 12 & 6l_b & -12 & 6l_b \\ 6l_b & (4+\phi) l_b^2 & -6l_b & (2-\phi) l_b^2 \\ -12 & -6l_b & 12 & -6l_b \\ 6l_b & (2-\phi) l_b^2 & -6l_b & (4+\phi) l_b^2 \end{bmatrix}, \tag{2.160}$$

which is symmetric in nature. Note that when the shear related term ϕ is neglected in Eqs. (2.157) and(2.160), the mass matrix and the stiffness matrix of the beam modelled using Timoshenko beam theory reduces to the mass and stiffness matrix of a Euler-Bernoulli beam as shown in the Eq. (2.20).

2.2.1.2 Finite Element Modeling of the Piezoelectric Element and the Piezoelectric Beam Element

The finite element modeling of the piezoelectric element is carried out as follows. Piezoelectric elements can be used as sensors and actuators in flexible structures for sensing and actuating purposes on the host structure. The dimensions of the piezoelectric patch are given in Table 2.8. The piezo sensor-actuator pair is also modeled using the Timoshenko beam theory. Employing the same procedure similar to the regular beam element in the previous sub-section 2.2.1:1, we get the equations of motion for the piezoelectric element as

$$M^p \ddot{\mathbf{q}} + K^p \mathbf{q} = \mathbf{f}^{\,p}, \tag{2.161}$$

where M^p, K^p are the local mass, stiffness matrices of the piezoelectric element or the elemental mass and stiffness matrices of size (4×4) and $\mathbf{f}^{\,p}$ is the force vector of size (4×1).

The mass matrix of the piezoelectric element is finally obtained as

$$[M^p] = \left[M_{\rho_p A_p}\right] + \left[M_{\rho_p I_p}\right]. \tag{2.162}$$

Here, in Eq. (2.162), $\left[M_{\rho_p A_p}\right]$ and $\left[M_{\rho_p I_p}\right]$ is associated with the translational inertia and the rotary inertia of the piezoelectric element as

$$\left[M_{\rho_p A_p}\right] = \frac{\rho_p A_p l_p}{210(1+\phi)^2} \begin{bmatrix} (70\phi^2 + 147\phi + 78) & (35\phi^2 + 77\phi + 44)\frac{l_p}{4} & (35\phi^2 + 63\phi + 27) & -(35\phi^2 + 63\phi + 26)\frac{l_p}{4} \\ (35\phi^2 + 77\phi + 44)\frac{l_p}{4} & (7\phi^2 + 14\phi + 8)\frac{l_p^2}{4} & (35\phi^2 + 63\phi + 26)\frac{l_p}{4} & -(7\phi^2 + 14\phi + 6)\frac{l_p^2}{4} \\ (35\phi^2 + 63\phi + 27) & (35\phi^2 + 63\phi + 26)\frac{l_p}{4} & 70\phi^2 + 147\phi + 78) & -(35\phi^2 + 77\phi + 44)\frac{l_p}{4} \\ -(35\phi^2 + 63\phi + 26)\frac{l_p}{4} & -(7\phi^2 + 14\phi + 6)\frac{l_p^2}{4} & -(35\phi^2 + 77\phi + 44)\frac{l_p}{4} & (7\phi^2 + 14\phi + 8)\frac{l_p^2}{4} \end{bmatrix} \tag{2.163}$$

and

$$\left[M_{\rho_p I_p}\right] = \frac{\rho_p I_p}{30(1+\phi)^2 l_p} \begin{bmatrix} 36 & -(15\phi-3)l_p & -36 & -(15\phi-3)l_p \\ -(15\phi-3)l_p & (10\phi^2+5\phi+4)l_p^2 & (15\phi-3)l_p & (5\phi^2-5\phi-1)l_p^2 \\ -36 & (15\phi-3)l_p & 36 & (15\phi-3)l_p \\ -(15\phi-3)l_p & (5\phi^2-5\phi-1)l_p^2 & (15\phi-3)l_p & (10\phi^2+5\phi+4)l_p^2 \end{bmatrix}. \tag{2.164}$$

Similarly, we obtain the stiffness matrix $\left[K^{piezo}\right]$ of the piezoelectric element as

$$K^p = \frac{E_p I_p}{(1+\phi)l_p^3} \begin{bmatrix} 12 & 6l_p & -12 & 6l_p \\ 6l_p & (4+\phi)l_p^2 & -6l_p & (2-\phi)l_p^2 \\ -12 & -6l_p & 12 & -6l_p \\ 6l_p & (2-\phi)l_p^2 & -6l_p & (4+\phi)l_p^2 \end{bmatrix}. \tag{2.165}$$

From the above discussions, we see that when the shear related term ϕ is neglected in the piezoelectric elements, the mass matrix in Eq. (2.163) and the stiffness matrix in Eq. (2.165) reduce to the mass and stiffness matrix of the piezoelectric material modelled with EB theory as given in the Eqs. (2.22) and (2.23).

The regular beam element and the piezoelectric beam element (top piezo patch + middle regular beam element + bottom piezo patch) are shown in Fig. 2.7. The piezoelectric beam element (top piezo patch + middle beam element + bottom piezo patch) is obtained by sandwiching the regular beam element in between a layer of 2 thin piezoelectric patches of thickness t_a or t_s as a collocated pair. Collocated piezoelectric sensor / actuators are used because they are supposed to be more robust (against parameter uncertainty) under feedback control action. The bottom layer acts as the sensor and the top layer acts as an actuator. At the same time, collocated piezo pairs improves the gain margin and phase margin of the feedback controller.

The mass matrix for the piezoelectric beam element is obtained by replacing the term $\rho_p A_p$ in Eq. (2.163) by $\rho A = b(\rho_b t_b + 2\rho_p t_p)$ and $\rho_p I_p$ in Eq. (2.164) by $\rho I = b(\rho_b I_b + 2\rho_p I_p)$. Here, ρA is called as the mass/unit length. From this, it is evident that the mass of the PE beam element is twice the mass of the PE element + mass of the regular beam element. Thus, the mass of the piezoelectric beam element is given by

$$[M] = \left[M^b\right] + [2\ M^p]. \tag{2.166}$$

The stiffness matrix for the piezoelectric beam element is obtained by replacing the term $E_p I_p$ in Eq. (2.165) by $EI = E_b I_b + 2E_p I_p$. Here, EI is called as the flexural rigidity. From this, it is evident that the stiffness of the PE beam element is twice the stiffness of the PE element + stiffness of the regular beam element. Thus, the stiffness of the piezoelectric beam element is given by

$$[K] = \left[K^b\right] + [2\ K^p]. \tag{2.167}$$

The mass and stiffness M and K of the piezoelectric elements and that of the piezoelectric beam elements are of the same size as that of the regular beam element. Note that the assembly of the regular beam element and the piezoelectric element can be done by adding the matrices of the regular beam element and the two matrices of the piezoelectric elements as given in Eqs. (2.166) and (2.167). It is assumed that there is continuity of shear stress at the interface of the piezo patches and the substrate beam and the rotations and displacements are the same in all the layers of the structure.

NOTE:

- The modeling of the piezoelectric strain rate sensors and actuators (sensor-actuator equations) is carried out on the similar lines as shown in the Section 2.1.1:4.
- The dynamic equation of the smart structure, the SISO state space model of the smart structure is also obtained on the similar lines as discussed in Section 2.1.1:5 and 2.1.1:6.
- Finally, the SISO state state space model of the smart structure modelled with finite element method and Timoshenko beam theory is given by Eq. (2.70)-(2.72) for 2 vibratory modes and Eqs. (2.84) - (2.86) for 3 vibratory modes.

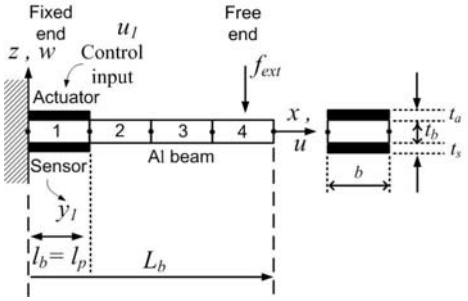

(a) Model 1 (PZT at FE position 1)

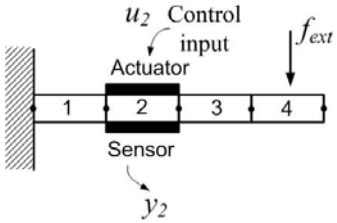

(b) Model 2 (PZT at FE position 2)

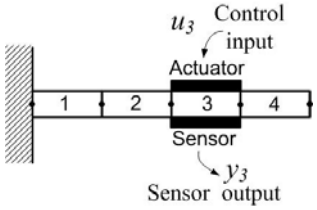

(c) Model 3 (PZT at FE position 3)

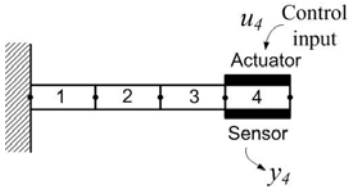

(d) Model 4 (PZT at FE position 4)

Fig. 2.7. Smart Timoshenko beam divided into 4 finite elements (piezo-patch placed at positions 1, 2, 3 and 4) - 4 SISO models

2.2.1.3 State Space Models of the Smart Timoshenko Beam

(i) State space model for 2 vibratory modes: (piezo position varied from fixed end to free end)

The cantilever beam is divided into 4 FE with piezo-patches bonded to the master structure as collocated sensor / actuator pairs at FE locations 1 or 2 or 3 or 4, thus giving rise to 4 SISO models of the same smart structure plant as shown in the Fig. 2.7(a)-(d). The 4 SISO models are obtained by varying the location of the sensor-actuator pair from the fixed end to the free end [73], [112].

State space model of the smart cantilever beam with sensor / actuator placed at FE position 1 (fixed end) as shown in Fig. 2.7(a) is given by

$$\dot{\mathbf{x}} = \mathbf{A}_{14}\,\mathbf{x}(t) + \mathbf{B}_{14}\,\mathbf{u}(t) + \mathbf{E}_{14}\,r(t) \;\text{ and }\; y(t) = \mathbf{C}_{14}^{T}\,\mathbf{x}(t) + \mathbf{D}_{14}\,\mathbf{u}(t) \tag{2.168}$$

with

$$\mathbf{A}_{14} = 10^{6}\begin{bmatrix} 0 & 0 & 0.0000 & 0 \\ 0 & 0 & 0 & 0.0000 \\ -0.0278 & -0.0000 & -0.0000 & -0.0000 \\ -0.0000 & -1.0435 & -0.0000 & -0.0000 \end{bmatrix},\; \mathbf{B}_{14} = \begin{bmatrix} 0 \\ 0 \\ -0.0006 \\ -0.0024 \end{bmatrix},$$

$$\mathbf{C}_{14}^{T} = \begin{bmatrix} 0 & 0 & -0.8440 & 2.6244 \end{bmatrix},\; \mathbf{D}_{14} = 0,\; \mathbf{E}_{14} = \begin{bmatrix} 0 \\ 0 \\ 0.7672 \\ 0.7505 \end{bmatrix}.$$

State space model of the smart cantilever beam with sensor / actuator placed at FE position 2 (nearby fixed end) as shown in Fig. 2.7(b) is given by

$$\dot{\mathbf{x}} = \mathbf{A}_{24}\,\mathbf{x}(t) + \mathbf{B}_{24}\,\mathbf{u}(t) + \mathbf{E}_{24}\,r(t) \;\text{ and }\; y(t) = \mathbf{C}_{24}^{T}\,\mathbf{x}(t) + \mathbf{D}_{24}\,\mathbf{u}(t) \tag{2.169}$$

with

$$\mathbf{A}_{24} = 10^{6}\begin{bmatrix} 0 & 0 & 0.0000 & 0 \\ 0 & 0 & 0 & 0.0000 \\ -0.0309 & 0.0000 & -0.0000 & 0.0000 \\ 0.0000 & -1.1672 & 0.0000 & -0.0000 \end{bmatrix},\; \mathbf{B}_{24} = \begin{bmatrix} 0 \\ 0 \\ -0.0015 \\ 0.0018 \end{bmatrix},$$

$$\mathbf{C}_{24}^{T} = \begin{bmatrix} 0 & 0 & -0.5305 & -3.2626 \end{bmatrix},\; \mathbf{D}_{24} = 0,\; \mathbf{E}_{24} = \begin{bmatrix} 0 \\ 0 \\ 0.8120 \\ 0.7969 \end{bmatrix}.$$

State space model of the smart cantilever beam with sensor / actuator placed at FE position 3 (middle) as shown in Fig. 2.7(c) is given by

$$\dot{\mathbf{x}} = \mathbf{A}_{34}\,\mathbf{x}(t) + \mathbf{B}_{34}\,\mathbf{u}(t) + \mathbf{E}_{34}\,r(t) \;\text{ and }\; y(t) = \mathbf{C}_{34}^{T}\,\mathbf{x}(t) + \mathbf{D}_{34}\,\mathbf{u}(t) \tag{2.170}$$

with

$$\mathbf{A}_{34} = 10^{6} \begin{bmatrix} 0 & 0 & 0.0000 & 0 \\ 0 & 0 & 0 & 0.0000 \\ -0.0307 & -0.0000 & -0.0000 & -0.0000 \\ -0.0000 & -1.1722 & -0.0000 & -0.0000 \end{bmatrix}, \quad \mathbf{B}_{34} = \begin{bmatrix} 0 \\ 0 \\ -0.0019 \\ -0.0035 \end{bmatrix},$$

$$\mathbf{C}_{34}^{T} = \begin{bmatrix} 0 & 0 & -0.2236 & -4.1608 \end{bmatrix}, \quad \mathbf{D}_{34} = 0, \quad \mathbf{E}_{34} = \begin{bmatrix} 0 \\ 0 \\ 0.8107 \\ 0.7966 \end{bmatrix}.$$

State space model of the smart cantilever beam with sensor / actuator placed at FE position 4 (free end) as shown in Fig. 2.7(d) is given by

$$\dot{\mathbf{x}} = \mathbf{A}_{44}\,\mathbf{x}(t) + \mathbf{B}_{44}\,\mathbf{u}(t) + \mathbf{E}_{44}\,r(t) \;\text{ and }\; y(t) = \mathbf{C}_{44}^{T}\,\mathbf{x}(t) + \mathbf{D}_{44}\,\mathbf{u}(t) \tag{2.171}$$

with

$$\mathbf{A}_{44} = 10^{3} \begin{bmatrix} 0 & 0 & 0.0001 & 0 \\ 0 & 0 & 0 & 0.0001 \\ -0.0305 & 0.0000 & -0.0000 & 0.0000 \\ 0.0000 & -1.1639 & 0.0000 & -0.0000 \end{bmatrix}, \quad \mathbf{B}_{44} = \begin{bmatrix} 0 \\ 0 \\ -0.0021 \\ -0.0069 \end{bmatrix},$$

$$\mathbf{C}_{44}^{T} = 10^{-4} \begin{bmatrix} 0 & 0 & -0.0363 & -1.1161 \end{bmatrix}, \quad \mathbf{D}_{44} = 0, \quad \mathbf{E}_{44} = \begin{bmatrix} 0 \\ 0 \\ 0.8086 \\ 0.7893 \end{bmatrix}.$$

(ii) State space model for 3 vibratory modes: (piezo position varied from fixed end to free end)

On the similar lines discussed in the above section 2.2.1:3(i) and in section 2.1.1:6(II), the state space model for 3 vibratory modes for the 4 SISO models of the Fig. 2.7 are given by

$$\textbf{Model 1 : } \mathbf{A}_{14} = 10^{6} \begin{bmatrix} 0 & 0 & 0 & 0.0000 & 0 & 0 \\ 0 & 0 & 0 & 0 & 0.0000 & 0 \\ 0 & 0 & 0 & 0 & 0 & 0.0000 \\ -0.0278 & -0.0000 & -0.0000 & -0.0000 & -0.0000 & -0.0000 \\ -0.0000 & -1.0435 & 0.0000 & -0.0000 & -0.0000 & 0.0000 \\ -0.0000 & 0.0000 & -7.8100 & -0.0000 & 0.0000 & -0.0001 \end{bmatrix}, \tag{2.172}$$

$$\mathbf{C}_{14}^{T} = \begin{bmatrix} 0 & 0 & 0 & -0.8440 & 2.6244 & -1.9399 \end{bmatrix}, \quad \mathbf{B}_{14} = \begin{bmatrix} 0 \\ 0 \\ 0 \\ -0.0006 \\ 0.0024 \\ -0.0041 \end{bmatrix}, \quad \mathbf{E}_{14} = \begin{bmatrix} 0 \\ 0 \\ 0 \\ 0.7672 \\ 0.7505 \\ 0.7286 \end{bmatrix},$$

$$\textbf{Model 2 : } \mathbf{A}_{24} = 10^6 \begin{bmatrix} 0 & 0 & 0 & 0.0000 & 0 & 0 \\ 0 & 0 & 0 & 0 & 0.0000 & 0 \\ 0 & 0 & 0 & 0 & 0 & 0.0000 \\ -0.0309 & 0.0000 & -0.0000 & -0.0000 & 0.0000 & -0.0000 \\ 0.0000 & -1.1672 & 0.0000 & 0.0000 & -0.0000 & 0.0000 \\ -0.0000 & 0.0000 & -8.7630 & -0.0000 & 0.0000 & -0.0001 \end{bmatrix}, \tag{2.173}$$

$$\mathbf{C}_{24}^T = \begin{bmatrix} 0 & 0 & 0 & -0.5305 & -3.2626 & 8.5763 \end{bmatrix}, \ \mathbf{B}_{24} = \begin{bmatrix} 0 \\ 0 \\ 0 \\ -0.0015 \\ 0.0018 \\ 0.0040 \end{bmatrix}, \ \mathbf{E}_{24} = \begin{bmatrix} 0 \\ 0 \\ 0 \\ 0.8120 \\ 0.7969 \\ 0.7727 \end{bmatrix},$$

$$\textbf{Model 3 : } \mathbf{A}_{34} = 10^6 \begin{bmatrix} 0 & 0 & 0 & 0.0000 & 0 & 0 \\ 0 & 0 & 0 & 0 & 0.0000 & 0 \\ 0 & 0 & 0 & 0 & 0 & 0.0000 \\ -0.0307 & -0.0000 & -0.0000 & -0.0000 & -0.0000 & -0.0000 \\ -0.0000 & -1.1722 & -0.0000 & -0.0000 & -0.0000 & -0.0000 \\ -0.0000 & -0.0000 & -8.7883 & -0.0000 & -0.0000 & -0.0001 \end{bmatrix}, \tag{2.174}$$

$$\mathbf{C}_{34}^T = \begin{bmatrix} 0 & 0 & 0 & -0.2236 & -4.1608 & -9.4795 \end{bmatrix}, \ \mathbf{B}_{34} = \begin{bmatrix} 0 \\ 0 \\ 0 \\ -0.0019 \\ -0.0035 \\ 0.0038 \end{bmatrix}, \ \mathbf{E}_{34} = \begin{bmatrix} 0 \\ 0 \\ 0 \\ 0.8107 \\ 0.7966 \\ 0.7747 \end{bmatrix},$$

$$\textbf{Model 4 : } \mathbf{A}_{44} = 10^6 \begin{bmatrix} 0 & 0 & 0 & 0.0000 & 0 & 0 \\ 0 & 0 & 0 & 0 & 0.0000 & 0 \\ 0 & 0 & 0 & 0 & 0 & 0.0000 \\ -0.0305 & 0.0000 & 0.0000 & -0.0000 & 0.0000 & 0.0000 \\ 0.0000 & -1.1639 & 0.0000 & 0.0000 & -0.0000 & 0.0000 \\ 0.0000 & 0.0000 & -8.7653 & 0.0000 & 0.0000 & -0.0001 \end{bmatrix}, \tag{2.175}$$

$$\mathbf{C}_{44}^T = \begin{bmatrix} 0 & 0 & 0 & -0.0363 & -1.1161 & -6.5536 \end{bmatrix}, \ \mathbf{B}_{44} = \begin{bmatrix} 0 \\ 0 \\ 0 \\ -0.0021 \\ -0.0069 \\ -0.0093 \end{bmatrix}, \ \mathbf{E}_{44} = \begin{bmatrix} 0 \\ 0 \\ 0 \\ 0.8086 \\ 0.7893 \\ 0.7656 \end{bmatrix}.$$

(iii) State space model for 3 vibratory modes with different aspect ratios :

The cantilever beam is divided into 4 FE with piezo patches bonded to the master structure as collocated sensor / actuator pairs placed at FE location number 2 only

as shown in the Fig. 2.7(b). The state space representation of the cantilever beam with surface mounted sensor / actuator in Eqs. (2.85) and (2.86) is obtained by using 3 regular beam elements and 1 piezoelectric beam element. Different state space models (3 cases) of the beam are obtained by varying the length to thickness ratio from 8 to 15 (i.e., the aspect ratio) [74].

State space model of the smart cantilever beam with aspect ratio of 8 is given by

$$\dot{\mathbf{x}} = \mathbf{A}_8\,\mathbf{x}(t) + \mathbf{B}_8\,\mathbf{u}(t) + \mathbf{E}_8\,r(t) \;\text{ and }\; y(t) = \mathbf{C}_8^T\,\mathbf{x}(t) + \mathbf{D}_8\,\mathbf{u}(t) \tag{2.176}$$

with

$$\mathbf{A_8} = \mathbf{10^8}\begin{bmatrix} 0 & 0 & 0 & 0.0000 & 0 & 0 \\ 0 & 0 & 0 & 0 & 0.0000 & 0 \\ 0 & 0 & 0 & 0 & 0 & 0.0000 \\ -0.0155 & 0.0000 & -0.0000 & -0.0000 & 0.0000 & -0.0000 \\ 0.0000 & -0.5836 & -0.0000 & 0.0000 & -0.0001 & -0.0000 \\ -0.0000 & -0.0000 & -4.3279 & -0.0000 & -0.0000 & -0.0004 \end{bmatrix},$$

$$\mathbf{B_8} = \begin{bmatrix} 0 \\ 0 \\ 0 \\ 0.0003 \\ -0.0013 \\ -0.0022 \end{bmatrix},\; \mathbf{D_8} = 0,\; \mathbf{E_8} = \begin{bmatrix} 0 \\ 0 \\ 0 \\ -8.1298 \\ -7.9431 \\ 7.6418 \end{bmatrix},$$

$$\mathbf{C}_8^T = \begin{bmatrix} 0 & 0 & 0 & 0.3402 & -0.7811 & 0.6556 \end{bmatrix}.$$

State space model of the smart cantilever beam with aspect ratio of 10 is given by

$$\dot{\mathbf{x}} = \mathbf{A}_{10}\,\mathbf{x}(t) + \mathbf{B}_{10}\,\mathbf{u}(t) + \mathbf{E}_{10}\,r(t) \;\text{ and }\; y(t) = \mathbf{C}_{10}^T\,\mathbf{x}(t) + \mathbf{D}_{10}\,\mathbf{u}(t) \tag{2.177}$$

with

$$\mathbf{A_{10}} = \mathbf{10^8}\begin{bmatrix} 0 & 0 & 0 & 0.0000 & 0 & 0 \\ 0 & 0 & 0 & 0 & 0.0000 & 0 \\ 0 & 0 & 0 & 0 & 0 & 0.0000 \\ -0.0099 & 0.0000 & -0.0000 & -0.0000 & 0.0000 & -0.0000 \\ 0.0000 & -0.3792 & 0.0000 & 0.0000 & -0.0000 & 0.0000 \\ -0.0000 & 0.0000 & -2.8641 & -0.0000 & 0.0000 & -0.0003 \end{bmatrix},$$

$$\mathbf{B_{10}} = \begin{bmatrix} 0 \\ 0 \\ 0 \\ -0.0003 \\ 0.0011 \\ -0.0020 \end{bmatrix},\; \mathbf{D_{10}} = 0,\; \mathbf{E_{10}} = \begin{bmatrix} 0 \\ 0 \\ 0 \\ 9.0991 \\ 8.9608 \\ 8.7426 \end{bmatrix},$$

$$\mathbf{C}_{10}^{T} = \begin{bmatrix} 0 & 0 & 0 & -0.3047 & 0.7019 & 0.6315 \end{bmatrix}.$$

State space model of the smart cantilever beam with aspect ratio of 15 is given by

$$\dot{\mathbf{x}} = \mathbf{A}_{15}\,\mathbf{x}(t) + \mathbf{B}_{15}\,\mathbf{u}(t) + \mathbf{E}_{15}\,r(t) \;\text{ and }\; y(t) = \mathbf{C}_{15}^{T}\,\mathbf{x}(t) + \mathbf{D}_{15}\,\mathbf{u}(t) \tag{2.178}$$

with

$$\mathbf{A_{15}} = \mathbf{10^{8}} \begin{bmatrix} 0 & 0 & 0 & 0.0000 & 0 & 0 \\ 0 & 0 & 0 & 0 & 0.0000 & 0 \\ 0 & 0 & 0 & 0 & 0 & 0.0000 \\ -0.0044 & -0.0000 & 0.0000 & -0.0000 & -0.0000 & 0.0000 \\ -0.0000 & -0.1711 & -0.0000 & -0.0000 & -0.0000 & -0.0000 \\ 0.0000 & -0.0000 & -1.3169 & 0.0000 & -0.0000 & -0.0001 \end{bmatrix},$$

$$\mathbf{B_{15}} = \begin{bmatrix} 0 \\ 0 \\ 0 \\ -0.0002 \\ -0.0009 \\ 0.0017 \end{bmatrix},\; \mathbf{D_{15}} = 0,\; \mathbf{E_{15}} = \mathbf{10^{2}} \begin{bmatrix} 0 \\ 0 \\ 0 \\ 11.1571 \\ -11.0714 \\ -10.9550 \end{bmatrix},$$

$$\mathbf{C}_{15}^{T} = \begin{bmatrix} 0 & 0 & 0 & -0.2491 & -0.5758 & -0.5568 \end{bmatrix}.$$

Control of these developed SISO state space models of the smart beam with different aspect ratios is obtained using fast output sampling feedback control law which is discussed in the subsequent chapters [74].

2.2.1.4 Justification of the Use of Timoshenko Beam Theory

The state space representation of the cantilever beam with surface mounted sensor / actuator in Eqs. (2.85) and (2.86) for 3 vibratory modes is obtained by using 3 regular beam elements and 1 piezoelectric beam element placed at finite element position 2 as shown in Fig. 2.7(b). Different state space models of the system are obtained by varying the length to thickness ratio from 8 to 15. The length of the beam is kept constant at 20 cm and the thickness is varied to change the aspect ratio. The width of the beam is taken as 3 cm. The first 3 natural frequencies of the 3 SISO models in (2.176) - (2.178) were calculated and compared with the corresponding natural frequencies obtained using the Euler-Bernoulli beam model. Figs. 2.8 to 2.10 show the variation of the first 3 natural frequencies of both Timoshenko and Euler-Bernoulli beam models with change in the length to thickness ratio.

It is clear from Fig. 2.8 that the first natural frequency predicted by both the theories is almost the same. Since many modes contribute to a structure's response, it can be inferred from Figs. 2.9 and 2.10 that there is a large difference in the second and third natural frequencies predicted by Timoshenko and Euler-Bernoulli beam theories especially for small length to thickness ratios (aspect ratio < 10). Thus,

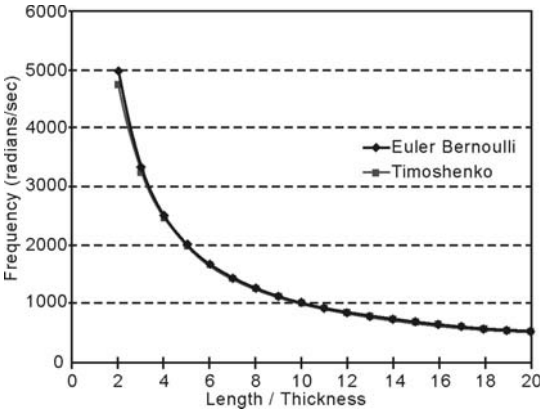

Fig. 2.8. Variation of first natural frequency with length / thickness ratio

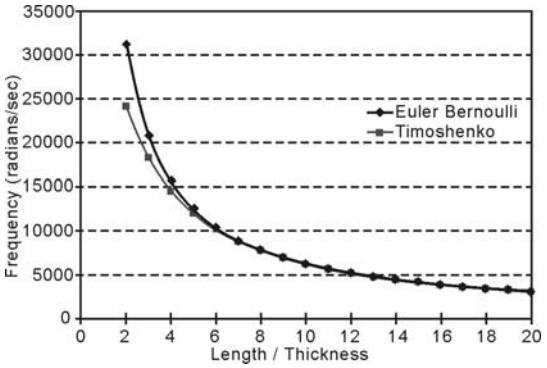

Fig. 2.9. Variation of second natural frequency with length / thickness ratio

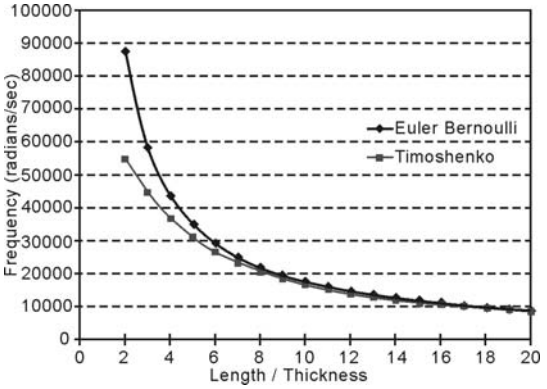

Fig. 2.10. Variation of third natural frequency with length / thickness ratio

the Timoshenko beam theory can predict the dynamic characteristics of the beam more accurately over the entire range of length by thickness ratio. Since Timoshenko beam model is closer to the actual model, it is used as the basis for controller design in our research work and the mathematical model obtained can be closer to an exact one.

2.2.2 Modeling of Smart Beams with Surface Mounted Sensors-Actuators for a MIMO Case

The dynamic equation of the smart structure, the multivariable state space model of the smart structure is also obtained on the similar lines as discussed in Section 2.1.2:1 and 2.1.2:2 for Euler-Bernoulli beams. Finally, the state state space model of the MIMO system with 2 inputs and 2 outputs is given by Eqs. (2.93) and (2.101) for 2 vibratory modes and Eqs. (2.103) and (2.104) for 3 vibratory modes with

$$\mathbf{A} = 1.0e+006 * \begin{bmatrix} 0 & 0 & 0.0000 & 0 \\ 0 & 0 & 0 & 0.0000 \\ -0.0306 & 0.0000 & -0.0000 & 0.0000 \\ 0.0000 & -1.1637 & 0.0000 & -0.0000 \end{bmatrix}, \ \mathbf{B} = \begin{bmatrix} 0 & 0 \\ 0 & 0 \\ -0.0015 & -0.0021 \\ 0.0018 & -0.0069 \end{bmatrix},$$

$$\mathbf{C}^T = \begin{bmatrix} 0 & 0 & -0.5283 & -3.2544 \\ 0 & 0 & -0.0364 & -1.1176 \end{bmatrix}, \ \mathbf{E} = \begin{bmatrix} 0 \\ 0 \\ 8.0789 \\ 7.9017 \end{bmatrix}, \tag{2.179}$$

$$\mathbf{D} = \text{a null matrix}$$

and

$$\mathbf{A} = 1.0e+006 * \begin{bmatrix} 0 & 0 & 0 & 0.0000 & 0 & 0 \\ 0 & 0 & 0 & 0 & 0.0000 & 0 \\ 0 & 0 & 0 & 0 & 0 & 0.0000 \\ -0.0306 & 0.0000 & 0.0000 & -0.0000 & 0.0000 & 0.0000 \\ 0.0000 & -1.1637 & -0.0000 & 0.0000 & -0.0000 & -0.0000 \\ 0.0000 & -0.0000 & -8.7691 & 0.0000 & -0.0000 & -0.0001 \end{bmatrix},$$

$$\mathbf{B} = \begin{bmatrix} 0 & 0 \\ 0 & 0 \\ 0 & 0 \\ -0.0015 & -0.0021 \\ 0.0018 & -0.0069 \\ 0.0040 & -0.0093 \end{bmatrix}, \ \mathbf{D} = 0, \ \begin{bmatrix} 0 \\ 0 \\ 0 \\ 8.0789 \\ 7.9017 \\ 7.6568 \end{bmatrix},$$

$$\mathbf{C}^T = \begin{bmatrix} 0 & 0 & 0 & -0.5283 & -3.2544 & 8.5826 \\ 0 & 0 & 0 & -0.0364 & -1.1176 & -6.5556 \end{bmatrix}. \tag{2.180}$$

By making 2 piezoelectric elements as active sensors / actuators at a time and by making other elements as regular beam elements, control of this MIMO state space model is obtained using various control techniques which is considered in the subsequent chapters. The characteristics of the smart cantilever beam as MIMO system are given in Tables 2.9 and 2.10 for 2 and 3 vibratory modes respectively.

Table 2.9. Characteristics of the smart Timoshenko beam with surface mounted sensor/actuator (2 inputs and 2 outputs)-2 modes

Position of sensor / actuator	Eigen values	Natural frequencies (Hz)
2, 4	$-0.12 \pm j\,24.74$	3.9369
	$-4.65 \pm j\,152.49$	24.2689

Table 2.10. Characteristics of the smart Timoshenko beam with surface mounted sensor/actuator (2 inputs and 2 outputs)-3 modes

Position of sensor / actuator	Eigen values	Natural frequencies (Hz)
	$-0.12 \pm j\,24.74$	3.9369
2, 4	$-4.65 \pm j\,152.49$	24.2689
	$-35.08 \pm j\,417.32$	66.4179

2.2.3 Modeling of Smart Timoshenko Cantilever Beam with Embedded Shear Sensors and Actuators as SISO and MIMO Systems

Many researchers have well established a mathematical finite element E-B model. These models do not consider the shear effects, axial effects, rotary inertia, etc.,. Modeling of embedded smart structures using shear deformable (Timoshenko) theory is limited. In this section, the effect of shear and axial displacement has been considered in the modeling [43] of sandwiched beams. A state space model of the smart beam with embedded shear sensors and actuators is presented in this context and its application in active vibration control is investigated [45].

Accurate model of the system is obtained when the shear effects and the axial displacement of the beam is considered in modeling of the smart structure [44]. Embedded shear sensors and actuators have been considered in this section instead of the surface mounted sensors and actuators for vibration suppression of beams because of lot of advantages over the latter since the surface bounded sensors and actuators are likely to be damaged by contact with the surrounding objects, environmental effects, stray noise pickups, thermal effects, magnetic fields, radio interference, etc., [30].

To overcome these problems, an adaptive sandwiched structure consisting of an axially poled piezoelectric core, sandwiched in between 2 thick aluminum beam layers can be used. Such actuators which are used in between the 2 beam layers are known as shear actuators. Once an electric field is applied to it, the piezoelectric will produce a shear deformation, which is the driving force for the transverse deflection of the structure.

2.2.3.1 Finite Element Modeling of the Sandwiched Beam Element

A sandwiched beam (piezo-laminated sandwiched beam) is shown in the Fig. 2.11 and consists of 3 layers, i.e., the piezo-patch with the rigid foam sandwiched in between two thick aluminum beam layers. The shear PZT layer functions as sensor or as actuator in the thickness shear mode. For shear actuation, rigid foam is introduced as a core along with PZT to obtain an equivalent sandwiched model.

The assumption made is that the middle layer is perfectly glued to the carrying structure and the thickness of the adhesive is neglected (thus, neglecting the effect of shear-lag, no slippage or delamination between the core layers during vibrations) as a result of which strong coupling exists between the master structure and the piezo-patches. The perfect bonding or the adhesive between the beam and the sensor / actuator and the bottom and top surfaces of the upper and lower aluminum beam have been assumed to add no mass or stiffness to the sensor / actuator.

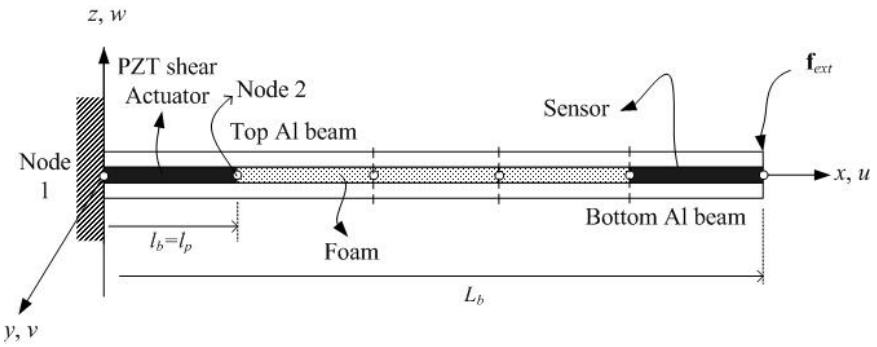

Fig. 2.11. The geometry of a 3 layered laminated beam with shear mode actuators and sensors and with the stacking sequence AL / PZT / AL

For the parts without piezoelectrics, the extra space at places where no piezoelectrics is present is being packed up fully with a non-structural material like rigid foam. There is strong coupling between the rigid foam and the structure. The beam is stacked properly and then used as a sandwiched structure for AVC. Thus, sandwich structures consisting of sheets and a relatively light-weight core such as honeycomb or rigid foam are highly efficient in producing bending and shear [32], [36].

In the modeling of the structure, the poling direction of the piezoelectric patch is done along the (axial) direction. The displacement field is based on a first order shear deformation theory. The element has constant moment of inertia, modulus of elasticity, mass density and length. The cable capacitance between sensor and signal-conditioning device has been considered negligible and the temperature effects have been neglected. The signal conditioning device gain is assumed as 100.

Consider a 2 node beam element as shown in Fig. 2.11. The longitudinal axis of the sandwiched beam element lies along the x-axis and the beam is subjected to vibrations in the $x-z$ plane. The beam element is assumed to have three structural DOF, viz., w, θ and u at each node, where w is the transverse displacement, θ is the bending rotation and u is the axial displacement of the node. A bending moment and

Table 2.11. Properties of the aluminum cantilever Timoshenko beam

Parameter (with units)	**Symbols**	**Numerical Values**
Length (cm)	L_b	20
Width (cm)	b	2
Thickness of the top layer and bottom aluminum beam layers (mm)	t_b	1
Young's Modulus (GPa)	E_b	193.06
Density (Kg/m^3)	ρ_b	8030
Damping Constants	α, β	$0.001, 0.0001$

Table 2.12. Properties of the piezoelectric shear sensor and actuator when the beam is divided into 5 FE

Parameter (with units)	**Symbols**	**Numerical Values**
Length (cm)	l_p	4
Width (cm)	c	2
Thickness (mm)	t_a, t_s	1
Young's Modulus (GPa)	E_p	84.1
Density (Kg/m^3)	ρ_p	7900
Piezoelectric strain constant (m/V)	d_{31}	-274.8×10^{-12}

a transverse shear force acts at each nodal point. The slope of the beam $\phi(x)$ consists of 2 parts, viz., $\frac{dw}{dx}$, the bending slope and the other, additional shear deformation angle $\gamma(x)$. An additional DOF, called as the electrical DOF (sensor voltage) comes into picture. Since the voltage is constant over the electrode, the number of electrical DOF is one for each element.

The equations of motion of a general piezo-laminated composite beam is obtained as follows [30], [43], [45]. The displacements of the beam $u(x)$ and $w(x)$ can be written as

$$u(x,z) = u_0(x) + z\theta(x,t), \qquad w(x,z) = w_0(x), \tag{2.181}$$

where $u_0(x)$ and $w_0(x)$ are the axial and transverse displacements of the point at the mid-plane assuming that there is incompressibility in the z direction and $\theta(x)$ is the bending rotation of the normal to the mid-plane, i.e., rotation of the beam about the y axis [104]. The strain components of the beam are given as

$$\varepsilon_x = \frac{\partial u_0}{\partial x} + z\frac{\partial \theta}{\partial x}, \quad \varepsilon_z = 0, \quad \gamma_{xz} = \frac{\partial u}{\partial x} + \frac{\partial w_0}{\partial x} = \left(\theta + \frac{\partial w_0}{\partial x}\right), \tag{2.182}$$

where ε_x, ε_z are the mechanical normal strain and transverse shear strain, γ_{xz} being the shear strain induced in the piezoelectric layer. The beam constitutive equations can be written as

$$\begin{bmatrix} N_x \\ M_x \\ Q_{xz} \end{bmatrix} = \begin{bmatrix} A_{11} & B_{11} & 0 \\ B_{11} & D_{11} & 0 \\ 0 & 0 & A_{55} \end{bmatrix} \begin{bmatrix} \frac{\partial u_0}{\partial x} \\ \frac{\partial \theta}{\partial x} \\ \theta + \frac{\partial w_0}{\partial x} \end{bmatrix} - \begin{bmatrix} E_{11} \\ F_{11} \\ G_{55} \end{bmatrix}, \tag{2.183}$$

where

$$N_x = \int_{-h/2}^{h/2} c\,\sigma_x\,dz, \quad M_x = \int_{-h/2}^{h/2} c\,\sigma_x\,z\,dz, \quad Q_{xz} = \int_{-h/2}^{h/2} c\,\tau_{xz}\,dz. \tag{2.184}$$

Here, $\sigma_x = \overline{Q}_{11}\varepsilon_x$ and $\tau_{xz} = \overline{Q}_{55}\gamma_{xz}$ are the normal and shear stresses respectively and c is the width of the beam. z is the depth of the material point measured from the beam reference plane along the vertical axis. h is the height of the beam + piezo patch, i.e., the thickness of the total structure which includes t_b, t_a, t_s, (thickness of the beam, thickness of the actuator and thickness of the sensor). N_x, M_x, Q_{xz} are the internal forces acting on the cross section of the beam and are the axial force, bending moment and the shear force respectively. A_{11}, B_{11}, D_{11} and A_{55} are the extensional, bending-extensional, bending and transverse shear stiffness coefficients. These are defined according to the lamination theory of composites [30], [43] as

$$A_{11} = c\sum_{k=1}^{N} \left(\overline{Q}_{11}\right)_k (z_k - z_{k-1}), \qquad B_{11} = \frac{c}{2}\sum_{k=1}^{N} \left(\overline{Q}_{11}\right)_k \left(z_k^2 - z_{k-1}^2\right), \tag{2.185}$$

$$D_{11} = \frac{c}{3}\sum_{k=1}^{N} \left(\overline{Q}_{11}\right)_k \left(z_k^3 - z_{k-1}^3\right), \qquad A_{55} = c\,\mathbb{K}\sum_{k=1}^{N} \left(\overline{Q}_{55}\right)_k (z_k - z_{k-1}). \tag{2.186}$$

Here, in Eqs. (2.185) and (2.186), z_k is the distance of the k^{th} layer from the x-axis, N is the number of layers, $\mathbb{K}$ is the shear correction factor, usually taken equal to $\frac{5}{6}$ and $\overline{Q}_{11}$, $\overline{Q}_{55}$ are calculated [113] according to the equations using the material properties of the piezoelectric material as given by [30], [43]

$$\overline{Q}_{11} = Q_{11}cos^4\lambda + Q_{22}sin^4\lambda + 2\,(Q_{12} + 1Q_{66})\,sin^2\lambda\,cos^2\lambda, \tag{2.187}$$

$$\overline{Q}_{55} = G_{13}cos^2\lambda + G_{23}sin^2\lambda. \tag{2.188}$$

The angle λ is the angle between the fiber direction and the longitudinal axis of the beam. The material constants Q_{11}, Q_{22}, Q_{12}, Q_{66}, Q_{13} and Q_{23} for foam, aluminum and piezoelectric material are calculated using the formulas given in the Appendix II. These constants are used to calculate the values of A_{11}, B_{11}, D_{11} and A_{55} using Eqs. (2.185) to (2.188). E_{11}, F_{11} and G_{55} in Eq. (2.183) are the actuator induced piezoelectric axial force, bending moment due to the constrained actuators and the shear force respectively, defined [30], [43] as

$$E_{11} = c\sum_{k=1}^{N_a} \left(\overline{Q}_{11}\right)_k^a V^k(x,t)\,d_{31}^k, \tag{2.189}$$

$$F_{11} = \frac{c}{2}\sum_{k=1}^{N_a} \left(\overline{Q}_{11}\right)_k^a V^k(x,t)\,d_{31}^k\,\left(z_{k+}^a - z_{k-}^a\right), \tag{2.190}$$

$$G_{55} = c\,\mathbb{K}\sum_{k=1}^{N_a}\left(\overline{Q}_{55}\right)_k^a\, V^k(x,t)\, d_{15}^k. \tag{2.191}$$

Since the piezoelectric layer is poled in the axial direction, $E_{11} = F_{11} = 0$. $V^k(x,t)$ is the applied voltage to the k^{th} actuator having a thickness of $(z_{k+}^a - z_{k-}^a)$ and d_{31}^k, d_{15}^k are the piezoelectric constants. $\left(\overline{Q}_{11}\right)_k^a$ and $\left(\overline{Q}_{55}\right)_k^a$ are the coefficients of the actuators calculated using the Eqs. (2.187) and (2.188) and using the material properties of the piezoelectric material. N_a is the number of actuators, where 'a' stands for w.r.t. 'actuator'. Using the Hamilton's principle (total strain energy is equal to the sum of the change in the kinetic energy + the work done due to the external forces, we get

$$\delta\Pi = \int_{t_1}^{t_2}\int_{0}^{l_b}\left(\delta U - \delta T + \delta W\right)\, dx\, dt, \tag{2.192}$$

where T is the kinetic energy, U is the strain energy, W is the external work done, l_b is the length of the beam element and t is the time.

The strain energy U of the beam element is given by

$$\delta U = N_x\left(\frac{\partial\,\delta U}{\partial x}\right) + M_x\left(\frac{\partial\,\delta\theta}{\partial x}\right) + Q_{xz}\left(\theta + \frac{\partial\,\delta w}{\partial x}\right). \tag{2.193}$$

The kinetic energy of the beam element is given by

$$\delta T = \left(I_1\dot{u} + I_2\dot{\theta}\right)\,\partial\dot{u} + I_1\dot{w}\,\partial\dot{w} + \left(I_2\dot{u} + I_3\dot{\theta}\right)\,\partial\dot{\theta}. \tag{2.194}$$

The external work done (i.e., force $\times$ displacement) is given by

$$\delta W = q_0\,\delta w, \tag{2.195}$$

where q_0 is the transverse distributed loading, which is nothing but the external force $\mathbf{f}_{ext}$ applied to the beam at its free end.

Here, in Eq. (2.194), I_1, I_2 and I_3 are the mass inertia characteristics [114] of the cross-section of the beam defined as

$$I_1 = c\int_{-h/2}^{h/2}\rho_b\, dz, \qquad I_2 = c\int_{-h/2}^{h/2} z\,\rho_b\, dz, \qquad I_3 = c\int_{-h/2}^{h/2} z^2\,\rho_b\, dz \tag{2.196}$$

or

$$(I_1,\ I_2,\ I_3) = c\int_{-h_1}^{h_2}\rho_b\ \left(1,\ z,\ z^2\right)\ dz, \tag{2.197}$$

where ρ_b is the mass density of each layer.

Substituting the values of strain energy, kinetic energy and external work done from Eqs. (2.193), (2.194) and (2.195) into Eq. (2.192), we get the governing equation of motion of a general shaped non-symmetric piezo-laminated beam with shear deformation and rotary inertia according to the first order shear deformation theory as

$$\frac{\partial}{\partial x}\left(A_{11}\frac{\partial u}{\partial x} + B_{11}\frac{\partial\theta}{\partial x} + E_{11}\right) = \frac{\partial}{\partial t}\left[I_1\dot{u} + I_2\dot{\theta}\right], \tag{2.198}$$

$$\frac{\partial}{\partial x}\left\{A_{55}\left(\theta+\frac{\partial w}{\partial x}\right)+G_{55}-P\frac{\partial w}{\partial x}\right\}=\frac{\partial}{\partial t}\left[I_1\dot{w}+q_0\right], \tag{2.199}$$

$$\frac{\partial}{\partial x}\left(B_{11}\frac{\partial u}{\partial x}+D_{11}\frac{\partial \theta}{\partial x}+F_{11}\right)-A_{55}\left(\theta+\frac{\partial w}{\partial x}\right)-G_{55}=\frac{\partial}{\partial t}\left[I_2\dot{u}+I_3\dot{\theta}\right], \tag{2.200}$$

which becomes

$$\frac{\partial}{\partial x}\left(A_{11}\frac{\partial u}{\partial x}+B_{11}\frac{\partial \theta}{\partial x}\right)=0, \tag{2.201}$$

$$\frac{\partial}{\partial x}\left\{A_{55}\left(\theta+\frac{\partial w}{\partial x}\right)\right\}=0, \tag{2.202}$$

$$\frac{\partial}{\partial x}\left(B_{11}\frac{\partial u}{\partial x}+D_{11}\frac{\partial \theta}{\partial x}+F_{11}\right)-A_{55}\left(\theta+\frac{\partial w}{\partial x}\right)-G_{55}=0, \tag{2.203}$$

for a static case and with constant properties of the beam. To facilitate the solution process for the coupled equations in Eqs. (2.201)-(2.203), the beam stiffness A_{55} and D_{11} are assumed to be uniform and constant throughout the length of the beam [30], [43], [44], [45].

Note that the influence of shear-induced strains appears in the above-coupled equations of motion for constant properties in the top and bottom layers of the embedded aluminum beam [115]. Let

$$w=a_1+a_2x+a_3x^2+a_4x^3, \tag{2.204}$$

$$\theta=b_1+b_2x+b_3x^2, \tag{2.205}$$

$$u=c_1+c_2x+c_3x^2, \tag{2.206}$$

be the solutions of the Eqs. (2.201)-(2.203) where and a_i, b_j and c_j's are the unknown coefficients $(i=1,..,4)$ and $(j=1,2,3)$ subject to the boundary conditions

$$\begin{array}{l} x=0,\ w=w_1,\ \theta=\theta_1,\ u=u_1,\\ x=l_b,\ w=w_2,\ \theta=\theta_2,\ u=u_2, \end{array} \tag{2.207}$$

where x is the local axial coordinate of the element. After applying boundary conditions from Eq. (2.207) into Eqs. (2.204)-(2.206), the unknown coefficients a_i, b_j and c_j's can be resolved. Since the axial displacement of a point not on the centerline is a linear function of θ as well as u, the degree of the polynomial used for θ must be the same as that used for u.

Consequently, the degree of the polynomial used for w must be one order higher than those used for u and θ in order to ensure compatibility. Therefore, the cubic polynomial used for the displacement w requires that quadratic functions be used for both axial displacement u and cross section rotation θ in order to be consistent [116]. Then, substituting the found out unknown coefficients into Eqs. (2.204)-(2.206) and writing them in matrix form, we get the expression for the axial displacement, transverse displacement and the bending rotation in terms of nodal displacements and shape functions as [117]

$$[u]=[N_u]\begin{bmatrix} u_1\\ w_1\\ \theta_1\\ u_2\\ w_2\\ \theta_2 \end{bmatrix},\qquad [w]=[N_w]\begin{bmatrix} u_1\\ w_1\\ \theta_1\\ u_2\\ w_2\\ \theta_2 \end{bmatrix},\qquad [\theta]=[N_\theta]\begin{bmatrix} u_1\\ w_1\\ \theta_1\\ u_2\\ w_2\\ \theta_2 \end{bmatrix}, \tag{2.208}$$

where $[N_w]$, $[N_w]$, $[N_\theta]$ are the mode shape functions due to the axial displacement, transverse displacement and due to the rotation or the slope, which are defined as

$$[N_u] = \begin{bmatrix} N_1 & N_2 & N_3 & N_4 & N_5 & N_6 \end{bmatrix}, \tag{2.209}$$

$$[N_w] = \begin{bmatrix} N_7 & N_8 & N_9 & N_{10} \end{bmatrix}, \tag{2.210}$$

$$[N_\theta] = \begin{bmatrix} N_{11} & N_{12} & N_{13} & N_{14} \end{bmatrix}. \tag{2.211}$$

The elements of the shape functions in (2.209)-(2.211) are given in Appendix III. Writing the 3 shape functions N_u, N_w and N_θ in matrix form, we get the relation between the vector of inertial forces $\mathbb{N}$ and the vector of nodal displacements $\mathbf{q}$ (displacement field) as $[\mathbb{N}] = [S]\,[\mathbf{q}]$ which is given by

$$\mathbb{N} = \begin{bmatrix} N_1 & N_2 & N_3 & N_4 & N_5 & N_6 \\ 0 & N_7 & N_8 & 0 & N_9 & N_{10} \\ 0 & N_{11} & N_{12} & 0 & N_{13} & N_{14} \end{bmatrix} \begin{bmatrix} u_1 \\ w_1 \\ \theta_1 \\ u_2 \\ w_2 \\ \theta_2 \end{bmatrix}. \tag{2.212}$$

The mass matrix of the regular beam element is given by

$$\left[M^b\right] = \int_0^{l_b} [\mathbb{N}]^T [I] [\mathbb{N}]\, dx, \tag{2.213}$$

where

$$I = \begin{bmatrix} I_1 & 0 & I_2 \\ 0 & I_1 & 0 \\ I_2 & 0 & I_3 \end{bmatrix} \tag{2.214}$$

is the inertia matrix and I_1, I_2, I_3 is given by Eqs. (2.196) and (2.197). The elemental mass matrix is given by [24]

$$\left[M^b\right] = \begin{bmatrix} M_{11} & M_{12} & M_{13} & M_{14} & M_{15} & M_{16} \\ M_{21} & M_{22} & M_{23} & M_{24} & M_{25} & M_{26} \\ M_{31} & M_{32} & M_{33} & M_{34} & M_{35} & M_{36} \\ M_{41} & M_{42} & M_{43} & M_{44} & M_{45} & M_{46} \\ M_{51} & M_{52} & M_{53} & M_{54} & M_{55} & M_{56} \\ M_{61} & M_{62} & M_{63} & M_{64} & M_{65} & M_{66} \end{bmatrix}. \tag{2.215}$$

Here, $\left[M^b\right]$ is a symmetric matrix called as the local mass matrix of size (6×6), i.e., the mass matrix of the small finite element [24], [118], [119]. The coefficients of the mass matrix are given in Appendix I.

The stiffness matrix of the regular beam element is given by

$$\left[K^b\right] = \int_0^{l_b} [B]^T [D] [B]\, A_b\, dx, \tag{2.216}$$

where A_b is the area of cross section of the beam element and

$$[B] = \frac{d[N]}{dx}, \qquad D = \begin{bmatrix} A_{11} & B_{11} & 0 \\ B_{11} & B_{11} & 0 \\ 0 & 0 & A_{55} \end{bmatrix}. \tag{2.217}$$

The stiffness matrix after further simplifying Eq. (2.216) is given by [24]

$$\left[K^b\right] = \begin{bmatrix} K_{11} & K_{12} & K_{13} & K_{14} & K_{15} & K_{16} \\ K_{21} & K_{22} & K_{23} & K_{24} & K_{25} & K_{26} \\ K_{31} & K_{32} & K_{33} & K_{34} & K_{35} & K_{36} \\ K_{41} & K_{42} & K_{43} & K_{44} & K_{45} & K_{46} \\ K_{51} & K_{52} & K_{53} & K_{54} & K_{55} & K_{56} \\ K_{61} & K_{62} & K_{63} & K_{64} & K_{65} & K_{66} \end{bmatrix}. \tag{2.218}$$

Here, $\left[K^b\right]$ is a symmetric matrix called as the local stiffness matrix [24], [118], [119] of size (6×6), whose coefficients are given in Appendix I. The mass M^b and stiffness matrix K^b of the regular beam element are obtained using foam as the core between two facing thick aluminum layers. The mass and stiffness matrices of the piezoelectric beam element are obtained on the similar lines as discussed in the previous paragraphs and in Sections 2.2.1:2 by using a shear piezoelectric patch between two facing thick aluminum layers as shown in Fig. 2.11 using the equations $M = M^p + 2M^b$ and $K = K^p + 2K^b$.

2.2.3.2 Sensor and Actuator Equations

In this Section, modeling of the shear sensor and actuator is presented.

Sensor equation

When a force acts upon a piezoelectric material, electric field is produced [3], [6]. This effect, which is called as the direct piezoelectric effect, is used to calculate the output charge produced by the strain in the structure. The external field produced by the sensor is directly proportional to the strain rate. The charge $q(t)$ accumulated on the piezoelectric sensor surfaces is given by the gauss law as

$$q(t) = \int\int_A D_3 \, dA, \tag{2.219}$$

where D_3 is the electric displacement in the thickness direction and A area of the shear PZT patches. If the poling is done along the axial direction of the sensors with the electrodes on the upper and lower surfaces, the electric displacement is given by

$$D_3 = \overline{Q}_{55} d_{15} \gamma_{xz} = e_{15} \gamma_{xz}, \tag{2.220}$$

Using Eq. (2.220) in (2.219) and further simplifying gives

$$q(t) = \int_A e_{15} \left(\theta + \frac{\partial w_0}{\partial x}\right) dA, \tag{2.221}$$

where e_{15} is the piezoelectric constant. On solving Eq. (2.221), we get

$$q(t) = e_{15} c \frac{6\eta}{-12\eta + l_p^2} \begin{bmatrix} 0 & 2 & -l_p & 0 & -2 & -l_p \end{bmatrix} \begin{bmatrix} u_1 \\ w_1 \\ \theta_1 \\ u_2 \\ w_2 \\ \theta_2 \end{bmatrix}. \tag{2.222}$$

Here, $\begin{bmatrix} u_1 \\ w_1 \\ \theta_1 \\ u_2 \\ w_2 \\ \theta_2 \end{bmatrix} = \mathbf{q}$ is the vector of nodal displacements, i.e., the vector of axial displacement, transverse displacement and slopes at node 1 and node 2 respectively. The current induced by the sensor surface is obtained by differentiating the total charge accumulated on the sensor surface and is given by

$$i(t) = \frac{d\, q(t)}{dt} \tag{2.223}$$

or

$$i(t) = e_{15} c \frac{6\eta}{-12\eta + l_p^2} \begin{bmatrix} 0 & 2 & -l_p & 0 & -2 & -l_p \end{bmatrix} \begin{bmatrix} \dot{u}_1 \\ \dot{w}_1 \\ \dot{\theta}_1 \\ \dot{u}_2 \\ \dot{w}_2 \\ \dot{\theta}_2 \end{bmatrix}. \tag{2.224}$$

i.e.,

$$i(t) = e_{15} c \frac{6\eta}{-12\eta + l_p^2} \begin{bmatrix} 0 & 2 & -l_p & 0 & -2 & -l_p \end{bmatrix} \dot{\mathbf{q}}. \tag{2.225}$$

Since the PE sensor is used as a strain rate sensor, this current can be converted into the open circuit sensor voltage $V^s(t)$ using a signal-conditioning device with a gain of G_c and applied to the actuator with the controller gain as

$$V^s(t) = G_c\, i(t), \tag{2.226}$$

$$V^s(t) = e_{15} c \frac{6\eta}{-12\eta + l_p^2} G_c \begin{bmatrix} 0 & 2 & -l_p & 0 & -2 & -l_p \end{bmatrix} [\mathbf{q}], \tag{2.227}$$

$$V^s(t) = \mathbf{p}^T \dot{\mathbf{q}}, \tag{2.228}$$

where $\dot{\mathbf{q}}$ is the time derivative of the nodal coordinate vector (strain rate) and $\mathbf{p}^T$ is a constant vector of size (1×6) for a 2 node beam element which depends on the type of sensor, its characteristics and its finite element location in the embedded structure and is given by

$$\frac{6\,\eta\, e_{15}\, c\, G_c}{-12\eta + l_p^2} \begin{bmatrix} 0 & 2 & -l_p & 0 & -2 & -l_p \end{bmatrix}. \tag{2.229}$$

The input voltage to the actuator is $V^a(t)$ and is given by

$$V^a(t) = \text{Controller gain} \times V^s(t), \tag{2.230}$$

$$V^a(t) = \text{Controller gain} \times \frac{6\ \eta\ e_{15}\ c\, G_c}{(-12\eta + l_p^2)} \begin{bmatrix} 0 & 2 & -l_p & 0 & -2 & -l_p \end{bmatrix} \dot{\mathbf{q}}, \tag{2.231}$$

Note that the sensor output voltage is a function of the second spatial derivative of the mode shape.

Actuator equation

The strain produced in the piezoelectric layer is directly proportional to the electric potential applied to the layer and is given by [3], [6]

$$\gamma_{xz} \propto E_f, \tag{2.232}$$

where γ_{xz} is the shear strain in the piezoelectric layer and E_f is the electric potential applied to the actuator, which is given by $E_f = \frac{V_a}{t_p}$, where t_p is the thickness of the shear PZT layer. Removing the constant of proportionality in Eq. (2.232), we get

$$\gamma_{xz} = d_{15}\, E_f. \tag{2.233}$$

Since the ratio of shear stress to shear strain is the modulus of rigidity $\mathbb{G}$, the shear stress is given by

$$\tau_{xz} = \mathbb{G}\, \gamma_{xz}. \tag{2.234}$$

Substituting the value of γ_{xz} from Eq. (2.233) into Eq. (2.234), we get

$$\tau_{xz} = \mathbb{G}\, d_{15}\, E_f. \tag{2.235}$$

Thus,

$$\tau_{xz} = \mathbb{G}\, d_{15}\, \frac{V^a}{t_p}. \tag{2.236}$$

Because of this stress, bending moments are induced in the beam at the nodes. The resultant moment M_a acting on the beam element is determined by integrating the stress throughout the structure thickness in Eq. (2.236). Finally, the resultant bending moment after simplification is given by

$$M_a = \mathbb{G}\, d_{15}\, V^a(t)\, \overline{h} = \mathbb{G}\, d_{15}\, K_c\, \mathbf{p}^T\, \dot{\mathbf{q}}\, \overline{h}, \tag{2.237}$$

where $\overline{h} = \left(\frac{t_a + t_b}{2}\right)$ is the distance from the neutral axis of the beam and the piezoelectric layer. The control force $\mathbf{f}_{ctrl}$ produced by the actuator that is applied on the beam elements is obtained by using Eq. (2.237) as

$$\mathbf{f}_{ctrl} = \mathbb{G}\, d_{15}\, \overline{h} \int_0^{l_p} N_\theta\, dx\, V^a(t) \tag{2.238}$$

or can be expressed as

$$\mathbf{f}_{ctrl} = \mathbf{h}\, V^a(t), \tag{2.239}$$

where $\mathbf{h}$ is a constant vector of size (6×1) for a 2 node beam element and depends on the type of actuator and its finite element location in the embedded structure and d_{15} is the piezoelectric strain constant. If any external forces described by the vector $\mathbf{f}_{ext}$ are acting then, the total force vector becomes

$$\mathbf{f}^t = \mathbf{f}_{ext} + \mathbf{f}_{ctrl}. \tag{2.240}$$

2.2.3.3 Dynamic Equation and the State Space Model of the Smart Structure for a SISO Case

So far, we have discussed the mass and stiffness of regular beam elements and that of the piezoelectric beam elements, which are called as the local matrices. Now, to obtain the equation of motion of the entire structure, consider the Fig. 2.12 in which the beam is divided into 5 FE and the shear actuator is placed at FE 1 whereas the sensor is placed at FE position 4. The dynamic equation of the embedded smart structure model (1 input and 1 output) is derived on the similar lines as explained in Section 2.1.1:5 by considering the the first 3 vibratory modes [76] and is given by

$$\mathbf{M}^*\ddot{\mathbf{g}} + \mathbf{C}^*\dot{\mathbf{g}} + \mathbf{K}^*\mathbf{g} = \mathbf{f}^*_{ext} + \mathbf{f}^*_{ctrl}, \tag{2.241}$$

where the generalized matrices (mass, stiffness, structural damping) are of size (3×3) and the force vectors $\mathbf{f}^*_{ext}$ and $\mathbf{f}^*_{ctrl}$ of sizes (3×1). The state space model is also obtained on the similar lines as explained in Section 2.1.1:6(II) and is given by

$$\begin{bmatrix} \dot{x}_1 \\ \dot{x}_2 \\ \dot{x}_3 \\ \dot{x}_4 \\ \dot{x}_5 \\ \dot{x}_6 \end{bmatrix} = \begin{bmatrix} 0 & I \\ -\mathbf{M}^{*-1}\mathbf{K}^* & -\mathbf{M}^{*-1}\mathbf{C}^* \end{bmatrix} \begin{bmatrix} x_1 \\ x_2 \\ x_3 \\ x_4 \\ x_5 \\ x_6 \end{bmatrix} + \begin{bmatrix} 0 \\ \mathbf{M}^{*-1}\mathbf{T}^T\mathbf{h} \end{bmatrix} u(t) + \begin{bmatrix} 0 \\ \mathbf{M}^{*-1}\mathbf{T}^T\mathbf{f} \end{bmatrix} r(t) \tag{2.242}$$

and

$$y(t) = \begin{bmatrix} 0 & \mathbf{p}^T\,\mathbf{T} \end{bmatrix} \begin{bmatrix} x_1 \\ x_2 \\ x_3 \\ x_4 \\ x_5 \\ x_6 \end{bmatrix}, \tag{2.243}$$

where the modal matrix $\mathbf{T}$ is of size (30×3) and the constant vectors $\mathbf{p}^T$, $\mathbf{h}$ are of sizes (1×30), (30×1) and the force vector $\mathbf{f}$ of size (30×1) respectively.

The two equations (2.242) and (2.243) can be written in compact form as

$$\dot{\mathbf{x}} = A\mathbf{x}(t) + B\mathbf{u}(t) + Er(t), \quad y(t) = \mathbf{C}^T\,\mathbf{x}(t) \,+\, \mathbf{D}\,\mathbf{u}(t), \tag{2.244}$$

where the state space matrices $\mathbf{A}$, $\mathbf{B}$, $\mathbf{C}$, $\mathbf{D}$, $\mathbf{E}$ are of sizes (6×6), (6×1), (1×6), Null matrix and (6×1). A cantilever beam of suitable dimensions as shown in Tables 2.11 and 2.12 is considered. The beam is divided into 5 FE and shear PZT's are embedded into the sandwiched structure as sensor / actuator [75], [76] at only one discrete location as non-collocated pair.

The actuator is sandwiched in between the 2 aluminum beam layers at finite element position 1 and the sensor is moved from the second position to the fifth position, thus giving rise to 4 SISO models of the same plant as shown in Figs. (2.12)(a)-(d). These models are obtained using the theory of piezoelectric bonding, the Timoshenko beam theory, FEM technique and the state space techniques by considering the first 3 vibratory modes ω_1, ω_2 and ω_3 [30], [43], [45]. An external force input $\mathbf{f}_{ext}$ is applied at the free end of the beam for all the 4 SISO models of the smart structure plant. There are 2 inputs to the plant. One is the external force

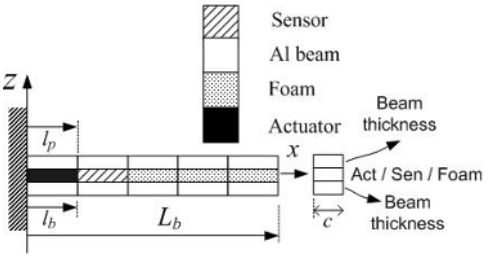

(a) Smart composite beam with actuator at FE 1, sensor at 2

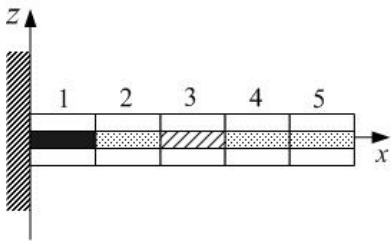

(b) Smart composite beam with actuator at FE 1, sensor at 3

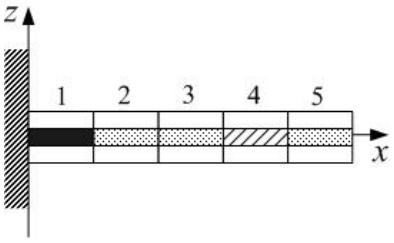

(c) Smart composite beam with actuator at FE 1, sensor at 4

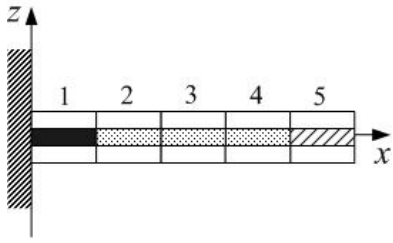

(d) Smart composite beam with actuator at FE 1, sensor at 5

Fig. 2.12. Smart sandwiched embedded Timoshenko beam divided into 5 finite elements (piezo-patch placed at positions 1, 2, 3 and 4) - 4 SISO models

input $\mathbf{f}_{ext}$, which is taken as a load matrix of 1 unit in the simulation. The other input is the control input u to the actuator from the controller.

The values of the **A**, **B**, **C**, **D**, **E** matrices for the model 1 with actuator at FE 1 and sensor at FE 2 of the smart beam as shown in Fig. 2.12(a) is given by

$$\mathbf{A} = 1\,e5 \begin{bmatrix} 0 & 0 & 0 & 0.00001 & 0 & 0 \\ 0 & 0 & 0 & 0 & 0.00001 & 0 \\ 0 & 0 & 0 & 0 & 0 & 0.00001 \\ -1.06 & -0.00 & 0.00 & -0.00 & -0.00 & 0.00 \\ -0.00 & -3.73 & 0.00 & -0.00 & -0.00 & -0.00 \\ 0.00 & -0.00 & -8.39 & 0.00 & -0.00 & -0.0001 \end{bmatrix}, \quad \mathbf{E} = \begin{bmatrix} 0 \\ 0 \\ 0 \\ -4.9470 \\ 0.0000 \\ 1.5310 \end{bmatrix},$$

$$\mathbf{D} = \text{Null matrix}, \ \mathbf{B} = 1e-4 \begin{bmatrix} 0 \\ 0 \\ 0 \\ 0.2346 \\ -0.0000 \\ -0.8647 \end{bmatrix}, \tag{2.245}$$

$$\mathbf{C}^T = \begin{bmatrix} 0 & 0 & 0 & -0.0001 & 0.0000 & 0.0014 \end{bmatrix}.$$

The characteristics of the smart cantilever beam with embedded non-collocated sensor and actuator as SISO system is given in Table 2.13. Similarly, the state space

Table 2.13. Characteristics of smart embedded beam as a SISO system - Model 1

Eigen values	Natural frequencies (Hz)
$-0.5344 \pm j\,326.92$	52.0312
$-1.8648 \pm j\,610.71$	97.1970
$-4.1968 \pm j\,916.16$	145.8111

models of the remaining 3 models and their characteristics are obtained. By making one pair of piezoelectric elements as non-collocated active sensors / actuator at a time and by making other elements as regular elements, control of these 4 SISO state space models are obtained using various types of control laws which are considered in the subsequent Chapters.

2.2.3.4 Dynamic Equation and the State Space Model of the Smart Structure for a MIMO Case

The dynamic equation of the MIMO model for the embedded case with 2 inputs and 2 outputs is derived on the similar lines as explained in section 2.1.2:1 and is given by

$$\mathbf{M}^*\ddot{\mathbf{g}} + \mathbf{C}^*\dot{\mathbf{g}} + \mathbf{K}^*\mathbf{g} = \mathbf{f}^*_{ext} + \mathbf{f}^*_{ctrl\,1} + +\mathbf{f}^*_{ctrl\,2}, \tag{2.246}$$

where the generalized matrices (mass, stiffness, structural damping) are of size (3×3) and the force vectors $\mathbf{f}^*_{ext}$ and $\mathbf{f}^*_{ctrl\ i}$ of sizes (3×1). The state space model is also obtained on the similar lines as explained in section 2.1.2:2 for 3 vibratory modes and is given by

$$\begin{bmatrix} \dot{x}_1 \\ \dot{x}_2 \\ \dot{x}_3 \\ \dot{x}_4 \\ \dot{x}_5 \\ \dot{x}_6 \end{bmatrix} = \begin{bmatrix} 0 & I \\ -\mathbf{M}^{*-1}\mathbf{K}^* & -\mathbf{M}^{*-1}\mathbf{C}^* \end{bmatrix}_{(6\times6)} \begin{bmatrix} x_1 \\ x_2 \\ x_3 \\ x_4 \\ x_5 \\ x_6 \end{bmatrix}$$

$$+\begin{bmatrix} 0 & 0 \\ \mathbf{M}^{*-1}\mathbf{T}^T\mathbf{h}_1 & \mathbf{M}^{*-1}\mathbf{T}^T\mathbf{h}_2 \end{bmatrix}_{(6\times2)} \begin{bmatrix} u_1 \\ u_2 \end{bmatrix} + \begin{bmatrix} 0 \\ \mathbf{M}^{*-1}\mathbf{T}^T\mathbf{f} \end{bmatrix}_{(6\times1)} r(t), \tag{2.247}$$

and

$$\begin{bmatrix} y_1 \\ y_2 \end{bmatrix} = \begin{bmatrix} 0 & \mathbf{p}_1^T\,\mathbf{T} \\ 0 & \mathbf{p}_2^T\,\mathbf{T} \end{bmatrix}_{(2\times6)} \begin{bmatrix} x_1 \\ x_2 \\ x_3 \\ x_4 \\ x_5 \\ x_6 \end{bmatrix}, \tag{2.248}$$

where the modal matrix $\mathbf{T}$ is of size (30×3) and the constant vectors $\mathbf{p}_i^T$, $\mathbf{h}_i$ are of sizes (1×30), (30×1) and the force vector $\mathbf{f}$ of size (30×1) respectively.

The two equations (2.247) and (2.248) can be written in compact form as

$$\dot{\mathbf{x}} = \mathbf{A}\mathbf{x}(t) + \mathbf{B}\mathbf{u}(t) + \mathbf{E}r(t), \quad y(t) = \mathbf{C}^T\,\mathbf{x}(t) + \mathbf{D}\,\mathbf{u}(t), \tag{2.249}$$

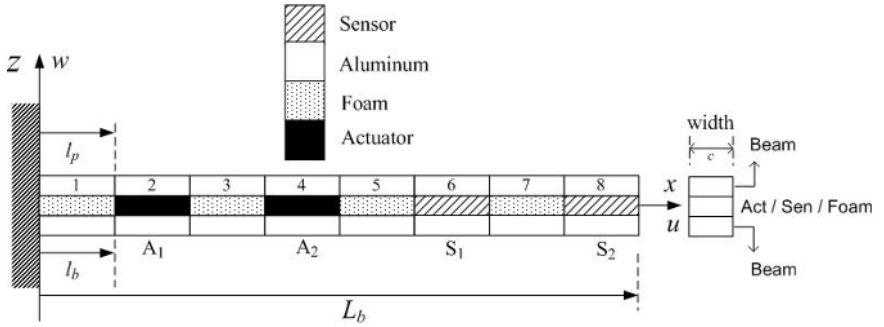

Fig. 2.13. A smart sandwiched embedded beam as a MIMO system with 2 inputs and outputs

where the state space matrices **A**, **B**, **C**, **D**, **E** are of sizes (6×6), (6×2), (2×6), Null matrix and (6×1).

A cantilever beam of suitable dimensions as given in Table 2.11 along with the PZT properties in Table 2.12 is considered. The beam is divided into 8 finite elements and shear PZT's are embedded into the master structure as sensors / actuators as shown in the Fig. 2.13. The actuators are sandwiched in between the 2 thick aluminum beam layers at finite element positions 2 and 4, whereas the sensors are placed at finite element positions 6 and 8, thus giving rise to a single multivariable model with 2 inputs and 2 outputs.

The MIMO model is obtained using the theory of piezoelectric bonding, the Timoshenko beam theory, FEM technique and the state space techniques by considering the first 3 dominant vibratory modes ω_1, ω_2 and ω_3 [30], [43], [44], [45]. An external force input $\mathbf{f}_{ext}$ is applied at the free end of the beam. There are three inputs to the plant. One is the external force input $\mathbf{f}_{ext}$ which creates the disturbance and is taken as a load matrix of 1 unit in the simulation. The other inputs are the control inputs u_1 and u_2 to the actuators from the controller.

The values of the **A**, **B**, **C**, **D**, **E** matrices for the MIMO state space model of the smart structure is given by

$$\mathbf{A} = 1\,e5 \begin{bmatrix} 0 & 0 & 0 & 0.00001 & 0 & 0 \\ 0 & 0 & 0 & 0 & 0.00001 & 0 \\ 0 & 0 & 0 & 0 & 0 & 0.00001 \\ -0.61 & 0.00 & -0.00 & -0.00 & 0.00 & -0.00 \\ 0.00 & -2.13 & -0.00 & 0.00 & -0.00 & -0.00 \\ -0.00 & -0.00 & -5.39 & -0.00 & -0.00 & -0.0001 \end{bmatrix}, \quad \mathbf{E} = \begin{bmatrix} 0 \\ 0 \\ 0 \\ 0.0037 \\ 0.0000 \\ 0.0015 \end{bmatrix},$$

$$\mathbf{C}^T = \begin{bmatrix} 0 & 0 & 0 & 0.0001 & -0.0000 & -0.0000 \\ 0 & 0 & 0 & 0.0001 & -0.0000 & -0.0011 \end{bmatrix}, \tag{2.250}$$

Table 2.14. Characteristics of the smart embedded beam for as a MIMO system

Eigen values	Natural frequencies (Hz)
$-0.3 \pm j\,246.43$	39.2205
$-1.07 \pm j\,461.97$	73.5245
$-2.7 \pm j\,734.23$	116.8571

$$\mathbf{D} = \text{Null matrix}, \quad \mathbf{B} = 1e-4 \begin{bmatrix} 0 & 0 \\ 0 & 0 \\ 0 & 0 \\ 0.0001 & -0.0011 \\ 0.0000 & -0.0000 \\ 0.0000 & -0.0031 \end{bmatrix}.$$

The characteristics of the smart cantilever beam as a MIMO system with the embedded non-collocated sensor and actuator pairs are given in Table 2.14. Control of this developed MIMO state space model is obtained using the multirate output feedback control techniques which is considered in the subsequent chapters.

2.2.4 Conclusions

Smart cantilever beam model containing piezoelectrics as surface mounted sensor / actuator is developed using the finite element method from which the state space model of the smart beam is obtained. This modeling approach allows us to place the sensor / actuator as collocated pairs at any desired location along the length of the beam by varying its position from the fixed end to the free end. Inclusion of sensor / actuator mass and stiffness and by positioning the sensor / actuator at different locations along the beam leads to various state space models and study their performance characteristics when subjected to a external disturbance with and without the controller.

The case of modeling a smart structure with more than one piezoelectric sensor / actuator at discrete locations is also dealt with in this modeling procedure. Some of the limitations of the Euler-Bernoulli theory such as the neglection of shear, rotary inertia and axial displacement are being considered here while modeling the beam. Embedded shear sensors and actuators have been considered in this chapter instead of the surface mounted sensors and actuators for vibration suppression of cantilever beams because of lot of advantages. Timoshenko beam theory corrects the simplifying assumptions made in Euler-Bernoulli beam theory and the model obtained can be closer to a exact one. These developed state space models are further used for designing the controllers in the subsequent chapters for vibration suppression of adaptive structures.

3

Periodic Output Feedback Controllers for Smart Structures

In this Chapter, we develop various types of control strategies for SISO and MIMO models of smart structure developed in the Chapter 2 using the Periodic Output Feedback (POF) control law, a type of multirate output feedback (MROF) technique. The various types of developed control strategies are used to control the vibrations of beams when they are subjected to an external disturbance (impulse or sinusoidal) at the free end of the cantilever beam. In the first part of this Chapter, the design of POF controllers for the active vibration suppression of flexible cantilever beams modelled with Euler-Bernoulli beam theory is discussed, while in the latter part of this Chapter, the design of POF controllers for the active vibration suppression of thick beams modelled with Timoshenko beam theory is presented. The performance of all the designed controllers are evaluated for AVC by observing the various responses. The results are compared and conclusions are finally drawn.

3.1 A Brief Review of the Periodic Output Feedback Control Technique

The problem of pole assignment by piecewise constant output feedback was studied by Werner [55], Chammas and Leondes [53], [54], [120] for LTI systems with infrequent observations. If a system is controllable and observable, then almost for all output sampling rates, they have shown that by the use of a periodically time-varying piecewise constant output feedback gain [47], the poles of the discrete time control system could be assigned arbitrarily (within the natural restriction that they should be located symmetrically with respect to the negative real axis) [51], provided the number of gain changes during one output sampling interval is not less than the controllability index of the system. Since the feedback gains are piecewise constants, their method could easily be implemented, guarantees the closed loop stability and indicated a new possibility in controller design. Such a control law can stabilize a much larger class of systems than by the use of static output feedback technique.

Consider a LTI continuous time system

$$\dot{x} = Ax + Bu, \quad y = Cx, \tag{3.1}$$

where $x \in \Re^n$, $u \in \Re^m$, $y \in \Re^p$, A, B, C are constant matrices of appropriate dimensions and $A \epsilon \Re^{n\times n}$, $B \epsilon \Re^{n\times m}$, $C \epsilon \Re^{p\times n}$.

Let $(\Phi_\tau, \Gamma_\tau, C)$ and (Φ, Γ, C) be the system in (3.1) sampled at τ and Δ secs respectively. It is assumed that $(\Phi_\tau, \Gamma_\tau, C)$ be named as the τ system and (Φ, Γ, C) be named as the Δ system. It is also assumed that τ system is completely observable and Δ system is completely controllable.

The output is measured at the time instants $t = k\tau, \;\; k = 0,\ 1,\ 2, ...$ We consider constant hold functions because they are more suitable for implementation. An output-sampling interval is divided into N sub-intervals of width $\Delta = \frac{\tau}{N}$ and the hold function is assumed to be constant on these sub-intervals as shown in Fig. 3.1. N should be greater $\geq$ the controllability index γ of (Φ_τ, Γ). Thus, the control law becomes

$$u(t) = K_l\ y(k\tau), \qquad ... (k\tau + l\Delta) \leq t \leq [k\tau + (l+1)\Delta], \quad K_{l+N} = K_l, \tag{3.2}$$

for $l = 0,\ 1,\ 2,\ ..., (N-1)$.

Note that a sequence of N gain matrices $\{K_0, K_1, ..., K_{N-1}\}$ when substituted into the Eq. (3.2), generates a time-varying piecewise constant output feedback gain $\mathbf{K}(t)$ for $0 \leq t \leq \tau$. To obtain the gain sequence $\mathbf{K}$, consider the delta system

$$x(k+1) = \Phi\ x(k) + \Gamma\ u(k), \quad y(k) = Cx(k). \tag{3.3}$$

Let

$$\mathbf{K} = \left[K_0\ K_1\ K_2 \cdots K_{N-1} \right]^T. \tag{3.4}$$

Let $u(t)$ be calculated using Eq. (3.2) and therefore, $\mathbf{u}(k\tau)$ becomes

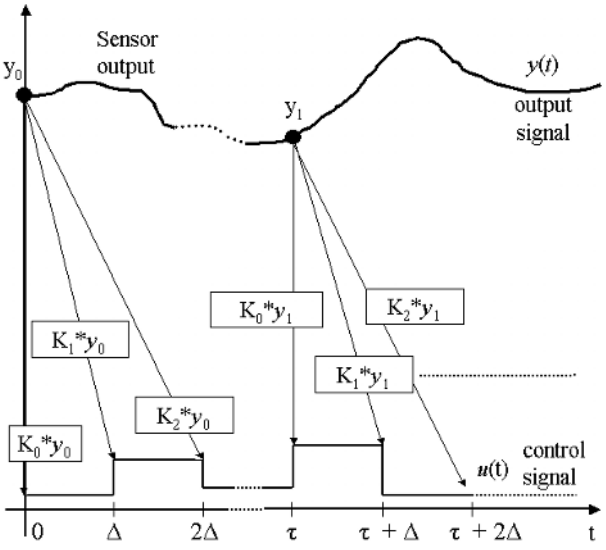

Fig. 3.1. Graphical illustration of the POF control law

$$\mathbf{u}(k\tau) = \mathbf{K}\ y(k\tau) = \begin{bmatrix} u(k\tau) \\ u(k\tau + \Delta) \\ \vdots \\ u(k\tau + \tau - \Delta) \end{bmatrix}. \tag{3.5}$$

Now, the tau system is written as

$$x(k\tau + \tau) = \mathbf{\Phi}^N x(k\tau) + \mathbf{\Gamma}\ \mathbf{u}(k\tau), \quad y(k\tau) = C\ x(k\tau), \tag{3.6}$$

where $\mathbf{\Gamma} = \left[\Phi^{N-1}\Gamma, \Phi^{N-2}\Gamma, ..., \Gamma\right]$.

Applying the control in Eq. (3.2), i.e., $\mathbf{K}\ y(k\tau)$ is substituted for $\mathbf{u}(k\tau)$, the closed loop system becomes

$$x(k\tau + \tau) = \left(\mathbf{\Phi}^N + \mathbf{\Gamma K} C\right) x(k\tau). \tag{3.7}$$

The problem has now taken the form of static output feedback [48]. Equation (3.7) suggests that an output injection matrix G be found such that

$$\rho\left(\mathbf{\Phi}^N + GC\right) < 1, \tag{3.8}$$

where $\rho(\cdot)$ denotes the spectral radius. By observability, one can always choose an output injection gain G to achieve any desired self-conjugate set of eigen values for the closed-loop matrix $\left(\mathbf{\Phi}^N + GC\right)$ and from $N \geq \nu$, it follows that one can find a POF gain $\mathbf{K}$ which realizes the output injection gain G by solving

$$\mathbf{\Gamma K} = G \tag{3.9}$$

for $\mathbf{K}$.

The problem with controllers obtained in this way is that, although they are stabilizing and achieve the desired closed loop behavior at the output sampling instants, they may cause an excessive oscillation between inter-sampling instants. The controller obtained using the above equation may give the desired behaviour, but might require excessive control action and the POF gains obtained may be very high. To reduce this effect, we relax the condition that $\mathbf{K}$ exactly satisfy the linear equation (3.9) and include a constraint on it. Solving $\mathbf{\Gamma K} = G$ may give a POF gain that is higher in magnitude, amplifying the noise in a system. Hence, the conditions on $\mathbf{K}$ is imposed during the controller design. These restrictions on $\mathbf{K}$ are posed as LMI problem [121]. Thus, we arrive at the following inequalities as

$$\| \mathbf{K} \| < \rho_1, \quad \| \mathbf{\Gamma}\ \mathbf{K} - G \| < \rho_2, \tag{3.10}$$

where ρ_2 small means that the POF controller with gain $\mathbf{K}$ is a good approximation of the original design, i.e., stability is not impaired and ρ_1 small means low noise sensitivity.

Using the schur complement, it is straight forward to bring these conditions in the form of Linear Matrix Inequalities (LMI) [49], [50], [121] as

$$\begin{bmatrix} \rho_1^2 I & \mathbf{K} \\ \mathbf{K}^T & -I \end{bmatrix} < 0, \quad \begin{bmatrix} \rho_2^2 I & (\Gamma\mathbf{K} - G) \\ (\Gamma\mathbf{K} - G)^T & -I \end{bmatrix} < 0. \tag{3.11}$$

In this form, the LMI toolbox of MATLAB can be used for the synthesis of $\mathbf{K}$. The POF controller obtained by this method requires only piecewise constant gains [122] and may be easier to implement in real time.

An alternative method to the above LMI technique is to use a performance index so that $\mathbf{\Gamma K} = G$ need not be forced exactly as used by Werner and Furuta [51], [55]. This constraint is replaced by a penalty function, which makes it possible to enhance the closed loop performance by allowing slight deviations from the original design and at the same time improving the behaviour. The performance index $J(k)$ is given by

$$J(k) = \sum_{l=0}^{\infty} \begin{bmatrix} x_l^T & u_l^T \end{bmatrix} \begin{bmatrix} \bar{Q} & 0 \\ 0 & R \end{bmatrix} \begin{bmatrix} x_l \\ u_l \end{bmatrix} + \sum_{k=1}^{\infty} \left(x_{kN} - x_{kN}^*\right)^T \bar{P} \left(x_{kN} - x_{kN}^*\right), \tag{3.12}$$

where $R \in \Re^{m \times m}$, $\bar{Q}$ and $\bar{P} \in \Re^{n \times n}$ are positive definite and symmetric weight matrices, x_l and u_l denote the states and the inputs of the delta system and x_{kN}^* denotes the state that would be reached at the instant kN, given $x_{(k-1)N}$, if K is solved to satisfy (3.9) exactly, i.e., $x_{kN}^* = \left(\mathbf{\Phi}^N + GC\right)\ x_{(k-1)N}$. The first term represents the averaged state and control energy whereas the second term penalizes the deviation of G. A trade-off between the closed loop performance and closeness to the chosen design is expressed by the above cost function.

3.2 Controller Design for Smart Structures Modelled Using EB Theory

In the following Sections, the design of the POF controllers for SISO and MIMO smart structure systems modelled using Euler-Bernoulli beam theory is presented.

3.2.1 Design of SISO Controllers for Smart Beam Divided into 3, 4, 5 Finite Elements

The POF control technique discussed in the previous Section 3.1 is used to design a controller to suppress the first 2 vibration modes of a flexible cantilever beam through smart structure concept for the various SISO state space models given in Section 2.1.1:6 I(i). The performance of the 3 type of systems is hereby evaluated for vibration control by carrying out the simulations in MATLAB and conclusions are drawn by observing the various responses [72], [87].

An external force $\mathbf{f}_{ext}$ (impulse disturbance) of 1 Newton is applied for duration of 1 sec at the free end of the beam for the individual models of the 3 systems shown in Figs. 2.3 and in A.1. The beam is subjected to vibrations and the open loop impulse response (plot of sensor outputs y as a function of t) of the various models of the 3 systems are observed.

The first task in designing the POF controller is the selection of the sampling interval τ. The maximum bandwidth for all the sensor / actuator locations on the beam are calculated (here, the second vibratory mode of the plant) and then by using the existing empirical rules [123] for selecting the sampling interval based on bandwidth, approximately 10 times of the maximum second vibration mode

frequency of the system has been selected. The sampling interval used is $\tau = 0.004$ seconds.

Consider the models of the 3 systems only at the fixed end. Let $(\Phi_{\tau 1j}, \Gamma_{\tau 1j}, C_{1j})$, $(j = 1,\ 2,\ 3)$ be the τ systems sampled at a rate of $\frac{1}{\tau}$ respectively. Thus,

$$\Phi_{\tau 11} = \begin{bmatrix} 0.6217 & -0.0000 & 0.0034 & -0.0000 \\ -0.0000 & 0.9819 & -0.0000 & 0.0040 \\ -175.4999 & -0.0000 & 0.6042 & -0.0000 \\ -0.0000 & -9.0062 & -0.0000 & 0.9810 \end{bmatrix}, \Gamma_{\tau 11} = 10^{-6} \begin{bmatrix} -0.09 \\ -0.01 \\ -40.46 \\ -3.70 \end{bmatrix}, \quad (3.13)$$

$$C_{11}^T = \begin{bmatrix} 0 & 0 & -0.0050 & -0.0028 \end{bmatrix},$$

$$\Phi_{\tau 12} = \begin{bmatrix} 0.6087 & -0.0000 & 0.0034 & -0.0000 \\ -0.0000 & 0.9860 & -0.0000 & 0.0040 \\ -180.9848 & -0.0000 & 0.5906 & -0.0000 \\ -0.0000 & -6.9747 & -0.0000 & 0.9853 \end{bmatrix}, \ \Gamma_{\tau 12} = 10^{-6} \begin{bmatrix} 0.06 \\ -0.00 \\ 27.07 \\ -1.82 \end{bmatrix}, \quad (3.14)$$

$$C_{12}^T = \begin{bmatrix} 0 & 0 & 0.0038 & -0.0016 \end{bmatrix},$$

$$\Phi_{\tau 13} = \begin{bmatrix} 0.6249 & 0.0000 & 0.0034 & 0.0000 \\ 0.0000 & 0.9881 & 0.0000 & 0.0040 \\ -174.1562 & 0.0000 & 0.6074 & 0.0000 \\ 0.0000 & -5.9265 & 0.0000 & 0.9875 \end{bmatrix}, \ \Gamma_{\tau 13} = 10^{-3} \begin{bmatrix} -0.0004 \\ -0.0000 \\ -0.1771 \\ -0.0108 \end{bmatrix}, \quad (3.15)$$

$$C_{13}^T = \begin{bmatrix} 0 & 0 & -0.0026 & -0.0010 \end{bmatrix}.$$

Here, for the sake of convenience, only the models of the 3 types of the systems for the piezo patch placed at the fixed end is given. It is found that the systems in Eqs. (3.13)-(3.15) are controllable and observable. Similarly, the tau systems of the other models of the 3 systems are obtained. The stabilizing output injection gains G_{1j}'s are obtained for the models of the 3 types of systems with the piezos at the fixed end such that the eigenvalues of $(\Phi_{\tau 1j} + G_{1j}\, C_{1j})$ lie inside the unit circle and the response of the system has a good settling time. Similarly, the output injection gains for the other models of the 3 systems are obtained. The impulse responses are observed with the output injection gains. The gains for the models at the fixed end of the 3 types of systems are obtained as

System 1, Model 1, Fixed end : $[\ -0.46\ -1.68\ -140.52\ -275.3\ ]^T$,
System 2, Model 1, Fixed end : $[\ -0.53\ -0.09\ \ 121.47\ \ -26.87\ ]^T$,
System 3, Model 1, Fixed end : $[\ -0.52\ -0.11\ \ 134.4\ \ -27.37\ ]^T$.

Let $(\Phi_{1j}, \Gamma_{1j}, C_{1j})$ be the delta systems of the various models of the 3 systems shown in the Fig. 2.3 with PZT's at the fixed end. The number of sub-intervals N is chosen as **10**. Thus,

$$\Phi_{11} = \begin{bmatrix} 0.9959 & -0.0000 & 0.0004 & -0.0000 \\ -0.0000 & 0.9998 & -0.0000 & 0.0004 \\ -20.3420 & -0.0000 & 0.9939 & -0.0000 \\ -0.0000 & -0.9064 & -0.0000 & 0.9997 \end{bmatrix}, \ \Gamma_{11} = 10^{-4} \begin{bmatrix} -0.0001 \\ -0.0000 \\ -0.4689 \\ -0.0372 \end{bmatrix}, \quad (3.16)$$

$$C_{11}^T = \begin{bmatrix} 0 & 0 & -0.0050 & -0.0028 \end{bmatrix},$$

$$\Phi_{12} = \begin{bmatrix} 0.9958 & -0.0000 & 0.0004 & -0.0000 \\ 0.0000 & 0.9999 & 0.0000 & 0.0004 \\ -21.0966 & -0.0000 & 0.9937 & -0.0000 \\ -0.0000 & -0.7009 & -0.0000 & 0.9998 \end{bmatrix}, \; \Gamma_{12} = 10^{-4} \begin{bmatrix} -0.0001 \\ -0.0000 \\ -0.3156 \\ -0.0183 \end{bmatrix}, \quad (3.17)$$

$$C_{12}^T = \begin{bmatrix} 0 & 0 & 0.0038 & 0.0016 \end{bmatrix},$$

$$\Phi_{13} = \begin{bmatrix} 0.9960 & 0.0000 & 0.0004 & 0.0000 \\ 0.0000 & 0.9999 & -0.0000 & 0.0004 \\ -20.1586 & 0.0000 & 0.9939 & 0.0000 \\ 0.0000 & -0.5951 & 0.0000 & 0.9998 \end{bmatrix}, \; \Gamma_{13} = 10^{-4} \begin{bmatrix} -0.0000 \\ -0.0000 \\ -0.2050 \\ -0.0109 \end{bmatrix}, \quad (3.18)$$

$$C_{13}^T = \begin{bmatrix} 0 & 0 & -0.0026 & -0.0010 \end{bmatrix}$$

As in the case of τ systems, the delta systems for the 3 types of systems where the piezo patch is placed at the fixed end is given here for in Eqs. (3.16)-(3.18). Similarly, the delta systems of the other models of the 3 systems are obtained. The POF gain matrix $\mathbf{K}$ for the systems are obtained by solving $\mathbf{\Gamma}_i \mathbf{K}_i \approx G_i$ using the LMI optimization method [121]. This reduces the amplitude of the control signal u. The POF gain matrix for the various SISO models of the 3 systems at the fixed end end is given by [72], [87].

Model 1 of system 1 : $10^{-2}[\ 7.17\ 6.25\ 5.37\ 4.54\ 3.77\ 3.06\ 2.41\ 1.84\ 1.34\ 0.92\ ]^T$,
Model 1 of system 2 : $10^{-2}[\ 3.55\ 3.08\ 2.62\ 2.19\ 1.79\ 1.44\ 1.11\ 0.86\ 0.65\ \ 0.5\ ]^T$,
Model 1 of system 3 : $10^{-2}[\ 3.61\ 3.18\ 2.75\ 2.34\ 1.94\ 1.58\ 1.24\ 0.94\ 0.68\ 0.46\ ]^T$.

Similarly, the POF gain matrices for the other models of the 3 systems are obtained. With the designed POF controller being put in the loop with the plant, the closed loop impulse responses (sensor outputs y) and the variation of the control signal u_i with time t for all the models in the 3 systems are observed. Here, for the sake of convenience, only the responses (open loop impulse response, closed loop impulse response with the output injection gain, closed loop impulse response with the POF gain, control effort required) for the models in which the piezo patches are placed at the fixed end and the free end of the 3 types of systems (2 modes) are shown in Figs. 3.2 - 3.7.

Responses are also observed for 3 vibration modes models with the piezo patches placed only at the fixed end. The responses are shown in the Figs. 3.8 - 3.10. The peak magnitudes of the open loop impulse responses, closed loop impulse responses with G_i, $\mathbf{K}_i$ and peak magnitude of the control effort u_i for the various models of the 3 systems (by retaining the first two vibratory modes) are given below.

Model 1 of System 1, Sensor / Actuator at 1 (fixed end)

Maximum positive	16.5	16.1	13.1	0.6
Maximum negative	16.5	13.5	12.3	0.63

Model 3 of System 1, Sensor / Actuator at 3 (free end)

Maximum positive	1.72	1.42	1.42	2.4
Maximum negative	1.62	0.83	1.32	1.16

Model 1 of System 2, Sensor / Actuator at 1 (fixed end)				
Maximum positive	12.1	10.5	11.4	0.32
Maximum negative	9.95	10.2	10	0.32
Model 4 of System 2, Sensor / Actuator at 4 (free end)				
Maximum positive	0.8	0.67	0.67	1.4
Maximum negative	0.75	0.5	0.62	0.32
Model 1 of System 3, Sensor / Actuator at 1 (fixed end)				
Maximum positive	8.5	8	8.9	0.23
Maximum negative	8.6	6.2	7.7	0.23
Model 5 of System 3, Sensor / Actuator at 5 (free end)				
Maximum positive	0.45	0.37	0.37	1.5
Maximum negative	0.44	0.37	0.34	0.2

3.2.1.1 Simulation Results and Discussions

Controllers are designed for the smart flexible cantilever beam using the POF control technique for the different models of the **3 systems** to suppress the first 2 vibratory modes [72], [87]. The various responses are obtained for each of the state space models of the 3 systems. The comparison and discussion of the simulation results for various cases of smart structure models are presented below.

From the simulation results, it is observed that modeling a smart structure by including the sensor / actuator mass and stiffness and by varying its location on the beam from the free end to the fixed end and by dividing it into a number of FE results in a considerable change in the system's structural vibration characteristics. Through the simulation results, it is inferred that when the plant is placed with this designed controller, the plant performs well and the vibrations die out quickly.

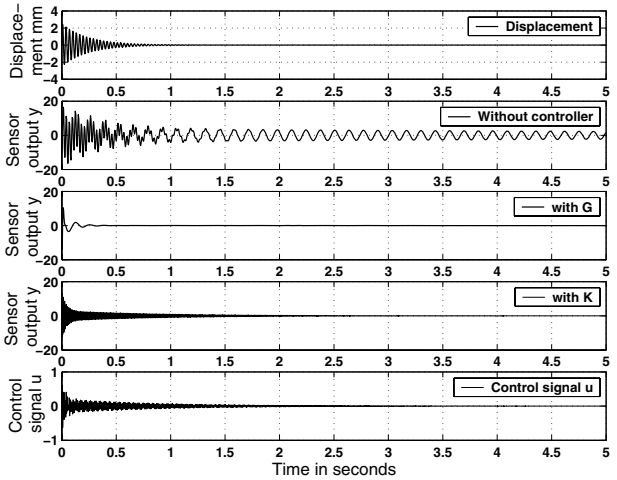

Fig. 3.2. Tip displacements, open and closed loop responses and control signal of model 1 of system 1 (Piezo placed at FE 1 - fixed end)

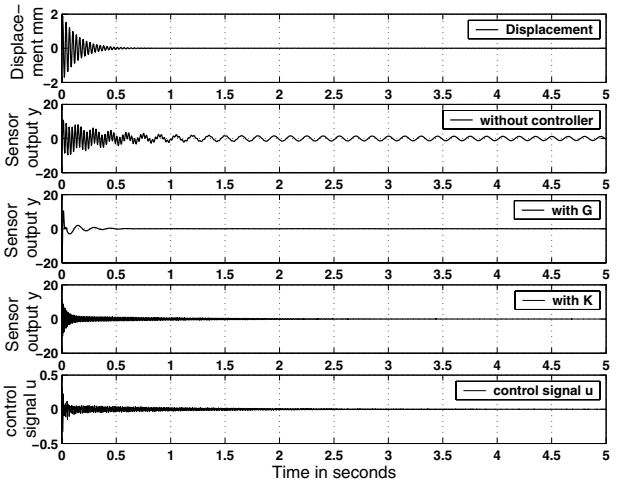

Fig. 3.3. Tip displacements, open and closed loop responses and control signal of model 1 of system 2 (Piezo placed at FE 1 - fixed end)

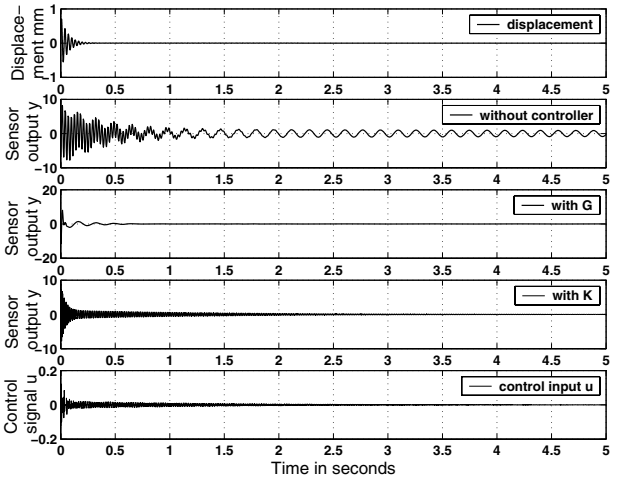

Fig. 3.4. Tip displacements, open and closed loop responses and control signal of model 1 of system 3 (Piezo placed at FE 1 - fixed end)

From the responses of the various models of each system, it is observed that when the piezoelectric element is placed near the clamped end, i.e., the fixed end, the sensor output voltage is greater. This is due to the heavy distribution of the bending moment near the fixed end, thus leading to a larger strain rate.

The sensor voltage is very less when the sensor / actuator pair is located at the free end as a result of which more control effort is required to damp out the vibrations. The sensitivity of the sensor / actuator pair thus depended on its location on the beam. From the output responses shown in the Figs. 3.2 - 3.10, it is observed

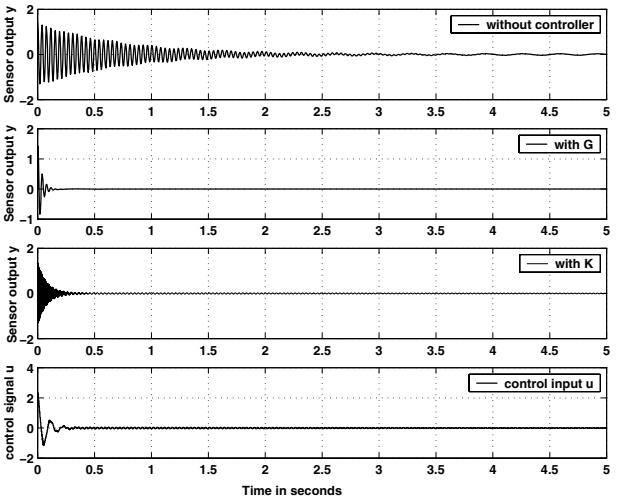

Fig. 3.5. Open and closed loop responses and control signal of model 3 of system 1 (Piezo placed at FE 3 - free end)

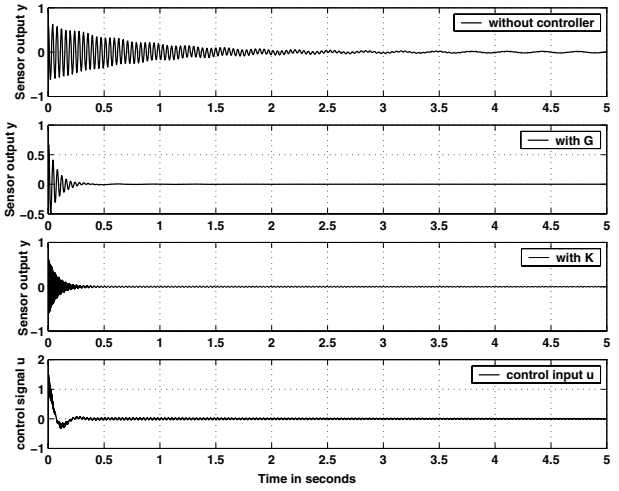

Fig. 3.6. Open and closed loop responses and control signal of model 4 of system 2 (Piezo placed at FE 4 - free end)

that the control effort u required from the controller gets reduced if the sensor / actuator placement location is moved towards the fixed end. A small magnitude of the control signal is sufficient to control the structural vibrations of each model of the systems 1, 2 and 3 when the piezos are at the fixed end.

An output injection gain for each discrete model of the three systems is obtained such that poles are placed inside the unit circle at appropriate locations and the CL

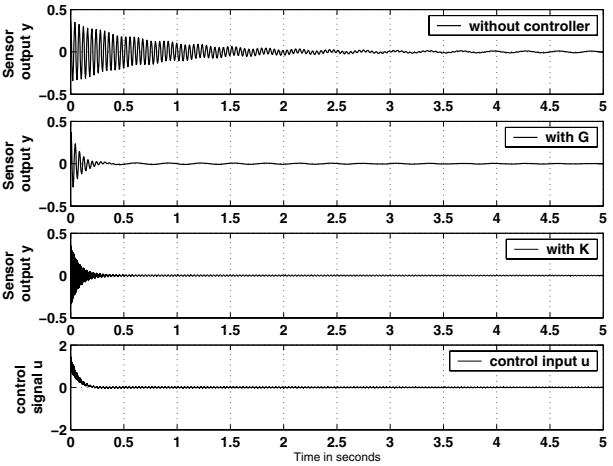

Fig. 3.7. Open and closed loop responses and control signal of model 5 of system 3 (Piezo placed at FE 5 - free end)

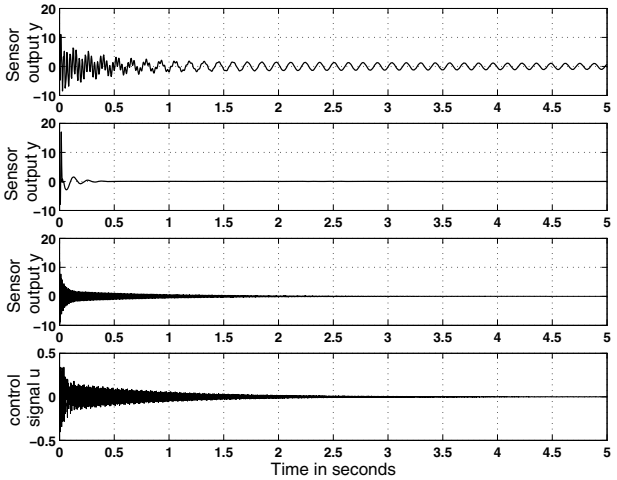

Fig. 3.8. Responses of model 1 of system 1 (Piezo placed at fixed end) : 3 modes

system has very good settling time. The individual models of the 3 systems are compared to obtain the best performance. Comparing the 3 systems, viz., system 1, 2 and 3, it is observed that when the smart beam is divided into 5 finite elements, the vibration characteristics was the best amongst all the models of the three systems. Hence, it can be concluded that, the best placement of the sensor / actuator pair is at the fixed end of the system 3, i.e., the model 1 of system 3. Comparing the responses of the various models of the 3 systems, it is observed that the model 1 of the system 3's vibration characteristics are the best for the vibration control of smart beam because of the following reasons.

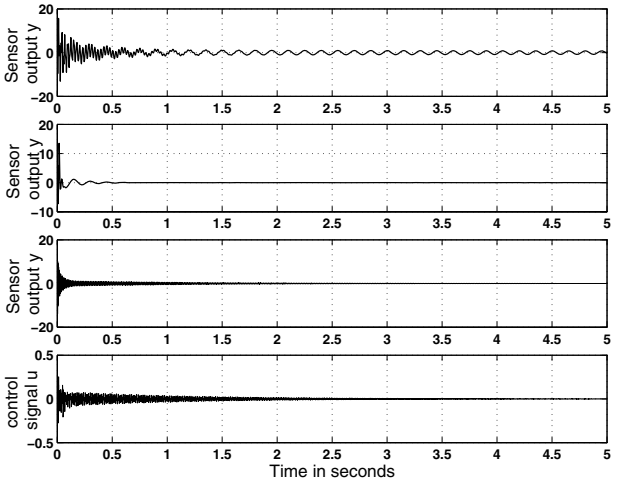

Fig. 3.9. Responses of model 1 of system 2 (Piezo placed at fixed end) : 3 modes

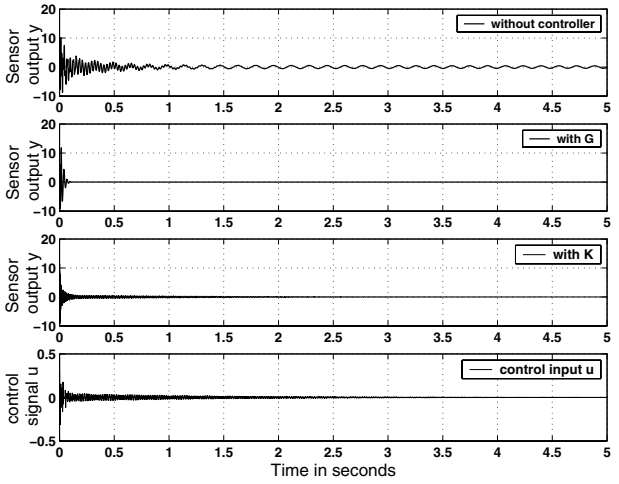

Fig. 3.10. Responses of model 1 of system 3 (Piezo placed at fixed end) : 3 modes

- A very small magnitude of control input u is required to damp out the vibrations compared to the systems 1 and 2 as a result of which less effort has to be put by the controller.
- The magnitude of the impulse response (closed loop) of both the continuous and the discrete time system is less compared to systems 1 and 2.
- Also, the response characteristics with G and $\mathbf{K}$ are the best.
- The vibrations are damped out quickly, i.e., the tip position settles quickly.

Further, the model 1 of system 3 is more sensitive to the first mode as the bending moment is maximum, strain rate is higher, minimum tip deflection, better sensor output and less requirement of the control input (control will be more effective at

the root), whereas at the free end of the system 3 (model 5 of system 3), because of the lesser strain rate and maximum deflection, more control energy is required to damp out the vibrations. The vibration characteristics of the system depended not only on the collocation of the piezo pair, but also on many factors such as the gain of the amplifier used, the mode number and the location of the piezo pair at the nodal points from the fixed end [11].

Further, responses are obtained by considering the first 3 vibratory modes also and are shown in Figs. 3.8 - 3.10. Results are compared with the controllers designed for first 2 vibratory modes. The responses without controller, with G, $\mathbf{K}$ and magnitude of the control input u are obtained. The obtained responses by retaining the first 3 modes were nearly (almost) the same as for the 2 vibration modes. Hence, it can be concluded that a fourth order model with 2 vibratory modes is sufficient to model a smart flexible beam and the control input u does not excite the remaining left out modes.

Thus, the observations are made with and without the controller to show the control effect. From the simulations, it was observed that without control the transient response was unsatisfactory, takes more time to settle and with control, the vibrations are suppressed. An integrated FE model to analyze the vibration suppression capability of a smart cantilever beam with surface mounted piezoelectric devices based on Euler-Bernoulli beam theory is presented in this section. Unlike static output feedback, the POF control technique always guarantees the stability of the closed loop system which can be observed from the simulation results [72], [87]. The designed POF controller requires constant gains and hence may be easier to implement in real time application.

3.2.2 Design of MIMO Controller for a Multivariable System

The POF control technique discussed in the Section 3.1 is used to design a controller to suppress the first 2 vibration modes of a smart cantilever beam through smart structure concept for the MIMO (multivariable) representation of the smart structure model. The performance of the smart beam modelled as MIMO system is hereby evaluated by carrying out the simulations in MATLAB and observing the various responses [77]. The effect of placing the sensor-actuator as collocated pair at 2 different finite element locations on the beam which led to the multivariable model of the smart beam is observed and the conclusions are drawn.

The MIMO system is given by the Eqs. (2.93) and (2.101) with its numerical value in Eq. (2.105). An external force $\mathbf{f}_{ext}$ (impulse disturbance) of 1 Newton is applied for duration of 1 sec at the free end of the beam as shown in Fig. 2.5. The beam is thus subjected to vibrations and the open loop impulse response (plot of sensor outputs as a function of time) is observed. As in the case of POF design for SISO system discussed in Section 3.2.1, here also τ is selected as 0.004 seconds.

Let $(\Phi_\tau, \Gamma_\tau, C)$ be the MIMO discrete state space model obtained by sampling the system given in Eq. (2.105) at a rate of $\frac{1}{\tau}$. Thus,

$$\Phi_\tau = \begin{bmatrix} -0.6356 & -0.000 & 0.003 & -0.000 \\ -0.0000 & 0.6729 & -0.000 & 0.0355 \\ -139.432 & -0.000 & -0.6496 & -0.000 \\ -0.0000 & -15.393 & -0.000 & 0.6713 \end{bmatrix}, \; \Gamma_\tau = 10^{-4} \begin{bmatrix} 0.0022 & 0.0035 \\ -0.0077 & -0.0078 \\ 0.1848 & 0.2984 \\ -0.3619 & -0.3692 \end{bmatrix}. \tag{3.19}$$

It is found that the system in Eq. (3.19) is controllable and observable. The stabilizing output injection gain G is obtained such that the eigenvalues of $(\Phi_\tau + G\,C)$ lie inside the unit circle and the response of the system has a good settling time. The impulse response with the output injection gain G for the multivariable model is observed. The output injection gain obtained is as

$$G = \begin{bmatrix} 0.1769 & 0.0422 \\ -7.1720 & -0.7254 \\ -88.7904 & -22.0246 \\ -71.8037 & 1.8034 \end{bmatrix} = \begin{bmatrix} G_1^T & G_2^T \end{bmatrix}. \tag{3.20}$$

Let (Φ, Γ, C) be the MIMO discrete state space model obtained by sampling the system given in Eq. (2.105) at a rate of $\frac{1}{\Delta}$, where $\Delta = \frac{\tau}{N} = 0.002$ secs. The number of sub-intervals N is chosen as **2**. The Φ, Γ matrices are given by

$$\Phi = \begin{bmatrix} 0.9659 & 0.0000 & 0.0011 & 0.0000 \\ -0.0000 & 0.9965 & -0.0000 & 0.0040 \\ -49.8947 & 0.0000 & 0.9609 & 0.0000 \\ -0.0000 & -1.7322 & -0.0000 & 0.9964 \end{bmatrix}, \quad \Gamma = 10^{-3} * \begin{bmatrix} 0.0000 & 0.0001 \\ -0.0001 & -0.0001 \\ 0.0661 & 0.1068 \\ -0.0407 & -0.0415 \end{bmatrix}. \tag{3.21}$$

The POF gain matrix $\mathbf{K}$ for the smart system is obtained by solving $\mathbf{\Gamma K} \approx G$ using the LMI optimization method [121]. This reduces the amplitude of the control effort u. The POF gain $\mathbf{K}$ obtained for the multivariable state space model of the smart structure system is obtained as

$$\mathbf{K}^T = 10^2 \begin{bmatrix} -1.7292 & -0.2801 \\ -3.2445 & -0.5041 \\ 2.3577 & 0.3176 \\ 3.2598 & 0.4500 \end{bmatrix} = \begin{bmatrix} \mathbf{K}_1^T & \mathbf{K}_2^T \end{bmatrix}. \tag{3.22}$$

With the designed POF controller being put in the loop with the plant, the closed loop impulse responses (sensor outputs y_1, y_2) with the the output injection gain G and the POF gain $\mathbf{K}$, the plot of control effort u_1, u_2 required to control the vibrations are observed and graphically displayed as shown in Figs. 3.11 - 3.13 respectively.

3.2.2.1 Simulation Results and Discussions

POF controller has been designed for the MIMO smart structure model developed using the EB beam theory [77]. The beam was divided into 4 FE with sensor / actuator placed at positions 2 and 4. The various responses are obtained for the developed MIMO state space model. Through the simulation results, it is shown that when the plant is placed with this controller, the plant performs well and the vibrations are suppressed quickly. It is also observed that modeling a smart structure by placing the sensor / actuator at 2 different locations introduces a considerable change in the structural vibration characteristics than placing the sensor / actuator pair at only one location as in [72], [87].

In this section, it is observed that when the pair is kept at 2 different locations, the closed loop responses of the MIMO system is less oscillatory compared to the SISO case because of the following reason. MIMO excitation is better than SISO

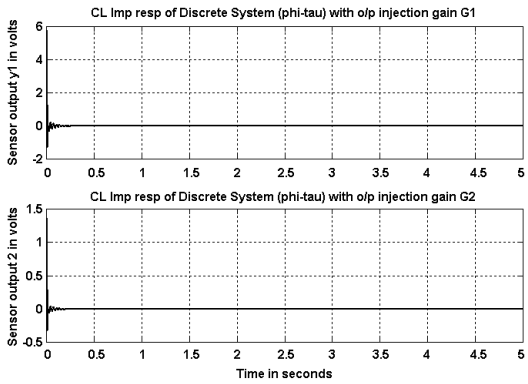

Fig. 3.11. CL responses y_1 and y_2 with the o/p injection gains G_1 and G_2 for the MIMO EB model

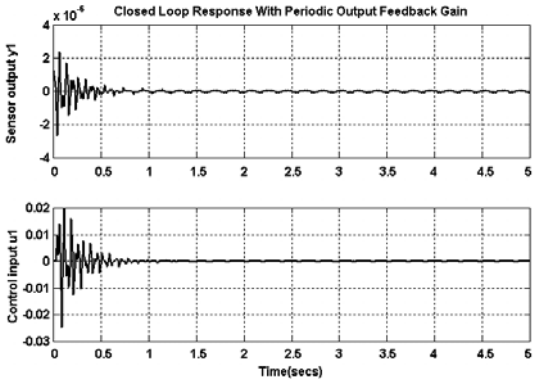

Fig. 3.12. CL response (sensor o/p) y_1 and control i/p u_1 with POF gain $\mathbf{K}_1$

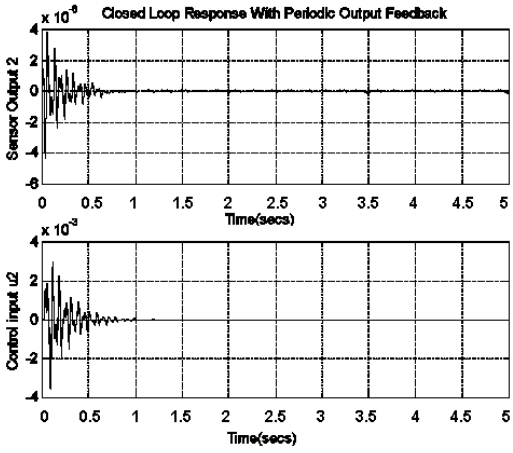

Fig. 3.13. CL response (sensor o/p) y_2 and control i/p u_2 with POF gain $\mathbf{K}_2$

excitation as only exciting the structure at a single point may cause poor distribution of input energy throughout the structure and may result in somewhat slightly disturbed frequency responses. A multi input test provides better energy distribution and even better actuation forces. Hence, it can be concluded that multivariable control of a smart structure is better compared to the single input single output control as there will be multiple interactions of the input and the output which will cause the vibrations in the system to damp out quickly.

The responses take lesser time to settle and the control effort required is also less. The impulse responses with the output injection gain and the POF gain show better performance. The output injection gain for the multivariable plant is so obtained that its poles are placed inside the unit circle at appropriate locations such that the system has a very good settling time. A overall better performance of the system is thus obtained. Responses were observed without control and were compared with the control to show the control effect. From the simulations, it was observed that without control, the transient response was unsatisfactory and with control, the vibrations are suppressed. The designed POF controller requires constant gains and hence may be easier to implement in real time. An integrated FEM-SS model to analyze the vibration suppression capability of a smart cantilever beam with surface mounted piezoelectric devices based on EB beam theory for a MIMO case is developed in this section.

3.2.3 Design of Robust Decentralized Fault Tolerant Controller for Smart Structures

3.2.3.1 Multimodel Synthesis

For the multimodel representation of a plant, it is necessary to design a controller which will robustly stabilize the multimodel system [55], [57]. Multimodel representation of plants can arise in several ways. When a non-linear system has to be stabilized at different operating points, linear models are sought to be obtained at those operating points. Even for parametric uncertain linear systems, different linear models can be obtained for extreme points of the parameters. These models are used for the stabilization of the uncertain system [81], [82]. Let us consider a family of plants $S = \{A_i, B_i, C_i\}$, defined by

$$\dot{x} = A_i x + B_i u, \quad y = C_i x, \quad i = 1, 2, ..., M. \tag{3.23}$$

By sampling at the rate of $\frac{1}{\Delta}$, we get a family of discrete systems (Φ_i, Γ_i, C_i). Assume that $\left(\Phi_i^{\tilde{N}},\ C_i\right)$ are observable. Then, we can find the output injection gains G_i such that $\left(\Phi_i^{\tilde{N}} + G_i\ C_i\right)$ has the required set of poles. Now, consider the augmented system defined as

$$\tilde{\Phi} = \begin{bmatrix} \Phi_1 & 0 & 0 & 0 \\ 0 & \Phi_2 & \cdot & \cdot \\ \cdot & \cdot & \cdot & \cdot \\ 0 & \cdot & \cdot & \Phi_M \end{bmatrix}, \quad \tilde{\Gamma} = \begin{bmatrix} \Gamma_1 \\ \Gamma_2 \\ \cdot \\ \Gamma_M \end{bmatrix}, \quad \tilde{G} = \begin{bmatrix} G_1 \\ G_2 \\ \cdot \\ G_M \end{bmatrix}. \tag{3.24}$$

The linear equation

$$\left[\tilde{\Phi}^{\tilde{N}-1}\tilde{\Gamma} \quad . \quad . \quad . \quad . \quad \tilde{\Gamma}\right] \begin{bmatrix} K_0 \\ K_1 \\ \cdot \\ \cdot \\ K^{\tilde{N}-1} \end{bmatrix} = \tilde{G} \tag{3.25}$$

has a solution if $\left(\tilde{\Phi}, \tilde{\Gamma}\right)$ is controllable with controllability index $\tilde{\gamma}$ and $\tilde{N} \geq \tilde{\gamma}$. This POF gain realizes the designed $\tilde{G}$ for all plants of the family. The controllability of the individual plants generically implies the controllability of the augmented system [51]. The controller obtained this way may be theoretically all right, but from the practical point of view, it may require excessive control action. To reduce this effect of gain on the control effort, we can approximate the condition given in Eq. (3.25) with a constraint on the gain. Thus, we consider the following inequality constraint equations,

$$\| \mathbf{K} \| < \rho_1, \quad \| \mathbf{\Gamma}_i \mathbf{K} - G_i \| < \rho_{2i}, \quad i = 1, 2, ..., M. \tag{3.26}$$

where ρ_1 and ρ_2 represent the upper bounds on the spectral norms of $\mathbf{K}$ and $(\mathbf{\Gamma}_i \mathbf{K} - G_i)$. These 2 objectives have been expressed by the upper bounds on matrix norms and each should be as small as possible. ρ_1 small means low noise sensitivity and ρ_2 small means that the POF controller with gain $\mathbf{K}$ is a good approximation of the original design. This can be formulated in the framework of Linear Matrix Inequalities as follows.

$$\begin{bmatrix} \rho_1^2 I & \mathbf{K} \\ \mathbf{K}^T & -I \end{bmatrix} < 0, \quad \begin{bmatrix} \rho_{2i}^2 I & (\Gamma_i \mathbf{K} - G_i) \\ (\Gamma_i \mathbf{K} - G_i)^T & -I \end{bmatrix} < 0. \tag{3.27}$$

In this form, the LMI Tool Box MATLAB [121] can be used for synthesis. The function *mincx*( ) of the LMI toolbox in Matlab is used to minimize the linear combination of ρ_1 and ρ_2. The robust POF controller obtained by the above method requires only constant gains and hence may be easier to implement in real time [57].

3.2.3.2 Fault Tolerant Controller Design

Control Problem **:** To design a fault tolerant control such that the vibrations are effectively controlled in the event of failure of one of the actuators. Such a failure mode can be modelled by replacing the i^{th} column of the input matrix by zero, i.e., the i^{th} column of B as zero indicates that the i^{th} actuator on the beam has failed. This consideration leads us to the problem of finding a control law that stabilizes the plant under normal operations and the 4 multivariable models corresponding to the 4 different failure modes.

The POF control technique discussed in the Sections 3.1 and 3.2.3:1 is used to design a robust controller to suppress the first 2 vibration modes of a flexible cantilever beam for the multimodel representation of the MIMO smart structure systems given by the Eqs. (2.112) and (2.118) with 4 inputs and 4 outputs when there is a failure of an actuator to function in the system dynamics. The performance of the smart beam is hereby evaluated for vibration control by carrying out the simulations in MATLAB and observing the various responses [81], [82]. The effect of failure of one of the 4 actuators on the beam is observed and the conclusions are drawn.

External disturbance is applied at the free end of the beam, thereby subjecting it into the vibrating mode. Now, when the system is in the vibrating mode and an actuator fails to perform (because of the reasons mentioned in section 2.1.3), a controller is designed in such a way that putting it in the loop with the plant during the actuator failure, will bring back the system to stability. As in the SISO and in the MIMO case of POF design, here also, the sampling interval τ is selected as 0.004 secs [123].

Consider a family of plant models, defined as $S = \{A, B_i, C_i\}$ and given by the state space representation as

$$\dot{x} = Ax + B_i u, \quad y_i = C_i x, \quad i \ = \ 1, 2, 3, 4. \tag{3.28}$$

Four models were obtained by considering 1 actuator failure at a time on the flexible beam. By sampling the 4 CT-SS models given in Eqs. (2.112) and (2.118) at a rate of $\frac{1}{\tau}$, we get a family of discrete systems $(\Phi_\tau, \Gamma_{\tau i}, C_i)$. One of these models, namely for the actuator failure at FE location 8 (fourth actuator), the tau system is

$$\Phi_{\tau 4} = \begin{bmatrix} -0.0798 & 0.0000 & -0.0135 & -0.0000 \\ -0.0000 & 0.2976 & 0.0000 & -0.0838 \\ 50.4855 & -0.0000 & -0.0748 & 0.0000 \\ 0.0000 & 10.7053 & -0.0000 & 0.2987 \end{bmatrix}, \quad \Gamma_{\tau 4} = 1.0e-3 * \begin{bmatrix} -0.0094 & -0.0017 & 0.0136 & 0 \\ -0.0185 & -0.0346 & -0.0449 & 0 \\ 0.4415 & 0.0774 & -0.6337 & 0 \\ 0.2820 & 0.5274 & 0.6884 & 0 \end{bmatrix},$$

$$C_4^T = 1.0e-3 * \begin{bmatrix} 0 & 0 & -0.2436 & -0.1598 \\ 0 & 0 & -0.427 & -0.2989 \\ 0 & 0 & 0.3496 & -0.3879 \\ 0 & 0 & 0.5134 & -0.4091 \end{bmatrix} \tag{3.29}$$

Similarly, the tau systems for the other 3 MIMO models are obtained. Stabilizing output injection gains G_i's are found such that the eigen values of $(\Phi_\tau + G_i C_i)$ lie within the unit circle and the responses has a good settling time. The closed loop impulse responses with the output injection is also observed.

Again by sampling the 4 models in Eqs. (2.112) and (2.118) at a rate of $\frac{1}{\Delta}$, where $\Delta = \frac{\tau}{N}$, we get a family of discrete systems (Φ, Γ_i, C_i). The number of sub-intervals is chosen as $N = 4$. One of these models, namely for the actuator failure at FE location 8 (fourth actuator), the delta system is

$$\Phi_4 = 10^3 * \begin{bmatrix} 0.9674 & 0.0000 & -0.0027 & -0.0000 \\ -0.0000 & 0.9912 & 0.0000 & -0.0112 \\ 9.9443 & 0.0000 & 0.9684 & 0.0000 \\ 0.0000 & 1.4257 & -0.0000 & 0.9914 \end{bmatrix}, \quad \Gamma_4 = 1e-3 * \begin{bmatrix} -0.0003 & -0.0001 & 0.0001 & 0 \\ -0.0002 & -0.0004 & -0.0006 & 0 \\ 0.0870 & 0.0152 & -0.1248 & 0 \\ 0.0376 & 0.0702 & 0.0911 & 0 \end{bmatrix} \tag{3.30}$$

Similarly, the delta systems for the other 3 multivariable models are obtained. Here, as we are dealing with robust stabilization for the multimodel system, we have to find a $\mathbf{K}$ which will satisfy $\mathbf{\Gamma}_i \mathbf{K}_i \approx G_i$, where $i = 1$ to 4 using the LMI optimization method. The LMI technique [121], [50] is used to find the RDPOF gain matrix $\mathbf{K}$, which realizes G_i by solving the equation $\mathbf{\Gamma}_i \mathbf{K}_i \approx G_i$ for different values of ρ. If the LMI constraints given in Eqs. (3.26) and (3.27) are solved using the above G_i, the robust POF gain matrix $\mathbf{K}$ may become full. This results in the control input of each actuator of the model being a function of the output of all the sensors. RDPOF control is achieved by making the off-diagonal elements of $\mathbf{K}_0, \mathbf{K}_1, \mathbf{K}_2, \cdots \mathbf{K}_{\tilde{N}-1}$ matrices zero. So, the structure of the resulting elements of $\mathbf{K}_i$ $(i = 0, 1, 2....., N-1)$ matrices for the 4 models of the multimodel system are assumed as

$$\mathbf{K}_i = Diag\ [\ k_{i11},\ k_{i22},\ k_{i33},\ k_{i44}] \ = \ \begin{bmatrix} k_{i11} & 0 & 0 & 0 \\ 0 & k_{i22} & 0 & 0 \\ 0 & 0 & k_{i33} & 0 \\ 0 & 0 & 0 & k_{i44} \end{bmatrix},\ i \ = \ 0, 1, .., (N-1). \tag{3.31}$$

With this structure of $\mathbf{K}_i$, the problem can be formulated in the framework of LMI and the desired matrices can be obtained. Now, it is evident that the control input u_i of each plant is a function of the output y_i of that plant model only and this makes the POF control technique based smart structure system a robust decentralized one [124]. The RDPOF gain matrix $\mathbf{K}$ for the multimodel system is given by

$$\begin{array}{rcllll} \mathbf{K}_0 & = & Diag\ [\ 6.52 & 4.16 & 3.75 & 2.33\ ] \\ \mathbf{K}_1 & = & Diag\ [\ 6.60 & 4.21 & 2.36 & 2.26\ ] \\ \mathbf{K}_2 & = & Diag\ [\ 6.66 & 4.25 & 3.91 & 3.51\ ] \\ \mathbf{K}_3 & = & Diag\ [\ 7.84 & 5.63 & 4.53 & 4.56\ ] \end{array} \tag{3.32}$$

The closed loop responses with this RDPOF gain $\mathbf{K}$ for all the 4 multivariable models of the smart structure plant (with one actuator failure at a time) are observed. The fault tolerant controller is able to stabilize the outputs in lesser time even though there is a failure of an actuator. The RDPOF controller obtained by this method requires only constant gains and hence may be easier to implement in real time. Simulation results of one of the four multi-models of the smart structure with fault taking place at finite element position numbering 8 are shown here in Figs. 3.14 - 3.18 with the RDPOF controller gain. Similarly, the simulation results are also observed when the fault takes place at FE positions 6 or 4 or 2 respectively due to the respective actuator failure.

3.2.3.3 Simulation Results and Discussions

RDPOF controller is designed for the multimodel system using the various multivariable models of the single plant when subjected to an actuator failure. The beam has been divided into 8 FE and sensor / actuator pair bonded to the master structure at even elements. 4 state space models have been obtained by considering the successive failure of one actuator at a time. Simulations are done in Matlab and the various responses (tip displacements, open loop, closed loop, magnitude of control inputs) are observed when a failure of one of the piezo-patches on the beam takes place. From the simulation results, it is inferred that when the plant is placed with the designed controller and when any one of the actuators fails to function, even then the controller stabilizes all the 4 models and damps out the oscillations quickly, stability is restored and the performance is not deteriorated.

In the control law presented, the control input to each actuator of the multimodel system is a function of the output of that corresponding sensor only and the gain matrix has got all off-diagonal elements zero. This makes the POF control technique a robust decentralized one. This would render better control as it requires only constant gains and hence implementation may become easier. Hence, MIMO control of a multimodel smart structure using RDPOF control technique is better compared to the SISO case [72], [87] as the vibrations decay out in a lesser time as there will be multiple interactions of the input-output with the system dynamics.

A robust control system has thus been designed with the constraint that the closed loop system be stable even if one of the input actuators has failed. It was

also observed from the simulations of the 4 models of the same plant that the initial transients for all the models were within acceptable limits and the outputs settles to final steady state value in lesser time. Comparing the 4 different failure rates of the 4 models of the plant, it is observed from the simulation results, the actuator failure at the FE position numbering 2 has more effect on the closed loop system dynamics rather than the failure at FE positions 4, 6 or 8.

When the actuator fails at position 2, the tip displacements takes more time to settle and more control effort is needed by the controller to bring the plant into equilibrium. This is because of the lesser strain rates available at the finite element locations which are far away from the fixed end. When the actuator fails to function at position 8, the tip displacement takes less time to settle and less control is needed for the system responses to settle because of the higher strain rates near the fixed end of the beam. Thus, it was observed that the fault taking place at finite element number 8 has less effect on the system dynamics.

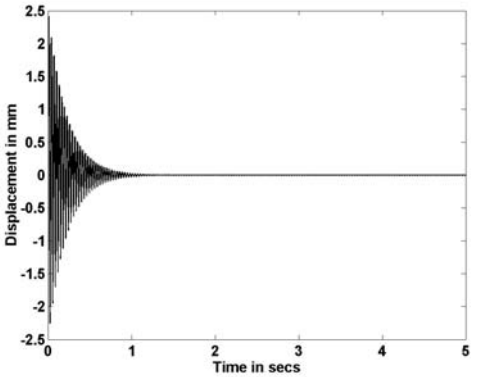

(a) Tip displacement, fault at FE 8 (w/o controller)

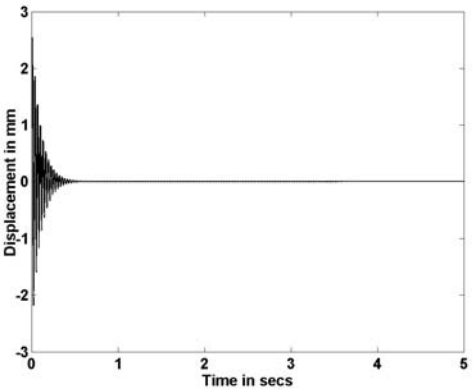

(b) Tip displacement, fault at FE 8 (with controller)

Fig. 3.14. Tip displacements when fault takes place at FE position numbering 8

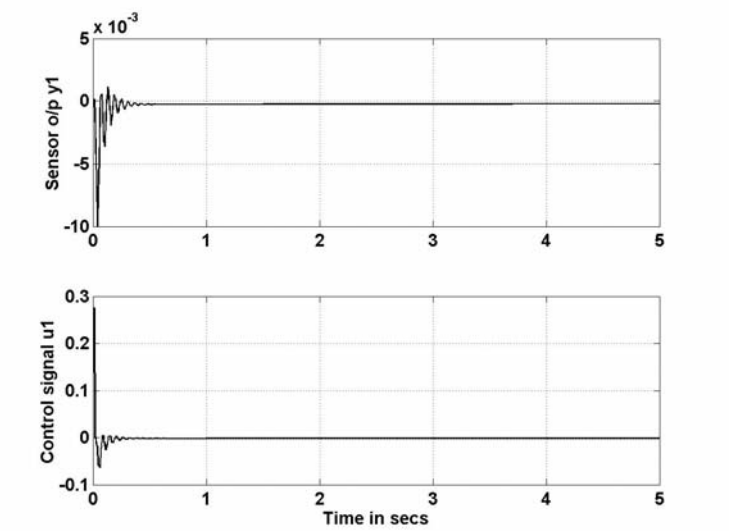

Fig. 3.15. Sensor o/p (CL response) y_1, control i/p u_1 for fault at FE position numbering 8 with the RDPOF gain

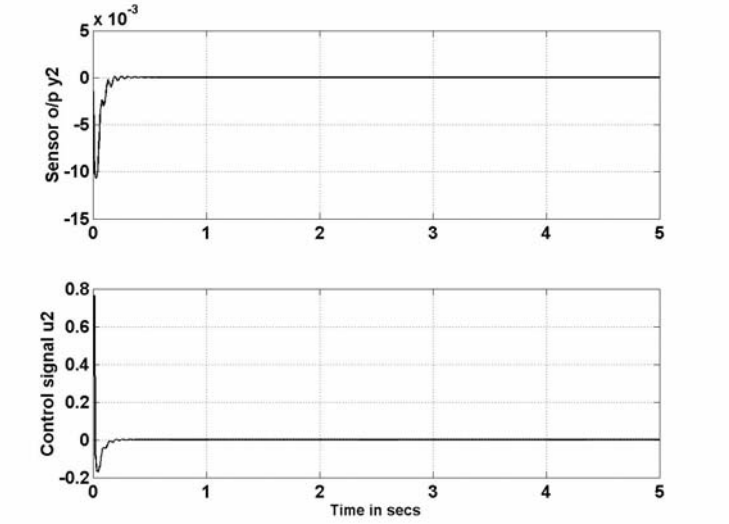

Fig. 3.16. Sensor o/p (CL response) y_2, control i/p u_2 for fault at FE position numbering 8 with the RDPOF gain

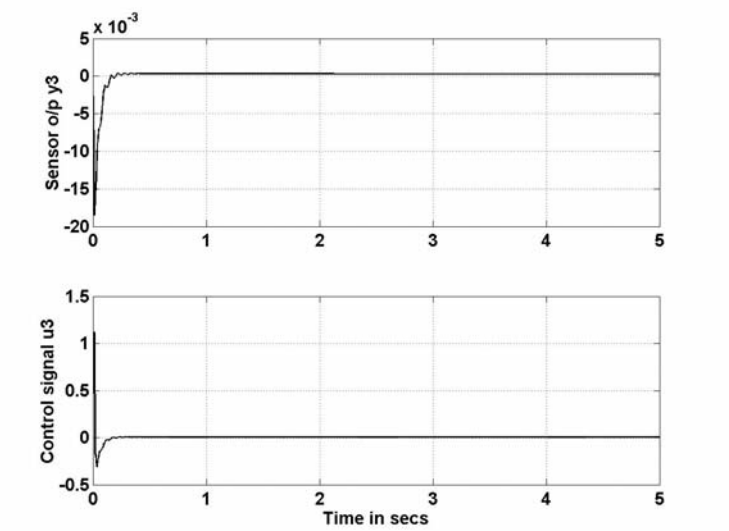

Fig. 3.17. Sensor output (CL response) y_3, control i/p u_3 for fault at FE position numbering 8 with the RDPOF gain

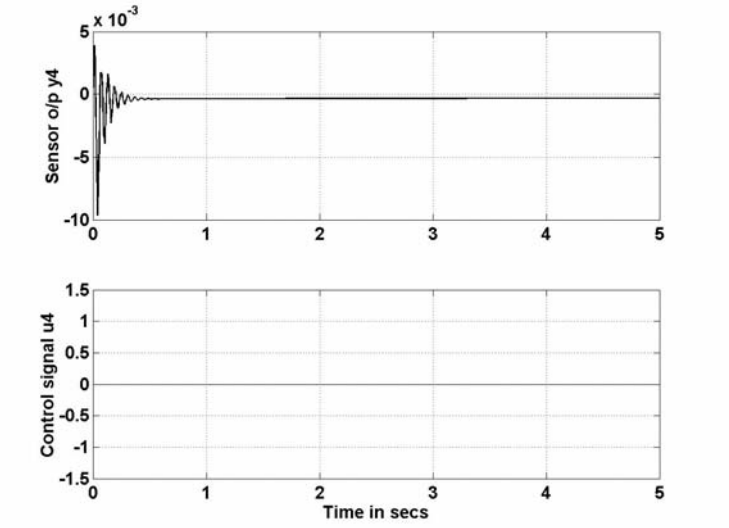

Fig. 3.18. Sensor output (CL response) y_4, control i/p u_4 for fault at FE position numbering 8 with the RDPOF gain

3.2.4 Robust Decentralized Periodic Output Feedback Controller Design via Reduced Order Model for Multimodel System

In this Section, the design of a RDPOF control technique for the AVC of smart structures for a multimodel case comprising of a family of multivariable plants is presented. The beam structure is modeled in state space form by dividing it into 4 FE and placing the PE sensor / actuator at 2 finite element locations (positions 2 and 4) as collocated pairs, i.e., as surface mounted sensor / actuator as shown in Fig. 2.5. Six vibratory modes are retained in modelling the beam [80]. A higher order multivariable system is thus obtained.

The state space model of the higher order system thus obtained is given by Eqs. (2.121) and (2.122) with the numerical values of the **A**, **B**, **C**, **D**, **E** matrices given by the Eq. (2.123) for the model 1. Five such multivariable models are obtained by varying the thickness parameter of the aluminum beam, thus giving rise to a multimodel system of the smart structure. Using model order reduction technique, the reduced order model of the higher order system is obtained [62]. RDPOF controllers are designed for the multimodel system consisting of 5 MIMO models. The performance of the multimodel system is hereby evaluated for AVC by carrying out the simulations.

The following few paragraphs gives a brief insight into the development of the RDPOF controller design using the model order reduction technique for a multimodel representation of the multivariable systems. Initially, we begin with a small review on the model order reduction technique and then followed by the design of robust decentralized controller using the model order reduction technique. For many complex processes or when the modes of a dynamical system are very high, the order of the state matrix may be quite large. It would be difficult to work with these large scale dynamical systems [102] in their original form. In such cases, it is common to study the process by approximating it to a simpler model. It is usually possible to describe the dynamics of a physical dynamical system by a number of linear differential equations with constant coefficients such as the state space forms. Consider the state space form of a physical dynamical system as

$$\dot{x} = Ax + Bu, \quad y = Cx, \tag{3.33}$$

where A is a $(n \times n)$ matrix.

One of the well-known techniques based on the dominant eigenvalue retention known as the Davison technique [61], [62] is used in this section. By this method, a system of higher order can be numerically approximated to one of smaller order. The method suggests that a large $(n \times n)$ system can be reduced to a simpler $(r \times r)$ model $(r \leq n)$ by considering the effects of the r most dominant (dominant in the sense of being closest to the instability) eigenvalues alone.

The principle of the method is to neglect the eigen values of the original system that are farthest from the origin and retain only the dominant eigenvalues and hence dominant time constants of the original system in the reduced order model. This implies that the overall behaviour of the approximated system will be very similar to that of the original system, since the contribution of the unretained eigenvalues to the system response are important only at the beginning of the response, whereas the eigenvalues retained are important throughout the whole of the response. For the system represented by the Eq. (3.33), consider the linear transformation,

$$x = P\ z \tag{3.34}$$

which transforms the model in Eq. (3.33) into the following form,

$$\dot{z} = \hat{A}z + \hat{B}u, \quad y = \hat{C}x, \tag{3.35}$$

where $\hat{A}$ is a $(r \times r)$ matrix and

$$\hat{A} = P^{-1}AP, \quad \hat{B} = P^{-1}B, \quad \hat{C} = CP. \tag{3.36}$$

Here, $\hat{A}$ is in the diagonal form as

$$\hat{A} = diag\ [\lambda_1, \lambda_2, ..., \lambda_n,] \tag{3.37}$$

and

$$Re(\lambda_1) \geq Re(\lambda_2) \geq ..... \geq Re(\lambda_n). \tag{3.38}$$

Further, assume that only r eigenvalues are dominant, i.e., the order of the reduced model is r and partition the model in Eq. (3.35) as

$$\dot{z}_1 = \hat{A}_1 z_1 + \hat{B}_1 u, \quad , \dot{z}_2 = \hat{A}_2 z_2 + \hat{B}_2 u, \quad , y = \hat{C}_1 z_1 + \hat{C}_2 z_2, \tag{3.39}$$

where

$$\hat{A}_1 = diag\ [\lambda_1, \lambda_2, ..., \lambda_r,], \quad \hat{A}_2 = diag\ [\lambda_{r+1}, \lambda_{r+2}, ..., \lambda_n,], \tag{3.40}$$

$$\hat{B}_1 = \text{first } r \text{ rows of } \hat{B}, \quad \hat{B}_2 = \text{remaining } (n-r) \text{ rows of } \hat{B} \tag{3.41}$$

and are respectively $(r \times r)$, $(n-r)\ \times\ (n-r)$, $(r \times m)$ and $(n-r)\ \times\ m$ matrices obtained by partitioning of $\hat{A}$ and $\hat{B}$ suitably. In Eq. (3.39), the order of z_1 is r and that of z_2 is $(n-r)$. Now, because the contribution of the modes represented by the eigenvalues $\lambda_{r+1}, \lambda_{r+2}, ..., \lambda_n$ is not significant, it may be assumed that $z_2 = 0$, whereby we have from Eq. (3.34),

$$\begin{bmatrix} x_1 \\ x_2 \end{bmatrix} = \begin{bmatrix} P_{11} \\ P_{21} \end{bmatrix}\ z_1, \tag{3.42}$$

where P_{11} and P_{21} are $(r \times r)$ and $(n-r)\ \times\ r$ sub-matrices obtained by partitioning of P matrix. Also, z_1 and z_2 are r and $(n-r)$ dimensional state vectors corresponding to the original state variables. It follows from Eq. (3.42) that

$$z_1 = P_{11}^{-1} x_1, \tag{3.43}$$

with which the model in Eq. (3.39) can be transformed to

$$\dot{x}_1 = P_{11}\hat{A}_1 P_{11}^{-1} x_1 + P_{11}\hat{B}_1 u = A_r x_1 + B_r u, \quad y = \hat{C}_1 P_{11}^{-1} x_1 = C_r x_1. \tag{3.44}$$

Moreover, from Eq. (3.42), and (3.43), we have

$$x_2 = P_{21} P_{11}^{-1} x_1. \tag{3.45}$$

Thus, the original n^{th} order model represented by Eq. (3.33) is reduced to an r^{th} order model given by Eq. (3.44). The state variables of the approximate model are the same as the first r state variables of the original higher-order model. The remaining state variables are given in terms of the first r state variables by Eq.

(3.45). This model order reduction technique is used to design a robust decentralized periodic output feedback controller for a multimodel system comprising of 5 multivariable models.

Let us consider a family of plants $S = \{A_i, B_i, C_i\}$ defined by

$$\dot{x} = A_i x + B_i u, \quad y = C_i x, \quad i = 1, 2, 3, ..., M, \tag{3.46}$$

where $M = 5$. The discrete time systems with sampling interval τ seconds can be represented as

$$x(k+1) = \Phi_{\tau i} x(k) + \Gamma_{\tau i} u(k), \quad y(k) = C_i x(k). \tag{3.47}$$

The adjoint or the dual for the above systems would be

$$\hat{x}(k+1) = \Phi_{\tau i}^T \hat{x}(k) + C_i^T \hat{u}(k), \quad \hat{y}(k) = \Gamma_{\tau i}^T \hat{x}(k). \tag{3.48}$$

There exists a transformation V_i, such that,

$$\hat{x} = V_i \hat{z} \tag{3.49}$$

transforms the above system in Eq. (3.48) into the following block modal form as

$$\hat{z}(k+1) = \hat{\Phi}_i \hat{z}(k) + \hat{C}_i \hat{u}(k), \quad \hat{y}(k) = \hat{\Gamma}_i \hat{z}(k), \tag{3.50}$$

where

$$\hat{\Phi}_i = \begin{bmatrix} \Phi_{1i} & 0 \\ 0 & \Phi_{2i} \end{bmatrix}, \quad \hat{C}_i = \begin{bmatrix} C_{1i} \\ C_{2i} \end{bmatrix}, \quad \hat{\Gamma}_i = \begin{bmatrix} \Gamma_{1i} \\ \Gamma_{2i} \end{bmatrix} \tag{3.51}$$

and the eigen values are arranged in the order of their dominance. We now extract an r^{th} order model, retaining the r dominant eigen values, by truncating the above systems. Using Eqs. (3.50) and (3.51), we get

$$\hat{z}_r(k+1) = \Phi_{1i} \hat{z}_r(k) + C_{1i} \hat{u}(k), \quad \hat{y}_r(k) = \Gamma_{1i} \hat{z}_r(k) \tag{3.52}$$

Let $\hat{u} = S_{ri} \hat{z}_r$ be a stabilizing control for the reduced order model in Eq. (3.52). Thus, the closed loop reduced model $(\Phi_{1i} + C_{1i} S_{ri})$ becomes stable. Now,

$$\hat{Z}_r = \begin{bmatrix} I_r & : & 0_{r*(n-r)} \end{bmatrix} \hat{z} = \begin{bmatrix} I_r & : & 0_{r*(n-r)} \end{bmatrix} V_i^{-1} \hat{x}. \tag{3.53}$$

$\therefore$, we get,

$$u(k) = S_{ri} \begin{bmatrix} I_r & : & 0_{r*(n-r)} \end{bmatrix} V_i^{-1} \hat{x} = S_i \hat{x} \tag{3.54}$$

which makes the closed loop system $\left(\Phi_{\tau i}^T + C_i^T S_i\right)$ stable. But the eigen values of $\left(\Phi_{\tau i}^T + C_i^T S_i\right)$ and $\left(\Phi_{\tau i}^T + C_i^T S_i\right)^T$ are the same. So, $\left(\Phi_{\tau i}^T + C_i^T S_i\right)$ will also be stable. Thus, $S_i^T \equiv G_i$ is the output injection gain for the system in Eq. (3.47). The POF gain $\mathbf{K}$ is thus realized using these output injection gains by solving the linear equation $\mathbf{\Gamma}_i \mathbf{K} \approx G_i$.

The problem with controllers obtained in this way is that, although they are stabilizing and achieve the desired closed loop behavior at the output sampling instants, they may cause an excessive oscillation between inter-sampling instants. The controller obtained using the above equation will give the desired behaviour, but might require excessive control action and the POF gains obtained may be very high. To reduce this effect, we relax the condition that $\mathbf{K}$ exactly satisfy the above linear equation and include a constraint on it.

Solving $\mathbf{\Gamma}_i\mathbf{K} = G_i$ may give a POF gain that is higher in magnitude, amplifying the noise in a system. Hence, the conditions on $\| \mathbf{K} \| < \rho_{1i}$ for noise and $\| \mathbf{\Gamma}_i \mathbf{K} - G_i \| < \rho_{2i}$ for stability is imposed during the controller design. These restrictions on $\mathbf{K}$ are posed as LMI problem [49], [50], [121]. Thus, we arrive at the following inequalities as

$$\| \mathbf{K} \| < \rho_{1i}, \quad \| \mathbf{\Gamma}_i \mathbf{K} - G_i \| < \rho_{2i}. \tag{3.55}$$

Using the schur complement, it is straight forward to bring these conditions in the form of Linear Matrix Inequalities (LMI) as

$$\begin{bmatrix} \rho_{1i}^2 I & \mathbf{K} \\ \mathbf{K}^T & -I \end{bmatrix} < 0, \quad \begin{bmatrix} \rho_{2i}^2 I & (\Gamma_i \mathbf{K} - G_i) \\ (\Gamma_i \mathbf{K} - G_i)^T & -I \end{bmatrix} < 0. \tag{3.56}$$

Here, the LMI toolbox of MATLAB can be used for the design of $\mathbf{K}$. If the LMI constraints given in Eqs. (3.55) and (3.56) are solved using the above G_i, the robust periodic output feedback gain matrix may become full. This results in the control input of each plant being a function of the output of all the plants. To obtain the RDPOF control, the off-diagonal elements of $K_0, K_1, K_2, ..., K_{N-1}$ matrices are made equal to zero. So, the structure of K_i $(i = 0, 1, 2, 3, ..., N-1)$ matrix is assumed as $K_i = diag\ [k_{i11}, k_{i22}, k_{i33}, ...]$ and the desired gain matrices can be obtained. Now, it is evident that the control input to each actuator of the plant model is a function of the output of that corresponding sensor only. This makes the POF control technique a robust decentralized one and is more feasible. The RDPOF controller gains obtained by this method requires only constant gains and hence may be easier to implement in real time.

The RDPOF controller design via reduced order model is designed as follows [80]. The 5 multivariable SS models of the multimodel system which are obtained by varying the thickness of the beam is considered as the preliminary step in the controller design. A 12^{th} order SS model of (12×12) is obtained on retaining the first 6 modes of vibration ω_1 to ω_6. This higher order system is reduced to a simpler 6^{th} order model of (6×6), by considering the effects of the 6 most dominant (dominant in the sense of being closed to instability) eigen values. The eigen values of the original system that are farthest from the origin are neglected and only dominant eigen values of the original system in the reduced order model is retained.

An external force $\mathbf{f}_{ext}$ of 1 N is applied for duration of 50 ms at the free end of the beam for all the 5 models of the Fig. 2.5 and the OL responses are observed. RDPOF controller is designed for the multimodel system to suppress the vibrations. The sampling interval used is $\tau = 0.004$ secs. The discrete models are obtained for sampling time of $\tau = 0.004$ secs and for $\Delta = 0.0004$ secs. The reduced order models are computed from the adjoint discrete models. Using the method discussed in the previous paragraphs, stabilizing gain matrices S_{ri} are obtained for each reduced order model using the DLQR theory. Using aggregation techniques [125], the output injection gain G_i can be calculated for each higher order (actual) models. The CL impulse responses with the output injection gain is observed. The RDPOF gain can be obtained which approximately realizes this designed G_i for all the models of the family.

Here, as we are dealing with robust stabilization, we have to find a $\mathbf{K}$ which will satisfy $\mathbf{\Gamma}_i\mathbf{K} \approx G_i$ $(i = 1$ to $5)$ using the LMI approach so that the magnitude of the control effort required is less. 10 gain sequences of $\mathbf{K}$ are chosen, i.e., $K_1, ..., K_{10}$. In our problem considered $N = 10$ had given good encouraging results. Using the

output injection gains G_i, LMI constraints given in Eqs. (3.55) and (3.56) are solved for different values of ρ_1 and ρ_2 to find the RDPOF gain matrix $\mathbf{K}$ for the actual models via the reduced order model. The RDPOF gain matrix is given by

$$\mathbf{K} = 10^2 * \begin{bmatrix} -1.6410 & 0 \\ 0 & 0.0173 \\ 0.2375 & 0 \\ 0 & -0.148 \\ 1.1130 & 0 \\ 0 & -0.0212 \\ 0.6873 & 0 \\ 0 & -0.0040 \\ -0.4794 & 0 \\ 0 & 0.0177 \\ -0.8435 & 0 \\ 0 & 0.0122 \\ 0.4678 & 0 \\ 0 & -0.0217 \\ 0.0804 & 0 \\ 0 & 0.0084 \\ -0.0489 & 0 \\ 0 & -0.0027 \\ 0.0035 & 0 \\ 0 & 0.0003 \end{bmatrix}_{(20\times 2)} \tag{3.57}$$

With the designed robust controller being put in the loop, the CL impulse responses (sensor outputs y_1 and y_2) and the variation of the control signal u_1 and u_2 with time for the multimodel system consisting of 5 MIMO plants are observed and shown in Figs. 3.19 - 3.28 respectively.

3.2.4:1 Simulation Results and Discussions

RDPOF Controller is designed for the multimodel representation of a family of multivariable smart structure plants via the reduced order model [80]. These multivariable models of the beam are obtained by varying the thickness parameter of the beam. Simulations are performed and the various responses are observed for the multimodel system. Through the simulation results, it is shown that when the plant is placed with the designed robust decentralized POF controller, all the models perform well. The stability is guaranteed and the vibrations die out quickly. Observations are made with and without the controller to show the control effect.

In the designed control law, the control input to each actuator of the multivariable plant is a function of the output of that corresponding sensor only and the gain matrix has got all off-diagonal elements zero. This makes the POF control technique a robust decentralized one. This would render better control and is more feasible. The robust decentralized POF controller designed by the above method requires only constant gains and hence may be easier to implement. The designed control method is thus applied simultaneously to all the MIMO models and thus resulted in satisfactory behaviour of the responses to damp out the vibrations, which can be seen from the simulation results.

In this Section, a new algorithm is presented for the design of robust decentralized controllers for a multivariable system using POF feedback technique via the reduced order model. The computation of the output injection gain, which is needed to obtain the decentralized POF feedback gain becomes very tedious when a number of modes, especially greater than 5 are considered. Hence, an output injection gain is computed from the reduced order model of the smart system and using the aggregation techniques [125], an output injection gain can be obtained for the higher order model.

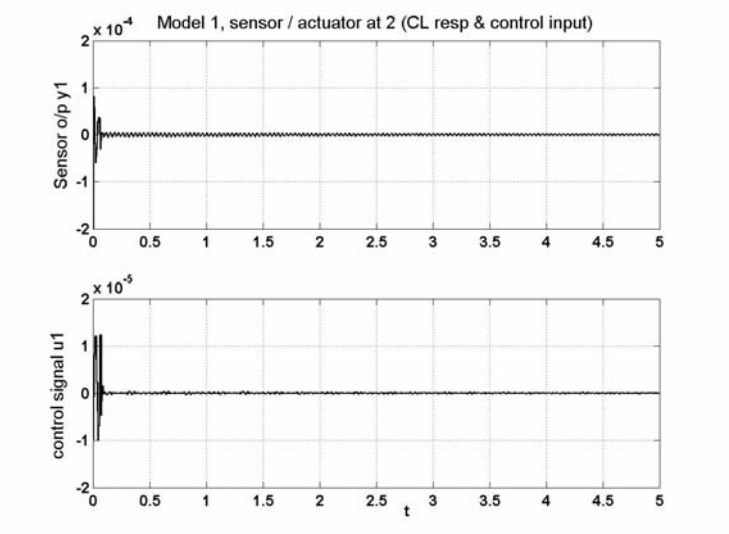

Fig. 3.19. CL response and control i/p (piezo placed at FE 2) : Model 1

The simulation results shows the effectiveness of the method presented. The RD-POF feedback gain which realizes this output injection gain, can be obtained for the actual model. It is found that the designed robust controller via the reduced order model provides good damping enhancement for all the models of the smart structure system. From the simulation results, it is inferred that as the thickness of the beam is increased, the sensor voltage reduces and more control effort is required to curb down the vibrations. An integrated FE model to analyze the vibration suppression capability of smart cantilever beams with surface mounted piezoelectric devices based on Euler-Bernoulli beam theory and reduced order modeling is presented in this Section [80].

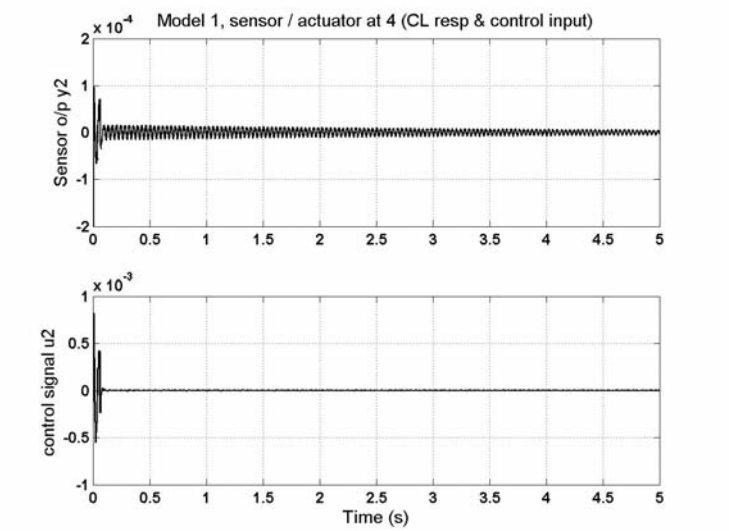

Fig. 3.20. CL response and control i/p (piezo placed at FE 4) : Model 1

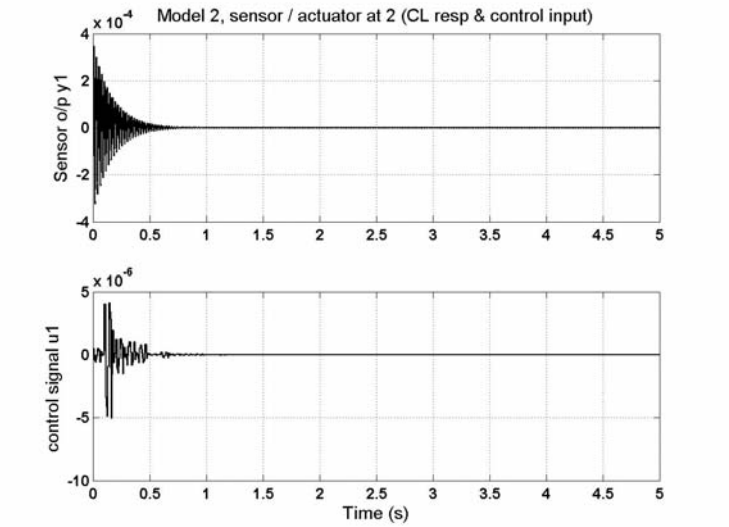

Fig. 3.21. CL response and control i/p (piezo placed at FE 2) : Model 2

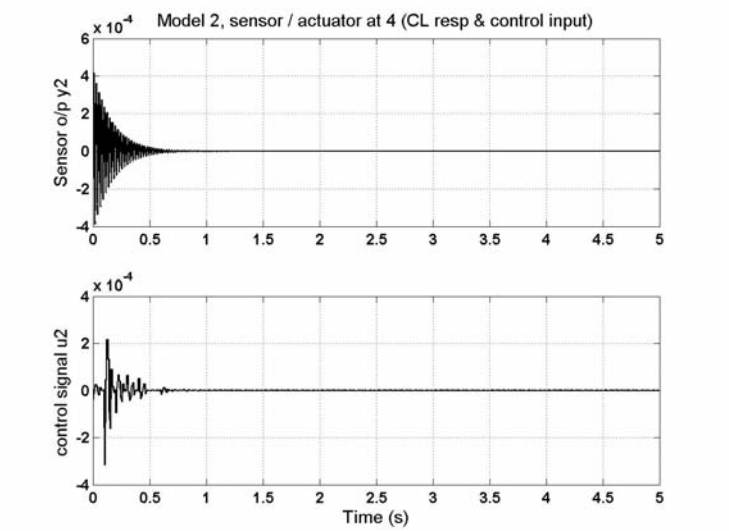

Fig. 3.22. CL response and control i/p (piezo placed at FE 4) : Model 2

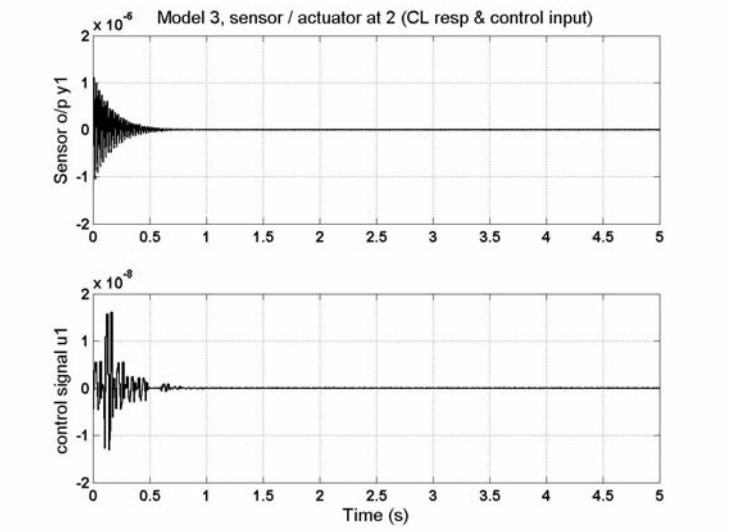

Fig. 3.23. CL response and control i/p (piezo placed at FE 2) : Model 3

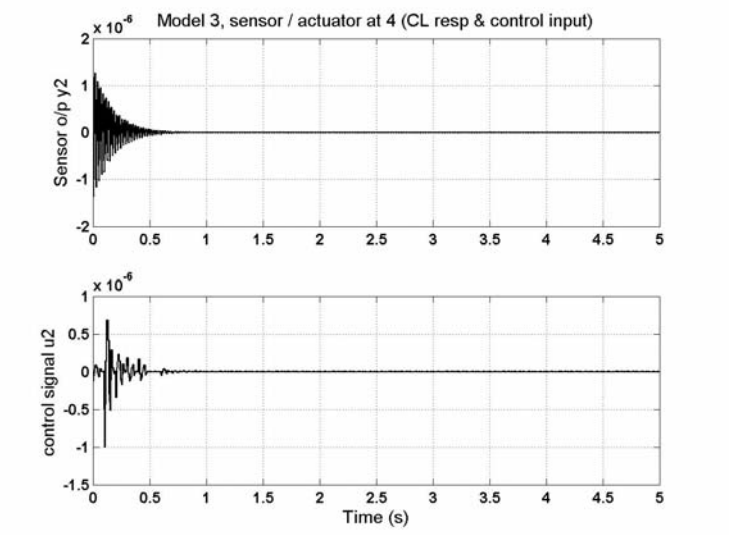

Fig. 3.24. CL response and control i/p (piezo placed at FE 4) : Model 3

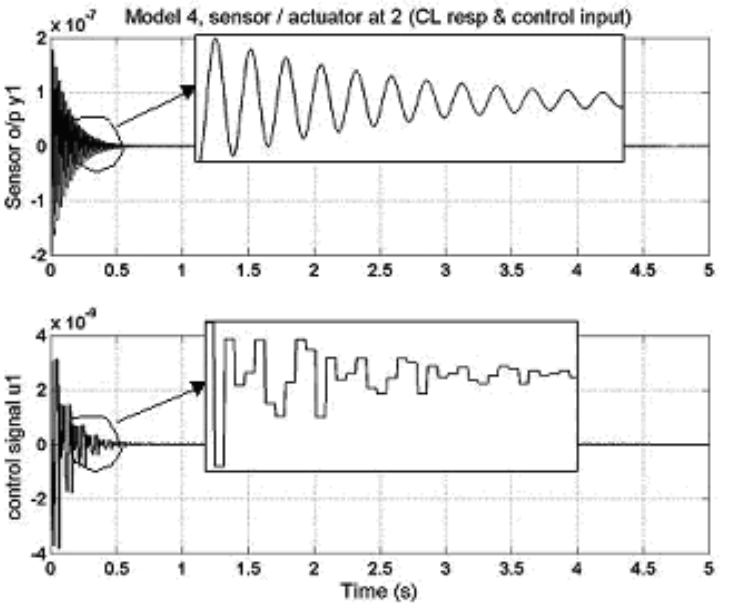

Fig. 3.25. CL response and control i/p (piezo placed at FE 2) : Model 4

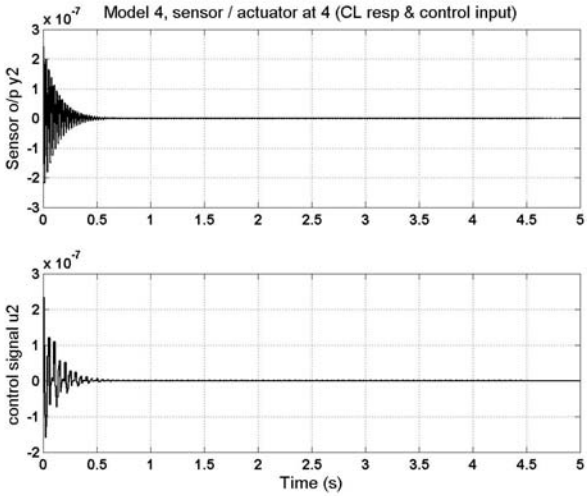

Fig. 3.26. CL response and control i/p (piezo placed at FE 4) : Model 4

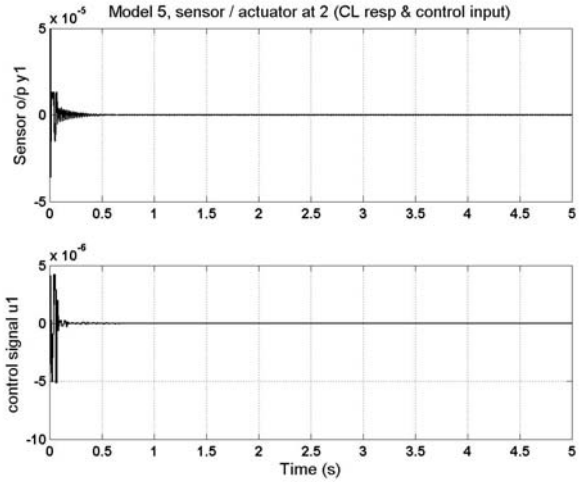

Fig. 3.27. CL response and control i/p (piezo placed at FE 2) : Model 5

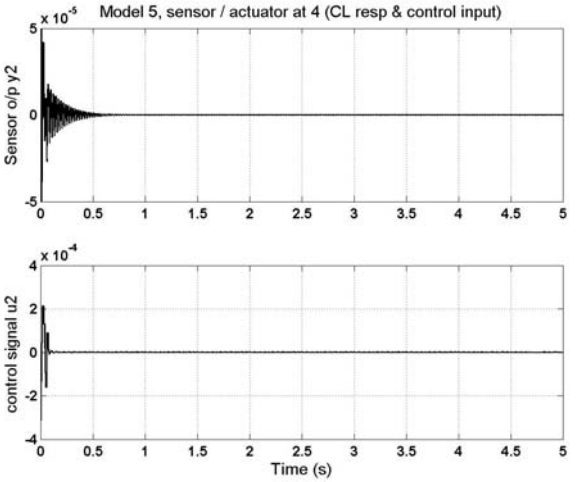

Fig. 3.28. CL response and control i/p (piezo placed at FE 4) : Model 5

3.3 Controller Design for Smart Structures Modelled Using Timoshenko Theory

In the following Sections, the design of the POF controllers for a smart structure modelled as SISO and MIMO systems using Timoshenko beam theory is presented.

3.3.1 Design of SISO Controllers for Smart Beams Using Surface Mounted Piezos

The POF control technique discussed in the section 3.1 is used to design the control strategy for the SISO representation of the developed smart structure model given in the Eqs. (2.172)-(2.175) with 1 actuator input and 1 sensor output for the various SISO models of the same plant shown in Fig. 2.7. A sixth order state space model of the system is obtained by retaining the first 3 modes of vibration of the system. The first 3 natural frequencies obtained are 3.75 Hz, 23 Hz and 62.5 Hz. The performance of the designed controller is evaluated for AVC by carrying out the simulations in MATLAB by observing the various responses. The effect of varying the sensor/actuator location at different FE positions (from fixed end to the free end) on the beam is observed and the conclusions are finally drawn for the best performance model.

The controller is designed on the similar lines as explained in the section 3.2.1 for Euler-Bernoulli beams modelled as an single input single output system. The sampling interval τ is taken as 0.004 secs and the number of sub-intervals N was taken as 10. An external force is applied at the free end of the beam, thus subjecting

it to vibrations. The OL responses are observed. The CT system in Eqs. (2.172)-(2.175) is sampled at a rate of $\frac{1}{\tau}$, thus giving rise to tau system as

$$\mathbf{\Phi}_\tau = 10^4 \begin{bmatrix} 0.0001 & -0.0000 & -0.0000 & 0.0000 & -0.0000 & -0.0000 \\ -0.0000 & 0.0001 & 0.0000 & -0.0000 & 0.0000 & 0.0000 \\ -0.0000 & 0.0000 & 0.0000 & -0.0000 & 0.0000 & 0.0000 \\ -0.0111 & -0.0000 & -0.0000 & 0.0001 & -0.0000 & -0.0000 \\ -0.0000 & -0.3880 & 0.0000 & -0.0000 & 0.0001 & 0.0000 \\ -0.0000 & 0.0000 & -1.7494 & -0.0000 & 0.0000 & -0.0000 \end{bmatrix}, \quad \mathbf{\Gamma}_\tau = 10^{-5} \begin{bmatrix} -0.0000 \\ 0.0000 \\ -0.0000 \\ -0.2234 \\ 0.8793 \\ -0.9155 \end{bmatrix}. \tag{3.58}$$

Similarly, the tau systems for the other SISO models of the smart beam are obtained. The stabilizing output injection gains are obtained for the tau system such that the eigenvalues of $\left(\mathbf{\Phi}_i^N + G_i C_i\right)$, $i = 1, .., 4$ are placed inside the unit circle at appropriate locations and the response of the system has a good settling time. The output injection gain obtained is as

$$G_1 = 10^3 \ * \ \begin{bmatrix} -0.0000 & 0.0000 & -0.0000 \\ -23.52 & 129.86 & -112.3952 \end{bmatrix} \tag{3.59}$$

for the model 1. Similarly, the output injection gains for the other 3 models are obtained. The CL impulse response of all the 4 models of the smart system with the output injection gain are observed. Now, the CT system given in Eqs. (2.172)-(2.175) is sampled at a rate of $\frac{1}{\Delta}$, thus giving rise to the delta system as

$$\mathbf{\Phi} = 10^3 \begin{bmatrix} 0.0010 & 0.0000 & -0.0000 & 0.0000 & -0.0000 & 0.0000 \\ 0.0000 & 0.0010 & -0.0000 & 0.0000 & 0.0000 & 0.0000 \\ 0.0000 & -0.0000 & 0.0010 & 0.0000 & -0.0000 & 0.0000 \\ -0.0111 & -0.0000 & 0.0000 & 0.0010 & -0.0000 & 0.0000 \\ -0.0000 & -0.4165 & 0.0000 & -0.0000 & 0.0010 & 0.0000 \\ -0.0000 & 0.0000 & -3.0725 & -0.0000 & 0.0000 & 0.0010 \end{bmatrix}, \quad \mathbf{\Gamma} = 10^{-5} \begin{bmatrix} -0.0000 \\ 0.0000 \\ -0.0000 \\ -0.0224 \\ 0.0944 \\ -0.1608 \end{bmatrix} \tag{3.60}$$

for the model 1.

Similarly, the delta systems for the other 3 SISO models are obtained. The POF gain matrix $\mathbf{K}$ for the smart system is obtained by solving $\mathbf{\Gamma}_i \mathbf{K}_i \approx G_i$ using the LMI optimization method which reduces the amplitude of the control signal u. The POF gain matrix for the SISO model 1 of the smart Timoshenko beam is given by

$$\mathbf{K}_1^T = 10^2 \begin{bmatrix} 16.88 & 10.85 & 5.73 & -4.33 & -3.42 & -1.78 \end{bmatrix}. \tag{3.61}$$

Similarly, the POF gains are obtained for the other 3 models of the smart structure plant. With the designed controller put in the loop, the closed loop impulse responses (sensor outputs) of the system and the variation of the control signal with time t for the 4 SISO state space models of the smart system are observed and shown in Figs. 3.29 - 3.36 respectively. The frequency response plot for the model 1 is shown in Fig. 3.37. Similarly, the bode plots of the other 3 SISO models of the smart system are also observed.

3.3.1.1 Simulation Results and Discussions

POF controllers are designed for the smart flexible cantilever beam for the 4 SISO models of the smart plant to suppress the first 3 vibratory modes. After observing the various responses as shown in the Figs. 3.29 - 3.37, the comparison and discussion of the simulation results of the vibration control are presented here for the best model required for AVC.

From the simulation results, it is observed that modeling a smart structure by including the sensor / actuator mass and stiffness and by varying its location on

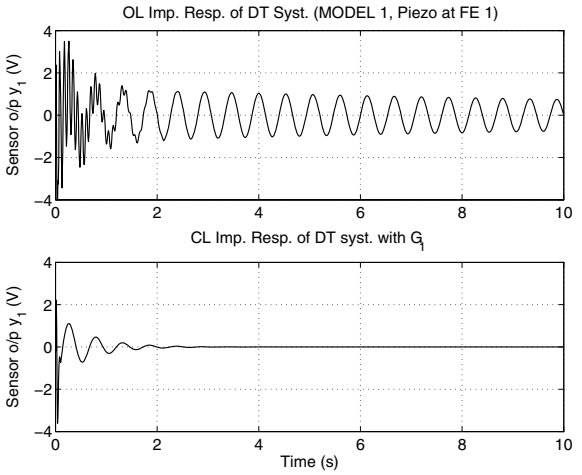

Fig. 3.29. OL, CL response with o/p injection gain G_1 (MODEL 1)

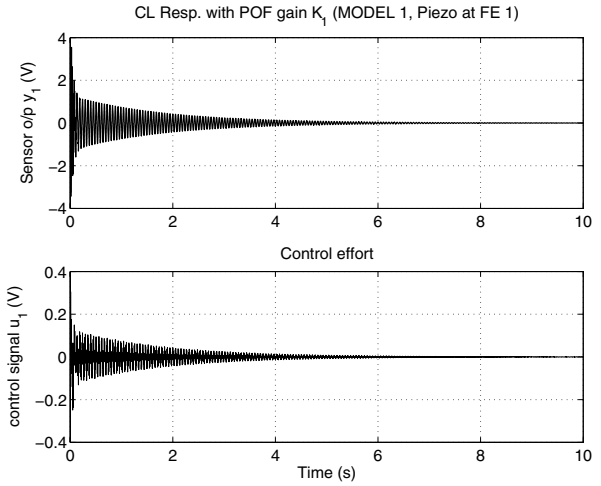

Fig. 3.30. CL response with POF gain $\mathbf{K}_1$ and control i/p u_1 (MODEL 1)

the beam from the free end to the fixed end introduces a considerable change in the system's structural vibration characteristics. Through the simulation results, it is inferred that when the plant is placed with this designed controller, the plant performs well and the vibrations are damped out quickly. The observations are made with and without the controller to show the control effect. It was observed that without control the transient response was unsatisfactory and with control the vibrations are suppressed.

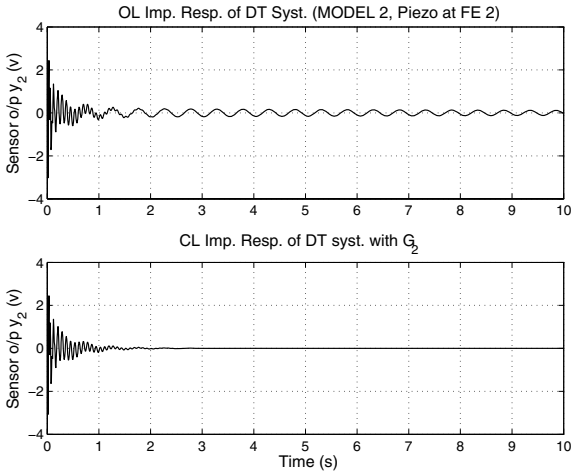

Fig. 3.31. OL, CL response with o/p injection gain G_2 (MODEL 2)

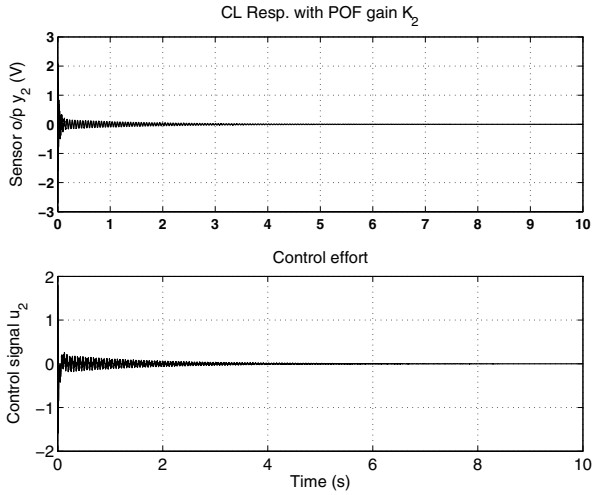

Fig. 3.32. CL response with POF gain $\mathbf{K}_2$ and control i/p u_2 (MODEL 2)

Model 1 can be used as the best model for AVC as the control will be more effective at the root. This is because of the following inferences observed after performing the simulations.

- The sensor output voltage is greater due to the heavy distribution of the bending moment near the fixed end, thus leading to a larger strain rate.
- Less control effort is required to damp out the vibrations.
- Sensitivity of the sensor / actuator pair depends on its location on the beam.
- The response characteristics with G and $\mathbf{K}$ are the best.

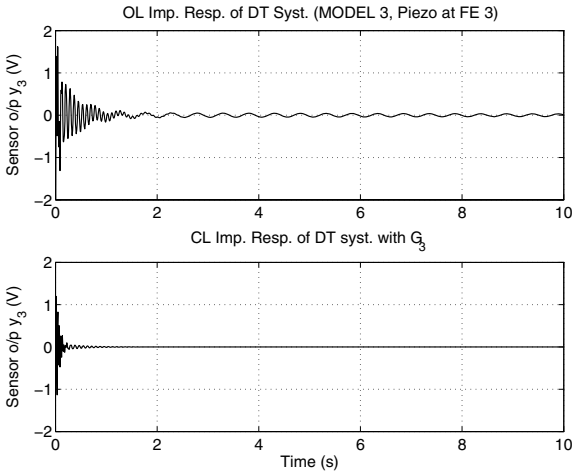

Fig. 3.33. OL, CL response with o/p injection gain G_3 (MODEL 3)

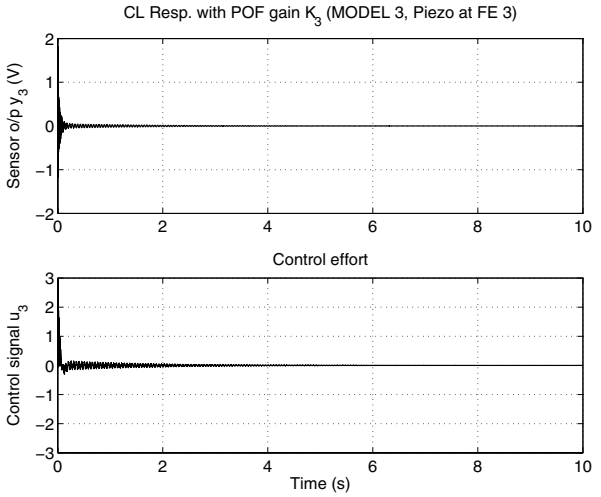

Fig. 3.34. CL response with POF gain $\mathbf{K}_3$ and control i/p u_3 (MODEL 3)

- Vibration characteristics of the system depended not only on the collocation of the piezo pair, but also on many factors such as the gain of the amplifier used, the mode number and the location of the piezo pair at the nodal points from the fixed end.

Further, responses are obtained by considering the first 2 vibratory modes also. Results are compared with the controllers designed for first 3 vibratory modes. The responses without controller, with G, $\mathbf{K}$ and magnitude of the control input u are obtained. The obtained responses by retaining the first 2 modes were nearly the same as the responses obtained when 3 vibration modes were considered. The designed

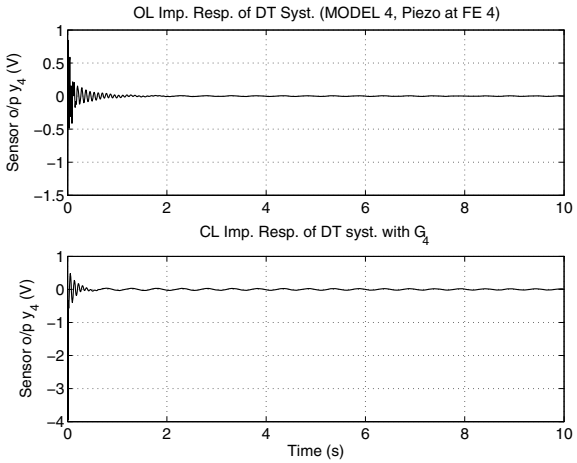

Fig. 3.35. OL, CL response with o/p injection gain G_4 (MODEL 4)

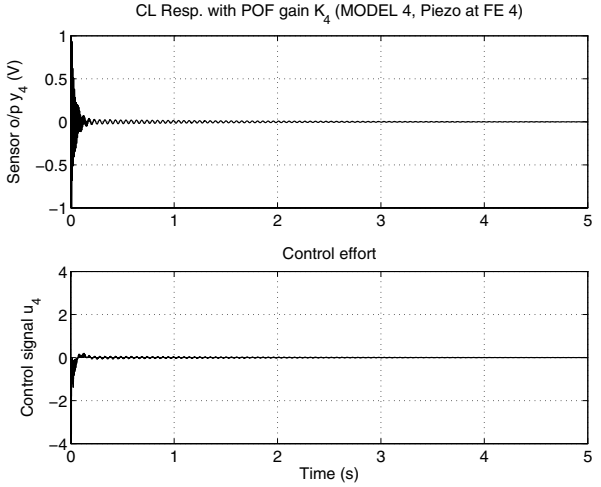

Fig. 3.36. CL response with POF gain $\mathbf{K}_4$ and control i/p u_4 (MODEL 4)

POF controller requires constant gains and hence may be easier to implement in real time. The limitations of Euler-Bernoulli beam theory such as the neglection of the axial displacements have been considered here while modeling the beam. Timoshenko beam theory corrects the simplifying assumptions made in Euler-Bernoulli beam theory and the model obtained can be closer to a exact one.

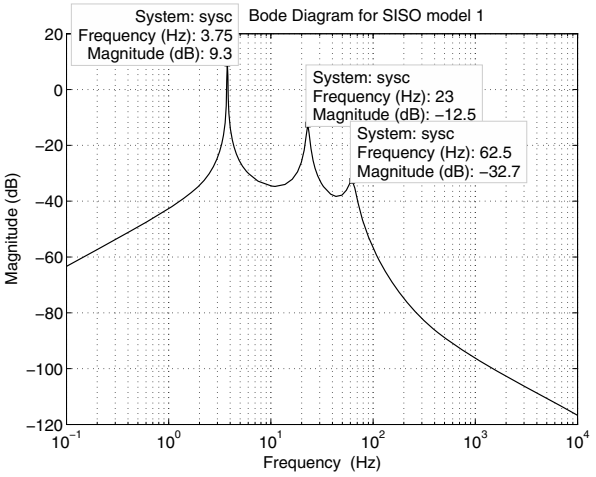

Fig. 3.37. Bode plot of MODEL 1

3.3.2 Design of MIMO Controllers for Smart Beam with Surface Mounted Piezos

In this Section, we develop the control system design using the POF control law discussed in 3.1 for the multivariable representation of the flexible cantilever beam given by the Eqs. (2.103) and (2.104) bonded with surface mounted sensors and actuators as collocated pairs through smart structure concept [78]. The numerical value of the state space matrices is given by the Eq. (2.180) in section 2.2.2. The performance of the MIMO smart beam is hereby evaluated for vibration control by carrying out the simulations by observing the various responses. The effect of placing the sensor-actuator pair at 2 different FE locations on the beam is observed and the conclusions are drawn. The multivariable controller is designed on the similar lines as explained in the section 3.2.2. The sampling interval τ is taken as 0.004 secs and the number of sub-intervals N was taken as 10. The POF gain matrix $\mathbf{K}$ for the MIMO model of the smart beam is given by

$$\mathbf{K}^T = 10^2 * \begin{bmatrix} -0.45 & 0.23 & -0.35 & -0.49 & 0.56 & -0.72 & 0.89 & 0.93 & 0.87 & 0.41 \\ -0.46 & 0.28 & -0.39 & -0.51 & 0.59 & -0.76 & 0.98 & 1.01 & 1.04 & 0.97 \end{bmatrix}, \quad (3.62)$$

$$= \begin{bmatrix} \mathbf{K}_1^T & \mathbf{K}_2^T \end{bmatrix}.$$

With the designed multivariable POF controller being put in the loop with the smart beam modelled using Timoshenko beam theory, CL impulse responses (sensor outputs y_1, y_2) with the the output injection gain G and the POF gain $\mathbf{K}$, the tip displacements with and without the controller, the control effort u_1, u_2 required to control the vibrations are observed and graphically displayed as shown in Figs. 3.38 - 3.40 respectively.

The MIMO simulation results are compared with the SISO simulation results as follows. A state space model is obtained by considering the mass and stiffness of

both the piezo patches at the 2 FE positions, but only one pair is considered active at a time. Hence, a SISO system is obtained with only 1 input and 1 output, say, the piezo placed at the free end is considered as active, whereas the pair placed at FE position 2 is inactive. The results of this SISO simulations for vibration suppression was observed and shown in Figs. 3.41 and 3.42.

3.3.2.1 Simulation Results and Discussions

POF controller has been designed for the MIMO smart structure model [78]. The beam was divided into 4 finite elements with sensor / actuator placed at positions 2 and 4. The various responses are obtained for the developed state space multivariable model. Through the simulation results, it is shown that when the plant is placed with this designed controller, it performs well and the vibrations are suppressed quickly. It is also observed that modeling a smart structure by including the sensor / actuator mass and stiffness and by placing the sensor / actuator at two different positions introduces a considerable change in the structural vibration characteristics than placing the sensor / actuator pair at only one location (Fig. 3.41).

The response takes lesser time to settle than the SISO case (Fig. 3.41) and the vibrations are damped out quickly. The control effort required is also less. The impulse responses with the output injection gain and the POF gain shows better performance. The sensor-actuator pair kept at position 2 controls the 2 vibratory modes at that finite element position 2, while the pair kept at position 4 also controls the 2 vibratory modes, but placed at that finite element position 4. A overall better performance of the system is obtained. Hence, it can be concluded that multivariable control of a smart structure is better compared to the SISO control as there will be multiple interactions of the input and output which will cause the vibrations in the system to damp out quickly. Responses were observed without control (open loop responses) and were compared with the control (closed loop responses) to show the control effect. From the simulations, it was observed that without control, the transient response was unsatisfactory and with control, the vibrations are suppressed to a larger extent.

MIMO dynamic analysis is able to identify pairs of modes that occur at nearly identical frequencies. SISO experiments are not actually reliable when it comes to accurate identification of mode pairs because they are unable to positively decipher mode pairs from signal noise in the measured Frequency Response Functions (FRF). Depending on the application, the smearing of the mode pairs into single modes may adversely affect the control algorithm, depending on the algorithm's sensitivity to the identified resonant frequencies of the system. MIMO excitation is better than SISO excitation as exciting only at a single point may cause poor distribution of input energy throughout the structure and may result in somewhat slightly disturbed frequency responses. A multi input test provides better energy distribution and even better actuation forces.

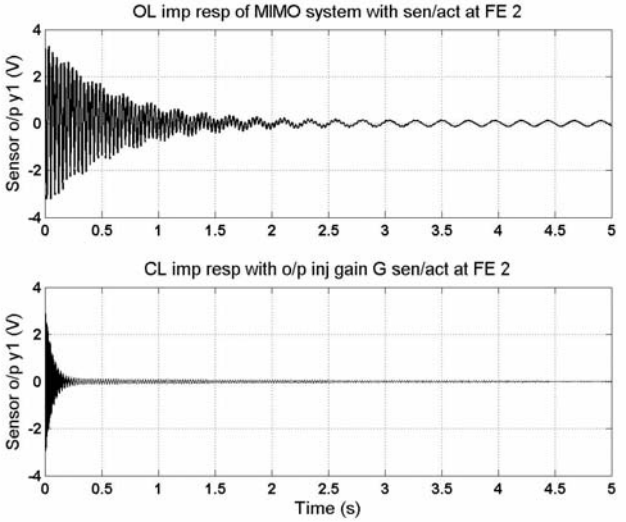

(a)

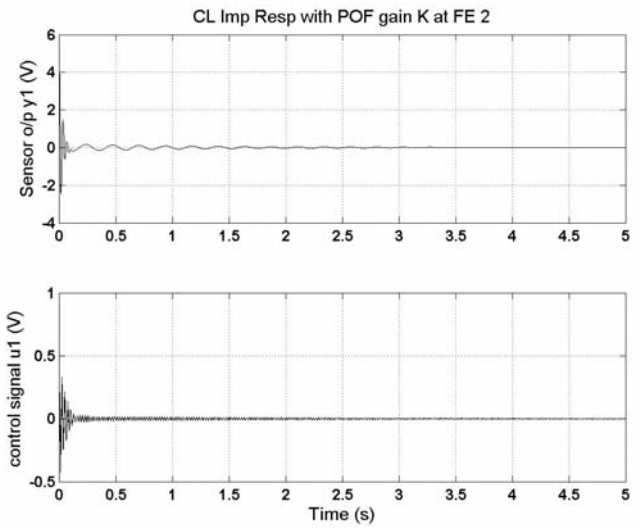

(b)

Fig. 3.38. OL and CL responses (with o/p injection gain G_1, POF gain $\mathbf{K}_1$), control i/p u_1 of the beam as a MIMO system (piezo patch placed at FE position 2)

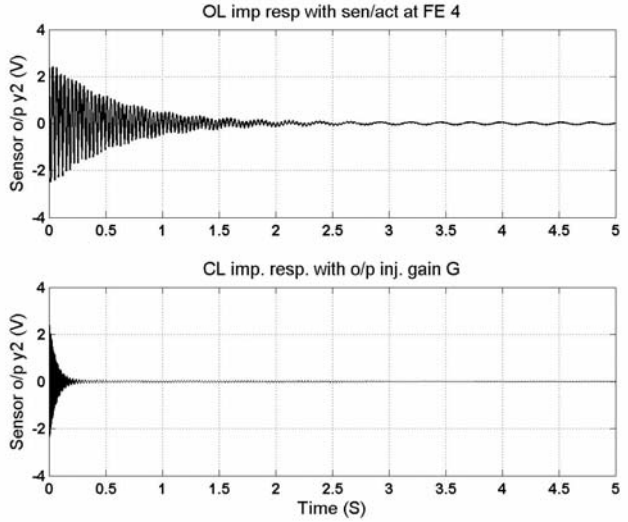

(a)

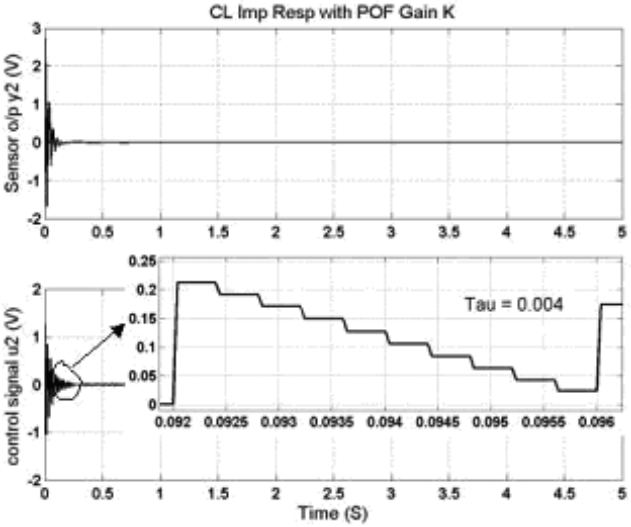

(b)

Fig. 3.39. OL and CL responses as a MIMO system (with o/p injection gain G_2, POF gain $\mathbf{K}_2$), control i/p u_2 of the beam as a MIMO system (piezo patch placed at FE position 4)

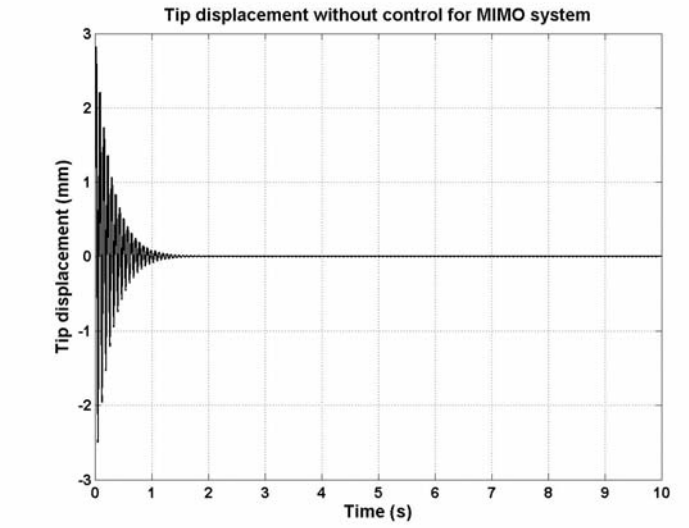

(a)

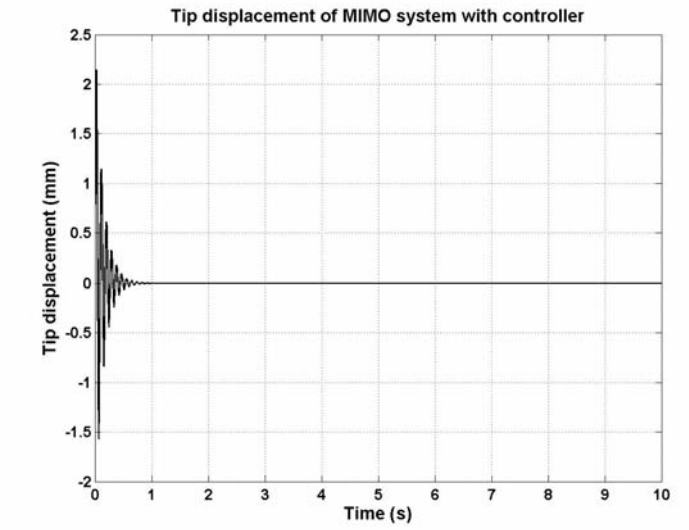

(b)

Fig. 3.40. Tip displacements of MIMO system without and with controller

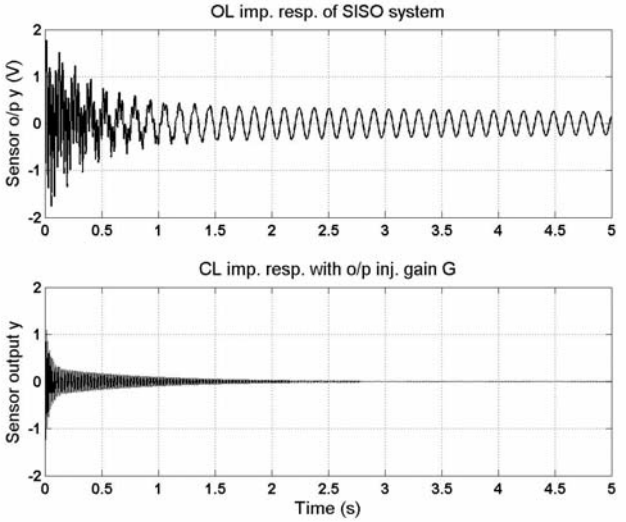

(a)

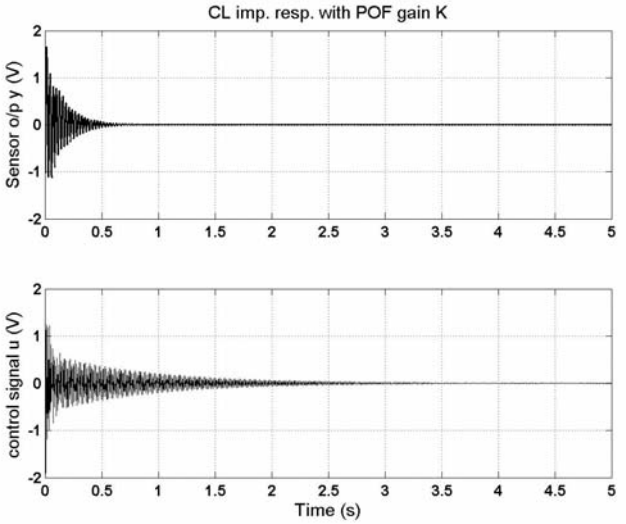

(b)

Fig. 3.41. OL and CL responses(with o/p injection gain G, POF gain $\mathbf{K}$), control i/p u of the beam as a SISO system (piezo patch placed at FE position 4)

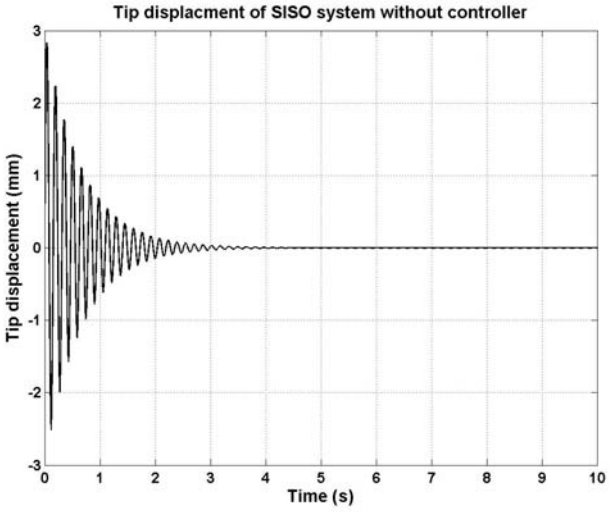

(a)

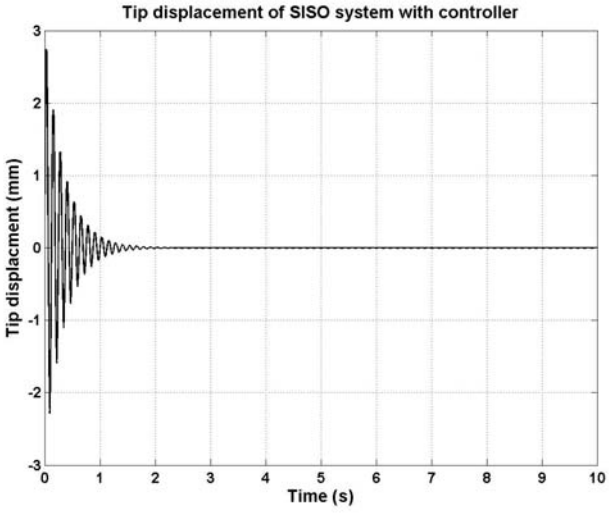

(b)

Fig. 3.42. Tip displacements of SISO system without and with controller (piezo at free end)

3.3.3 Design of SISO Controllers for Smart Beams Using Embedded Piezos

In the following Section, we develop the control strategy [75] for the developed smart structure model given in the Eqs. (2.242)-(2.243) using the POF control law discussed in the Section 3.1 for the various SISO models of the same plant. The sandwiched beam is divided into 5 FE and the control actuator is placed at FE position 1, whereas the sensor is varied from position 2 to 5, i.e., from the nearby fixed end to the free end. Four state space SISO models (1 input and 1 output) are thus developed for the 4 different configurations of the beam considered as shown in Fig. 2.12.

In all the 4 cases, the length of the beam is 20 cm and its cross section is 1 mm by 2 cm. The length of the piezo patch is 6 cm and its cross section is 1 mm by 2 cm. The only change in all the 4 models is in the location of the sensor. A sixth order state space model of the system is obtained on retaining the first 3 modes of vibration of the system. The first 3 natural frequencies obtained are 52.03 Hz, 97.21 Hz and 145.81 Hz. The designed POF controller is used to control the first 3 vibration modes of the sandwiched cantilever beam embedded with shear sensors and actuators through smart structure concept [75]. The performance of the controller is evaluated for vibration control by carrying out the simulations in MATLAB by observing the various responses. The effect of placing the sensor at different locations in the embedded sandwiched structure as non-collocated pair is observed and the conclusions are finally drawn.

The controller is designed on the similar lines as explained in the section 3.2.1 for Euler-Bernoulli beams and in section 3.3.1 for Timoshenko beams. The sampling interval τ is taken as 0.004 secs and the number of sub-intervals N was taken as 10. An external force is applied at the free end of the beam, thus subjecting it to vibrations. The OL responses are observed. The discrete models are obtained by sampling the system in (2.242)-(2.243) at a rate of $\frac{1}{\tau}$ and $\frac{1}{\Delta}$ respectively giving rise to $(\Phi_{\tau i}, \Gamma_{\tau i}, C_i)$-tau systems and (Φ_i, Γ_i, C_i)-delta systems respectively $(i = 1, .., 4)$ as

$$\Phi_\tau = \begin{bmatrix} 0.2611 & -0.0000 & 0.0000 & 0.0029 & -0.0000 & 0.0000 \\ -0.0000 & -0.7580 & -0.0000 & -0.0000 & 0.0010 & -0.0000 \\ 0.0000 & -0.0000 & -0.8541 & 0.0000 & -0.0000 & -0.0005 \\ -314.9974 & -0.0000 & -0.0000 & 0.2580 & -0.0000 & 0.0000 \\ -0.0000 & -389.9351 & 0.0000 & -0.0000 & -0.7619 & -0.0000 \\ -0.0000 & 0.0000 & 450.0271 & 0.0000 & -0.0000 & -0.8496 \end{bmatrix}, \quad \Gamma_\tau = 10^{-7} \begin{bmatrix} 0.0016 \\ -0.0000 \\ -0.0019 \\ 0.6915 \\ -0.0000 \\ 0.4636 \end{bmatrix} \tag{3.63}$$

and

$$\Phi = \begin{bmatrix} 0.9915 & -0.0000 & 0.0000 & 0.0004 & -0.0000 & 0.0000 \\ 0.0000 & 0.9703 & 0.0000 & -0.0000 & 0.0004 & 0.0000 \\ 0.0000 & 0.0000 & 0.9631 & 0.0000 & -0.0000 & -0.0003 \\ -42.6203 & 0.0000 & -0.0000 & 0.9910 & -0.0000 & -0.0000 \\ -0.0000 & -147.5971 & -0.0000 & -0.0000 & 0.9688 & 0.0000 \\ 0.0000 & 0.0000 & 236.7758 & 0.0000 & 0.0000 & 0.9655 \end{bmatrix}, \quad \Gamma = 10^{-7} \begin{bmatrix} 0.0000 \\ -0.0000 \\ -0.0000 \\ 0.0936 \\ 0.0000 \\ 0.2440 \end{bmatrix} \tag{3.64}$$

for the model 1.

Similarly, the tau and delta systems for the other SISO models of the embedded beam are obtained. It is found that all the discrete models were controllable and observable. The stabilizing output injection gains are obtained for the tau system such that the eigenvalues of $\left(\mathbf{\Phi}_i^N + G_i C_i\right),\ i = 1, .., 4$ lie inside the unit circle and the response of the system has a good settling time. The output injection gain for the SISO model 1 is obtained as

$$G_i = \begin{bmatrix} -4.05 & 5.32 & 2.24 & 1.81 & -8.62 & 3.63 \end{bmatrix}. \tag{3.65}$$

Similarly, the output injection gain for the other 3 models is obtained. The closed loop impulse response of the 4 models of the system with the output injection gain is also observed. The POF gain matrix $\mathbf{K}$ for the smart beam model is obtained by solving $\mathbf{\Gamma}_i\mathbf{K}_i \approx G_i$ using the LMI optimization method which reduces the amplitude of the control signal u. With the designed controller put in the loop, the closed loop impulse response (sensor output) with the POF gain $\mathbf{K}$ for the different SISO models of the smart system are observed. The POF gain matrix for the SISO model 1 of the smart Timoshenko beam is given by

$$\mathbf{K}_1^T = \begin{bmatrix} 32.10 & -45.78 & 45.32 & -32.78 & 12.92 & 12.49 \\ & & & -36.69 & 49.68 & -49.34 & 37.73 \end{bmatrix}. \tag{3.66}$$

Similarly, the POF gains are obtained for the other 3 models of the smart structure plant. The closed loop impulse responses (sensor outputs) of all the models with the POF gain K of the system is observed. Also, the variation of the control signal with time for the 4 models of the sandwiched system is observed [75]. The comparisons of the quantitative results of the OL and CL responses (with output injection gain, POF gain) and with the magnitude of the control efforts, their settling times required is shown in Table 3.1.

Table 3.1. Quantitative comparative results of POF simulations for the SISO system (terms inside the brackets indicate the settling values), only the +ve values shown

Model	OL	CL with G	CL with K	Control i/p u
1	8 mV (12 secs)	7 mV 4 (secs)	6 mV (4 secs)	1 V
2	7 mV (15 secs)	5 mV 4.5 (secs)	4 mV (5 secs)	1.8 V
3	6 mV (18 secs)	4 mV 5 (secs)	3.6 mV (5.5 secs)	2.9 V
4	5 mV (20 secs)	3.2 mV 5.5 (secs)	3 mV (6 secs)	3.8 V

3.3.3.1 Simulation Results and Discussions

Different smart cantilever beam models with embedded shear sensors / actuators are developed using the Timoshenko beam theory for different sensor locations keeping the actuator location fixed. POF controllers are designed for the 4 SISO models of the smart embedded sandwiched structure to suppress the first 3 vibratory modes. The various responses are obtained for each of the SISO models. The comparison and discussion of the simulation results of the vibration control for the best model required for AVC is arrived at.

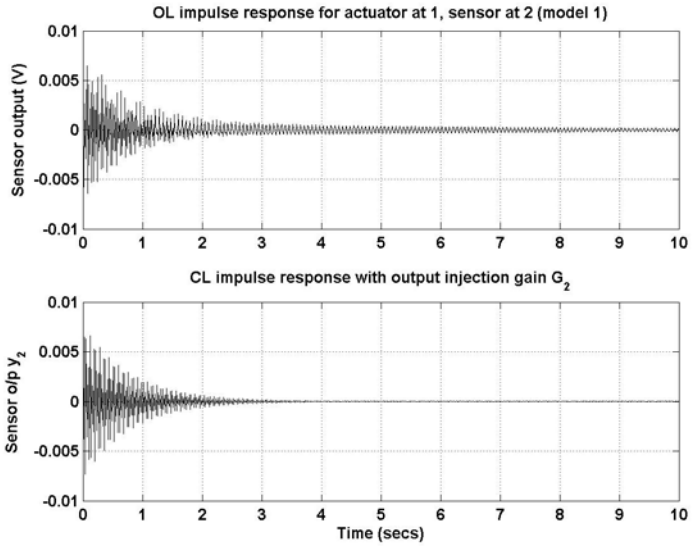

(a) OL response and CL response with G

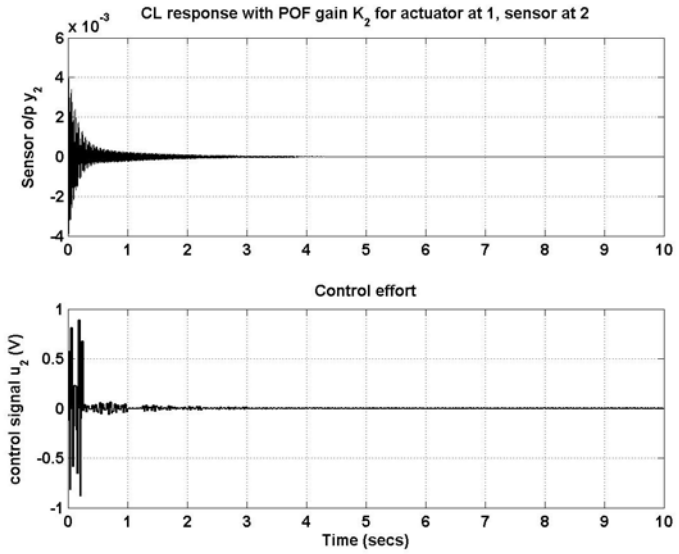

(b) CL response with **K** and control u

Fig. 3.43. OL and CL responses with G, **K** and control effort u (Model 1)

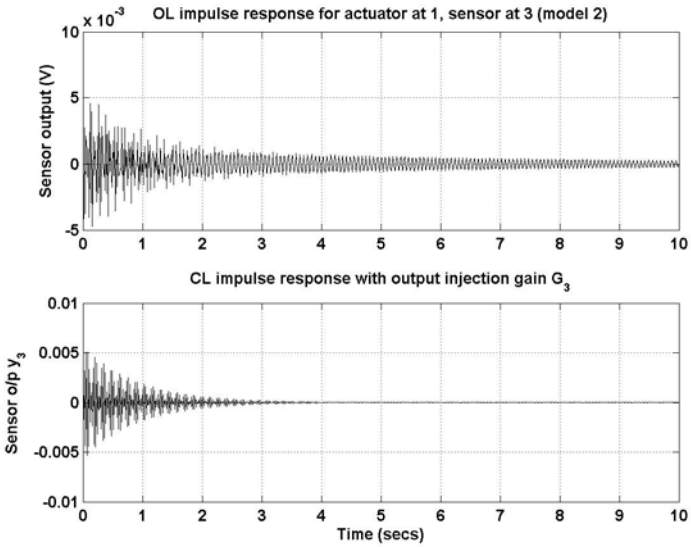

(a) OL response and CL response with G

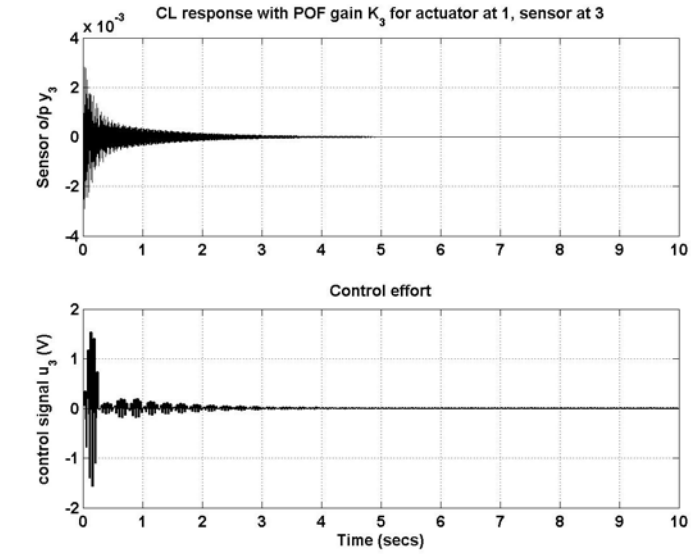

(b) CL response with **K** and control u

Fig. 3.44. OL and CL responses with G, **K** and control effort u (Model 2)

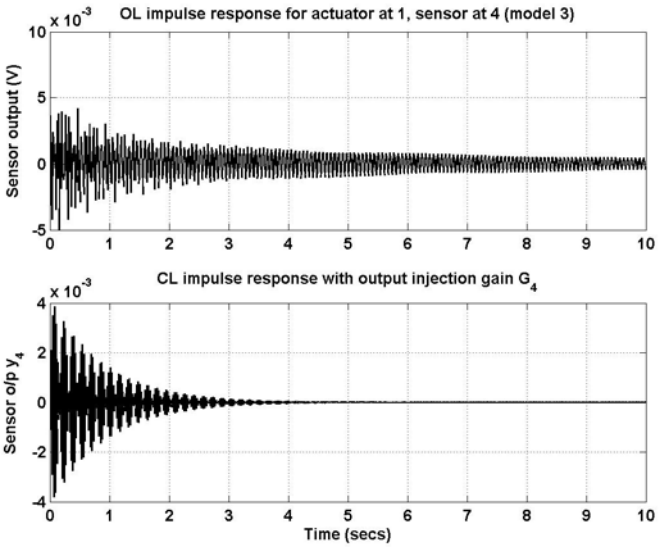

(a) OL response and CL response with G

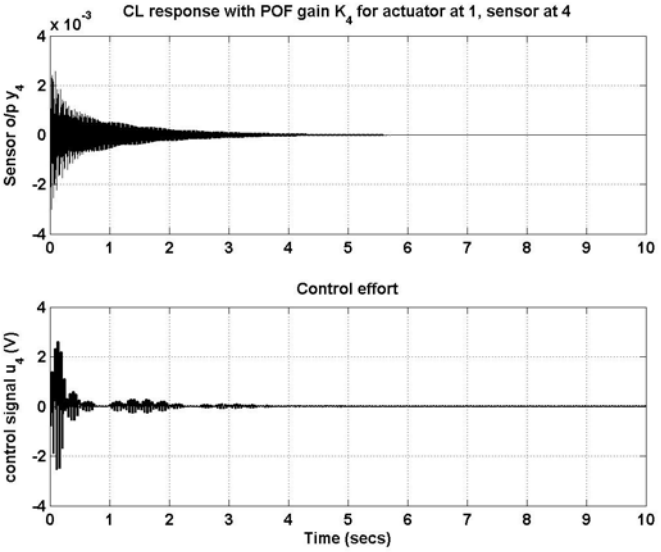

(b) CL response with **K** and control u

Fig. 3.45. OL and CL responses with G, **K** and control effort u (Model 3)

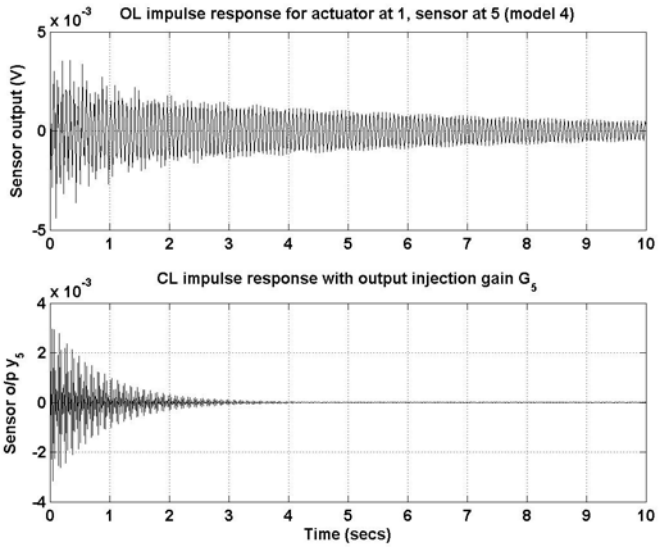

(a) OL response and CL response with G

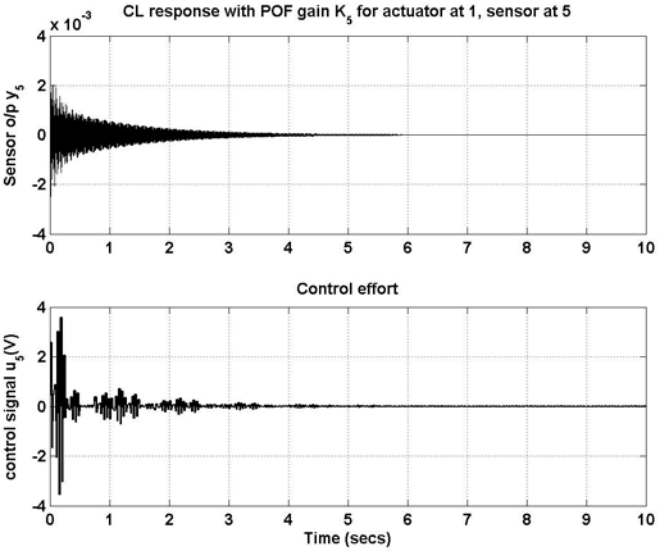

(b) CL response with **K** and control u

Fig. 3.46. OL and CL responses with G, **K** and control effort u (Model 4)

From the simulation results, it is observed that by varying the sensor location on the beam from the free end to the fixed end introduces a considerable change in the system's structural vibration characteristics. From the simulation results, it is inferred that when the plant is placed with this designed controller, the plant performs well and the responses settles in a quicker time than the open loop counterpart. The magnitude of the control signal required increases as the position of the sensor is changed from the nearby fixed end and moved towards the free end of the smart cantilever beam. The impulse responses show better performance when the sensor is at the nearby fixed end rather than at the free end.

It is also observed that the maximum amplitude of the control voltage required to damp out the vibrations is less when the sensor is placed at FE position 2 than at the free end. Thus, the observations are made with and without the controller to show the control effect. The designed POF controller requires constant gains and hence may be easier to implement in real time. The simulation results show that a periodic output feedback controller based on Timoshenko beam theory is able to satisfactorily control the first 3 modes of vibration of the smart cantilever beam and this shows the effectiveness of the designed controller.

Surface mounted piezoelectric collocated sensors and actuators (piezo-patches bonded to the master structure at top and bottom of the single flexible beam) are usually placed at the root of the structure (near by the fixed end) as collocated pairs, one above and the other below the beam in order to achieve most effective sensing and actuation. This subjects the sensors / actuators to high longitudinal stresses that might damage the brittle piezo-electric material. Furthermore, surface mounted sensors / actuators are likely to be damaged by the contact with surrounding objects. The temperature effects, stray magnetic fields, noise signals, environmental conditions, etc., may have some effects on the behavior of the PZT's.

Due to these reasons, there may be some changes in the plant behavior. Embedded shear sensors / actuators can be used to alleviate these problems. The natural frequencies were found to be little on the higher side in the case of embedded beams. The limitations of Euler-Bernoulli beam theory such as the neglection of the shear and axial displacements have been considered here while modeling the beam. Timoshenko beam theory corrects the simplifying assumptions made in Euler-Bernoulli beam theory and the model obtained can be a exact one.

3.3.4 Design of MIMO Controller for Smart Beams Using Embedded Piezos

In the following Section, we develop the control strategy for the multivariable representation of the developed smart structure model given in Eqs. (2.247)-(2.248) for an MIMO case shown in the Fig. 2.13 with its numerical values given in Eq. (2.250) using the POF control law discussed in the Section 3.1. The embedded beam is divided into 8 FE and the control actuators are embedded into the sandwiched structure at FE positions 2 and 4, whereas the sensors are embedded into the structure at FE positions 6 and 8 respectively. An external force is applied at the free end of the beam, thereby subjecting it to vibrations.

The vibrations are damped out quickly by the incorporation of a POF controller being put in the feedback loop with the plant. The designed POF controller is used to suppress the first 3 vibration modes of the sandwiched beam. The multivariable

controller is designed on the similar lines as explained in section 3.2.2 for Euler-Bernoulli beams and in section 3.3.2 for Timoshenko beams. The performance of the smart beam is hereby evaluated for vibration control by carrying out the simulations and observing the various responses.

The effect of placing the sensor-actuator pair at 2 different FE locations in between the beam layers as non-collocated pairs is observed and the conclusions are finally drawn. The sampling interval τ is taken as 0.004 secs and the number of sub-intervals N was taken as 10. OL response of the system is obtained after subjecting it to vibrations. The discrete models are obtained by sampling the system in (2.250) at a rate of $\frac{1}{\tau}$ and $\frac{1}{\Delta}$ giving rise to $(\Phi_\tau, \Gamma_\tau, C)$-tau system and (Φ, Γ, C)-delta system respectively as

$$\Phi_\tau = \begin{bmatrix} 0.9552 & 0.0000 & -0.0000 & -0.0010 & 0.0000 & -0.0000 \\ 0.0000 & -0.4258 & 0.0000 & 0.0000 & -0.0018 & 0.0000 \\ -0.0000 & 0.0000 & 0.4787 & -0.0000 & 0.0000 & -0.0010 \\ 58.8471 & -0.0000 & 0.0000 & 0.9558 & 0.0000 & -0.0000 \\ -0.0000 & 391.7526 & 0.0000 & 0.0000 & -0.4219 & 0.0000 \\ 0.0000 & 0.0000 & 535.5225 & -0.0000 & 0.0000 & 0.4841 \end{bmatrix},$$

$$\Gamma_\tau = 10^{-5} \begin{bmatrix} 0.0000 & -0.0001 \\ 0.0000 & -0.0000 \\ 0.0000 & -0.0003 \\ -0.0001 & 0.1067 \\ -0.0000 & 0.0000 \\ -0.0007 & 0.3109 \end{bmatrix} \tag{3.67}$$

and

$$\Phi = \begin{bmatrix} 0.9982 & 0.0000 & 0.0000 & -0.0001 & 0.0000 & 0.0000 \\ 0.0000 & 0.9737 & -0.0000 & -0.0000 & -0.0004 & -0.0000 \\ 0.0000 & -0.0000 & 0.9814 & -0.0000 & 0.0000 & -0.0001 \\ 6.0251 & 0.0000 & 0.0000 & 0.9982 & -0.0000 & -0.0000 \\ -0.0000 & 92.8365 & -0.0000 & 0.0000 & 0.9746 & 0.0000 \\ 0.0000 & 0.0000 & 71.4111 & -0.0000 & -0.0000 & 0.9822 \end{bmatrix},$$

$$\Gamma = 10^{-6} \begin{bmatrix} 0.0000 & -0.0000 \\ -0.0000 & -0.0000 \\ 0.0000 & -0.0001 \\ -0.0001 & 0.1092 \\ 0.0000 & 0.0000 \\ -0.0010 & 0.4146 \end{bmatrix}. \tag{3.68}$$

It is found that the discrete model was controllable and observable. Stabilizing output injection gain is obtained for the tau system such that the eigenvalues of $\left(\mathbf{\Phi}^N + GC\right)$ lie inside the unit circle and the response of the system has a good settling time. The output injection gain obtained is as

$$G = 10^{-6} \begin{bmatrix} -0.2095 & 0.0054 \\ 0.0000 & -0.0000 \\ -0.0200 & 0.4930 \\ 210.5816 & -5.4808 \\ 0.0000 & -0.0000 \\ -15.1199 & -837.9257 \end{bmatrix}. \tag{3.69}$$

The closed loop impulse response of the system with the output injection gain is also observed. The POF gain matrix $\mathbf{K}$ for the smart system is obtained by solving $\mathbf{\Gamma K} \approx G$ using the LMI optimization method which reduces the amplitude of the control signal u. The POF gain matrix $\mathbf{K}$ for the MIMO model of the smart beam is given by

$$\mathbf{K} = \begin{bmatrix} 0.0014 & 0.0529 \\ -1.2572 & -22.5487 \\ -0.0013 & -0.0552 \\ 1.0720 & 23.5198 \\ 0.0001 & 0.0422 \\ 0.9789 & -18.0520 \\ -0.0004 & -0.0171 \\ 0.3341 & 7.2781 \\ 0.0004 & -0.0135 \\ -1.0629 & 5.7890 \\ 0.0012 & 0.0411 \\ -1.2904 & -17.4790 \\ -0.0013 & -0.0580 \\ 0.9529 & 24.7388 \\ 0.0004 & 0.0594 \\ 0.8790 & -25.3775 \\ -0.0010 & -0.0442 \\ 0.6992 & 18.8384 \\ 0.0009 & 0.0163 \\ -1.2104 & -6.9271 \end{bmatrix} = [\, \mathbf{K}_1 \quad \mathbf{K}_2]\,. \tag{3.70}$$

With the designed multivariable POF controller being put in the loop with the smart beam, the CL impulse responses (sensor outputs y_1, y_2) with the POF gain $\mathbf{K}$ the control effort u_1, u_2 required to control the vibrations are observed and graphically displayed as shown in Figs. 3.47 - 3.48 respectively. The comparisons of the quantitative results of the OL and CL responses (with output injection gain, POF gain) and with the magnitude of the control efforts, their settling times required is shown in Table 3.2.

Table 3.2. Quantitative comparative results of POF simulations of the embedded beam as a MIMO system (terms inside the brackets indicate the settling values), only the +ve values shown here

FE location	**OL**	**CL with G**	**CL with K**	**Control i/p u**
y_1	3.6 V	3.7 V	3.7 V	18 V
FE 6	32 (secs)	10 (secs)	(4 secs)	
y_2	1.8 V	1.8 V	1.9 V	39 V
FE 8	11 (secs)	9 (secs)	(8 secs)	

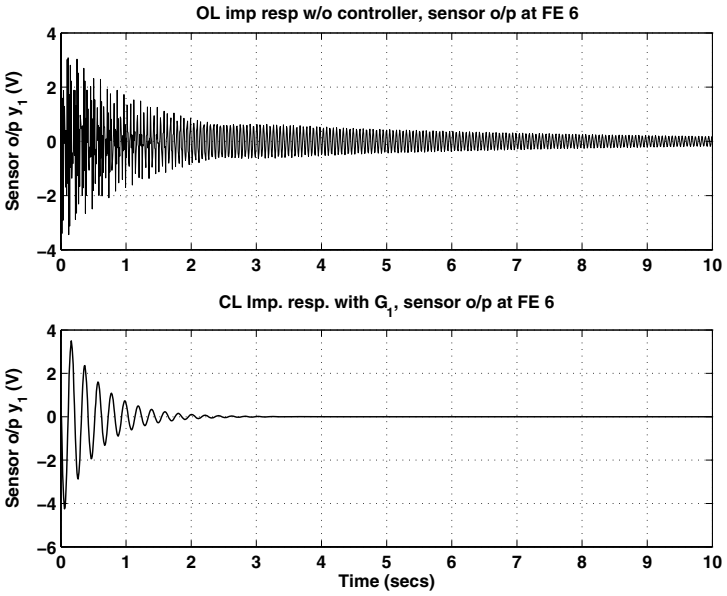

(a) OL and CL response with G

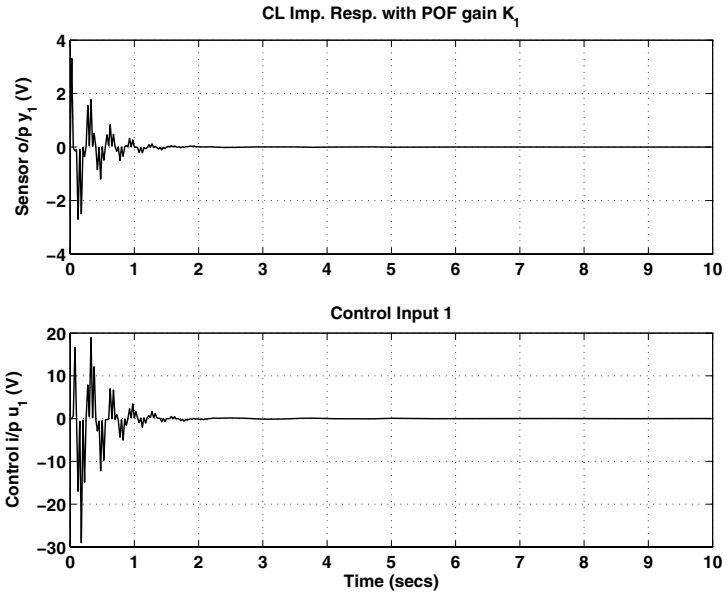

(b) CL response with $\mathbf{K}$ and control u

Fig. 3.47. OL and CL responses with G_1, $\mathbf{K}_1$ and control effort u_1)

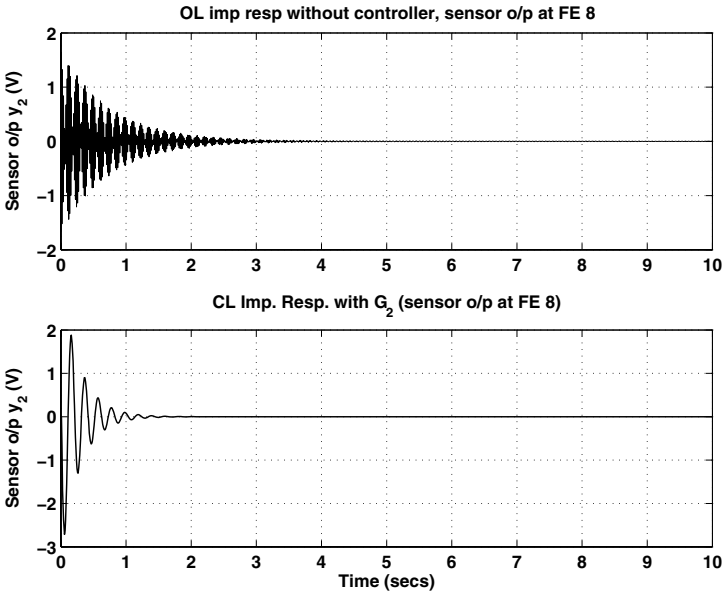

(a) OL and CL response with G

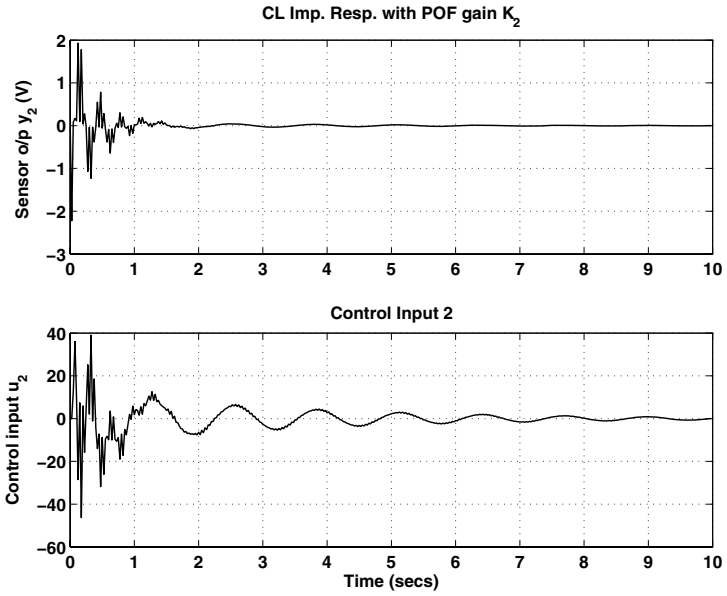

(b) CL response with $\mathbf{K}$ and control u

Fig. 3.48. OL and CL responses with G_2, $\mathbf{K}_2$ and control effort u_2)

3.3.4.1 Simulation Results and Discussions

POF controller has been designed for the MIMO model of the sandwiched smart structure and when put in feedback loop with the plant, the transient oscillations die out quickly in lesser time and steady state is reached quickly. It is also observed that modeling a smart structure by including the sensor / actuator mass and stiffness and by placing the sensor / actuator at two different positions in between the beam layers introduces a considerable change in the structural vibration characteristics than placing the sensor / actuator pair at only one location (Figs. 3.43 - 3.46). The response takes lesser time to settle than the SISO case (Figs. 3.43 - 3.46) and the vibrations are damped out quickly. A overall better performance of the system is obtained as there will be multiple interactions of the input and the output which will cause the vibrations in the system to be damped out quickly.

Responses were observed without control and were compared with the control to show the control effect. From the simulations, it was observed that without control the transient response was unsatisfactory, takes a lot of time to settle and with control, the vibrations are suppressed. The limitations of Euler-Bernoulli beam theory such as the neglection of the shear and axial displacements have been considered here while modeling the beam. Timoshenko beam theory corrects the simplifying assumptions made in Euler-Bernoulli beam theory and the model obtained can be closer to a exact one.

3.4 Conclusions

POF controllers are designed successfully to control the first few vibratory modes of a smart cantilever beam modelled using 2 type of beam theories, viz., Euler-Bernoulli beam theory and Timoshenko beam theory. New AVC schemes to control the flexural vibrations of SISO and MIMO smart models were presented. Different sensor / actuator locations bonded to the master structure (flexible cantilever beam) either as surface mounted piezos or as embededd type piezos were considered. It is observed that the the control effort required gets reduced when the piezo pair is moved towards the root of the structure.

Better performances are obtained when the piezo pair is at the root (fixed end) rather than at the free end. The open loop impulse responses of the plants (without the controller) shows an oscillatory time response and takes more time for the vibrations to decay out. The closed loop responses of the plant with the POF gain shows that the performance obtained by the output injection gain is realized with the POF gain and the vibrations are suppressed quickly by the introduction of the POF controller. Multivariable control of a smart structure is inferred to be better compared to the SISO control as there will be multiple interactions of the input and the output which will cause the vibrations in the system to be damped out quickly than the earlier case.

A multi input multi output test provides better energy distribution and even better actuation forces. Unlike static output feedback, the POF control always guarantees the stability of the closed loop system and all the states are not needed for control purposes. Fault tolerant control in the event of an actuator failure in a multimodel system is also proposed which showed that even when an actuator fails to

function in a multivariable system, the system stabilizes. A higher order smart structure model is designed by considering more number of vibratory modes. A reduced order model is thus obtained and a robust controller is designed via the reduced order model and then applied to the higher order model which works satisfactorily.

4

Fast Output Sampling Feedback Controllers for Smart Structures

In the fourth Chapter of this monograph, various types of control strategies for the SISO and MIMO state space models of the smart structure developed in the Chapter 2 using the fast output sampling feedback control law (a type of multirate output feedback technique) is presented. The main aim of developing these control strategies is to control and damp out the flexural or transverse vibrations of flexible beams when they are subjected to an external disturbance, say an impulse or a sinusoidal disturbance at the free end of the flexible beam or due to an actuator failure in a multivariable system. In the first part of this Chapter, the design of Fast Output Sampling (FOS) feedback controllers for the active vibration suppression of beams modelled with Euler-Bernoulli beam theory is discussed, while in the latter part of this chapter, the design of FOS controllers for the active vibration suppression of beam modelled with Timoshenko beam theory is presented. The performance of all the designed controllers are evaluated by performing the simulations and observing the various responses. Conclusions are finally drawn regarding the simulated results.

4.1 A Brief Review of the Fast Output Sampling Feedback Control Technique

The problem of FOS was studied by Werner and Furuta [51], [126] for LTI systems. They have shown that the poles of the DT control system could be assigned arbitrarily using the FOS feedback control technique. As the constant gains are used in FOS technique, this method could easily be implemented and indicated a new possibility. Such a control law can stabilize a much larger class of systems. In this control law, the output of the system is sampled at a faster rate than the control input. A brief introduction to this type of control technique is as follows.

Consider a plant described by a LTI state space model given by

$$\dot{x}(t) = Ax(t) + Bu(t), \qquad y(t) = Cx(t), \tag{4.1}$$

where $x \in \Re^n$, $u \in \Re^m$, $y \in \Re^p$, A, B, C are constant matrices of appropriate dimensions and $A \epsilon \Re^{n\times n}$, $B \epsilon \Re^{n\times m}$, $C \epsilon \Re^{p\times n}$.

Let $(\Phi_\tau, \Gamma_\tau, C)$ be the system in (4.1) sampled at τ secs and given by

$$x((k+1)\tau) = \Phi_\tau x(k\tau) + \Gamma_\tau u(k\tau), \qquad y(k\tau) = Cx(k\tau). \tag{4.2}$$

It is assumed that $(\Phi_\tau, \Gamma_\tau, C)$ be named as the τ system and is completely controllable. Assume that the plant is to be controlled by a digital computer with sampling interval τ and a sampled data state feedback design has been carried out to find a state feedback gain F such that the closed loop system

$$x(k\tau + \tau) = (\Phi_\tau + \Gamma_\tau F)\, x(k\tau) \tag{4.3}$$

has desirable properties. i.e., an state feedback gain matrix F is designed such that the eigen values of $(\Phi_\tau + \Gamma_\tau F)$ are placed inside the unit circle at appropriate locations (no eigen values at the origin) and the closed loop system has a good settling time. Here,

$$\Phi_\tau = e^{A\tau} \tag{4.4}$$

and

$$\Gamma_\tau = \int_0^\tau e^{As}\, ds\; B. \tag{4.5}$$

Instead of using a state observer, the following sampled data control can be used to realize the effect of the state feedback gain F by output feedback and then applied to this discretized system. Let $\Delta = \frac{\tau}{N}$, i.e., an output-sampling interval τ is divided into N sub-intervals of width $\Delta = \frac{\tau}{N}$, where N being greater $\geq$ the observability index ν of (Φ, C) and the hold function is assumed to be constant over these sub-intervals as shown in Fig. 4.1. The block-diagrammatic view of the FOS control technique is shown in Fig. 4.2. The control signal $u(t)$, which is applied during the interval $k\tau < t < (k+1)\tau$, is then constructed as a linear combination of the last N output observations as

$$u(t) = \begin{bmatrix} L_0 & L_1 & L_2 \cdots & L_{N-1} \end{bmatrix} \begin{bmatrix} y(k\tau - \tau) \\ y(k\tau - \tau + \Delta) \\ \vdots \\ \vdots \\ y(k\tau - \Delta) \end{bmatrix} = \mathbf{L}\; y_k, \tag{4.6}$$

where the matrix blocks L_j represent the output feedback gains and (weights for the individual output samples) the notations $\mathbf{L}$, y_k has been introduced here for convenience. Note that $\frac{1}{\tau}$ is the rate at which the loop is closed, whereas the output samples are taken at the N-times faster rate $\frac{1}{\Delta}$.

To show how a FOS feedback controller in Eq. (4.6) can be designed to realize the given sampled data state feedback gain F for a controllable and observable system (A, B, C), we construct a fictitious, lifted system for which the Eq. (4.6) can be interpreted as static output feedback [48]. To see the relationship between the gain sequence and the closed loop behavior, consider the CT system in (4.1) sampled at the rate of $\frac{1}{\Delta}$, giving rise to the delta system, (Φ, Γ, C). Consider the discrete time system at time $t = k\tau$, having the input $u_k = u(k\tau)$, the state $x_k = x(k\tau)$ and the output as y_k. Then, we have a lifted system given as

$$x_{k+1} = \Phi_\tau\; x_k \;+\; \Gamma_\tau\; u_k, \quad y_{k+1} = \mathbf{C}_0\; x(k) + \mathbf{D}_0\; u(k), \tag{4.7}$$

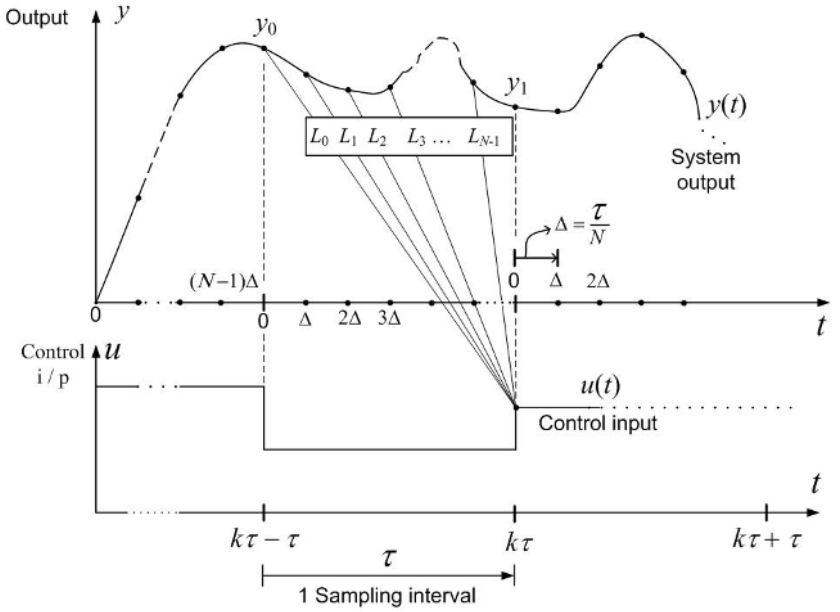

Fig. 4.1. Graphical illustration of the FOS control law

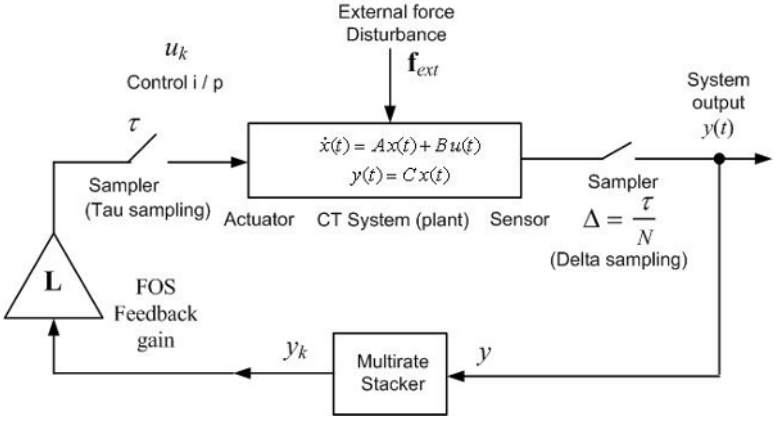

Fig. 4.2. Block diagrammatic representation of the FOS control law

where $\mathbf{C}_0$ and $\mathbf{D}_0$ are the matrices of the lifted system given as

$$\mathbf{C}_0 = \begin{bmatrix} C \\ C\Phi \\ C\Phi^2 \\ \vdots \\ C\Phi^{N-1} \end{bmatrix}, \quad \mathbf{D}_0 = \begin{bmatrix} 0 \\ C\Gamma \\ C\Phi\Gamma \\ \vdots \\ C\sum_{j=0}^{N-2} \Phi^j \Gamma \end{bmatrix}. \tag{4.8}$$

Now, since the state feedback gain F has already been designed, then assuming that in the interval $k\tau \leq t \leq (k\tau + \tau)$,

$$u(t) = F\ x(k\tau), \tag{4.9}$$

one can define the fictitious measurement matrix as

$$\mathbf{C}(F, N) = (\mathbf{C}_0 + \mathbf{D}_0 F)\ \ (\Phi_\tau + \Gamma_\tau F)^{-1}, \tag{4.10}$$

which satisfies the fictitious measurement equation

$$y_k = \mathbf{C}\ x_k. \tag{4.11}$$

The measurement matrix of this fictitious system can almost be made equal to have full column rank so that any sampled data SFB gain for the system in (4.1) can be realized by the control law (4.6). Then, the feedback law in (4.6) can be interpreted as static output feedback control law as

$$u_k = \mathbf{L}\ y_k \tag{4.12}$$

for the system in (4.7) with the measurement matrix $\mathbf{C}$. For $\mathbf{L}$ to realize the effect of F in the Eqs. (4.7) and (4.8), it must satisfy the equation

$$\mathbf{L}\ \mathbf{C}\ =\ F. \tag{4.13}$$

Let ν denote the observability index of $(\Phi, \mathbf{C})$. It can be shown that for $N > \nu$, generically, $\mathbf{C}$ has full column rank, so that any state feedback gain F can be realized by a FOS feedback gain $\mathbf{L}$. At $t = 0$, the control signal $u(t) = u_0$ for $0 < t \leq \tau$ cannot be computed from Eq. (4.6) since the output measurements are not available for $t < 0$. If the initial state x_0 is known, one can take $u_0 = Fx_0$. If x_0 is unknown and estimated with error Δx_0, the value of u_0 will differ by $\Delta u_0 = F\Delta x_0$ from the control signal which would be applied if the initial states were known and there will be an error $\Delta u_k = u_k - F\ x_k$. For $k \geq 1$, u_k can be computed from Eq. (4.6), but if $\Delta u_0 \neq 0$, the assumption $u_k = F\ x_k$ and therefore $y_k = \mathbf{C}\ x_k$ does not hold good and the effect of initial error Δu_0 would propagate through the closed loop response of the system. One can verify that the closed loop dynamics is governed by

$$\begin{bmatrix} x_{k+1} \\ \Delta u_{k+1} \end{bmatrix} = \begin{bmatrix} \Phi_\tau + \Gamma_\tau F & \Gamma_\tau \\ 0 & \mathbf{L}\mathbf{D}_0 - F\Gamma_\tau \end{bmatrix} \begin{bmatrix} x_k \\ \Delta u_k \end{bmatrix}. \tag{4.14}$$

The system in Eq. (4.7) under the application of control law in Eq. (4.12) is stable if and only if F stabilizes (Φ_τ, Γ_τ) and the matrix $(\mathbf{L}\mathbf{D}_0 - F\Gamma_\tau)$ has all its eigen values inside the unit circle. To see this, apply the coordinate transformation,

$$T = \begin{bmatrix} I & 0 \\ -F & I \end{bmatrix} \tag{4.15}$$

to the equation

$$\begin{bmatrix} x_{k+1} \\ u_{k+1} \end{bmatrix} = \begin{bmatrix} \Phi_\tau & \Gamma_\tau \\ \mathbf{L}\mathbf{C}_0 & \mathbf{L}\mathbf{D}_0 \end{bmatrix} \begin{bmatrix} x_k \\ u_k \end{bmatrix} \tag{4.16}$$

and use Eq. (4.10). Thus, we have the eigen values of the closed loop system under a FOS control law in (4.6) as those of $(\Phi_\tau + \Gamma_\tau F)$ together with those of $(\mathbf{L}\mathbf{D}_0 - F\Gamma_\tau)$.

This suggests that the state feedback F should be obtained so as to ensure the stability of both $(\Phi_\tau + \Gamma_\tau F)$ and $(\mathbf{L}\mathbf{D}_0 - F\Gamma_\tau)$.

It is realized that with this designed FOS feedback controller, 2 problems are required to be addressed.

The first problem is the unknown states are estimated implicitly using the measured output samples and assuming that the initial control is generated by the state feedback. If the external disturbances cause an estimation error, then decay of this error will be determined by the eigen values of the matrix $(\mathbf{L}\mathbf{D}_0 - F\mathbf{\Gamma}_\tau)$ which depends on $\mathbf{L}$ and whose dimensions equals the number of control inputs. For stability, these eigen values have to be inside the unit disc and for fast decay, they should be as close to the origin as possible. This problem must be taken into account while designing $\mathbf{L}$.

The second problem is as follows. The problem with controllers obtained in this way is that, although they are stabilizing and achieve the desired closed loop behavior at the output sampling instants, they may cause an excessive oscillation between inter-sampling instants. The controller obtained using (4.13) may give the desired behaviour, but might require excessive control action and the FOS gains obtained may be very high. In practice, these high gains may amplify measurement noise, saturate the actuator and it is desirable to keep these values low. When trying to deal with these problems, it turns out that it is better not to insist on an exact solution to the design equation $\mathbf{L}\ \mathbf{C}\ =\ F$ and one can allow a small deviation and use an approximation $\mathbf{L}\ \mathbf{C} \approx F$, which hardly effects the desired closed loop dynamics, but may have considerable effect on the 2 problems discussed above. Thus, we are putting a constraint on the gain $\mathbf{L}$.

Instead of looking for an exact solution to the inequalities, the following inequalities given below are solved.

$$\| L \| < \rho_1, \quad \| \mathbf{L}\mathbf{D}_0 - F\Gamma_\tau \| < \rho_2, \quad \| \mathbf{L}\mathbf{C} - F \| \leq \rho_3. \tag{4.17}$$

Here, in Eq. (4.17), the 3 objectives have been expressed by the upper bounds on the matrix norms, and each should be as small as possible. ρ_1 small means means low noise sensitivity, ρ_2 small means fast decay of observation error, and most importantly, ρ_3 small means that the FOS controller with gain $\mathbf{L}$ is a good approximation of the originally designed state feedback controller. If $\rho_3 = 0$, then $\mathbf{L}$ is a exact solution. If the bounds ρ_1 and ρ_2 are known, one can keep these bounds fixed and minimize ρ_3 under these constraints. This requires a search for a FOS controller which gives the best approximation of the given SFB designed under the constraints represented by ρ_1 and ρ_2. It should be noted here that CL stability requires $\rho_2 < 1$, i.e., the eigen values which determine the error dynamics must lie within the unit disc.

Using the schur compliment, it is straight forward to bring these conditions in the form of LMI [121] [50] as

$$\begin{bmatrix} \rho_1^2 I & \mathbf{L} \\ \mathbf{L}^T & -I \end{bmatrix} < 0, \tag{4.18}$$

$$\begin{bmatrix} \rho_2^2 I & \mathbf{L}\mathbf{D}_0 - F\mathbf{\Gamma}_\tau \\ (\mathbf{L}\mathbf{D}_0 - F\mathbf{\Gamma}_\tau)^T & -I \end{bmatrix} < 0, \tag{4.19}$$

$$\begin{bmatrix} \rho_3^2 I & \mathbf{L}\mathbf{C} - F \\ (\mathbf{L}\mathbf{C} - F)^T & -I \end{bmatrix} < 0. \tag{4.20}$$

In this form, the function *mincx*( ) of the LMI control toolbox [121], [50] can be used to minimize a linear combination of ρ_1, ρ_2 and ρ_3 for the synthesis of $\mathbf{L}$.

4.2 Controller Design for Smart Structures Modelled Using EB Theory

In the following sections, the design of the FOS feedback controllers for SISO and MIMO models of the smart structure modelled using Euler-Bernoulli beam theory is presented.

4.2.1 Design of SISO Controllers for Smart Beam Divided into 3, 4, 5 Finite Elements

The FOS control technique discussed in the previous Section 4.1 is used to design a controller to suppress the first 2 vibration modes of a cantilever beam through smart structure concept for the various SISO state space models of the 3 types of systems given in Section 2.1.1:6 I(i). The performance of the 3 type of systems is hereby evaluated for vibration control by carrying out the simulations and observing the various responses. Finally, the conclusions are drawn with the discussions on the simulation results [91], [92].

The sampling interval τ is selected as 0.004 secs. The number of sub-intervals N is chosen as 4. An external force is applied at the free end of the beam, thus subjecting it to vibrations. The OL responses (without the controller) are observed. τ systems $(\Phi_{\tau 1j}, \Gamma_{\tau 1j}, C_{1j})$ of the various models of the 3 systems (j = 1, 2, 3) at the fixed end as shown in the Fig. 2.3 are obtained by sampling the CT systems given in (2.73)-(2.75) at a rate of $\frac{1}{\tau}$. The tau systems for the SISO models are given by the Eqs. (3.13)-(3.15) for the piezo-patches placed only at the fixed end.

Similarly, the tau systems of the other SISO models of the 3 systems are also obtained. It is found that the systems in Eqs. (3.13)-(3.15) are controllable and observable. The stabilizing SFB gains are obtained for each of the SISO models of the 3 systems such that the eigenvalues of $(\Phi_\tau + \Gamma_\tau F)$ are placed inside the unit circle at appropriate locations such that the closed loop system has a good settling time. The impulse response of all the models of the 3 systems with the SFB gain F is observed.

Delta systems $(\Phi_{1j}, \Gamma_{1j}, C_{1j})$ of the various models of the 3 systems with the piezo patches at the fixed end are obtained by sampling the CT systems given in (2.73)-(2.75) at a rate of $\frac{1}{\Delta}$ respectively. The delta systems for the SISO models are given by the Eqs. (3.16)-(3.18) for the piezo-patches placed only at the fixed end. Similarly, the delta systems of the other SISO models of the 3 systems are obtained. The FOS feedback gain for the SISO models with the PZT's at the fixed end is obtained by solving $\mathbf{LC} \approx F$ using the LMI optimization method [121], [50] and is given by

$$\begin{aligned} &\textit{Model 1 of System 1 :}\ \mathbf{L}_{11} = [78.82 \quad 54.16 \quad -83.75 \quad -72.33]\,, \\ &\textit{Model 1 of System 2 :}\ \mathbf{L}_{12} = [66.60 \quad -54.21 \quad -62.36 \quad 61.26]\,, \\ &\textit{Model 1 of System 3 :}\ \mathbf{L}_{13} = [-26.66 \quad 24.25 \quad -13.91 \quad 11.51]\,. \end{aligned} \tag{4.21}$$

Similarly, the FOS gain matrices for the other SISO models of the 3 systems are obtained. With the designed FOS feedback controller being put in the loop with the smart plant, the CL impulse responses (sensor outputs y) and the variation of the control signal u_i with time t for all the SISO models of the 3 systems are observed [91], [92].

Here, for the sake of convenience, only the responses such as the CL impulse response with the FOS feedback gain and the control efforts required for the SISO models of the 3 systems in which the piezos are placed at the fixed and free end are shown in the Figs. 4.3 - 4.5. Also, the tip displacements for the same are observed and displayed graphically in Figs. 4.6 - 4.8. The frequency response plots for the SISO models when the piezo patches are placed at the fixed end is shown in Fig 4.9(a)-(c) respectively. Simulations were also performed by considering 3 vibratory modes and the responses were observed.

4.2.1.1 Simulation Results and Discussions

Controllers are designed for the smart flexible cantilever beam using the FOS feedback control technique for the different models of the **3 systems** to suppress the first 2 vibratory modes [91], [92]. The various responses are observed for each of the state space models of the 3 systems. The comparison and discussion of the simulation results for the best model required for AVC is presented here.

From the simulation results, it is observed that modeling a smart structure by including the sensor / actuator mass and stiffness and by varying the position of the sensor / actuator pair on the beam from the fixed end to the free end and by dividing it into a number of finite elements, introduces a considerable change in the system's structural vibration characteristics, which was observed through the simulation results. It is inferred that when the plant is placed with this designed FOS controller, the plant performs well and the vibrations die out quickly than its open loop counterpart.

From the output responses shown in the Figs. 4.3 - 4.8, it is observed that the control effort u required from the controller gets reduced if the sensor / actuator placement location is moved towards the fixed end. A small magnitude of the control signal is sufficient to control the structural vibrations of each model of the systems 1, 2 and 3 when the piezos are placed at the fixed end.

The individual models of the 3 systems are compared to obtain the best performance. Comparing the 3 systems, viz., system 1, 2 and 3, it is observed that if the smart beam is divided into 5 finite elements, the vibration characteristics is improved. Hence, it can be concluded that, the best placement of the sensor / actuator pair is at the fixed end of the system 3, i.e., the model 1 of system 3. Comparing the responses of the various models of the 3 systems, it is observed that the model 1 of the system 3's vibration characteristics are the best for the vibration control of smart beam because of the following reasons.

- A very small magnitude of control input u is required to damp out the vibrations compared to the systems 1 and 2 as a result of which less effort has to be put by the controller.
- The magnitude of the impulse response (closed loop) of both the continuous and the discrete time system is less compared to systems 1 and 2.

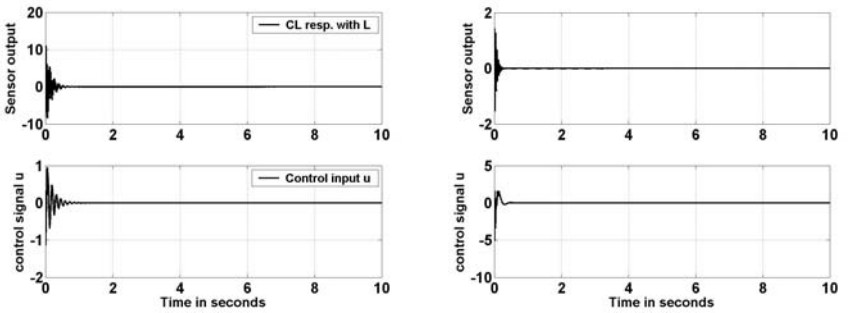

(a) Fixed end (b) Free end

Fig. 4.3. CL impulse response with FOS feedback gain $\mathbf{L}$ (sensor output y) and control input u, beam divided into 3 FE, PZT placed at fixed and free end

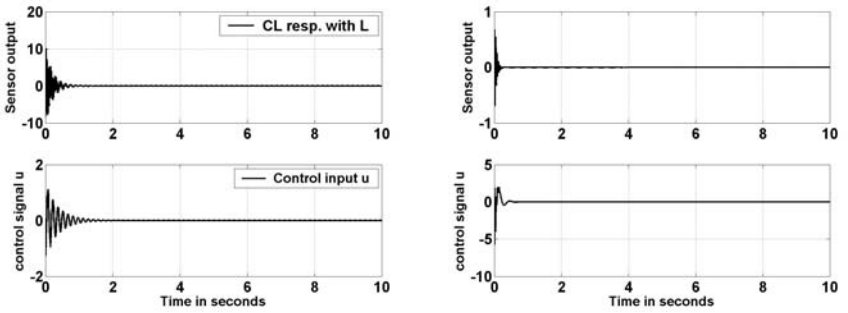

(a) Fixed end (b) Free end

Fig. 4.4. CL impulse response with FOS feedback gain $\mathbf{L}$ (sensor output y) and control input u, beam divided into 4 FE, PZT placed at fixed and free end

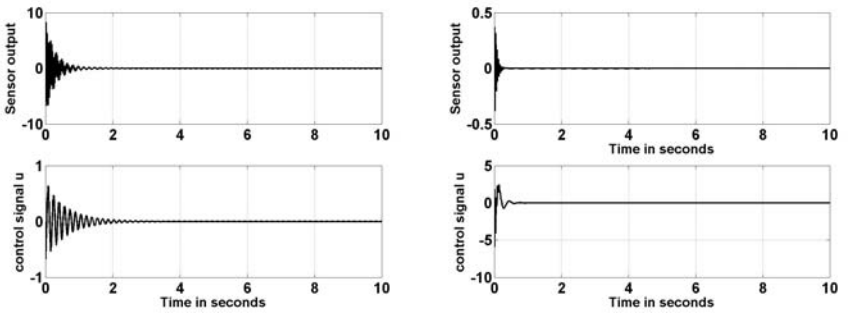

(a) Fixed end (b) Free end

Fig. 4.5. CL impulse response with FOS feedback gain $\mathbf{L}$ (sensor output y) and control input u, beam divided into 5 FE, PZT placed at fixed and free end

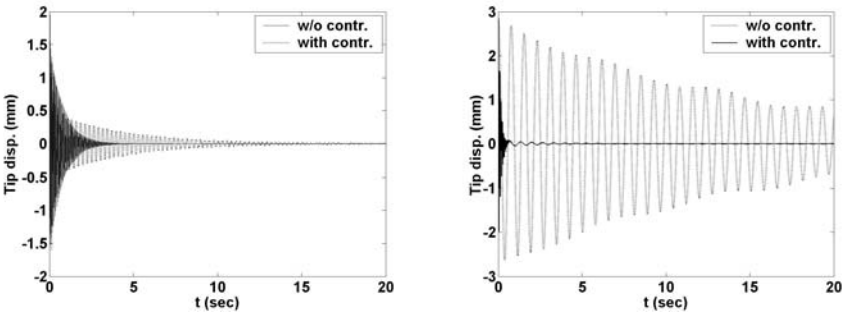

(a) Fixed end (b) Free end

Fig. 4.6. Tip displacement for SISO model (fixed, free end) of beam - 3 FE

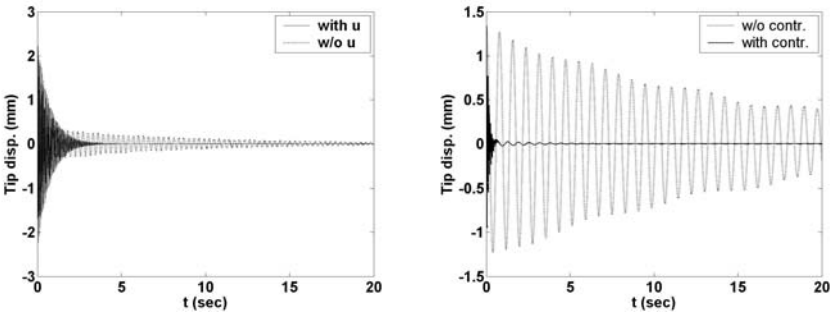

(a) Fixed end (b) Free end

Fig. 4.7. Tip displacement for SISO model (fixed, free end) of beam - 4 FE

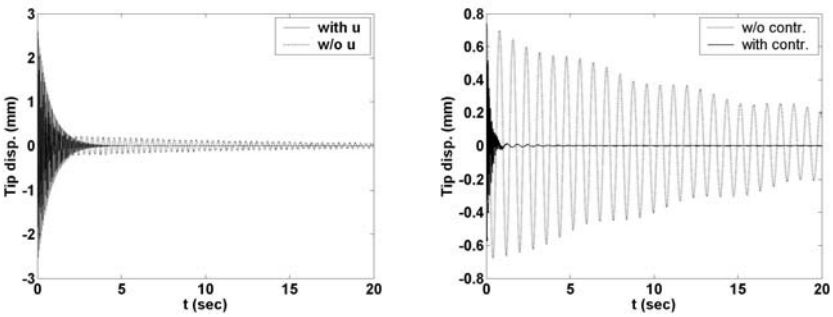

(a) Fixed end (b) Free end

Fig. 4.8. Tip displacement for SISO model (fixed, free end) of beam - 5 FE

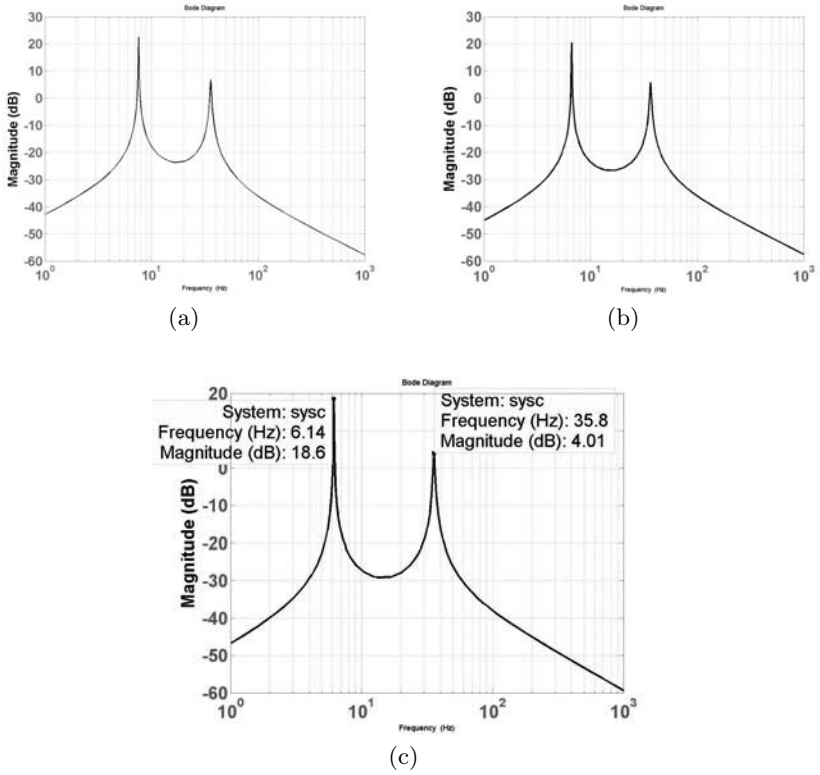

Fig. 4.9. Bode plots for the SISO models at fixed end

- Also, the response characteristics with F and $\mathbf{L}$ are best amongst all the other models of the 3 systems.
- The vibrations are damped out quickly and the tip position settles quickly to its equilibrium position.

Further, the model 1 of system 3 is more sensitive to the first mode as the bending moment is maximum, strain rate is higher, minimum deflection at the tip, better sensor output and less requirement of the control input (control will be more effective at the root), whereas at the free end of the system 3 (model 5 of system 3), because of the lesser strain rate and maximum deflection, more control energy is required to damp out the vibrations. The vibration characteristics of the system depended not only on the collocation of the piezo pair, but also on many factors such as the gain of the amplifier used, the mode number and the location of the piezo pair at the nodal points from the fixed end.

Further, responses are obtained by considering the first 3 vibratory modes also. Results were compared with the FOS controllers designed for first 2 vibratory modes. The obtained responses by retaining the first 3 modes were nearly the same as in the case of 2 vibration modes. Hence, it can be concluded that a fourth order model with 2 vibratory modes is sufficient to model a smart flexible beam and the control

input u does not excite the remaining left out modes. The quantitative results of the tip displacements for the models of Figs. 2.3 and A.1 with piezo-patches at fixed end and free end are shown in Tables 4.1 and 4.2 respectively.

Table 4.1. Tip displacement (in mm with + and - values); simulation results for the fixed end of the EB SISO models with settling time in secs.

Models	Fixed end					
	With controller			Without controller		
Mod 1, Sys 1	1.8 mm	-1.9 mm	5.3 sec	2.9 mm	-2.7 mm	53 sec
Mod 1, Sys 2	0.9 mm	-0.9 mm	4.8 sec	1.3 mm	-1.3 mm	40 sec
Mod 1, Sys 3	0.78 mm	-0.6 mm	3.8 sec	0.8 mm	-0.7 mm	48 sec

Table 4.2. Tip displacement (in mm with + and - values); simulation results for the free end of the EB SISO models with settling time in secs.

Models	Free end					
	With controller			Without controller		
Mod 3, Sys 1	2.6 mm	-2.6 mm	5.5 sec	2.9 mm	-2.8 mm	25 sec
Mod 4, Sys 2	2.1 mm	-2.1 mm	5 sec	2.7 mm	-2.6 mm	22 sec
Mod 5, Sys 3	1.5 mm	-1.5 mm	4 sec	2 mm	-1.8 mm	15 sec

Thus, the observations are made with and without the controller to show the control effect. It was observed that without control the transient response was unsatisfactory, takes more time to settle and with control, the vibrations are suppressed. Thus, an integrated FE model to analyze the vibration suppression capability of a smart cantilever beam with surface mounted piezoelectric devices based on Euler-Bernoulli beam theory is presented in this section. To conclude, unlike static output feedback, the FOS feedback control technique always guarantees the stability of the closed loop control system, requires constant gains and easy to implement [91], [92].

4.2.2 Design of MIMO FOS Controller for a Multivariable System

The FOS control technique discussed in Section 4.1 is used to design a controller to suppress the first 2 vibration modes of a smart cantilever beam through smart structure concept for the multivariable representation of the smart structure plant (Fig. 2.5). The MIMO model is given by the Eqs. (2.93) and (2.101) with its numerical value by the Eq. (2.105). The performance of the smart beam is hereby evaluated by carrying out the simulations. The effect of placing the sensor-actuator as collocated pairs at 2 different FE locations on the beam is observed and the conclusions are drawn [93].

The sampling interval τ is selected as 0.004 secs. The number of sub-intervals N is chosen as 2. An external force is applied at the free end of the beam, thus subjecting it to vibrations. The OL responses (without the controller) are observed.

The τ system $(\Phi_\tau, \Gamma_\tau, C)$ is obtained by sampling the CT system (2.105) at a rate of $\frac{1}{\tau}$ and is given by Eq. (3.19). It is found that the τ system is controllable and observable. The stabilizing SFB gains are obtained for the tau system such that the eigenvalues of $(\Phi_\tau + \Gamma_\tau F)$ are placed inside the unit circle at appropriate locations and the response of the CL system has a good settling time. The state feedback gain obtained is as

$$F = 10^2 \begin{bmatrix} 2.2210 & 0.3116 & -1.7156 & 0.4210 \\ -1.2302 & 0.2118 & 1.0015 & -0.3153 \end{bmatrix}. \tag{4.22}$$

The impulse response of the MIMO system with the SFB gain F is observed and is shown in the Figs. 4.10 and 4.11.

The delta system (Φ, Γ, C) is obtained by sampling the CT system (2.105) at a rate of $\frac{1}{\Delta}$ and is given by Eq. (3.21). The FOS feedback gain the MIMO model is obtained by solving $\mathbf{LC} \approx F$ using the LMI optimization method [121], [50] and is given by

$$\mathbf{L} = 10^{-4} \begin{bmatrix} 2.29.7 & 1.4650 \\ -1.1108 & -0.0686 \\ 4.0057 & 3.2805 \\ -3.4527 & -2.3226 \end{bmatrix}. \tag{4.23}$$

With the designed multivariable FOS feedback controller put in the loop with the plant, the CL impulse responses (sensor outputs y_1 and y_2), the variation of the control signal u_1 and u_2 with time t for the MIMO model is observed and shown in Figs. 4.12 and 4.13.

4.2.2.1 Simulation Results and Discussions

FOS feedback controller has been designed for the MIMO model of the smart structure developed using the EB beam theory [93]. The beam was divided into 4 FE with sensor / actuator placed at FE positions 2 and 4. The various responses are obtained for the developed multivariable state space model of the beam without and with the controller. Through the simulation results, it is shown that when the plant is placed with this designed controller, the plant performs well and the vibrations are suppressed quickly.

It is also observed that modeling a smart structure by including the sensor / actuator mass and stiffness and by placing the sensor / actuator at 2 different positions introduces a considerable change in the structural vibration characteristics than placing the sensor / actuator pair at only one location as in [91], [92]. In this section, it is observed that when the pair is kept at 2 different locations, the closed loop responses of the MIMO system is less oscillatory compared to the single input single output case.

The response take lesser time to settle than the SISO case and the vibrations are damped out quickly. The control effort required is also less. The impulse responses with the SFB gain and the FOS feedback gain show better performance. The stabilizing SFB gain for the multivariable plant is obtained so that its poles are placed inside the unit circle at appropriate locations such that the system has a very good settling time. The sensor-actuator pair kept at position 2 controls the 2 vibratory modes at that FE position 2, while the pair kept at position 4 also controls the 2 vibratory modes, but placed at that FE position 4. An overall better performance of the system is thus obtained.

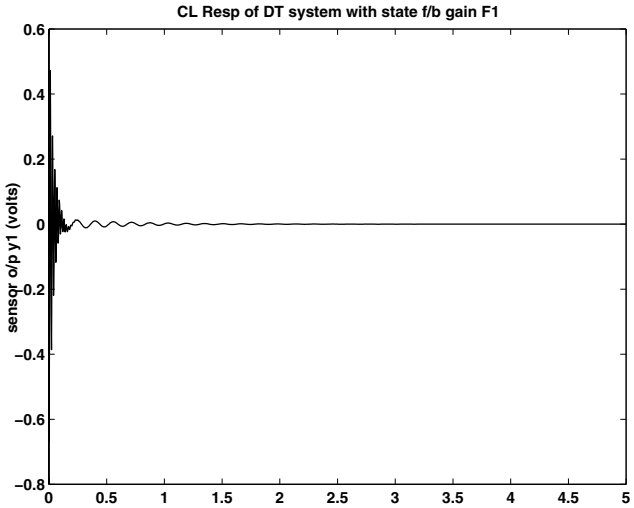

Fig. 4.10. Response y_1 with SFB gain F_1 (MIMO model of the beam : FOS control)

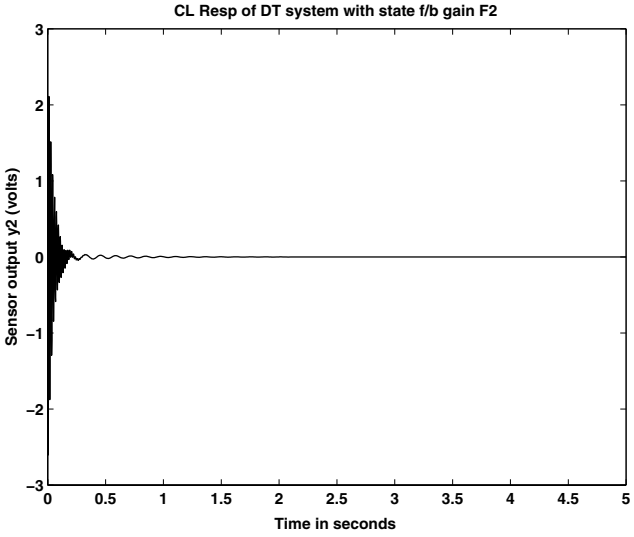

Fig. 4.11. Response y_2 with SFB gain F_2 (MIMO model of the EB beam : FOS control)

Hence, it can be concluded that multivariable control of a smart structure is better compared to the single input single output control as there will be multiple interactions of the input and the output which will cause the vibrations in the system to damp out quickly. MIMO excitation is better than SISO excitation as only

exciting at a single point may cause poor distribution of input energy throughout the structure and may result in somewhat slightly disturbed frequency responses.

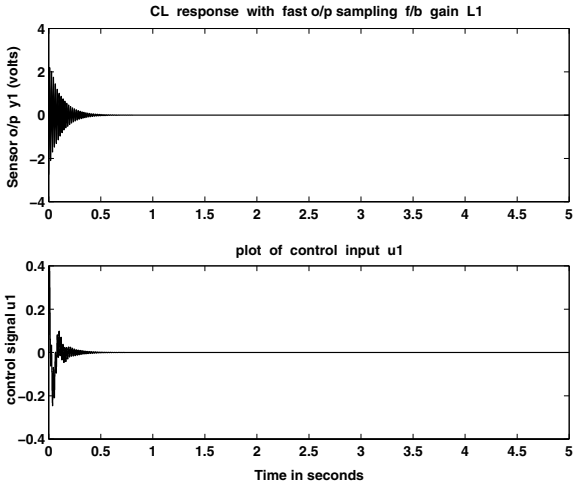

Fig. 4.12. Response y_1 with FOS feedback gain $\mathbf{L}_1$ (MIMO model of the EB beam: FOS control)

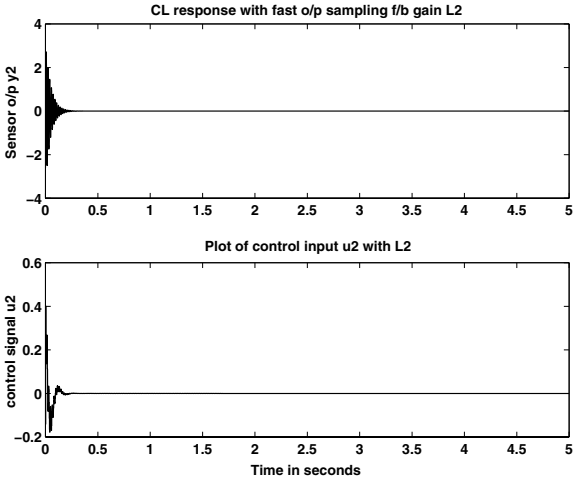

Fig. 4.13. Response y_2 with FOS feedback gain $\mathbf{L}_2$ (MIMO model of the EB beam: FOS control)

A multi input test provides better energy distribution and even better actuation forces. Responses were observed without control and were compared with the control to show the control effect. From the simulations, it was observed that without control, the transient response was unsatisfactory and with control, the vibrations are suppressed to a greater extent. An integrated FEM-SS model to analyze the vibration suppression capability of a smart cantilever beam with surface mounted piezoelectric devices based on EB beam theory for a MIMO case is developed in this Section.

4.2.3 Design of Robust Decentralized Fault Tolerant Controller for Smart Structures

4.2.3.1 Multimodel Synthesis

As in the case of POF design for multimodel system discussed in section 3.2.3:1, FOS controller can also be designed for the multimodel system [52]. This is briefly discussed in the following paragraphs. Consider a family of plant models $\{A_i, B_i, C_i\}$ defined by

$$\dot{x} = A_i x + B_i u, \quad y = C_i x, \quad i = 1, 2, 3, 4, ..., M. \tag{4.24}$$

By sampling at the rate of $\frac{1}{\Delta}$, we get a family of discrete systems (Φ_i, Γ_i, C_i). Now, consider the augmented system defined as

$$\tilde{\Phi} = diag(\Phi_1, ..., \Phi_M) = \begin{bmatrix} \Phi_1 & 0 & 0 & \cdots \\ 0 & \Phi_2 & \cdots & \vdots \\ \vdots & \vdots & \ddots & \vdots \\ 0 & 0 & \cdots & \Phi_M \end{bmatrix}, \tag{4.25}$$

$$\tilde{\Gamma} = diag(\Gamma_1, ..., \Gamma_M) = \begin{bmatrix} \Gamma_1 & 0 & 0 & \cdots \\ 0 & \Gamma_2 & \cdots & \vdots \\ \vdots & \vdots & \ddots & \vdots \\ 0 & 0 & \cdots & \Gamma_M \end{bmatrix}, \tag{4.26}$$

and

$$\tilde{C} = [\, C_1, \;\; C_2 \;\; .... \;\; C_M], \quad i = 1 \text{ to } M, \;\; M = 4. \tag{4.27}$$

Consider the family of discrete time systems in Eq. (4.24) having at time $t = k\tau$, the input $u_k = u(k\tau)$, the state vector $x_k = x(k\tau)$ and the output y_k as

$$x_{k+1} = \Phi_{\tau i} \; x_k \; + \; \Gamma_{\tau i} \; u(k), \quad y_{k+1} = \mathbf{C}_{0i} x(k) + \mathbf{D}_{0i} u(k), \tag{4.28}$$

where $\mathbf{C}_{0i}$ and $\mathbf{D}_{0i}$ are the matrices of the lifted system given as

$$\mathbf{C}_{0i} = \begin{bmatrix} C_i \\ C_i\Phi_i \\ C_i\Phi_i^2 \\ \vdots \\ C_i\Phi_i^{N-1} \end{bmatrix}, \quad \mathbf{D}_{0i} = \begin{bmatrix} 0 \\ C_i\Gamma_i \\ C_i\Phi_i\Gamma_i \\ \vdots \\ C_i \sum_{j=0}^{N-2} \Phi_i^j \; \Gamma_i \end{bmatrix}. \tag{4.29}$$

Assume that the discrete models $(\Phi_{\tau i}, \Gamma_{\tau i})$ are controllable. Then, we can find a robust state feedback gain F such that $(\Phi_{\tau i} + \Gamma_{\tau i} F)$ has no eigen values at the origin, CL poles are placed at the appropriate locations and the system responses has a good settling time. Then, assuming that in the interval $k\tau \leq t \leq (k\tau + \tau)$,

$$u(k\tau) = F\ x(k\tau), \tag{4.30}$$

one can define the fictitious measurement matrix,

$$\mathbf{C}_i(F, N) = (\mathbf{C}_{0i} + \mathbf{D}_{0i} F_i)\ \ (\Phi_{\tau i} + \Gamma_{\tau i} F_i)^{-1}, \tag{4.31}$$

which satisfies the fictitious measurement equation

$$y_k = \mathbf{C}_i\ x_k, \tag{4.32}$$

i.e, to design the FOS controller for the multi-model system, the initial part of design upto the calculation of the measurement matrix is done independently for each plant. For robustness, FOS feedback controller gains $\mathbf{L}$ are obtained by solving the equation

$$\mathbf{L}\ \mathbf{C}_i\ =\ F, \quad i = 1 \text{ to } M, \quad M = 4, \tag{4.33}$$

which can be rewritten as

$$\mathbf{L}\ \tilde{\mathbf{C}}\ =\ F, \tag{4.34}$$

where

$$\tilde{\mathbf{C}}\ =\ [\ C_1 \quad C_2 \quad C_3 \quad C_4\ ] \tag{4.35}$$

are the new fictitious output measurement matrices for the individual plant models and

$$F\ =\ [\ F_1 \quad F_2 \quad F_3 \quad F_4\ ]. \tag{4.36}$$

IF $\tilde{\nu}$ denotes the observability index of $(\tilde{\Phi}, \tilde{C})$, it can be shown that for $N \geq \tilde{\nu}$, generically, $\tilde{C}$ has full column rank so that the robust SFB gain can be realized by a FOS feedback gain $\mathbf{L}$. With a FOS feedback gain which satisfies the Eq. (4.33), for each model the closed loop eigen values are the eigen values of the following matrix

$$\begin{bmatrix} \Phi_{\tau i} + \Gamma_{\tau i} F_i & \Gamma_{\tau i} \\ 0 & \mathbf{L}\mathbf{D}_{0i} - F_i \Gamma_{\tau i} \end{bmatrix}, \quad i = 1, 2, 3, 4, \tag{4.37}$$

which shows that the CL eigen values are still the ones for which the state feedback gains F_i have been designed, together with those of $(\mathbf{L}\mathbf{D}_{0i} - F_i \Gamma_{\tau i})$.

Thus, we have the eigen values of the closed loop system under a FOS control law in (4.33) as those of $(\Phi_{\tau i} + \Gamma_{\tau i} F_i)$ and $(\mathbf{L}\mathbf{D}_{0i} - F_i \Gamma_{\tau i})$. This suggests that the state feedback F should be obtained so as to ensure the stability of both $(\Phi_{\tau i} + \Gamma_{\tau i} F_i)$ and $(\mathbf{L}\mathbf{D}_{0i} - F_i \Gamma_{\tau i})$. The lifted system in Eq. (4.28) is stable if and only if F stabilizes $(\Phi_{\tau i}, \Gamma_{\tau i})$ and the matrix $(\mathbf{L}\mathbf{D}_{0i} - F_i \Gamma_{\tau i})$ has all its eigen values inside the unit circle.

Thus, the designed FOS gain $\mathbf{L}$ for the multimodel system realizes the designed F for all plants of the family. The controller obtained may be all right, but from the practical point of view, it may require excessive control action and the FOS gain values may be very high. To reduce this effect of gain on the control effort, we put a constraint on the gain using the spectral norms and then solve the linear equation (4.34) using the LMI optimization method [121], [50] for the multimodel system. The inequality constraint equations given in (4.17) - (4.20) can be used to solve the multimodel optimization problem.

4.2.3.2 Fault Tolerant Controller Design

In this Section, we design a fault tolerant control strategy such that the vibrations are effectively controlled in the event of failure of one of the actuators in the system dynamics. Such a failure mode can be modelled by replacing the i^{th} column of the input matrix by zero, i.e., the i^{th} column of B as zero indicates that the i^{th} actuator on the beam has failed. This consideration leads us to the problem of finding a control law that stabilizes the plant under normal operations and the 4 multivariable models corresponding to the 4 different failure modes. Sections 4.1 and 4.2.3:1 are used for the controller design here. The performance of the smart beam is hereby evaluated for vibration control by carrying out the simulations and observing the various responses and studying the effect of actuator failure [83], [84].

External disturbance is applied at the free end of the beam, thereby subjecting it into the vibrating mode. Now, when the system is in the vibrating mode, when a actuator fails to perform (because of the reasons mentioned in section 2.1.3), a robust controller is designed in such a way that putting it in the loop with the plant during the actuator failure, will bring back the system to stability. 4 models were obtained by considering 1 actuator failure at a time on the flexible beam. The sampling interval used is $\tau = 0.004$ seconds. The number of sub-intervals N is chosen as 4.

By sampling the 4 CT-SS models given in the Eqs. (2.112) and (2.118) at a rate of $\frac{1}{\tau}$ and $\frac{1}{\Delta}$, we get a family of tau systems $(\Phi_\tau, \Gamma_{\tau i}, C_i)$ and delta systems (Φ, Γ_i, C_i). One of these models, namely for the actuator failure at FE location 8, i.e., the fourth actuator, the tau and delta system is given by Eqs. (3.29) and (3.30). Similarly, the tau and delta systems for the other 3 MIMO models are obtained.

Stabilizing SFB gains are obtained such that the eigen values of $(\Phi_\tau + \Gamma_\tau F)$ are placed inside the unit circle at appropriate locations and the response of the system has a good settling time. The CL impulse responses with the SFB gain F is observed. Here, as we are dealing with robust stabilization, we have to find a $\mathbf{L}$ which will satisfy $\mathbf{L}\mathbf{C}_i = F,\ (i = 1, .., 4)$ using the LMI optimization approach. Using LMI theory, the Eqs. (4.17) - (4.20) are solved for different values of ρ_1, ρ_2 and ρ_3 and to find the RDFOS feedback gain matrix $\mathbf{L}$.

Using this F, if the LMI constraints given in the Eqs. (4.17) - (4.20) are solved, the robust FOS feedback gain matrix for the multi-model system may become full. This results in the control input of each actuator of the model being a function of the output of all the sensors. Decentralized robust FOS feedback control can be achieved by making the off-diagonal elements of L_0, L_1, L_2,...,L_{N-1} matrices zero. So, the structure of the resulting elements of $\mathbf{L}_i$ $(i = 0, 1, 2, 3, ..., N-1)$ matrices for the 4 models of the plant are assumed as

$$\mathbf{L}_i = Diag\ [\ L_{i11},\ L_{i22},\ L_{i33},\ L_{i44}] \ = \ \begin{bmatrix} L_{i11} & 0 & 0 & 0 \\ 0 & L_{i22} & 0 & 0 \\ 0 & 0 & L_{i33} & 0 \\ 0 & 0 & 0 & L_{i44} \end{bmatrix},\ i \ = \ 0, 1, .., (N-1). \tag{4.38}$$

With this structure of $\mathbf{L}_i$, the problem can be formulated in the framework of LMI and the desired matrices can be obtained. Now, it is evident that the control input u_i of each plant model is a function of the output y_i of that plant model only and this makes the FOS feedback control technique based smart structure system a

robust decentralized one. The RDFOS controller obtained by the designed method requires only constant gains, easier to implement in real time. The RDFOS gain matrix $\mathbf{L}$ for the multimodel system is given by

$$\begin{array}{rcl} \mathbf{L}_0 & = & Diag\ [\ 30.86 \quad -40.79 \quad 36.75 \quad -22.33\ ] \\ \mathbf{L}_1 & = & Diag\ [\ -60.60 \quad 47.21 \quad 21.36 \quad -15.26\ ] \\ \mathbf{L}_2 & = & Diag\ [\ 63.66 \quad -55.25 \quad 23.91 \quad -31.51\ ] \\ \mathbf{L}_3 & = & Diag\ [\ 70.84 \quad -65.63 \quad -52.53 \quad 40.56\ ] \end{array} \tag{4.39}$$

The closed loop responses with this RDFOS feedback gain $\mathbf{L}$ for all the 4 multivariable models of the smart structure plant (with one actuator failure at a time) are observed.

4.2.3.3 Simulation Results and Discussions

RDFOS feedback controller is designed for the multimodel smart system using the multivariable models of the single plant when subjected to an actuator failure [83], [84]. The beam has been divided into 8 FE and sensor / actuator pair bonded to the master structure at even FE. Four state space models have been obtained by considering the successive failure of one actuator at a time. Simulations are done in Matlab and the various responses (tip displacements, OL, CL, magnitude of control inputs) are observed when a failure of one of the piezo-patches on the beam takes place.

From the simulation results, it is inferred that when the plant is placed with the designed controller and when any one of the actuators fails to function, even then the controller stabilizes all the 4 models and damps out the oscillations quickly, stability is restored and the performance is not deteriorated. In the control law presented, the control input to each actuator of the multimodel system is a function of the output of that corresponding sensor only and the gain matrix has got all off-diagonal elements zero. This makes the FOS feedback control technique a robust decentralized one. This would render better control as it requires only constant gains and hence implementation may become easier. A robust control system has thus been designed with the constraint that the CL system be stable even if one of the input actuators has failed.

The transverse vibrations of the tip (i.e., tip displacement which is nothing but the first state variable x_1 plotted as a function of time t) for the multimodel system when the fault takes place at FE position 2 or 4 or 6 or 8 is shown in Figs. 4.14 and 4.15 respectively (with and without controller). From these figures, it is inferred that the actuators placed at FE position numbering 2 or 4 or 6 or 8 fails, the tip displacements of the beam w.r.t. the neutral axis of the beam takes a lot of time to decay out without the controller, whereas with the controller the vibrations are damped out quickly.

Thus, the tip displacements are well controlled and within the limits and the plots of tip displacements show a good damping enhancement, which can also be seen from the quantitative results displayed in Table 4.3. The plots of time derivative of the tip displacement, i.e., the sensor outputs y (CL impulse responses) as a function of time when the fault takes place at FE positions numbering 2 or 4 or 6 or 8 with and without the controllers is shown in Figs. 4.17 - 4.19 respectively.

The CL responses with the designed RDFOS gain $\mathbf{L}$ for the multimodel system with one actuator failure on the beam are observed and are found to be satisfactory.

What we mean by this statement is, the CL responses of the sensor outputs are well within limits, exhibiting a damped behavior, bringing the system back to stability and without going towards instability inspite of an actuator failure. Comparatively, the CL responses settle quickly than the OL responses and the controller effect is thus seen. The simulations of the 4 multivariable models of the multimodel system subjected to faults showed satisfactory results as the initial transients for all the models were within acceptable limits and the outputs settles in lesser times, i.e., in approximately 2 to 5 secs. By fault-tolerant control, we mean that even after a component failure, the smart system maintains stability.

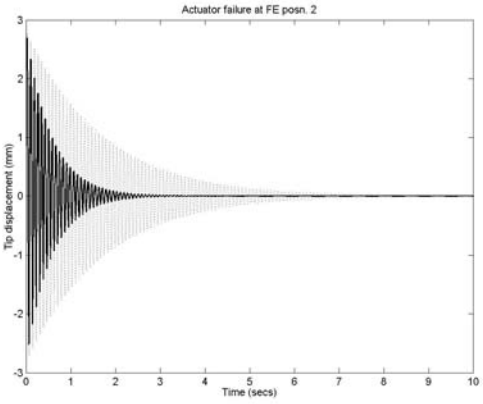

(a) Fault at FE 2

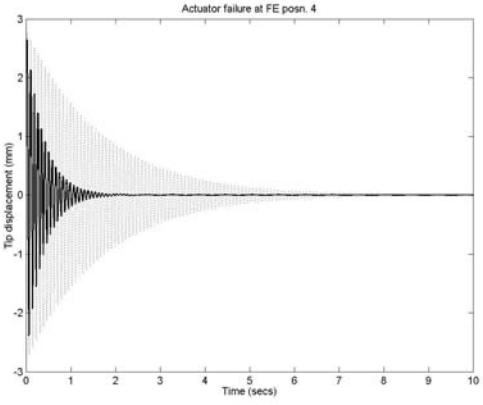

(b) Fault at FE 4

Fig. 4.14. Tip displacement when fault takes place at FE positions numbering 2 and 4 (without / with controller) for RDFOS f/b control

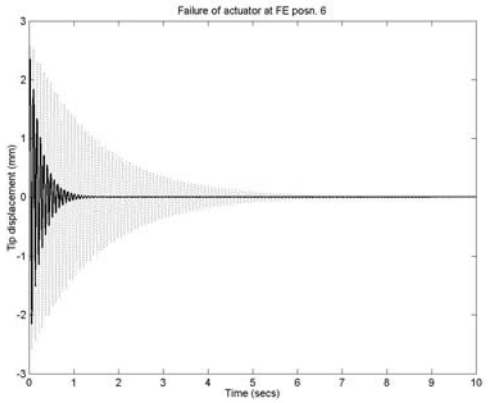

(a) Fault at FE 6

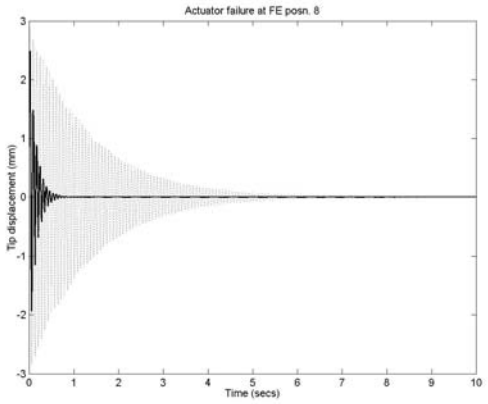

(b) Fault at FE 8

Fig. 4.15. Tip displacement when fault takes place at FE positions numbering 6 and 8 (without / with controller) for RDFOS f/b control

The comparisons of the graphical results are shown quantitatively in Table 4.4. It can be concluded that the CL system has good fault tolerance. The eigen values of the multimodel system were also found to be stable and within the unit circle even after the failure of the actuator. It can also be concluded that multivariable control of a smart structure using robust design is better compared to the SISO case [91], [92]. This is due to the fact that there is redundancy in the selection of sensor / actuator pairs on the beam, i.e., in the SISO case, if there is a sensor / actuator failure, then the system may go towards instability, but this is not so in the case of multivariable systems.

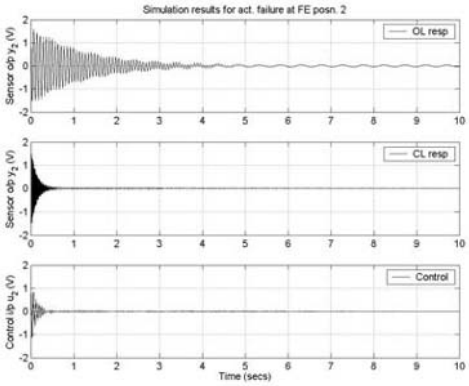

(a) Fault at FE 2, output of sensor 2

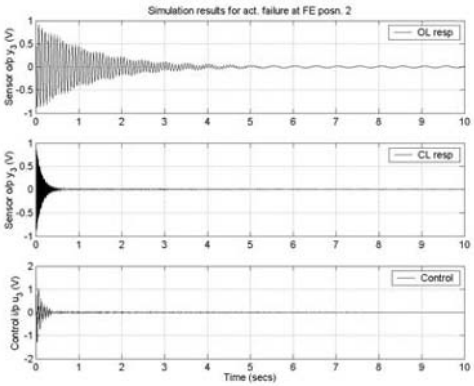

(b) Fault at FE 2, output of sensor 3

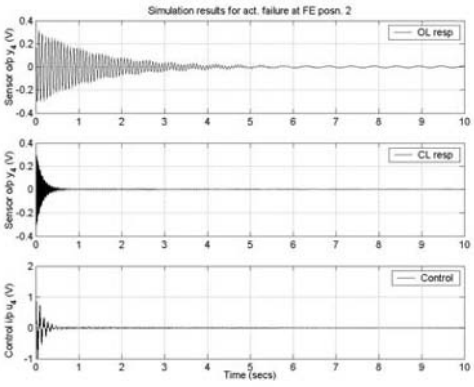

(c) Fault at FE 2, output of sensor 4

Fig. 4.16. OL / CL responses with RDFOS gain and control i/p for fault at FE position 2)

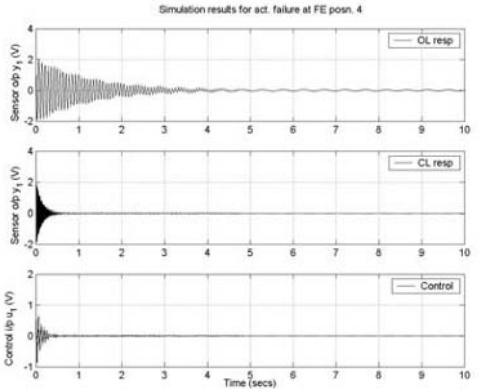

(a) Fault at FE 4, output of sensor 1

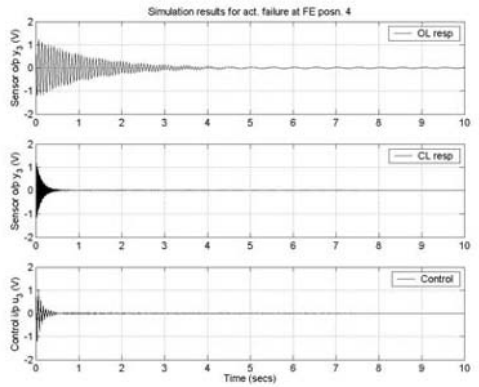

(b) Fault at FE 4, output of sensor 3

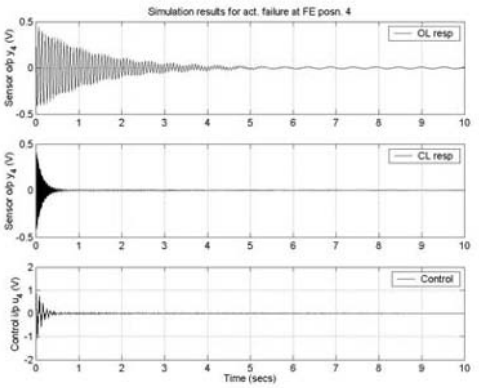

(c) Fault at FE 4, output of sensor 4

Fig. 4.17. OL / CL responses with RDFOS gain and control i/p for fault at FE position 4)

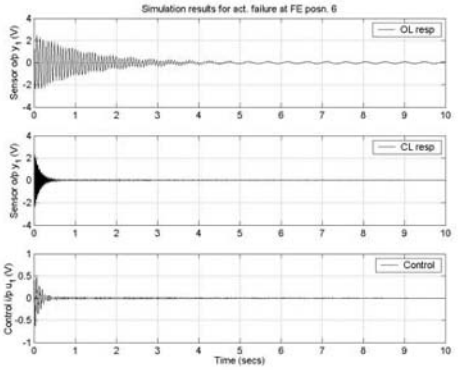

(a) Fault at FE 6, output of sensor 1

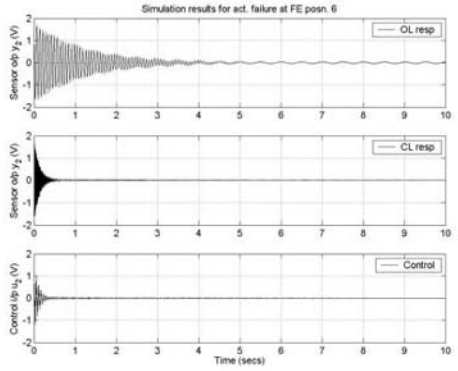

(b) Fault at FE 6, output of sensor 2

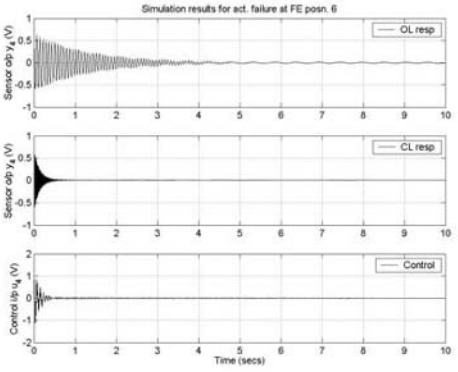

(c) Fault at FE 6, output of sensor 4

Fig. 4.18. OL / CL responses with RDFOS gain and control i/p for fault at FE position 6)

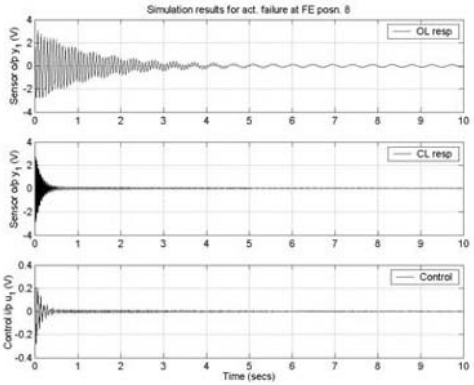

(a) Fault at FE 8, output of sensor 1

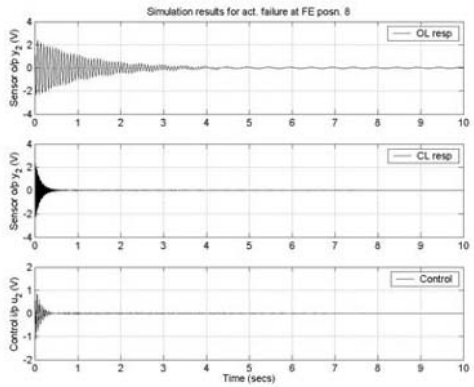

(b) Fault at FE 8, output of sensor 2

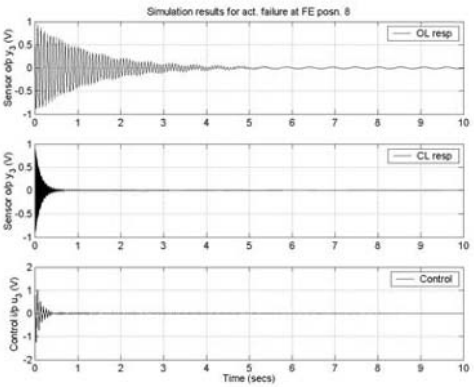

(c) Fault at FE 8, output of sensor 3

Fig. 4.19. OL / CL responses with RDFOS gain and control i/p for fault at FE position 8)

Table 4.3. Tabulation of the comparison results of simulation (tip displacements) of RDFOS f/b control

Actuator failure at FE position	Settling time (secs)		
	Without control	With control	% Damping (reduction in settling time)
Position 2	0.8	3.2	$\cong$ 60 %
Position 4	8.1	2.4	$\cong$ 70 %
Position 6	6.5	1.7	$\cong$ 80 %
Position 8	6.1	0.8	$\cong$ 90 %

Table 4.4. Tabulation of the comparison results of simulation (OL / CL responses with F, $\mathbf{L}$ and control for RDFOS f/b control)

for the multimodel system

Parameters	Failure of the piezo-actuator at FE location			
	Position 2	Position 4	Position 6	Position 8
Sensor o/p y_1				
OL	-	3.2 (10)	3.3 (10)	3.9 (10)
CL	-	3.2 (3)	3.3 (3)	3.8 (3)
control u_1	-	1.6	0.8	0.36
Sensor o/p y_2				
OL	1.8 (10)	-	1.9 (9.5)	3.6 (9.5)
CL	1.8 (3)	-	1.9 (2.5)	3.6 (2.5)
control u_2	0.9	-	1.5	1.8
Sensor o/p y_3				
OL	0.9 (9.9)	1.6 (9.5)	-	1 (9)
CL	0.9 (2.5)	1.6 (2)	-	1 (2)
control u_3	1.6	1.5	-	1.3
Sensor o/p y_4				
OL	0.4 (9.8)	0.5 (9)	1.5 (9)	-
CL	0.36 (2)	0.49 (1.5)	0.8 (2)	-
control u_4	1.9	1.2	0.6	-

Similar to the conclusions drawn in the case of RDPOF at the end of the simulation results, here also the same conclusions are met for the case of RDFOS feedback. The simulation results showed that the FOS feedback controller gain maintained the performance achieved by the SFB gain. Thus, unlike static output feedback, the FOS feedback control always guarantees the stability of the CL system.

4.2.4 Robust Decentralized Fast Output Sampling Feedback Controller Design via Reduced Order Model for Multivariable Systems

In this Section, the design of a RDFOS feedback control technique for the AVC of smart structures for a multimodel case comprising of a family of multivariable plants is presented [79]. The beam structure is modeled in state space form by dividing it into 4 FE and placing the PE sensor / actuator at 2 finite element locations (positions 2 and 4) as collocated pairs, i.e., as surface mounted sensor / actuator as shown in Fig. 2.5. Six vibratory modes are retained in modelling the beam. A higher order multivariable system is thus obtained.

The state space model of the higher order system thus obtained is given by Eqs. (2.121) and (2.122) with the numerical values of the **A**, **B**, **C**, **D**, **E** matrices given by the Eq. (2.123) for the model 1. Five such multivariable models are obtained by varying the thickness parameter of the aluminum beam, thus giving rise to a multimodel system of the smart structure. Using model order reduction technique, the reduced order model of the higher order system is obtained [62]. RDFOS feedback controllers are designed for the multimodel system consisting of 5 MIMO models using the reduced order model technique. The performance of the multimodel system is hereby evaluated for AVC by carrying out the simulations. A brief review about the model order reduction technique was presented in Section 3.2.4.

Consider a family of plants $S = \{A_i, B_i, C_i\}$ defined by

$$\dot{x} = A_i x + B_i u, \quad y = C_i x, \qquad i \; = \; 1, 2, 3, ..., M, \tag{4.40}$$

where $M = 5$. The discrete systems with sampling interval τ seconds can be represented as

$$x(k+1) = \Phi_{\tau i} x(k) + \Gamma_{\tau i} u(k), \quad y(k) = C_i x(k). \tag{4.41}$$

There exists a transformation V_i, such that,

$$x = V_i \; z \tag{4.42}$$

transforms the above system in Eq. (4.41) into the following block modal form as

$$z(k+1) = \hat{\Phi}_i z(k) + \hat{\Gamma}_i u(k), \quad y(k) = \hat{C}_i z(k), \tag{4.43}$$

where

$$\hat{\Phi}_i = \begin{bmatrix} \Phi_{1i} & 0 \\ 0 & \Phi_{2i} \end{bmatrix}, \quad \hat{C}_i = \begin{bmatrix} C_{1i} \\ C_{2i} \end{bmatrix}, \quad \hat{\Gamma}_i = \begin{bmatrix} \Gamma_{1i} \\ \Gamma_{2i} \end{bmatrix} \tag{4.44}$$

and the eigen values are arranged in the order of their dominance. We now extract an r^{th} order model, retaining the r dominant eigen values, by truncating the above systems. Using Eqs. (4.43) and (4.44), we get

$$z_r(k+1) = \Phi_{1i} z_r(k) + \Gamma_{1i} u(k), \quad y(k) = C_{1i} z_r(k) \tag{4.45}$$

Let $u(k) = S_r\ z_r$ be a stabilizing control for the reduced order model in Eq. (4.45). Thus, the closed loop reduced model $(\Phi_{1i} + \Gamma_{1i} S_r)$ becomes stable. Now,

$$Z_r = \left[I_r\ :\ 0_{r*(n-r)}\right]\ z = \left[I_r\ :\ 0_{r*(n-r)}\right] V^{-1}\ x. \tag{4.46}$$

$\therefore$, we get,

$$u(k) = S_r \left[I_r\ :\ 0_{r*(n-r)}\right] V^{-1} x = S_i\ x, \tag{4.47}$$

which makes the CL system $(\Phi_{\tau i} + \Gamma_{\tau i} S_i)$ stable and has no eigen values at the origin. Thus, $S_i \equiv F_i$ are the stabilizing SFB gains for the system in Eq. (4.41). Using these SFB gains F_i , the following inequalities are solved to obtain $\mathbf{L}$.

$$\| \mathbf{L} \| < \rho_{1i}, \quad \| \mathbf{L}\mathbf{D}_{0i} - F_i \Gamma_{\tau i} \| < \rho_{2i}, \quad \| \mathbf{L}\mathbf{C}_i - F_i \| \leq \rho_{3i}, \quad i = 1, 2, ..., M. \tag{4.48}$$

The controller obtained from the above equation will give desired behavior, but might require excessive control action. To reduce this effect, we relax the condition that $\mathbf{L}$ exactly satisfy the linear equation $\mathbf{LC} \approx F$ and include a constraint on the gain $\mathbf{L}$. Thus, this can be formulated in the framework of Linear Matrix Inequalities (LMI) as given in the following equations as

$$\begin{bmatrix} \rho_{1i}^2 I & \mathbf{L} \\ \mathbf{L}^T & -I \end{bmatrix} < 0, \tag{4.49}$$

$$\begin{bmatrix} \rho_{2i}^2 I & \mathbf{L}\mathbf{D}_{0i} - F_i \Gamma_{\tau i} \\ (\mathbf{L}\mathbf{D}_{0i} - F_i \Gamma_{\tau i})^T & -I \end{bmatrix} < 0, \tag{4.50}$$

$$\begin{bmatrix} \rho_{3i}^2 I & \mathbf{L}\mathbf{C}_i - F_i \\ (\mathbf{L}\mathbf{C}_i - F_i)^T & -I \end{bmatrix} < 0. \tag{4.51}$$

If the LMI constraints given in Eqs. (4.48) - (4.51) are solved using the above F_i, the robust FOS feedback gain may become full. This results in the control input of each model being a function of the outputs of all the models. To obtain the RDFOS feedback control, the off-diagonal elements of $L_0, L_1, L_2, ..., L_{N-1}$ matrices are made equal to zero as a result of which the control input to each actuator is a function of the output of that corresponding sensor only. This makes the FOS control technique a robust decentralized one and is more feasible, requires only constant gains and may be easier to implement.

The RDFOS feedback controller via reduced order model is designed as follows. The 5 multivariable SS models of the multimodel system is considered as the preliminary step in the controller design. A 12^{th} order SS model of of (12×12) is obtained by retaining the first 6 modes of vibration ω_1 to ω_6. This higher order system is reduced to a simpler 6^{th} order model of (6×6), by considering the effects of the 6 most dominant (dominant in the sense of being closed to instability) eigen values. The eigen values of the original system that are farthest from the origin are neglected and only dominant eigen values of the original system in the reduced order model is retained.

An external force $\mathbf{f}_{ext}$ of 1 N is applied for duration of 50 ms at the free end of the beam for all the 5 models of the Fig. 2.5 and the OL responses are observed. RDPOF controller is designed to take care of the fault, stabilize the system and damp out the vibrations in quicker time. The sampling interval used is $\tau = 0.004$ secs. The discrete models are obtained for sampling time of $\tau = 0.004$ secs and for $\Delta = 0.0004$ secs.

Using the method discussed in the previous paragraphs from Eqs. (4.40) - (4.48) and in section 3.2.4, RDFOS feedback gain is obtained which approximately realizes the designed SFB gain F_i for all the models of the family. Here, as we are dealing with robust stabilization, we have to find a $\mathbf{L}$ which will satisfy $\mathbf{LC}_i = F_i,\ i \approx 1, .., 5$ all these equations using the LMI approach so that the magnitude of the control effort required to control the vibrations is less. 10 gain sequences of $\mathbf{L}$ are obtained, i.e., $L_1, ..., L_{10}$. In our problem considered, $N = 10$ had given good encouraging results. Using the SFB gains F_i, the LMI constraints given in Eqs. (4.48) - (4.51) are solved for different values of ρ_1, ρ_2 and ρ_3 to find the RDFOS feedback gain matrix $\mathbf{L}$ for the actual models via the reduced order model. The RDFOS feedback gain matrix is given by

$$\mathbf{L} = \begin{bmatrix} 172.1137 & 0 & -79.0428 & 0 & -176.0630 & 0 & -68.3585 \\ 0 & -144.1840 & 0 & 108.1592 & 0 & 92.7216 & 0 \end{bmatrix}$$

$$\begin{bmatrix} 0 & 169.2613 & 0 & -9.8467e-6 & 0 & 0.0016 & 0 \\ 2.2531 & 0 & -86.7592 & 0 & 1.289e-5 & 0 & -0.0020 \end{bmatrix}$$

$$\begin{bmatrix} -0.0968 & 0 & 2.6812 & 0 & -34.4828 & 0 \\ 0 & 0.1069 & 0 & -2.6288 & 0 & 34.4253 \end{bmatrix}. \quad (4.52)$$

With the designed robust controller being put in the loop, the CL impulse responses with the RDFOS feedback gain of the system and the variation of the control signals with time for the multimodel system comprising of 5 MIMO plants are observed and shown in Figs. 4.20 - 4.24 respectively.

4.2.4.1 Simulation Results and Discussions

Robust decentralized fast output sampling feedback Controller is designed for the multimodel representation of multivariable plants via the reduced order modeling [79]. These multivariable models of the smart beam are obtained by varying the thickness parameter of the beam. Simulations are performed and the various responses are observed for the multimodel system. Through the simulation results, it is shown that when the plant is placed with the designed robust decentralized FOS controller, all the models perform well and the vibrations die out quickly. Observations are made with and without the controller to show the control effect.

A new algorithm is presented for the design of robust decentralized controllers for a multivariable system using FOS feedback technique via the reduced order model. The computation of the SFB gain, which is needed to obtain the decentralized FOS feedback based smart structure system, becomes very tedious when a number of modes, especially greater than 5 are considered. Here, a SFB gain is computed from the reduced order model of the smart system and using the aggregation techniques [125], a state feedback gain can be obtained for the higher order model.

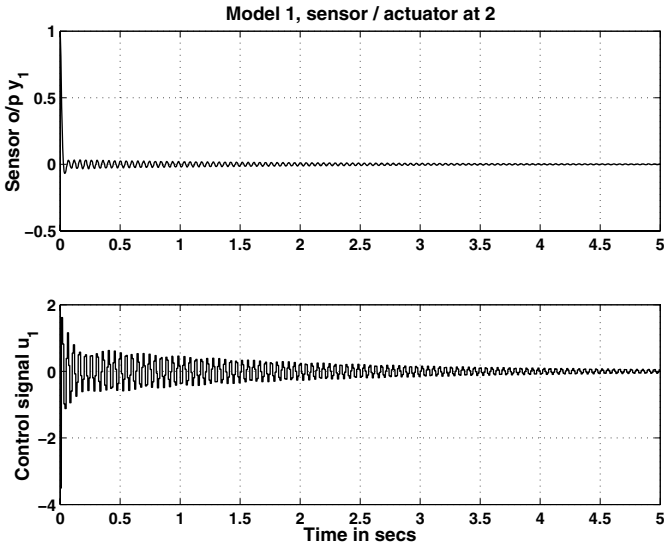

(a) FE 2

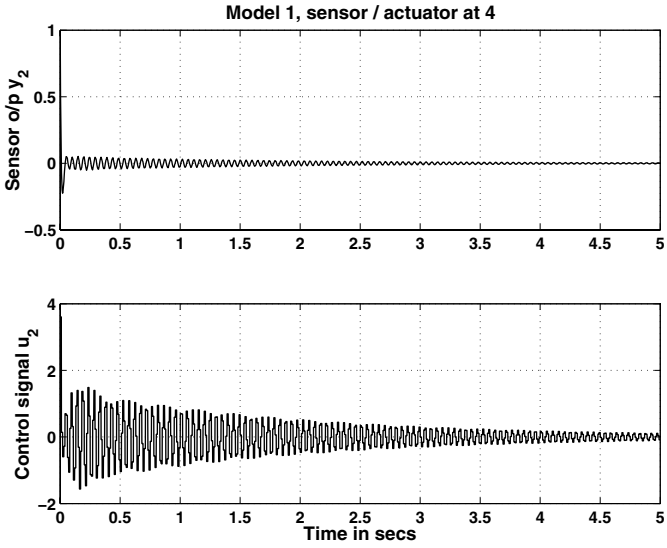

(b) FE 4

Fig. 4.20. CL responses and control inputs (sensor / actuator placed at FE positions 2, 4) : Model 1

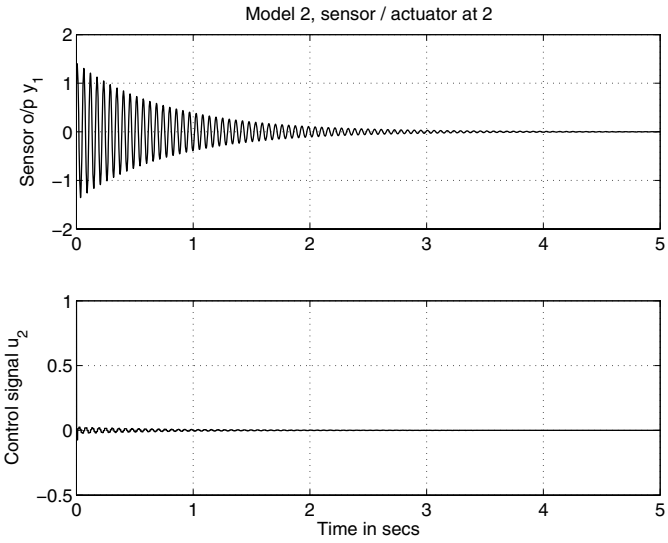

(a) FE 2

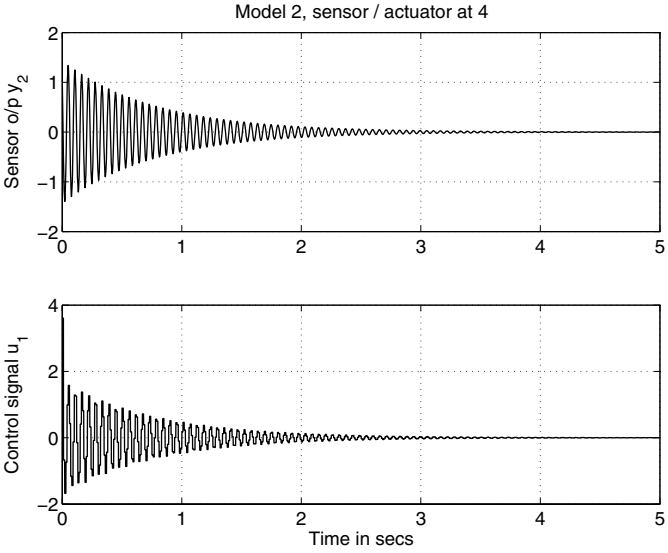

(b) FE 4

Fig. 4.21. CL responses and control inputs (sensor / actuator placed at FE positions 2, 4) : Model 2

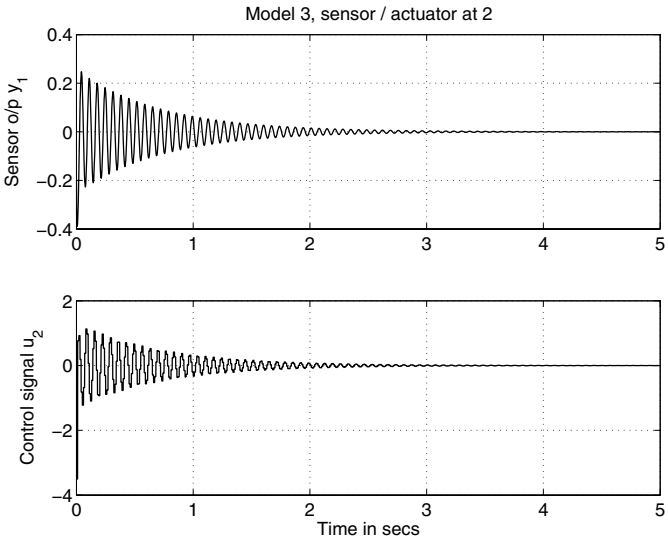

(a) FE 2

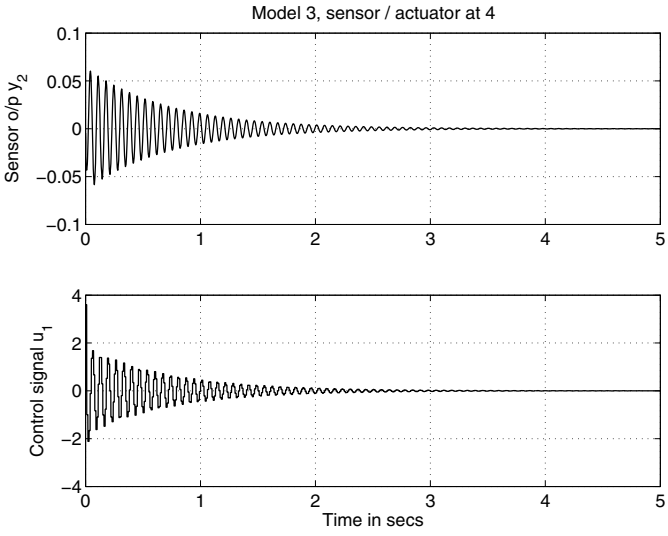

(b) FE 4

Fig. 4.22. CL responses and control inputs (sensor / actuator placed at FE positions 2, 4) : Model 3

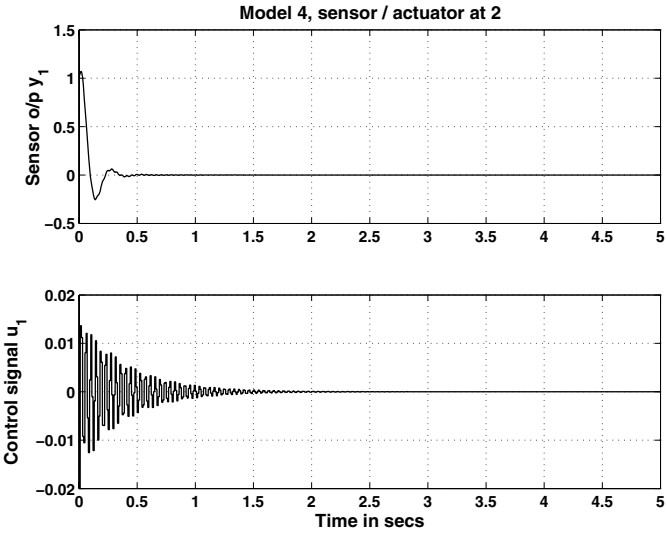

(a) FE 2

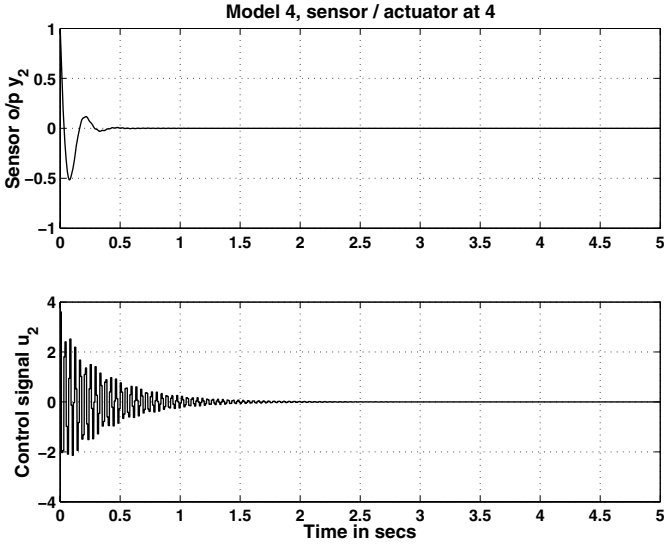

(b) FE 4

Fig. 4.23. CL responses and control inputs (sensor / actuator placed at FE positions 2, 4) : Model 4

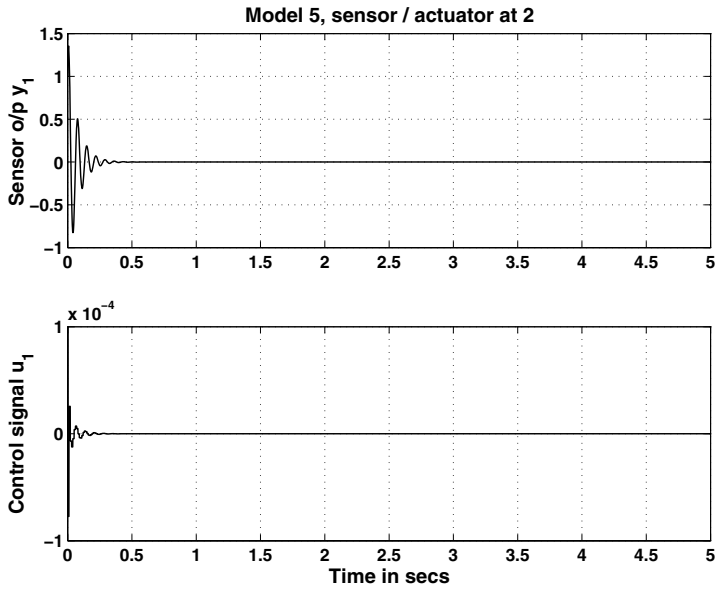

(a) FE 2

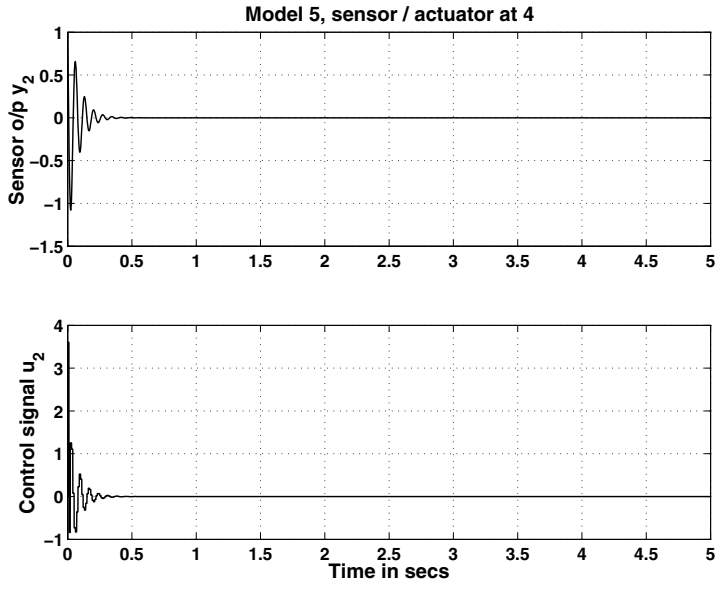

(b) FE 4

Fig. 4.24. CL responses and control inputs (sensor / actuator placed at FE positions 2, 4) : Model 5

The RDFOS feedback gain which realizes this SFB gain, can be obtained for the actual model. It is found that the designed RDFOS controller via the reduced order model provides good damping enhancement for the models of the smart structure system. In the designed control law, the control input to each actuator of the multivariable plant's multimodel is a function of the output of that corresponding sensor only and the gain matrix has got all off-diagonal elements zero or very small compared to the diagonal terms. This makes the FOS control technique a robust decentralized one and would render better control.

4.3 Controller Design for Smart Structures Modelled Using Timoshenko Theory

In the following Sections, the design of the FOS controllers for a smart structure modelled as SISO and MIMO systems using Timoshenko beam theory is presented.

4.3.1 Design of SISO Controllers for Smart Beams Using Surface Mounted Piezos

The FOS control technique discussed in the Section 4.1 is used to design the control strategy for the SISO representations of the developed smart structure models as shown in Fig. 2.7 with surface mounted collocated piezo patches [73]. The various SISO models are given in the Eqs. (2.172)-(2.175). A sixth order state space model of the system is obtained by retaining the first 3 vibratory modes of the system. The first 3 natural frequencies obtained are 3.75 Hz, 23 Hz and 62.5 Hz. The performance of the designed controller is evaluated for AVC by carrying out the simulations and by observing the various responses. The effect (role) of varying the sensor/actuator location at different FE positions (from fixed end to the free end) on the beam is observed and the conclusions are drawn for the best model required for AVC.

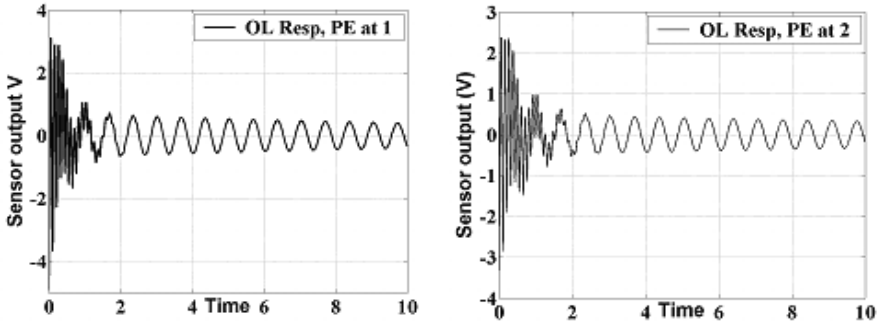

(a) Model 1 (b) Model 2

Fig. 4.25. OL responses for PZT at FE positions 1 and 2 for SISO models of Timoshenko beam (surface mounted PZT)

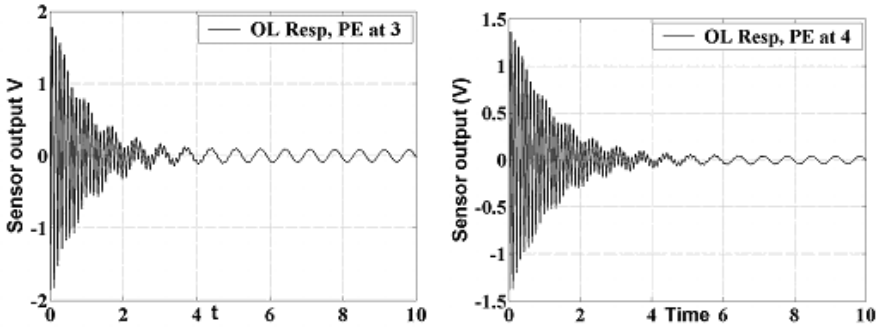

(a) Model 3 (b) Model 4

Fig. 4.26. OL responses for PZT at FE positions 3 and 4 for SISO models of Timoshenko beams (surface mounted PZT)

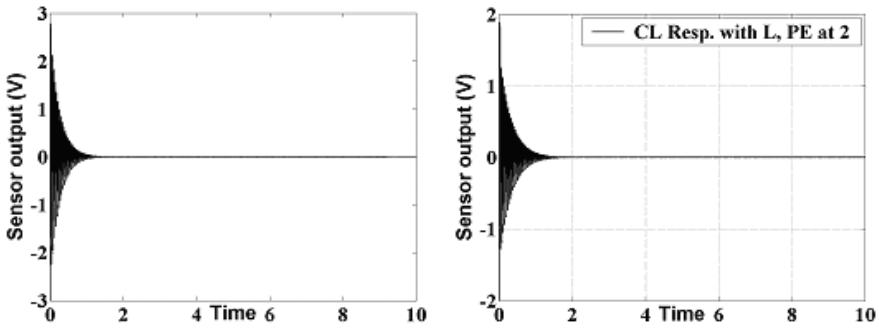

(a) Model 1 (b) Model 2

Fig. 4.27. CL responses for PZT at FE positions 1 and 2 for SISO models of Timoshenko beams (surface mounted PZT)

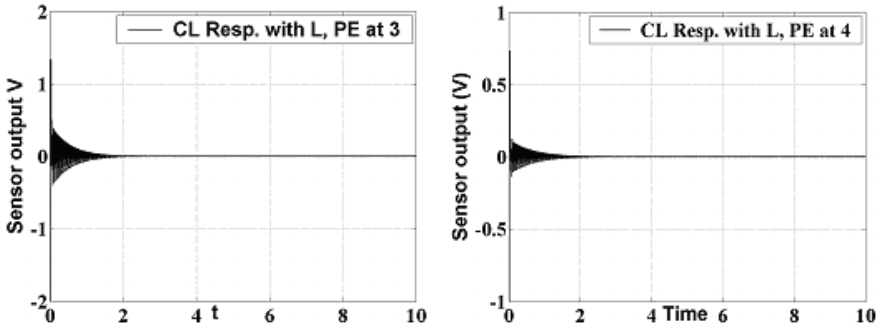

(a) Model 3 (b) Model 4

Fig. 4.28. CL responses for PZT at FE positions 3 and 4 for SISO models of Timoshenko beams (surface mounted PZT)

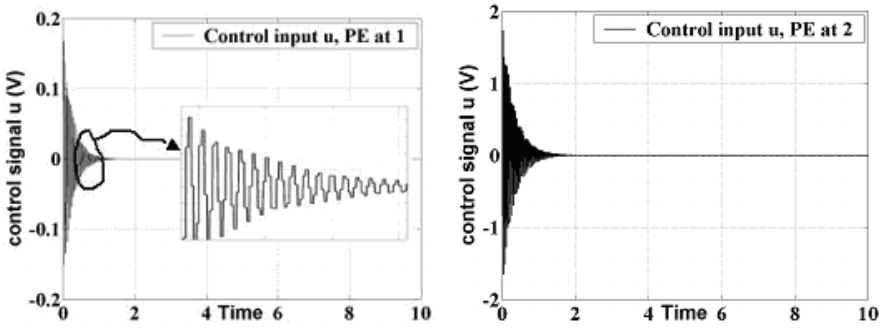

(a) Model 1 (b) Model 2

Fig. 4.29. Control inputs at FE positions 1 and 2 for SISO models of Timoshenko beams (surface mounted PZT)

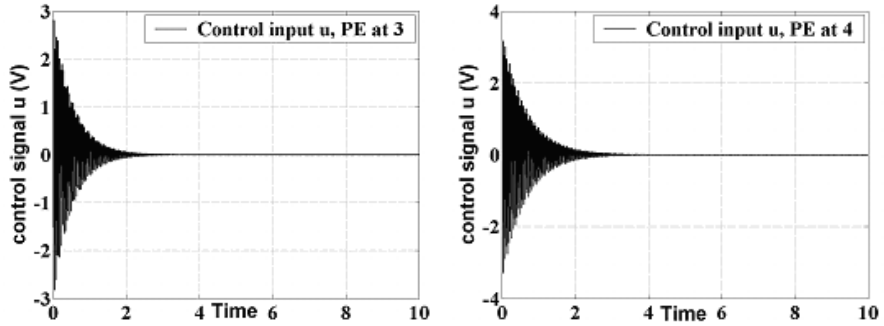

(a) Model 3 (b) Model 4

Fig. 4.30. Control inputs at FE positions 3 and 4 for SISO models of Timoshenko beams (surface mounted PZT)

An external force is applied at the free end of the beam, thus subjecting it to vibrations. The OL responses are observed and shown in the Figs. 4.25 and 4.26. The controller is designed on the similar lines as explained in the Section 4.2.1 on Euler-Bernoulli beams modelled as SISO systems. The sampling interval τ is taken as 0.004 secs and the number of sub-intervals N was taken as 4. The CT system in Eqs. (2.172)-(2.175) is sampled at a rate of $\frac{1}{\tau}$, thus giving rise to tau systems. The tau system for the model 1 is given by the Eq. (3.58). Similarly, the tau systems for the other SISO models of the smart beam are obtained. It is found that the tau systems are controllable and observable. The stabilizing SFB gains are obtained for each of the SISO models of the smart beam such that the eigenvalues of $(\Phi_\tau + \Gamma_\tau F)$ are placed inside the unit circle at appropriate locations and the response of the system has a good settling time. The CL impulse responses of all the 4 SISO models with the SFB gain F is observed.

Now, the CT system given in Eqs. (2.172)-(2.175) is sampled at a rate of $\frac{1}{\Delta}$, thus giving rise to delta systems. The delta system for the model 1 is given by the Eq.

(3.60). Similarly, the delta systems for the other SISO models of the smart beam are obtained. The FOS feedback gain $\mathbf{L}$ for the 4 SISO models (model 1, 2, 3 and 4) of the smart beam is obtained by solving $\mathbf{L}\ \mathbf{C}\ \approx\ F$ using the LMI optimization method [121], [50] and is given by

$$\begin{array}{l} \mathbf{L}_1 = [-19.2078 \quad 29.2089 \quad 16.6960 \quad -10.1007]\,, \\ \mathbf{L}_2 = [-37.1699 \quad 54.8758 \quad 33.0538 \quad -17.5525]\,, \\ \mathbf{L}_3 = [-86.5273 \quad 88.2034 \quad 89.3166 \quad -79.0370]\,, \\ \mathbf{L}_4 = [-89.5000 \quad 96.1000 \quad 91.9000 \quad -86.8000]\,. \end{array} \tag{4.53}$$

With the designed FOS feedback controller being put in the loop with the smart plant, the CL impulse responses (sensor outputs y_i) and the variation of the control signal u_i with time t for all the 4 SISO models of the smart beam are observed as shown in Figs. 4.27 and 4.28.

4.3.1.1 Simulation Results and Discussions

FOS feedback controllers are designed for the 4 SISO models of the smart structure modelled using Timoshenko beam theory in order to suppress the first 3 vibratory modes [73]. After observing the various responses as shown in the Figs. 4.25 - 4.30, the comparison and discussion of the simulation results of the vibration control for the smallest magnitude of the control effort u and the best model for AVC is presented here. As in the case of the results on the POF control of SISO models modelled using Timoshenko beam theory with surface mounted PZT's, here also, the best model required for AVC is the model 1, i.e., the SISO model with PZT at the fixed end of Fig. 2.7. The model 1 is selected because of the following reasons.

- Control will be more effective at the root.
- The sensor output voltage is greater due to the heavy distribution of the bending moment near the fixed end for the fundamental mode, thus leading to a larger strain rate.
- Less control effort is required to damp out the vibrations.
- Sensitivity of the sensor / actuator pair depends on its location on the beam.
- The response characteristics with F and $\mathbf{L}$ are the best amongst all the SISO models.
- Vibration characteristics of the system depended not only on the collocation of the piezo pair, but also on many factors such as the gain of the amplifier used, the mode number and the location of the piezo pair at the nodal points from the fixed end.
- Controller output required is very less.

Further, responses are obtained by considering the first 2 vibratory modes also. Results are compared with the controllers designed for first 3 vibratory modes. The obtained responses by retaining the first 2 modes were almost the same as in the case of 3 vibration modes. The limitations of Euler-Bernoulli beam theory such as the neglection of axial displacement has been considered here while modeling the beam. Timoshenko beam theory corrects the simplifying assumptions made in Euler-Bernoulli beam theory and the model obtained can be closer to a exact one.

4.3.2 Design of MIMO FOS Controller for Smart Beam Using Surface Mounted Piezos

In this Section, we develop the control system design using the FOS feedback control law discussed in Section 4.1 for the multivariable representation of the flexible cantilever beam given by the Eqs. (2.103) and (2.104) and bonded with surface mounted sensors and actuators as collocated pairs through the smart structure concept as shown in Section 2.2.2. First 3 vibratory modes are considered. The numerical values of the state space matrices of the MIMO model are given by the Eqs. (2.180).

The performance of the smart beam as a multivariable system is evaluated for vibration control by carrying out the simulations and observing the various responses. The effect of placing the sensor-actuator pair at 2 different FE locations on the beam is observed and the conclusions are drawn. The multivariable controller is designed on the similar lines as explained in the section 4.2.2 for EB beams. The sampling interval τ is taken as 0.004 secs and the number of sub-intervals N was taken as 10. The FOS gain matrix $\mathbf{L}$ for the MIMO model of the surface mounted smart beam modelled using Timoshenko beam theory is given by

$$\mathbf{L} = 10^2 \begin{bmatrix} -0.4568 & 0.3563 & -0.5583 & 0.6347 \\ -0.4896 & 0.3986 & -0.6125 & 0.7125 \end{bmatrix}. \tag{4.54}$$

4.3.2.1 Simulation Results and Discussions

FOS controller has been designed for the MIMO smart structure model. The beam was divided into 4 FE with sensor / actuator placed at positions 2 and 4. The various responses are obtained for the developed state space multivariable model. Through the simulation results, it is shown that when the plant is placed with this controller, the plant performs well and the vibrations are suppressed quickly. It is also observed that modeling a smart structure by including the sensor / actuator mass and stiffness and by placing the sensor / actuator at two different positions introduces a considerable change in the structural vibration characteristics than placing the sensor / actuator pair at only one location (Figs. 4.25 - 4.30).

The response takes lesser time to settle than the SISO case and the vibrations are damped out quickly. The control effort required is also less. The impulse responses with the output injection gain and the FOS gain shows better performance. The sensor-actuator pair kept at position 2 controls the 2 vibratory modes at that FE position 2, while the pair kept at position 4 also controls the 2 vibratory modes, but placed at that FE position 4. A overall better performance of the system is obtained. Hence, it can be concluded that multivariable control of a smart structure is better compared to the SISO control as there will be multiple interactions of the input and the output which will cause the vibrations in the system to damp out quickly. Responses were observed without control and were compared with the control to show the control effect. From the simulations, it was observed that without control the transient response was predominant and with control, the vibrations are suppressed.

MIMO dynamic analysis is able to identify pairs of modes that occur at nearly identical frequencies. SISO experiments are not actually reliable when it comes to accurate identification of mode pairs because they are unable to positively decipher

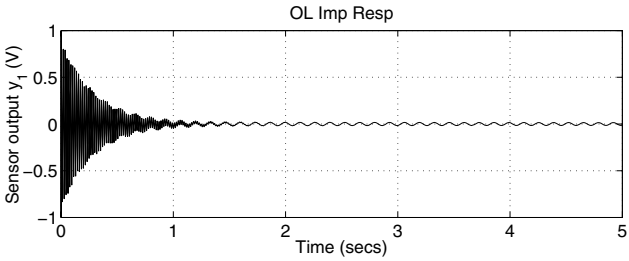

(a) OL Impulse response

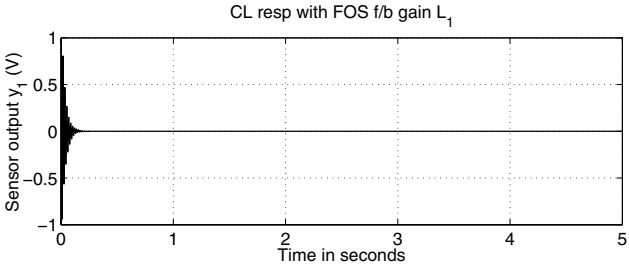

(b) CL impulse response with F_1

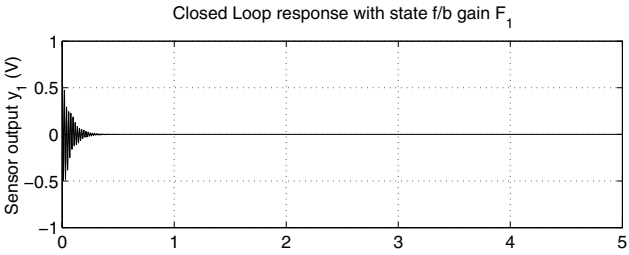

(c) CL impulse response with $\mathbf{L}_1$

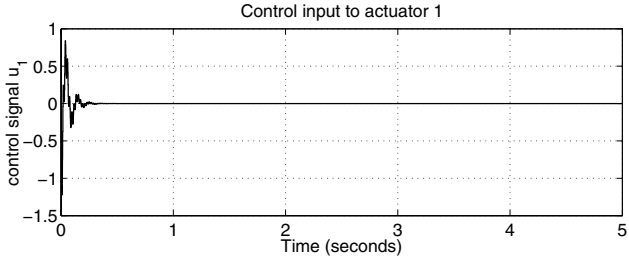

(d) Control input u_1

Fig. 4.31. Responses of MIMO system at FE 2 for surface mounted PZT's of Timoshenko beams

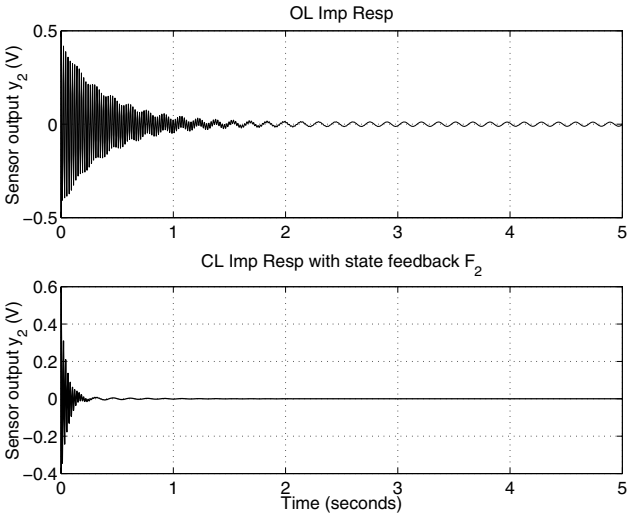

(a) OL and CL Impulse response with F_2

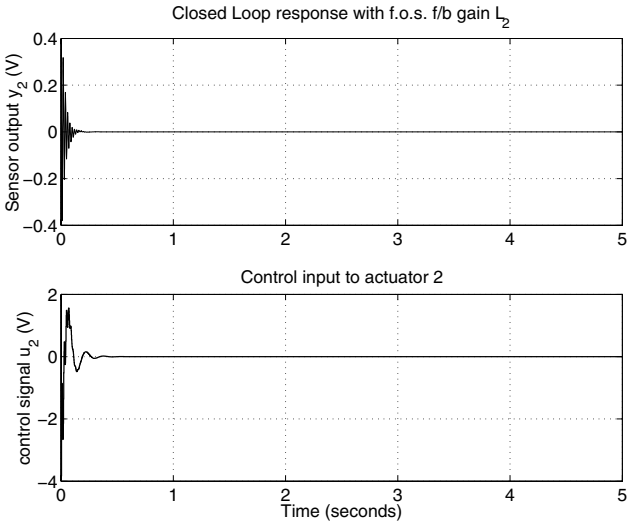

(b) CL impulse response with $\mathbf{L}_2$, control u_2

Fig. 4.32. Responses of MIMO system at FE 4 for surface mounted PZT's of Timoshenko beams

mode pairs from signal noise in the measured Frequency Response Functions (FRF). Depending on the application, the smearing of the mode pairs into single modes may adversely affect the control algorithm, depending on the algorithm's sensitivity to the identified resonant frequencies of the system. MIMO excitation is better than SISO excitation as exciting only at a single point may cause poor distribution of

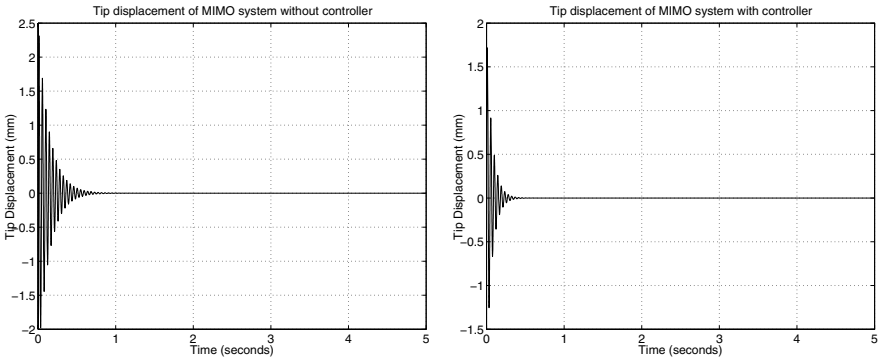

(a) (b)

Fig. 4.33. Tip displacements of MIMO Timoshenko beam with surface mounted PZT's

input energy throughout the structure and may result in somewhat slightly disturbed frequency responses. A multi-input test provides better energy distribution and even better actuation forces.

4.3.3 Design of SISO Controllers for Smart Beams Using Embedded Piezos

In the following Section, we develop the control strategy for the SISO representation of the developed smart structure model given in the Eqs. (2.242)-(2.243) using the FOS feedback control law discussed in the Section 4.1 for the various SISO models of the same plant [76] with embedded shear sensors and actuators. Four different configurations of the beam are considered as shown in Fig. 2.12. In all the 4 cases, the length of the beam is 20 cm and its cross section is 1 mm by 2 cm. The length of the piezo patch is 6 cm and its cross section is 1 mm by 2 cm. The only change in all the 4 models is in the location of the sensor whereas the actuator location is fixed at FE position 1.

A sixth order state space model of the system is obtained on retaining the first 3 modes of vibration of the system. The first 3 natural frequencies obtained are 52.03 Hz, 97.21 Hz and 145.81 Hz. The performance of the designed controller is evaluated for vibration control by carrying out the simulations and observing the various responses. The effect of placing the sensor at different locations in the embedded composite structure as non-collocated pair is observed and the conclusions are finally drawn for the best performance model required for the AVC [76].

The controller is designed on the similar lines as explained in the Section 4.2.1 for Euler-Bernoulli beams and in Section 4.3.1 for Timoshenko beams. The sampling interval τ is taken as 0.004 secs and the number of sub-intervals N was taken as 10. An external force is applied at the free end of the beam, thus subjecting it to vibrations. The OL responses are observed. The discrete models are obtained by sampling the system in (2.242) and (2.243) at a rate of $\frac{1}{\tau}$ and $\frac{1}{\Delta}$ respectively giving rise to $(\Phi_{\tau i}, \Gamma_{\tau i}, C_i)$-tau systems and (Φ_i, Γ_i, C_i)-delta systems respectively $(i = 1, .., 4)$.

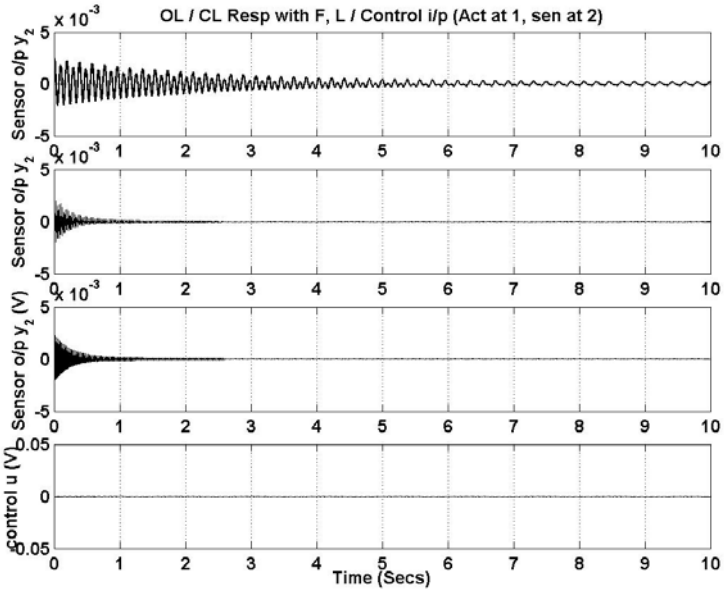

Fig. 4.34. OL / CL response with F and $\mathbf{L}$ / control u for model 1 (embedded Timoshenko beam)

The tau and delta system for the model 1 is given by the Eqs. (3.63) and (3.64). Similarly, the tau and delta systems for the other 3 models are obtained. It is found that all the discrete models were controllable and observable. The stabilizing SFB gains are obtained for the tau system such that the eigenvalues of $(\Phi_{\tau i} + \Gamma_{\tau i} F_i)$ lie inside the unit circle and the response of the system has a good settling time. The SFB gain for the model 1 is obtained as

$$F_1 = [\ -2.0322 \quad 0.0006 \quad 0.0024 \quad 0.0081 \quad -0.0003 \quad 0.0002]. \tag{4.55}$$

Similarly, the SFB gains for the other SISO models are obtained. The CL impulse responses of the 4 models of the system with the output injection gain is observed and shown in Figs. 4.34 - 4.37. The FOS feedback gain matrix $\mathbf{L}$ for the smart system given is obtained by solving $\mathbf{LC} \approx F$ using the LMI optimization method, which reduces the amplitude of the control signal u. With the designed controller put in the loop, the CL impulse responses (sensor outputs) of the different SISO models of the smart system are observed. The FOS feedback gain matrix for the SISO model 1 of the smart Timoshenko beam with embedded sensor /actuator is given by

$$\mathbf{L} = \big[\ 0.1111 \quad 0.0734 \quad 0.039 \quad 0.0095 \quad -0.038 \quad -0.0304 \quad -0.0403 \quad -0.0440 \quad -0.0426 \quad -0.0377\big]. \tag{4.56}$$

Similarly, the FOS gains are obtained for the other 3 models of the smart structure plant. With the designed FOS controller put in loop with the plant, the CL impulse responses (sensor outputs) of all the 4 SISO models and the variation of

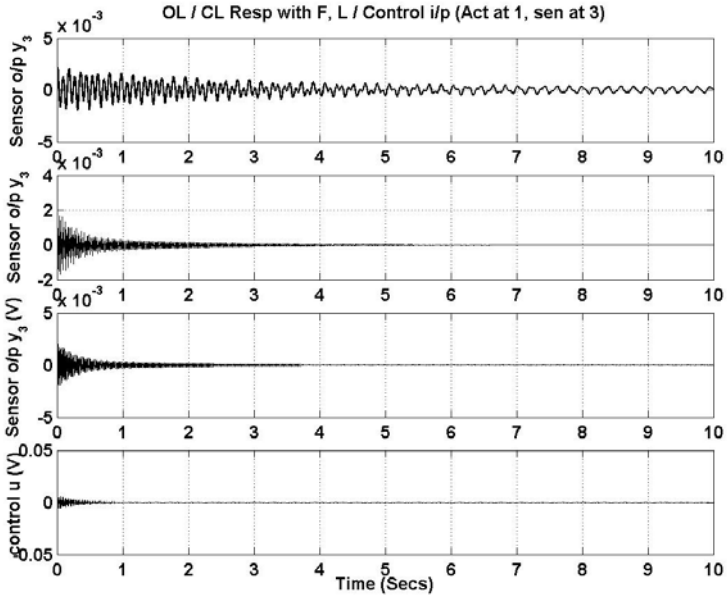

Fig. 4.35. OL / CL response with F and $\mathbf{L}$ / control u for model 2 (embedded Timoshenko beam)

the control effort required for the 4 models of the sandwiched system to damp out the vibrations are observed and shown in Figs. 4.34 - 4.37. The comparisons of the quantitative results of the OL and CL responses and with the magnitude of the control efforts, their settling times required is given in Table 4.5.

4.3.3.1 Simulation Results and Discussions

FOS Controllers are designed for the 4 SISO models of the smart embedded sandwiched structure to suppress the first 3 vibratory modes [76]. The various responses are obtained for each of the SISO models. The comparison and discussion of the simulation results of the vibration control for the smallest magnitude of the control effort u required to control the vibrations of the smart composite beam is presented here. From the simulation results, it is observed that by varying the sensor location on the beam from the free end to the fixed end introduces a considerable change in the system's structural vibration characteristics.

Through the simulation results, it is inferred that when the plant is placed with this designed controller, the plant performs well and the responses settles in a quicker time. The magnitude of the control signal required increases as the position of the sensor is changed from the nearby fixed end and moved towards the free end of the smart cantilever beam. The impulse responses show better performance when the sensor is at the nearby fixed end rather than at the free end. It is also observed that the maximum amplitude of the control voltage required to damp out the vibrations is less when the sensor is placed at FE position 2 than at the free end.

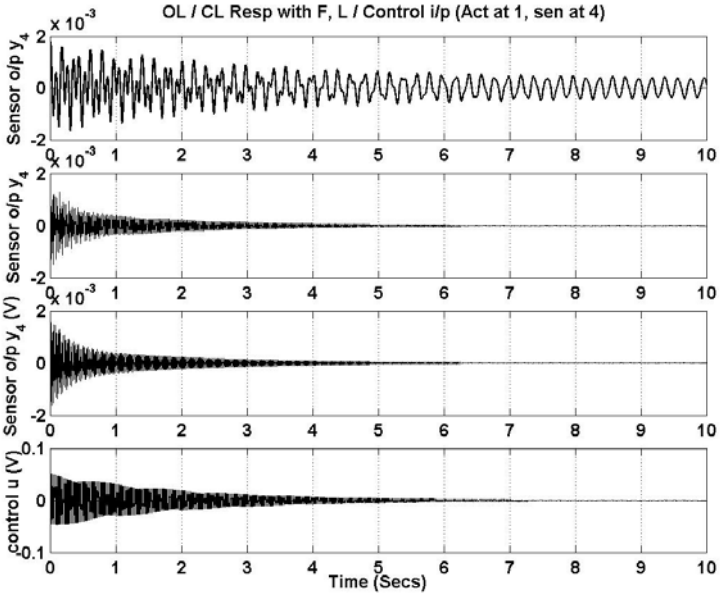

Fig. 4.36. OL / CL response with F and $\mathbf{L}$ / control u for model 3 (embedded Timoshenko beam)

Table 4.5. Quantitative comparative results of FOS simulations for the embedded Timoshenko beam as SISO systems (terms inside the brackets indicate the settling values), only the +ve values shown

Model	OL	CL with F	CL with L	Control i/p u
1	10 mV (11 secs)	25 mV 5 (secs)	25 mV (4 secs)	0.005 V
2	22 mV (15 secs)	22 mV 6 (secs)	22 mV (5 secs)	0.01 V
3	20 mV (19 secs)	19 mV 7 (secs)	19 mV (6 secs)	0.05 V
4	18 mV (22 secs)	18 mV 8 (secs)	18 mV (7 secs)	0.06 V

Thus, the observations are made with and without the controller to show the control effect. The designed FOS controller requires constant gains and hence may be easier to implement in real time. The simulation results show that a FOS feedback controller based on Timoshenko beam theory is able to satisfactorily control the first 3 modes of vibration of the smart cantilever beam and this shows the effectiveness of the designed controller. The advantages of using the embedded technology in smart

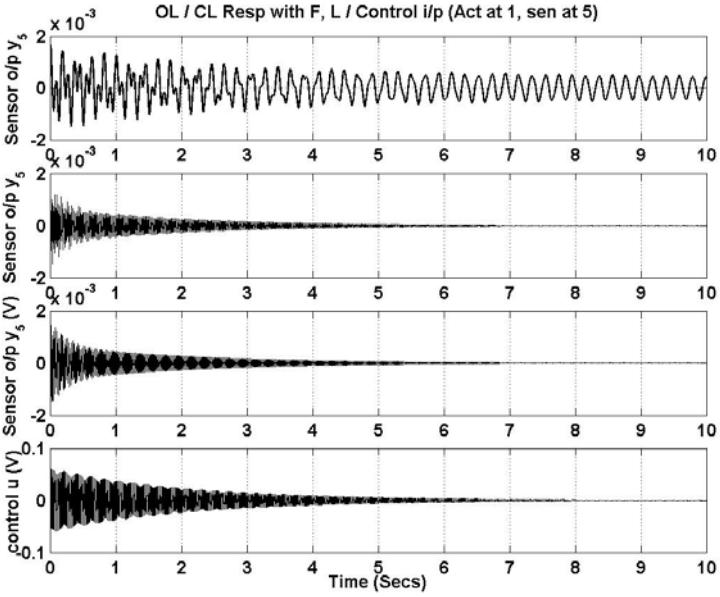

Fig. 4.37. OL / CL response with F and $\mathbf{L}$ / control u for model 4 (embedded Timoshenko beam)

structures is discussed in the last paragraph in the conclusion Section 3.3.3:1 for AVC of embedded beams using POF.

4.3.4 Design of MIMO Controller for Smart Beams Using Embedded Piezos

In the following Section, we develop the control strategy for the multivariable representation of the developed smart structure model given in the Eqs. (2.247)-(2.248) for an embedded multivariable case with its numerical values given in the Eq. (2.250) using the FOS control law discussed in the Section 4.1 (Fig. 2.13). An external force is applied at the free end of the beam, thereby subjecting it to vibrations.

The vibrations are damped out quickly by the incorporation of a FOS controller being put in the feedback loop with the plant. The designed FOS controller is used to suppress the first 3 vibration modes of the composite beam. The multivariable controller is designed on the basis of similar lines as explained in Section 4.2.2 for Euler-Bernoulli beams and in Section 4.3.2 for Timoshenko beams. The performance of the MIMO smart composite beam is hereby evaluated for vibration control by carrying out the simulations and observing the responses.

The effect of placing the sensor-actuator pair at 2 different FE locations in between the beam layers as non-collocated pairs is observed and the conclusions are finally drawn. The sampling interval τ is taken as 0.004 secs and the number of subintervals N was taken as 10. OL response of the system is obtained after subjecting

it to vibrations. The discrete models are obtained by sampling the system in (2.250) at a rate of $\frac{1}{\tau}$ and $\frac{1}{\Delta}$ respectively giving rise to $(\Phi_\tau, \Gamma_\tau, C)$-tau system and (Φ, Γ, C)-delta system respectively as shown in Eqs. (3.67) and (3.68).

It is found that the discrete model is controllable and observable. Stabilizing SFB gain is obtained for the tau system such that the eigenvalues of $(\Phi_\tau + \Gamma_\tau F)$ lie inside the unit circle and the response of the system has a good settling time. The SFB gain is given by

$$F = \begin{bmatrix} 10.4076 & -0.0000 & 63.1936 & -0.0901 & 0.0000 & -0.0235 \\ 3.7078 & -0.0000 & 1.0254 & 0.0028 & 0.0000 & 0.0007 \end{bmatrix} \tag{4.57}$$

The CL impulse response of the system is observed and shown in the Figs. 4.38 and 4.39 respectively. The FOS feedback gain matrix $\mathbf{L}$ for the smart beam is obtained by solving $\mathbf{LC} \approx F$ using the LMI optimization method which reduces the amplitude of the control signal u. The FOS gain matrix $\mathbf{L}$ for the MIMO model of the smart beam is given by

$$\mathbf{L} = \begin{bmatrix} -0.2891 & -0.6602 & -0.3868 & 0.3400 & 1.2074 \\ -3.8510 & 4.0246 & 3.4152 & -0.2986 & -3.2085 \\ 1.8044 & 1.6476 & 0.2116 & -3.0399 & -8.6228 \\ -3.2732 & -0.4981 & 3.1102 & 3.8097 & -3.4195 \end{bmatrix} \tag{4.58}$$

With the designed multivariable FOS controller being put in the loop with the smart beam, the CL impulse responses (sensor outputs y_1, y_2), the control effort

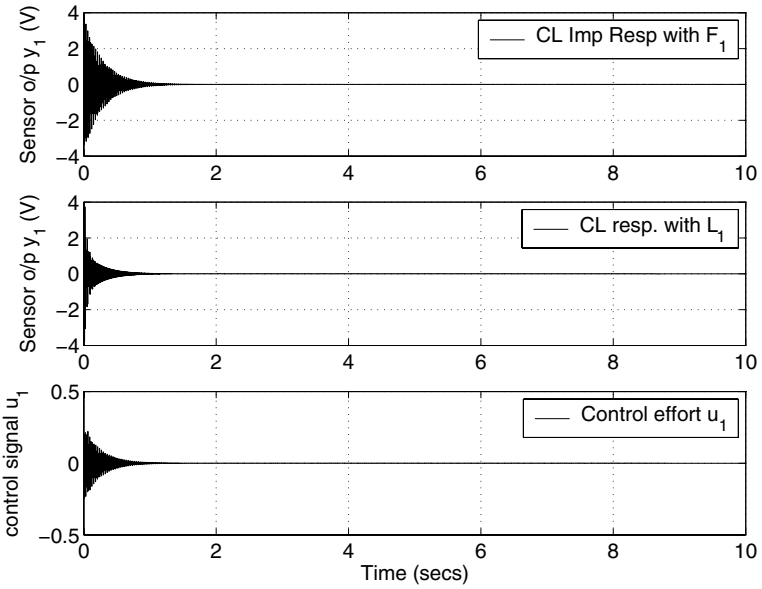

Fig. 4.38. OL / CL response with F and $\mathbf{L}$ / control u for PZT pair at FE 2 (MIMO embedded model)

u_1, u_2 required to control the vibrations are observed and shown in Figs. 4.38 - 4.39 respectively. The comparisons of the quantitative results of the OL and CL responses with the magnitude of the control efforts, their settling times required is shown in Table 4.6.

4.3.4.1 Simulation Results and Discussions

FOS controller has been designed for the smart structure as a multivariable system with embedded piezos and when put in feedback loop with the plant, the transient oscillations die out quickly in lesser times and steady state is reached quickly. It is also observed that modeling a smart structure by including the sensor / actuator mass and stiffness and by placing the sensor / actuator at 2 different positions introduces a considerable change in the structural vibration characteristics than placing the sensor / actuator pair at only one location (Figs. 4.34 - 4.37). The response takes lesser time to settle than the SISO case and the vibrations are damped out quickly. A overall better performance of the system is obtained as there will be multiple interactions of the input and the output which will cause the vibrations in the system to be damped out quickly.

Responses were observed without control and were compared with the control to show the control effect. From the simulations, it was observed that without control the transient response was unsatisfactory and with control, the vibrations are suppressed. The limitations of Euler-Bernoulli beam theory such as the neglection of the shear and axial displacements have been considered here while modeling

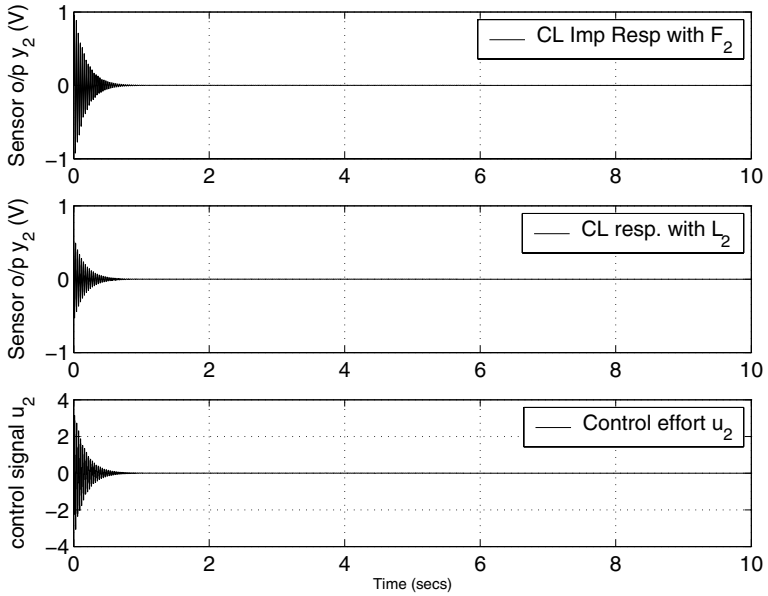

Fig. 4.39. OL / CL response with F and $\mathbf{L}$ / control u for PZT pair at FE 4 (MIMO embedded model)

Table 4.6. Quantitative comparative results of FOS simulations for the embedded beam as a MIMO system (terms inside the brackets indicate the settling values), only the +ve values shown here

FE location	**OL**	**CL with** F	**CL with L**	**Control i/p** u
y1	3.9 V	3.9 V	3.9 V	0.4 V
FE 6	30 (secs)	2 (secs)	(1.5 secs)	
y2	0.95 V	0.95 V	0.9 V	4 V
FE 8	14 (secs)	1 (secs)	(0.8 secs)	

the beam. Timoshenko beam theory corrects the simplifying assumptions made in Euler-Bernoulli beam theory and the model obtained can be closer to a exact one. The designed FOS controller requires constant gains and hence may be easier to implement in real time applications.

4.4 Conclusions

FOS feedback controllers are designed successfully to control the first few vibratory modes of a smart cantilever beam modelled using 2 type of beam theories, viz., Euler-Bernoulli beam theory and Timoshenko beam theory. New AVC schemes to control the flexural vibrations of SISO and MIMO smart models were presented. Different sensor / actuator locations bonded to the master structure (flexible cantilever beam) either as surface mounted piezos or as embededd type piezos were considered, thus giving rise to many state space models of the smart structure beam. It is observed that the control effort required to dampen out the vibrations gets reduced when the piezo pair is moved from the free end towards the root of the structure. The role of sensor / actuator position in the controller design is analyzed. The optimum sensor / actuator location is identified as the position near the fixed end.

Better performances are obtained when the piezo pair is at the root (fixed end) rather than at the free end. The open loop impulse responses of the plants (without the controller) shows an oscillatory time response and takes more time for the vibrations to decay out. The closed loop responses of the plant with the FOS gain shows that the performance obtained by the state feedback gain is realized with the FOS gain. It is also noticed from the closed loop responses that it is the FOS gain **L** which controls the first few modes of vibration. Multivariable control of a smart structure is inferred to be better compared to the SISO control as there will be multiple interactions of the input and the output which will cause the vibrations in the system to be damped out quickly than the earlier case.

A multi input multi output test provides better energy distribution and even better actuation forces. Unlike static output feedback, the FOS control always guarantees the stability of the closed loop system and all the states are not needed for control purposes. Fault tolerant control in the event of an actuator failure in a multimodel system is also presented which showed that even when an actuator fails to function in a multivariable system, the system stabilizes. A higher order smart structure model is designed by considering more number of vibratory modes. A reduced

order model is thus obtained and a robust controller is designed for the reduced order model and then applied to the higher order model gave satisfactory results.

From the developed control strategies seen in the Chapter, we conclude the following. One one hand, the location and placement of the number of piezo pairs on the beam or in a composite structure played a very important role in the design procedure and in the system dynamics. On the other, actuator and sensor locations affects the controllability and observability of a controlled structure and has a influence on the control system and the required control effort in order to satisfy a given desired criterion. Thus, the placement of actuator and sensor is one of the main problems in the design of adaptive structures today which has been dealt with in this Chapter. The effectiveness of the overall smart structure depended to a great extent on the number and distribution of the active materials included in the structure as well as on the designed controller. Further, the FOS results of the AVC of beams were found to be more impressive than the POF counterpart.

5

Discrete Time Sliding Mode Control for Smart Structures

Various types of control strategies for the SISO and MIMO state space representations of the smart structure using the Multirate Output Feedback (MROF) based Discrete Sliding Mode Control (DSMC) techniques is presented in the fifth Chapter of this monograph. The main aim of developing these control strategies is to control and damp out the flexural or transverse vibrations of flexible beam when they are subjected to an external disturbance. Two different methods of discrete time sliding mode control strategies have been used in this application. The first one uses a switching function in the control and results in quasi sliding mode motion, the other one does not use the switching in the control function and hence eliminates chattering. These two methods do not need the measurement of the system states for feedback as they makes use of only the output samples for designing the controller. The methodology adopted is more practical and may be easy to implement in real time applications.

The design of MROF based DSMC controllers for the active vibration suppression of cantilever beams modelled as SISO and MIMO models using Euler-Bernoulli beam theory and Timoshenko beam theory with surface mounted piezos and embedded piezo sensors and actuators is presented in this context. The performance of all the designed controllers are evaluated for vibration control by performing the simulations and observing the various responses.

5.1 Discrete Time Sliding Mode Control with Switching Function

In this Section, application of the discrete sliding mode control technique using the output samples [70] is made for controlling the vibrations of smart structures. This control technique uses a switching function in the control that results in quasi sliding mode motion. Recently, a FOS sliding mode control algorithm (FOSSMC) was proposed in [127], which uses the reaching law approach. The output is corrected before being used for feedback purpose. The output feedback gain $\mathbf{L}$ is obtained from the state feedback gain F using the relation $\mathbf{LC} = F$ [52]. An improvement of this technique was proposed in [128] where output correction is not required to generate the control signal. Finally, in [70], it is shown that the switching function and the

control law can be directly obtained in terms of output samples and immediate past control input. A deep insight into the control technique used in this section is as follows.

State feedback SMC :

Consider the discrete system

$$x(k+1) = \Phi_\tau x(k) + \Gamma_\tau u(k), \quad y(k) = Cx(k). \tag{5.1}$$

A reaching law for the sliding mode control of a DT system is proposed in [69] and has the following form

$$s(k+1) - s(k) = -q\ \tau s(k) - \varepsilon\ \tau\ sgn(s(k)), \tag{5.2}$$

where $\tau > 0$ is the sampling period, $\varepsilon > 0$, $q > 0$, $1 - q\tau > 0$. $s(k)$ is the switching function defined as a function of the system states as

$$s(k) = c^T x(k) = 0. \tag{5.3}$$

Using the reaching law in (5.2), the control law $u(k)$ for the system represented by the Eq. (5.1) has been obtained in [69] as

$$u(k) = F\ x(k) + \gamma\ sgn(s(k)), \tag{5.4}$$

where

$$F = -(c^T\Gamma_\tau)^{-1}\left[c^T\Phi_\tau - c^T I + q\tau c^T\right] \tag{5.5}$$

and

$$\gamma = -\left(c^T\Gamma_\tau\right)^{-1}\varepsilon\tau. \tag{5.6}$$

The width of the quasi-sliding mode band δ within which the system trajectory remains in steady state is given by [129] as

$$2\delta \leq \frac{2\varepsilon\tau}{2 - q\tau}. \tag{5.7}$$

Sliding mode control and switching surface from output samples (DQSMC):

In order to determine the expression for the discrete sliding mode control using output samples, consider the system in Eq. (4.7) with $k = 0$ as

$$x(\tau) = \Phi_\tau x(0) + \Gamma_\tau u(0), \tag{5.8}$$

$$y_\tau = C_0 x(0) + D_0 u(0). \tag{5.9}$$

As the output samples are not known before $t = 0$, the control $u(0)$ can be obtained from Eq. (5.4) with $k = 0$. Now, at τ sampling instant, the expression for 's' and the control 'u' in terms of the past output samples are derived using Eqs. (5.8) and (5.9) as

$$s(\tau) = c^T\Phi_\tau C_0^{-1} y_\tau + c^T\left(\Gamma_\tau - \Phi_\tau C_0^{-1} D_0\right) u(0). \tag{5.10}$$

and

$$u(\tau) = F\Phi_\tau C_0^{-1} y_\tau + F\left(\Gamma_\tau - \Phi_\tau C_0^{-1} D_0\right) u(0) + \gamma\ sgn\left(s(\tau)\right). \tag{5.11}$$

Similarly, for 2τ instants, s and u can be obtained as

$$s(2\tau) = c^T \Phi_\tau C_0^{-1} y_{2\tau} + c^{2T}\left(\Gamma_\tau - \Phi_\tau C_0^{-1} D_0\right) u(\tau), \tag{5.12}$$

$$u(2\tau) = F\Phi_\tau C_0^{-1} y_{2\tau} + F\left(\Gamma_\tau - \Phi_\tau C_0^{-1} D_0\right) u(\tau) + \gamma\ sgn\left(s(2\tau)\right). \tag{5.13}$$

It is assumed here that $N = n$. Since the system is observable, C_0^{-1} exists. Hence, extending the above algorithm, a generalized expression for the switching surface and the sliding mode control can be derived and is given [70] as

$$s(k) = c^T \Phi_\tau C_0^{-1} y_k + c^T\left[\Gamma_\tau - \Phi_\tau C_0^{-1} D_0\right] u(k-1) \tag{5.14}$$

and

$$u(k) = F\Phi_\tau C_0^{-1} y_k + F\left[\Gamma_\tau - \Phi_\tau C_0^{-1} D_0\right] u(k-1) + \gamma\ sgn(s(k)). \tag{5.15}$$

Thus, it can be seen from Eqs. (5.14) and (5.15) that the states of the system are needed neither for switching function evaluation nor for the feedback purposes. The main advantage of this algorithm is that a single expression is used to compute the switching function. It does not depend on whether a trajectory is in reaching phase or in switching phase. However, this control law brings only quasi-sliding mode motion. This means when the trajectory crosses the switching plane for the first time, it will cross and recross the plane again in every successive sampling interval resulting in zig-zag motion about the switching plane and the size of each step is not increasing. The trajectory stays in the band. The width of the quasi-sliding mode band 2δ within which the system remains in steady state is the same as given in Eq. (5.7). The application of this control law to the various smart structure models developed in Chapter 2 is presented in the following Sections.

5.1.1 Controller Design for Euler–Bernoulli Smart Beams as SISO Systems

The control technique discussed in Section 5.1 is used to design a controller to suppress the first 2 vibration modes of a cantilever beam through smart structure concept for the various SISO state space models of the smart beam given in Section 2.1.1:6 I(ii) for the piezo patches placed at different FE locations along the length of the beam [97]. The cantilever beam is divided into 4 FE. PZT's are bonded to the beam at one FE position only as a collocated pair, say, at fixed end (FE location 1) or at FE position 2 or at FE position 3 or at FE position 4 (free end), thus giving rise to 4 SISO models of the same smart structure as shown in Fig. 2.4. The performance of these 4 SISO models is evaluated for AVC by carrying out the simulations and observing the various responses. Finally, discussions on the simulation results for optimal performance of the sensor / actuator location on the beam is presented.

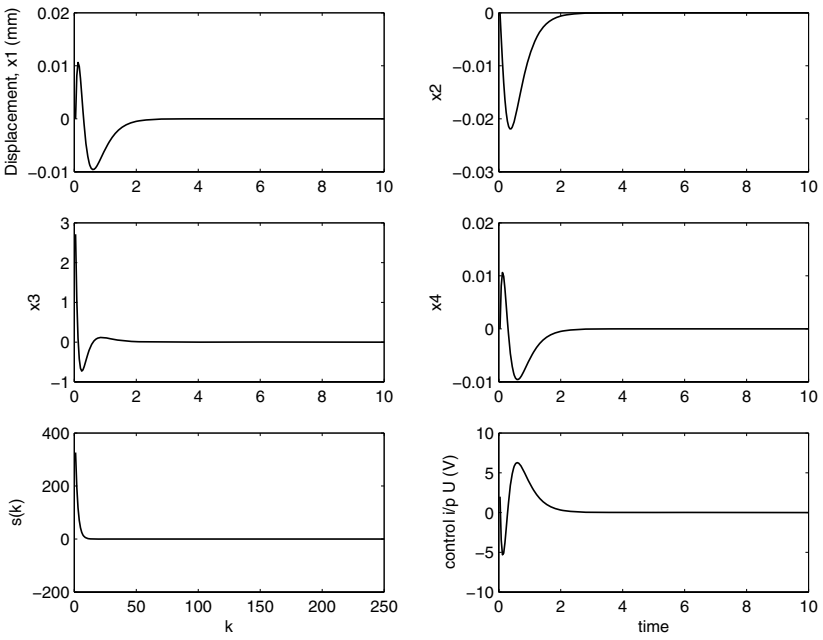

Fig. 5.1. Plot of states, switching f/n, control for model 1 (EB beam modelled as SISO system with surface mounted PZT)

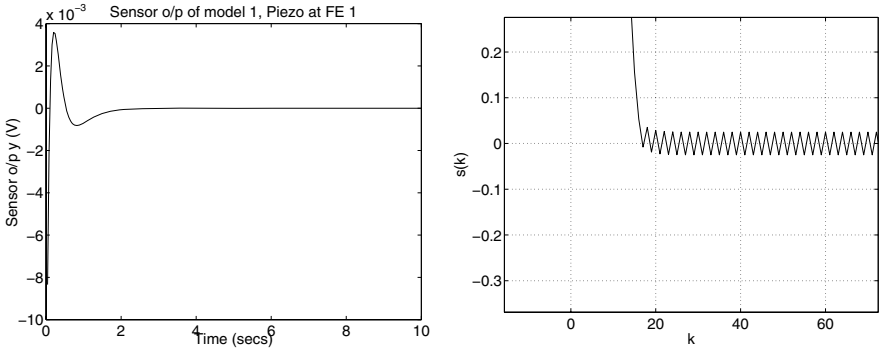

(a) Sensor o/p (b) Chattering phenomenon

Fig. 5.2. Plot of sensor o/p and chattering for model 1 (EB beam modelled as SISO system with surface mounted PZT)

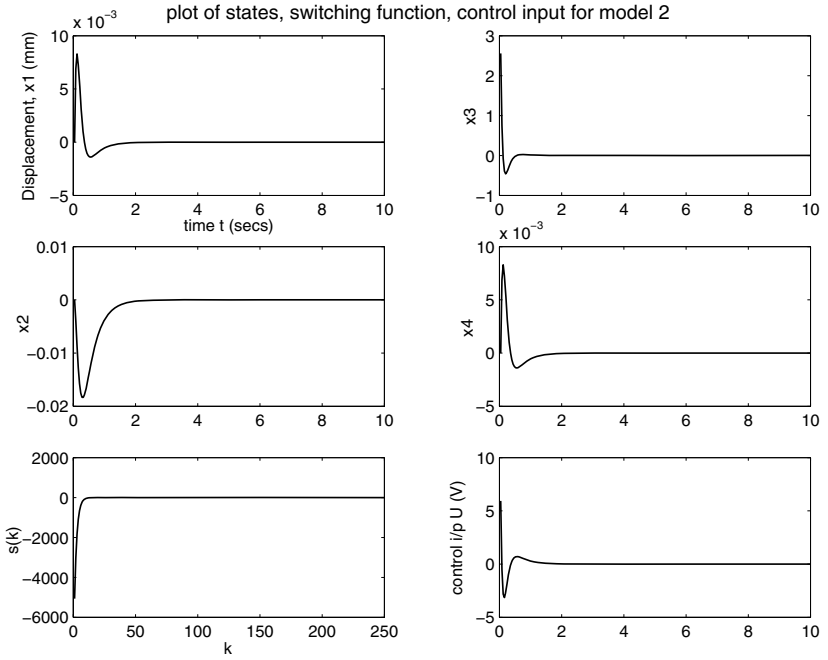

Fig. 5.3. Plot of states, switching f/n, control for model 2 (EB beam modelled as SISO system with surface mounted PZT)

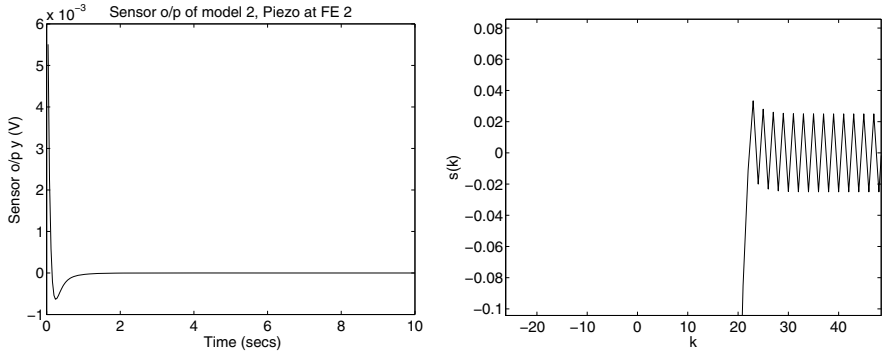

(a) Sensor o/p (b) Chattering phenomenon

Fig. 5.4. Plot of sensor o/p and chattering for model 2 (EB beam modelled as SISO system with surface mounted PZT)

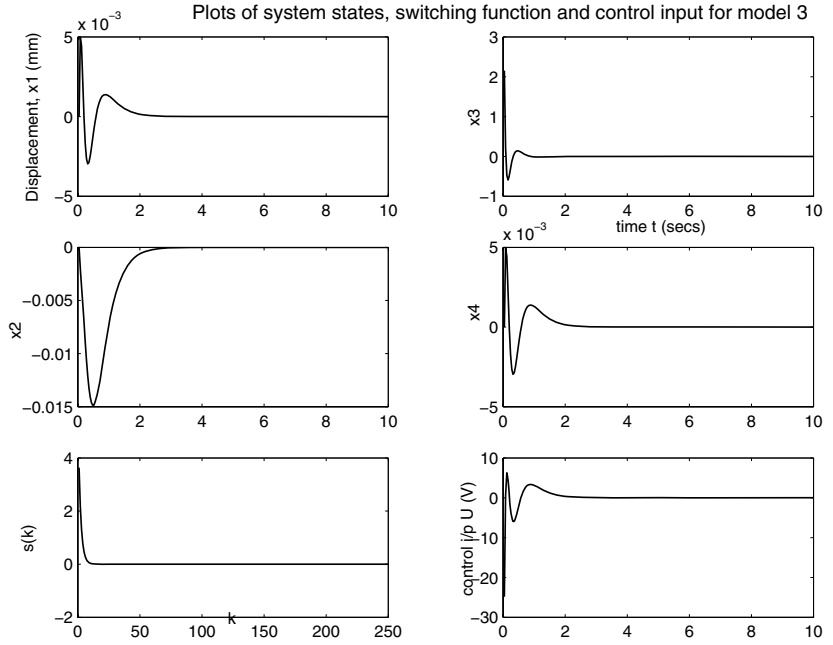

Fig. 5.5. Plot of states, switching f/n, control for model 3 (EB beam modelled as SISO system with surface mounted PZT)

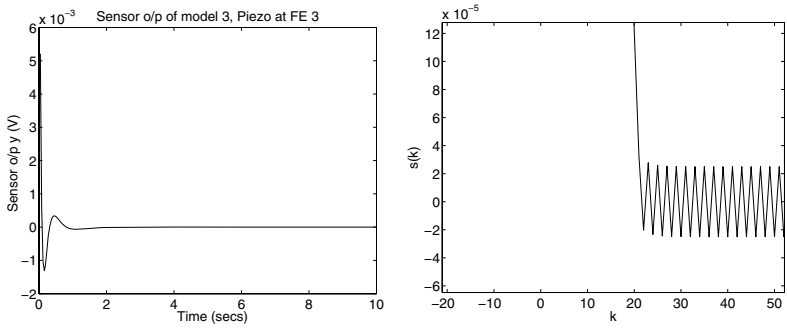

(a) Sensor o/p (b) Chattering phenomenon

Fig. 5.6. Plot of sensor o/p and chattering for model 3 (EB beam modelled as SISO system with surface mounted PZT)

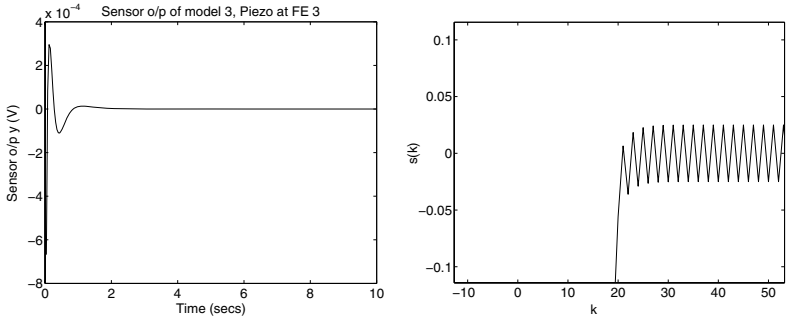

(a) Sensor o/p (b) Chattering phenomenon

Fig. 5.7. Plot of sensor o/p and chattering for model 4 (EB beam modelled as SISO system with surface mounted PZT)

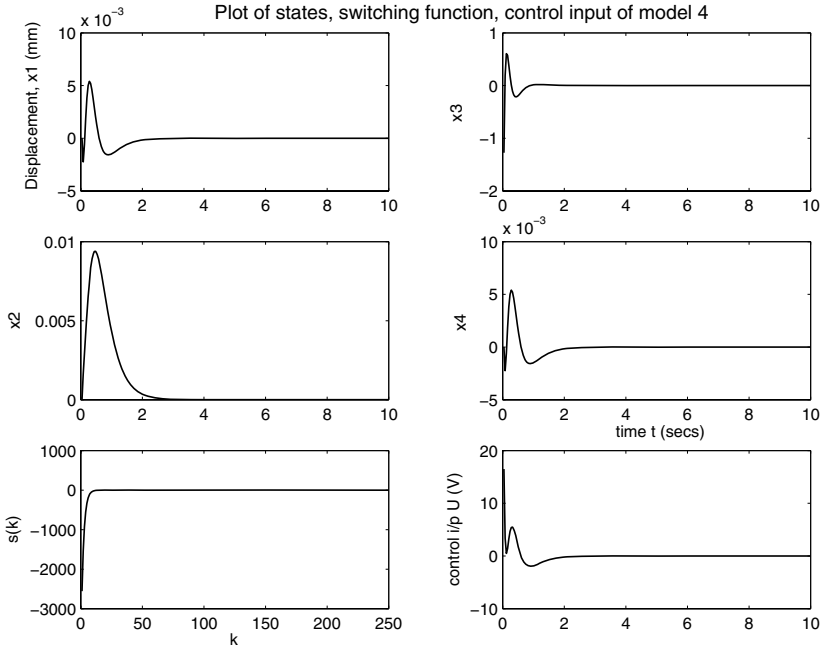

Fig. 5.8. Plot of states, switching f/n, control for model 4 (EB beam modelled as SISO system with surface mounted PZT)

The 4 SISO state space models of the smart beam are given by the Eqs. (2.76) - (2.79). The smart beam is excited by an impulse signal applied at the free end of the beam for the individual SISO models shown in the Fig. 2.4. The beam is thus subjected to vibrations and the OL impulse response (plot of sensor outputs y as a function of t) of the various SISO models are observed. The designed controller is put in loop with the plant and the various responses are observed for all the 4 SISO models of the same smart structure plant. Simulation is performed with a set of controller parameter values of q, τ, N, δ, ε. The plot of the various states of the system, the switching functions, control inputs, sensor outputs and the chattering band during the sliding mode are shown in Figs. 5.1 - 5.8 respectively.

Here, the comparison and discussion of the simulation results of the vibration control for the smallest magnitude of the control effort u required to control the vibrations of the smart cantilever beam is presented [97]. Model 1 is inferred to be the best model for AVC because of the inferences mentioned in (a) - (h) below.

(a) Modeling a smart structure by including the sensor / actuator mass and stiffness and by varying its location on the beam from the free end to the fixed end introduces a considerable change in the system's structural vibration characteristics,
(b) The uncontrolled system takes much longer time to damp out the oscillations as compared to the system with the designed sliding mode control input, i.e., without control the transient response was predominant and with control, the vibrations are suppressed,
(c) When the piezo element is placed near the root, the sensor output voltage is greater because of the heavy distribution of the bending moment near the fixed end, thus leading to a larger strain rate,
(d) Sensor voltage is less when the piezo pair is located at the free end because of lesser strain rate and hence require more control effort,
(e) Sensitivity of the sensor / actuator pair depends on its location on the beam from the root hub, collocation of the piezo pair and the gain of the amplifier used,
(f) System responds well in CL and does not exhibit undesirable chattering phenomenon. Neither does the system vibrate much,
(g) MROF based DSMC uses the signum function in the control input and the control is computed from the immediate past control value and the past output samples,
(h) Comparing the 4 SISO models, it is observed that if the smart beam is divided into 4 FE with piezo pair placed at the fixed end (SISO model 1), the vibration characteristics are the best to demonstrate the AVC of smart beams because of the above mentioned inferences.

Hence, it may be concluded that an effective vibration control technique is demonstrated here [97].

5.1.2 Controller Design for Euler–Bernoulli Smart Beam as MIMO System

The control technique discussed in Section 5.1 is used to design a controller to suppress the first 2 vibration modes of a smart cantilever beam modelled as MIMO

system given in Section 2.1.2 through smart structure concept. The MIMO system is given by the Eqs. (2.93) and (2.101) with its numerical value in Eq. (2.105). The performance of the beam is evaluated for AVC by carrying out the simulations and observing the various responses.

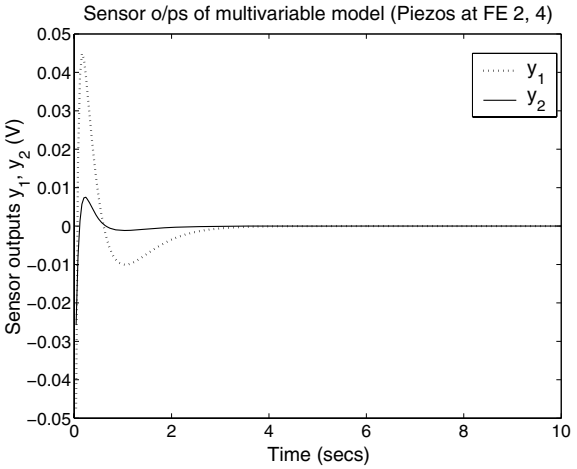

Fig. 5.9. Plot of sensor outputs for the EB-MIMO model

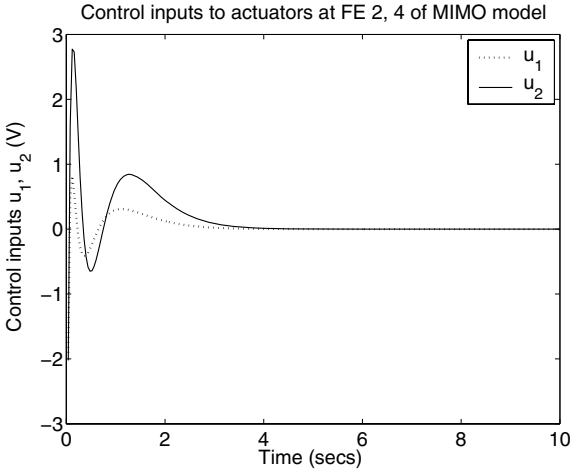

Fig. 5.10. Plot of control inputs to the actuators for the EB-MIMO model

The smart beam is excited by an impulse signal applied at the free end of the beam. DSMC using output samples for the multivariable system is designed on the similar lines as explained in Section 5.1.1 for the SISO systems. The designed output feedback controller is put in loop with the plant and the system responses (sensor

outputs y_1 and y_2) and the generated control inputs (u_1 and u_2) from the controller are observed for the multivariable plant and shown in Figs. 5.9 and 5.10 respectively. The evolution of the sliding function (S_1 and S_2) is also observed.

Simulation study has been carried out for a set of parameters of the controller by assuming the values of q, τ, N, δ, ε. Assuming a set of initial conditions, for the states, the switching surface is obtained using Eq. (5.14) and the sliding mode control using the output samples is computed using Eq. (5.15). The plot of Fig. 5.10 shows the control input which settles to zero because there is no reference. The plot of the response of the states also converges to zero from the given initial condition. Also, the switching function decreases towards zero from the initial value and stays within a small band in the neighborhood of the switching line which is nothing but the width of the quasi sliding mode band δ.

MIMO control is better than the SISO control because of the following inferences made from the simulation results.

- Multiple interactions of the input and output.
- Sensor output at FE 2 is more as the strain rate is high than the sensor output at FE 4 where the sensor output is low because of lesser strain rate.
- Control effort required at FE 2 is less than the control effort required at FE 4.
- Overall control effort required by the MIMO controller is less than the SISO controller [97].
- Placing the piezos at 2 different finite element positions on the beam introduces a considerable change in the system structural characteristics than placing it at only 1 location.
- DSMC can be directly obtained in terms of the output samples and immediate past control function.
- The algo does not need the system states neither for feedback purposes nor for switching function evaluation.

5.1.3 Controller Design for Timoshenko Smart Beams with Surface Mounted PZT's as SISO Systems

The control technique discussed in Section 5.1 is used to design a DSM controller using output samples to suppress the first 2 vibration modes of a cantilever beam through smart structure concept for the various SISO state space models of the smart beam given in Section 2.2.1:3(i) for the piezo patches placed at different FE locations along the length of the beam as shown in the Fig. 2.7. The performance of these 4 SISO models is evaluated for AVC by carrying out the simulations and observing the various responses. Conclusions are drawn finally on the simulation results for best location of the placement of sensor-actuator pair on the beam. Here, the comparison and discussion of the simulation results of the vibration control for the smallest magnitude of the control effort u required to control the vibrations of the smart cantilever beam is presented. For convenience, only the responses at the fixed end are shown in Figs. 5.11 and 5.12. Similarly, the responses are observed for other models also. Model 1 is found to be the best model that can be used for AVC because of the inferences / observations presented in (a) - (i) in Section 5.1.1.

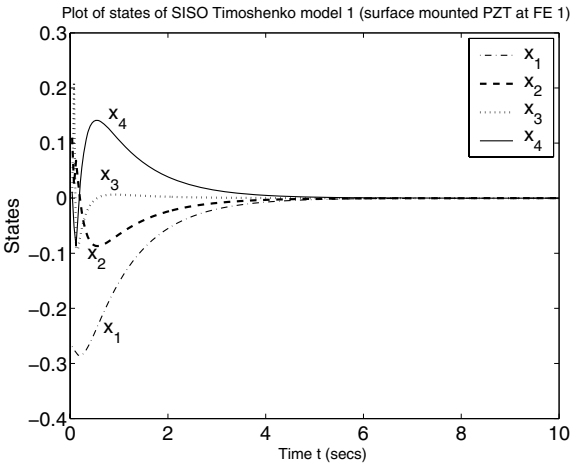

Fig. 5.11. Plot of the four states for the Timoshenko SISO model 1 with surface mounted PZT

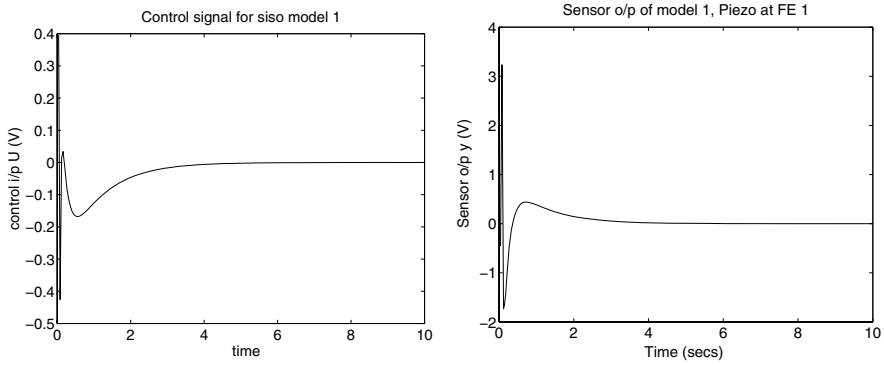

(a) Control effort (b) Sensor output

Fig. 5.12. Plot of control, sensor o/p for Timoshenko beam modelled as SISO system (model 1)

5.1.4 Controller Design for Timoshenko Smart Beams with Surface Mounted PZT's as MIMO System

The control technique discussed in Section 5.1 is used to design a DSM controller using output samples in order to suppress the first 2 vibration modes of a smart cantilever beam modelled as a MIMO system in Section 2.2.2 (Fig. 2.5) through smart structure concept. The MIMO state space model of the smart beam is given in Eq. (2.179). The performance of this MIMO model is evaluated for the AVC by carrying out the simulations and observing the various responses and finally concluding with the discussions on the simulation results.

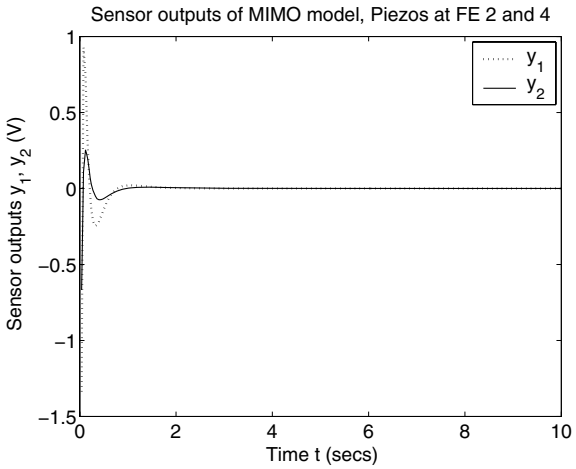

Fig. 5.13. Plot of sensor outputs for Timoshenko beam modelled as MIMO system with surface mounted PZT

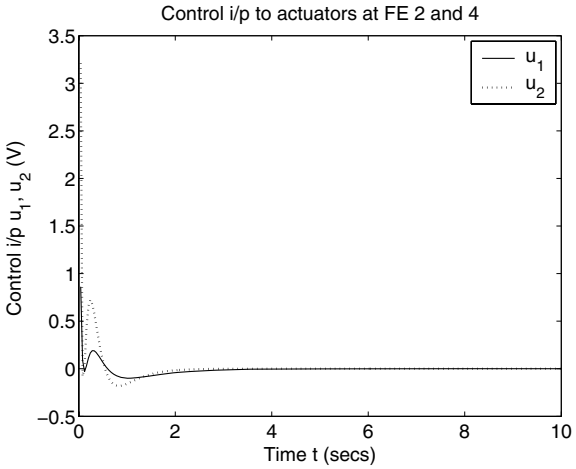

Fig. 5.14. Plot of control inputs for Timoshenko beam modelled as MIMO system with surface mounted PZT

The controller is designed on the similar lines as explained in the previously discussed control designs for MIMO based system. With the designed controller put in loop with the plant, the responses such as the sensor output, control input and the switching function are observed and shown in Figs. 5.13 - 5.15 respectively. From the simulation results, it is observed that the multivariable control is better than the SISO control because of the observations mentioned in Section 5.1.2 at the end which can also be seen in many of the topics on AVC of MIMO based smart structures in Chapters 3 and 4.

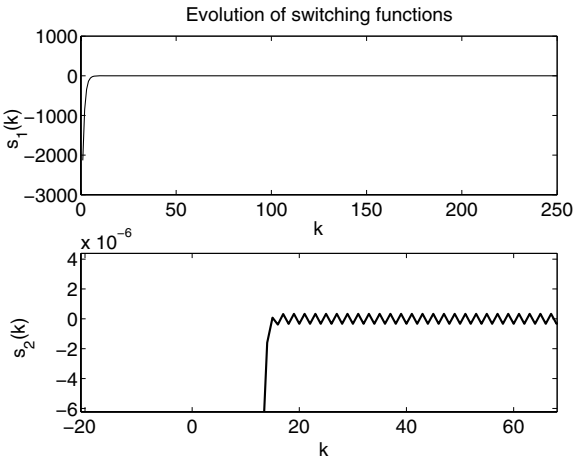

Fig. 5.15. Plot of switching functions for Timoshenko beam modelled as MIMO system with surface mounted PZT

5.1.5 Controller Design for Timoshenko Smart Beams with Embedded PZT's for a SISO Case

The control technique discussed in Section 5.1 is used to design a controller to suppress the first 2 vibration modes of a cantilever beam through smart structure concept for the various SISO state space models of the smart beam given in Section 2.2.3:3. Four SISO models are obtained by embedding the shear actuator in between two top and bottom aluminum beam layers at FE position 1 and moving the shear sensor position from FE 2 to FE 5 as shown in Fig. 2.12. The 4 SISO state space models of the smart embedded beam is given by Eqs. (2.242) and (2.243) with its numerical value in Eq. (2.245) for the model 1. Three vibratory modes are considered. The performance of these 4 SISO models is evaluated for AVC by carrying out the simulations, observing the various responses and finally concluding with the discussions on the simulation results for the best location of the placement of the sensor / actuator pair on the beam.

The controller is designed on the similar lines as explained in the previously discussed control designs for SISO based systems for all the 4 SISO models. Here, the comparison and discussion of the simulation results of the vibration control for the smallest magnitude of the control effort u required to control the vibrations of the smart cantilever beam and the best model for AVC is presented. The same inferences / observations presented in (a) - (h) in Section 5.1.1 are also valid here for the AVC of SISO based smart Timoshenko beams with embedded PZT's. Here, for the sake of convenience, only the responses of the model 1 such as the sensor output, control input and the switching function are shown in Figs. 5.16 and 5.17 as the best model for AVC in the 4 SISO models is the model 1. Similarly, the responses are observed for the other 3 models also.

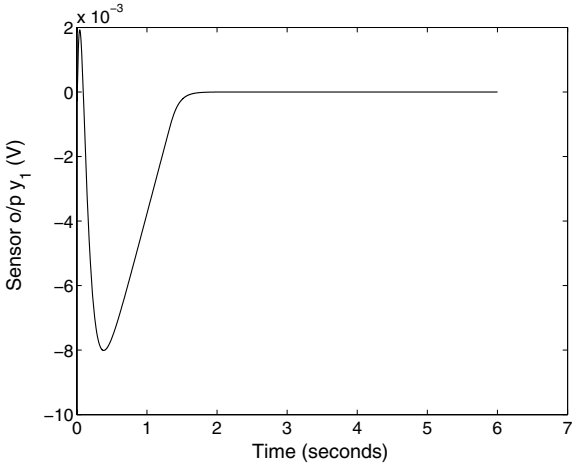

Fig. 5.16. Plot of sensor o/p for Timoshenko beam modelled as SISO system with embedded piezos (model 1)

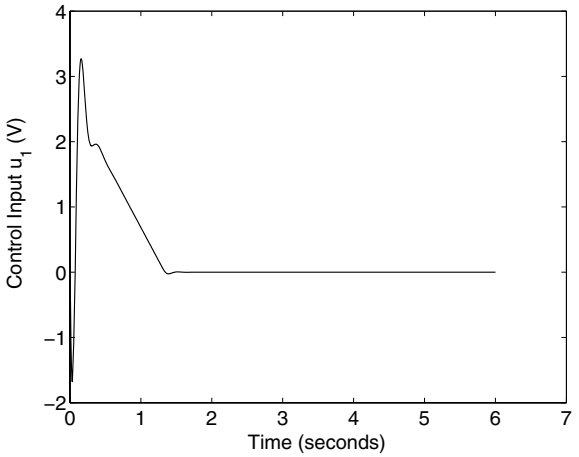

Fig. 5.17. Plot of control i/p for Timoshenko beam modelled as SISO system with embedded piezos (model 1)

5.1.6 Controller Design for Timoshenko Smart Beam with Embedded PZT's for a MIMO Case

The control technique discussed in Section 5.1 is used to design a controller to suppress the first 2 vibratory modes of a cantilever beam embedded with shear sensors and actuators and modelled as a multivariable system as given in Section 2.2.3:4. The MIMO model of the smart beam is obtained by embedding the shear actuators in between top and bottom aluminum layers at FE positions 2, 4 and sensors at FE positions 6, 8, thereby giving rise to a multivariable system with 2

inputs and 2 outputs (Fig. 2.13). The MIMO state space model of the smart beam is given by Eqs. (2.247) and (2.248) with its numerical value in Eq. (2.250). Three vibratory modes are considered. The performance of this MIMO model is evaluated for AVC by carrying out the simulations and observing the various responses and finally concluding with the discussions on the simulation results. The controller is designed on the similar lines as explained in the previously discussed control designs for MIMO based systems. The responses such as the sensor output, control input and the switching function are observed. From the simulation results, it was observed that the multivariable control is better than the SISO control because of the observations mentioned in Section 5.1.2 at the end.

5.2 Discrete Time Sliding Mode Control Without Switching Function

Bartoszewicz [71] proposed a quasi-sliding mode control strategy that does not use switching function in control and has the property of finite time convergence to the quasi-sliding mode band. In addition, it also eliminates chattering due to not using signum function in the control input. In this Section, a discrete output feedback sliding mode control algorithm in [56] based on Bartoszewicz's control law [71] and multirate output feedback [57] is used for the control of vibrations of smart smart structures.

Here, the disturbance is the external force signal $r(t)$, i.e., an impulse disturbance which is applied to the beam at its free end as shown in Figs. 2.4, 2.5, 2.7, 2.12 and 2.13. The beam is thus subjected to vibrations under the application of the disturbance, which is bounded in nature. DSM controllers based on MROF techniques are designed and put in the loop with the plant to damp out the vibrations as quickly as possible and thus saving the structure from getting damaged from wear and tear further. The method used is briefly discussed in the following paragraphs.

Consider a CT SISO system that is sampled with a sampling interval of τ secs and given by

$$x(k+1) = \Phi_\tau x(k) + \Delta\Phi_\tau x(k) + \Gamma_\tau u(k) + f(k), \quad y(k) = C\ x(k), \tag{5.16}$$

where $\Delta\Phi_\tau$ is the uncertainty in the state, $f(k)$ is an external disturbance vector of $(n \times 1)$ and Φ_τ, Γ_τ and C are matrices of appropriate dimensions with (Φ_τ, Γ_τ) being controllable and (Φ_τ, C) being observable. Let us define the disturbance vector as

$$\tilde{d}(k) = \Delta\Phi_\tau x(k) + f(k). \tag{5.17}$$

Let the desired sliding manifold be governed by the parameter vector c^T such that $c^T\Gamma_\tau \neq 0$ and the resulting quasi-sliding motion is stable and let the disturbance be bounded such that

$$d(k) = c^T\tilde{d}(k) \tag{5.18}$$

satisfies the inequality

$$d_l \leq d(k) \leq d_u, \tag{5.19}$$

where d_l and d_u are the known lower and upper bounds on the disturbance respectively. Now, we define the following terms.

$$d_0 = 0.5(d_l + d_u), \quad \delta_d = 0.5(d_u - d_l). \tag{5.20}$$

The switching surface is given by

$$s(k) = c^T \; x(k). \tag{5.21}$$

The quasi-sliding mode is defined as the motion such that $|s(k)| \leq \varepsilon$, where the positive constant ε is called the quasi-sliding-mode bandwidth. A significant reduction of the control effort and improved quality of the QSMC is observed. A reaching law proposed by Bartoszewicz [71] is of the form

$$s(k+1) = d(k) - d_0 + s_d(k+1), \tag{5.22}$$

where, $d(k)$ is defined by Eq. (5.19) and $s_d(k)$ is a apriori known function that satisfies the following two conditions given when

$$|s(0)| > 2\delta_d \text{ and } |s(0)| \leq 2\delta_d \tag{5.23}$$

as

Condition 1 : If $|s(0)| > 2\delta_d$, then
$s_d(0) = s(0)$,
$s_d(k)\; s_d(0) \geq 0$, for any $k \geq 0$,
$s_d.(k) = 0$, for any $k \geq k^*$,
$|s_d(k+1)| < |s_d(k)| - 2\; \delta_d$, for any $k < k^*$.

Condition 2 : If $|s(0)| \leq 2\delta_d$, then
$s_d(k) = 0)$, for any $k \geq 0$.

The value of the positive integer k^* is chosen by the designer so as to have a trade off between faster convergence and the magnitude of the control input u. By controlling the rate of decay (tuning k^*), the convergence of $s(k) = 0$ is tuned. The reaching law in Eq. (5.22) together with the two conditions of the function $s_d(k)$ imply that the reaching law condition is satisfied and that, for any $k \geq k^*$, the QSM in the δ_d vicinity of the sliding plane $s(k) = c^T x(k) = 0$ exists. One possible function for $s_d(k)$, when $|s(0)| > 2\delta_d$, can be described as

$$s_d(k) = \frac{k^* - k}{k^*} \; s(0), \quad k = 0, 1, 2, ..., k^*, \tag{5.24}$$

where

$$k^* < \frac{|s(0)|}{2\delta_d}. \tag{5.25}$$

The control law that satisfies the reaching law defined in Eq. (5.22) and achieves sliding mode for the system with disturbance described in Eq. (5.19) can be computed to be

$$u(k) = \left(c^T \Gamma_\tau\right)^{-1} (c^T \Phi_\tau x(k) + d_0 - s_d(k+1)). \tag{5.26}$$

When the control input described in Eq. (5.26) is fed into the system, it would guarantee that for any $k > k^*$, the switching function would satisfy the inequality

$$|s(k)| = |d(k-1) - d_0| \leq \delta_d. \tag{5.27}$$

Hence, the states of the system settle within a quasi-sliding mode band whose width is less than half the width of the band described in [69]. From [56], a multirate

output feedback based algorithm using a modified reaching law can be obtained. Let the modified reaching law be [56] given as

$$s(k+1) = d(k) - d_0 + e(k-1) - e_0 + s_d(k+1), \tag{5.28}$$

where a new variable $e(k)$ is introduced. The control input generated using the algorithm in [56] can be represented as

$$u(k) = -(c^T\ \Gamma_\tau)^{-1}(c^T\Phi_\tau L_y y_k + c^T\Phi_\tau L_u u(k-1) + d_0 + e_0 - s_d(k+1)), \tag{5.29}$$

where,

$$L_y = \Phi_\tau C_0^{-1},\quad L_u = \Gamma_\tau - C_0^{-1}D_0,\quad L_d = I - C_0^{-1}C_d, \tag{5.30}$$

$$C_0 = \begin{bmatrix} C \\ C\Phi \\ C\Phi^2 \\ \vdots \\ C\Phi^{N-1} \end{bmatrix},\quad D_0 = \begin{bmatrix} 0 \\ C\Gamma \\ C(\Phi\Gamma+\Gamma) \\ \vdots \\ C\sum_{i=0}^{N-2}\Phi^i\Gamma \end{bmatrix},\quad C_d = \begin{bmatrix} 0 \\ C\left(\sum_{i=0}^{N-1}\Phi^i\right)^{-1} \\ C\left(\sum_{i=0}^{1}\Phi^i\right)\left(\sum_{i=0}^{N-1}\Phi^i\right)^{-1} \\ \vdots \\ C\left(\sum_{i=0}^{N-2}\Phi^i\right)\left(\sum_{i=0}^{N-1}\Phi^i\right)^{-1} \end{bmatrix}, \tag{5.31}$$

and $e_0 = 0.5(e_l + e_u)$ and $\delta_e = 0.5(e_u - e_l)$ are the mean (average value) and the variation (maximum deviation) of the function of the uncertainty. e_l and e_u are the lower and upper bounds of $e(k)$. The new variable $e(k)$, which is the effect of disturbance on the sampled output is defined as

$$e(k) = c^T\Phi_\tau L_d\tilde{d}_k, \tag{5.32}$$

where the bounds on $e(k)$ is given by $e_l \le e(k) \le e_u$, since the disturbance $\tilde{d}(k)$ is bounded. The value of N is chosen to be > the observability index υ of the system defined as "the observability index of a system represented by the triplet (A, B, C) is the minimum integer value of υ such that"

$$Rank\begin{pmatrix} C \\ CA \\ \vdots \\ CA^{\upsilon-1} \end{pmatrix} = Rank\begin{pmatrix} C \\ CA \\ \vdots \\ CA^{\upsilon} \end{pmatrix}. \tag{5.33}$$

Hence, the control input can be computed using the past output samples and the immediate past input signal. But, at $k = 0$, there are no past outputs for use in control, hence $u(0)$ is obtained by ignoring $e(k-1)$ and e_0 (as we expect no disturbance before the instant $k = 0$ to affect the system) and assuming an initial state $x(0)$ to obtain

$$u(0) = -(c^T\Gamma_\tau)^{-1}\left(c^T\Phi_\tau x_0 + d_0 - s_d(1)\right). \tag{5.34}$$

When the control input deduced from Eq. (5.29) is applied to the system, it obeys the reaching law

$$s(k+1) = d(k) - d_0 + e(k-1) - e_0 + s_d(k+1), \tag{5.35}$$

$$s(k) = d(k-1) - d_0 + e(k-2) - e_0 + s_d(k). \tag{5.36}$$

When $k > (k^*, 2)$, $s_d(k) = 0$ and therefore

$$s(k) = d(k-1) - d_0 + e(k-2) - e_0. \tag{5.37}$$

Thus, we have

$$|s(k)| = |d(k-1) - d_0 + e(k-2) - e_0|, \tag{5.38}$$

i.e.,

$$|s(k)| \leq |d(k-1) - d_0| + |e(k-2) - e_0|, \tag{5.39}$$

which can be written as

$$|s(k)| \leq \delta_d + \delta_e. \tag{5.40}$$

It can be seen that this algorithm does not need the measurement of the states of the system for the generation of the control input. But, as a trade off, the width of the quasi-sliding mode band is increased by δ_e. The control technique discussed in the previous paragraphs is used to design a MROF based DSMC control scheme to suppress the vibrations in a smart structure, which is modelled using Euler-Bernoulli beam theory and Timoshenko beam theory for 2 and 3 vibratory modes.

5.2.1 Controller Design for Euler-Bernoulli Smart Beams as SISO Systems

The control technique discussed in the previous Section 5.2 is used to design a controller to suppress the first 2 vibration modes of a flexible cantilever beam through smart structure concept for different SISO state space models of the smart beam given in section 2.1.1:6 I(ii). The cantilever beam is divided into 4 FE. PZT's are bonded to the beam as surface mounted piezos at one FE position only as a collocated pair, say, at fixed end (FE location 1) or at FE position 2 or at FE position 3 or at FE position 4 (free end), thus giving rise to 4 SISO models of the same smart structure plant as shown in Fig. 2.4. The performance of these 4 SISO models is evaluated for AVC by carrying out the simulations and observing the various responses [94].

The 4 SISO state space models are given by Eqs. (2.76) - (2.79). The beam is excited by an impulse signal applied at the free end of it as shown in Fig. 2.4. The beam is thus subjected to vibrations and the open loop impulse response (plot of sensor outputs y as a function of t) of the various SISO models are observed without the controller. The designed DSMC controller is put in loop with the plant and the closed loop system responses, the control input and the sliding function are observed for all the 4 SISO models of the same smart structure plant. Here, for the sake of convenience, only the responses for the SISO model with piezo patches placed at the fixed end of the beam are shown in the Figs. 5.18 and 5.19.

Here, the comparison and discussion of the simulation results of the vibration control for the smallest magnitude of the control effort u required to control the vibrations of the smart cantilever beam is presented. The best model for AVC is also arrived at, which is nothing but the SISO model 1 because of the inferences mentioned in (a)-(h) in Section 5.1.1. Hence, it may be concluded that an effective vibration control technique is demonstrated here [94].

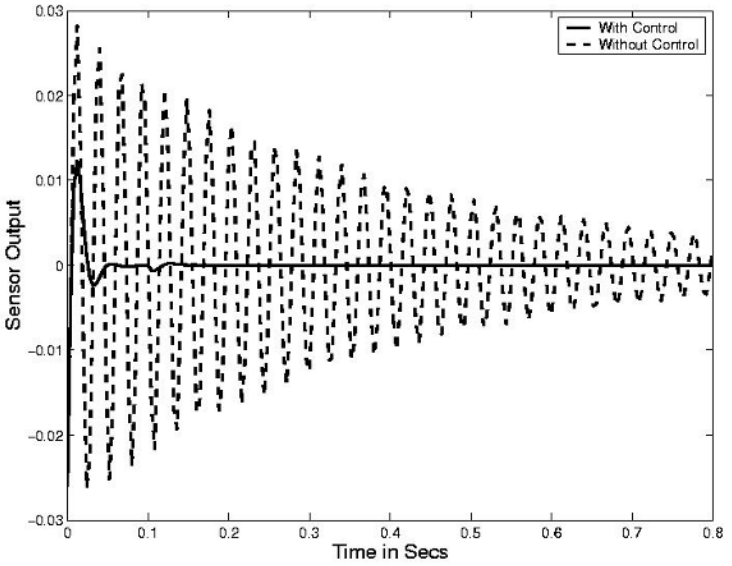

Fig. 5.18. Plot of sensor output y_1 without control (OL response) and with control input (CL response) due to impulse excitation : Model 1 (PZT placed at fixed end)

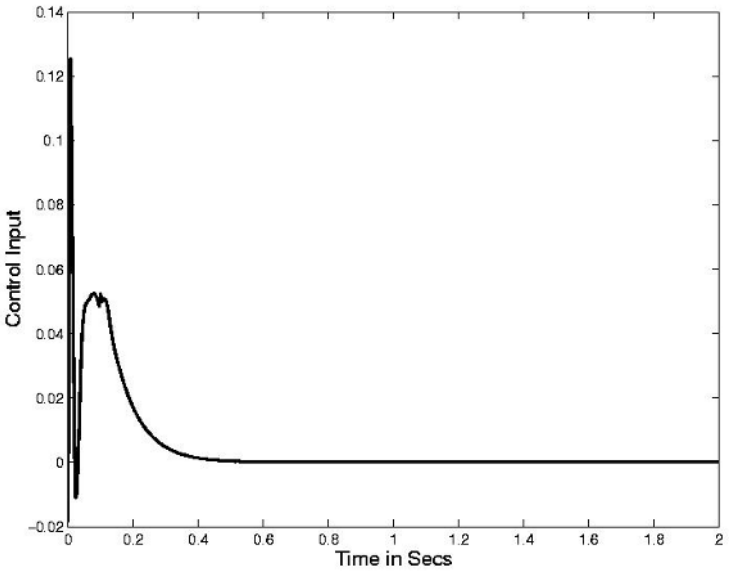

Fig. 5.19. Plot of control input u_1 v/s t (for impulse i/p excitation : Model 1)

5.2.2 Controller Design for Euler–Bernoulli Smart Beam as a MIMO System

Here, the control technique discussed in Section 5.2 is used to design a controller [96] to suppress the first 2 vibration modes of a smart cantilever beam modelled as MIMO system given in Section 2.1.2 through the smart structure concept (Fig. 2.5). The cantilever beam is divided into 4 finite elements. Collocated PZT pairs are bonded to the master structure at even FE positions, thus giving rise to a MIMO system of the smart structure. The MIMO state space model of the smart structure is given in Eq. (2.93) and (2.101) with its numerical value is (2.105). The performance of the beam as a multivariable system is hereby evaluated for AVC by carrying out the simulations and observing the various responses.

The smart beam is excited as in the earlier cases. The beam is thus subjected to vibrations and the OL impulse response is observed without the controller. The designed DSMC controller is put in loop with the plant and the system responses (sensor outputs y_1 and y_2), the control inputs (u_1 and u_2) and the evolution of the sliding function (S_1 and S_2) are observed for the multivariable plant and is shown in Fig. 5.20.

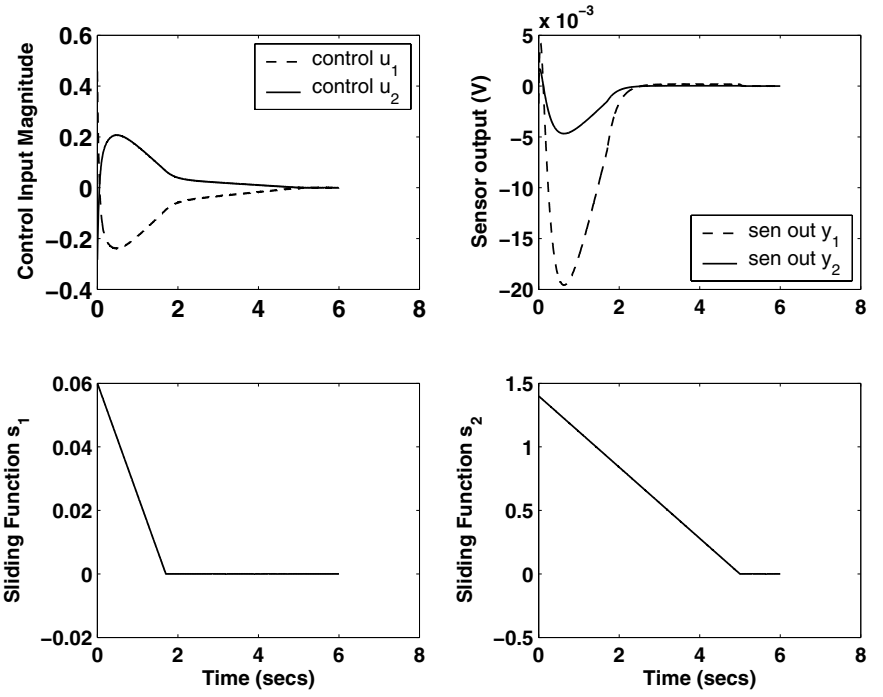

Fig. 5.20. Plots of sensor outputs y_1 and y_2, control inputs u_1 and u_2 and sliding functions S_1 and S_2 of the EB MIMO system with 2 inputs and 2 outputs

As in the case of control of MIMO model of the smart beam discussed in the Chapters 3 and 4, similar observations are arrived at as mentioned in Section 5.1.2. It is observed that modeling a smart structure by including the sensor / actuator mass and stiffness and by placing the sensor / actuator at 2 different FE positions along the beam [96] introduces a considerable change in the structural vibration characteristics than placing the sensor / actuator pair at only one location as in [94].

It can be argued that multivariable control of a smart structure is better compared to the single input single output control as there will be multiple interactions of the input and the output. From the simulation results, we infer that the system responds well in CL and does not exhibit undesirable chattering phenomenon. Neither does the system vibrate much. The values of δ_d and δ_e are determined to be $\delta_d = 10^{-4}\begin{bmatrix}0.176 & 0.066\end{bmatrix}^T$ and $\delta_e = 10^{-3}\begin{bmatrix}0.007 & 0.743\end{bmatrix}^T$.

5.2.3 Controller Design for Smart Timoshenko Beam with Surface Mounted PZT's as SISO System

The control technique discussed in Section 5.2 is used to design a MROF based DSM controller to suppress the first 2 vibration modes of a smart cantilever beam modelled as SISO system given in section 2.2.1:3(i) with the piezo patches placed at different FE locations along the length of the beam from the free end to the fixed end [112].

PZT's are bonded to the beam at one FE position only as a collocated pair, say, at fixed end (FE location 1) or at FE position 2 or at FE position 3 or at FE position 4 (free end), thus giving rise to 4 SISO models (1 actuator input u and 1 sensor output y) of the same smart structure plant as shown in the Fig. 2.7. The performance of these 4 SISO models is evaluated for AVC by carrying out the simulations and observing the various responses. The best model for the demonstrating the AVC concept for smart beams is presented.

The 4 SISO state space models of the smart beam is given by the Eqs. (2.168) - (2.171). The smart beam is excited as in the earlier cases. The beam is thus subjected to vibrations and the OL impulse response (plot of sensor outputs y as a function of t) are observed without the controller. The designed DSMC controller is put in loop with the plant and the system responses, the control input and the sliding surface are observed for all the 4 SISO models of the same smart structure plant. The responses of the 4 SISO models are shown in Figs. 5.21 and 5.22.

As in the case of control of SISO models of the smart beams discussed in the Chapter 3 and 4, similar observations are arrived at. Here, the comparison and discussion of the simulation results of vibration control for the smallest magnitude of the control effort u required to control the vibrations of the smart cantilever beam is presented [112] along with the best model for AVC, which is the model 1. The same inferences / observations presented in (a) - (h) in Section 5.1.1 are also valid here for the AVC of SISO based smart Timoshenko beams with surface mounted PZT's.

5.2.4 Controller Design for Smart Timoshenko Beam with Surface Mounted PZT's for a MIMO Case

The control technique discussed in Section 5.2 is used to design a controller to suppress the first 2 vibration modes of a smart cantilever beam modelled as MIMO

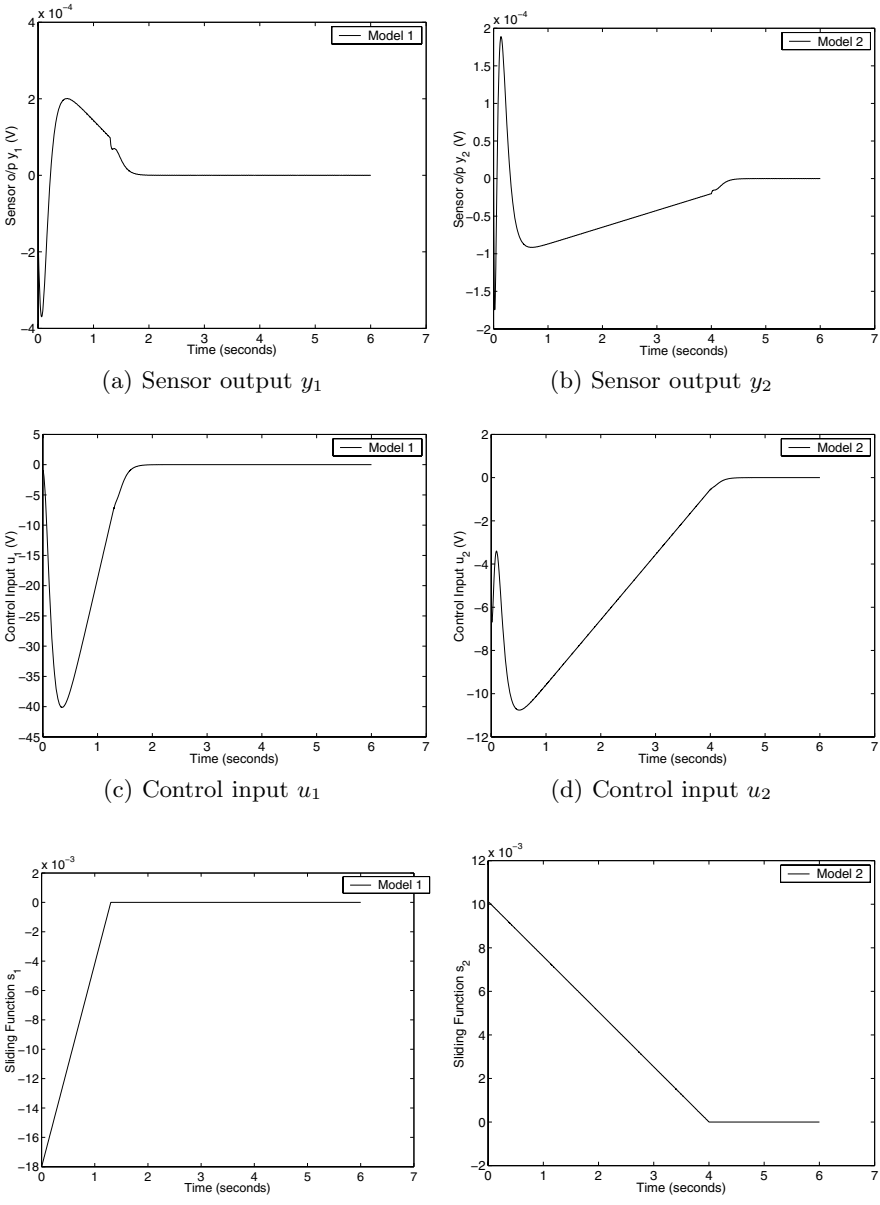

Fig. 5.21. Responses of Model 1 (piezo at FE 1) and model 2 (piezo at FE 2) for the smart Timoshenko beam modelled as SISO systems with surface mounted piezos

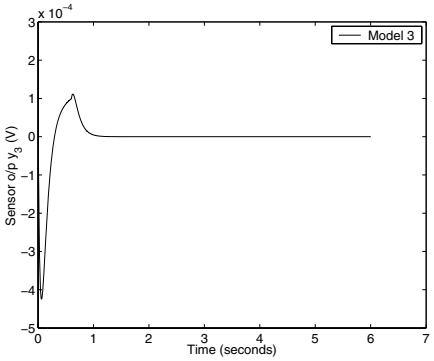

(a) Sensor output y_3

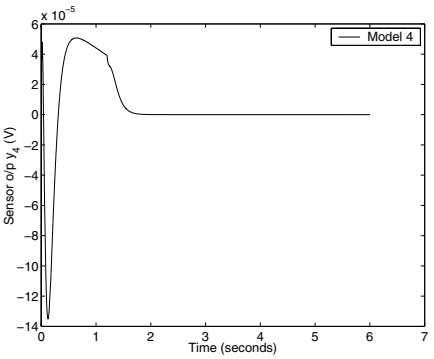

(b) Sensor output y_4

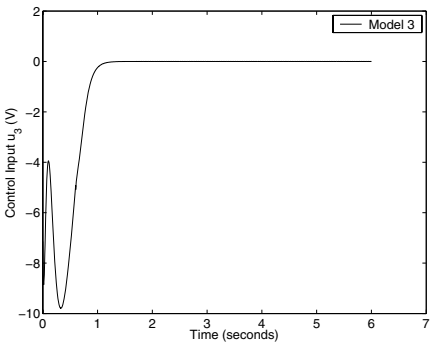

(c) Control input u_3

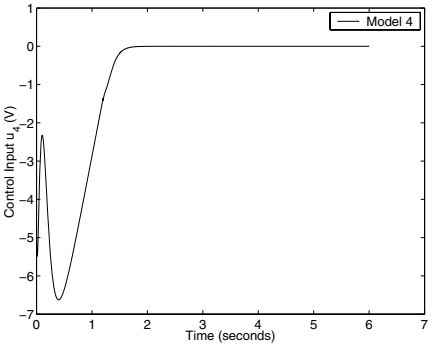

(d) Control input u_4

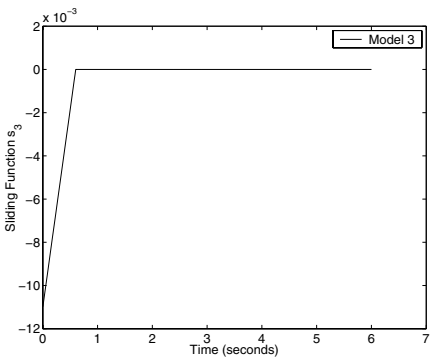

(e) Sliding function S_3

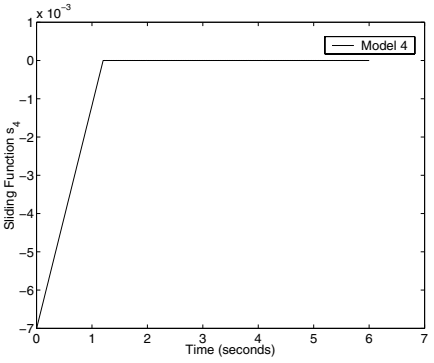

(f) Sliding function S_4

Fig. 5.22. Responses of Model 3 (piezo at FE 3) and model 4 (piezo at FE 4) for the smart Timoshenko beam modelled as SISO systems with surface mounted piezos

system as given in Section 2.2.2 for the Fig. 2.5 through the smart structure concept. Collocated PZT pairs are bonded to the master structure at even FE positions, thus giving rise to a MIMO model of the smart structure which is given in Eqs. (2.93) and (2.101) with its numerical value in Eq. (2.180) for 3 modes. The performance of this beam modelled as a multivariable system is hereby evaluated for AVC by carrying out the simulations and observing the various responses.

The smart beam is excited as in the earlier cases and the OL impulse response is observed without the controller. The designed DSMC controller is put in loop with the plant and the system responses (sensor outputs y_1 and y_2) and the control inputs (u_1 and u_2) are observed and shown in Fig. 5.23. The evolution of the sliding function (S_1 and S_2) is also shown in Fig. 5.24.

As in the case of MIMO EB models, similar observations has been made for the MIMO Timoshenko models. It is observed that modeling a smart structure

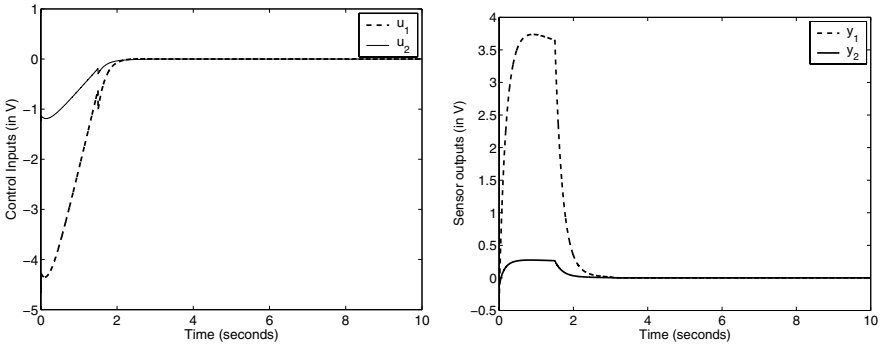

(a) Control inputs u_1, u_2 (b) Sensor outputs y_1, y_2

Fig. 5.23. Plot of controls, sensor o/p's for the Timoshenko beam with surface mounted PZT's as a MIMO system

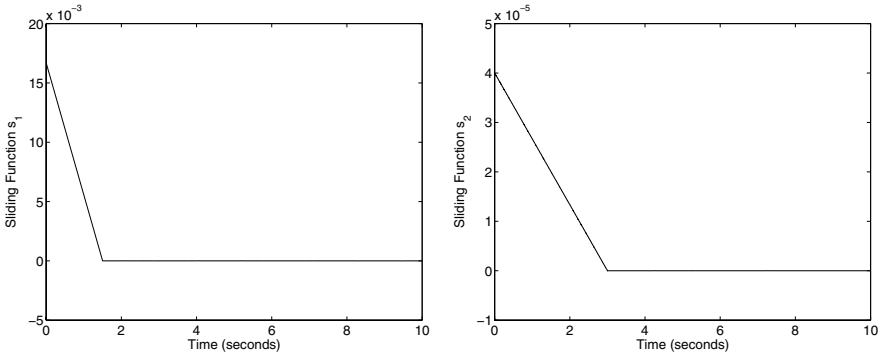

(a) Sliding function s_1 (b) Sliding function s_2

Fig. 5.24. Plot of sliding functions $s(k)$ for the Timoshenko beam with surface mounted PZT's as a MIMO system

by including the sensor / actuator mass and stiffness and by placing the sensor / actuator at 2 different FE positions along the beam introduces a considerable change in the structural vibration characteristics than placing the sensor / actuator pair at only one location as in [94]. The values of δ_d and δ_e are determined to be $\delta_d = 10^{-8}\begin{bmatrix}0.2719 & 0.2690\end{bmatrix}^T$ and $\delta_e = 10^{-7}\begin{bmatrix}0.8940 & 0.0817\end{bmatrix}^T$.

5.2.5 Controller Design for Smart Timoshenko Beams with Embedded PZT's as SISO Systems

The control technique discussed in Section 5.2 is used to design a controller to suppress the first 2 vibration modes of a smart cantilever beam modelled as MIMO system as given in Section 2.2.3:3 through smart structure concept. Four SISO models are obtained by embedding the shear actuator in between the top and bottom aluminum beam layers at FE position 1 and moving the shear sensor position from FE 2 to FE 5 as shown in Fig. 2.12. The 4 SISO state space models of the smart embedded beam is given by Eqs. (2.242) and (2.243) with its numerical value in Eq. (2.245). Three vibratory modes are considered. The performance of these 4 SISO models is evaluated for AVC by carrying out the simulations and observing the various responses and finally concluding with the discussions on the simulation results for best location of the placement of the sensor / actuator pair on the beam.

The controller is designed on the similar lines as explained in the previously discussed control designs for SISO models. Here, the comparison and discussion of the simulation results of the vibration control for the smallest magnitude of the control effort u required to control the vibrations of the smart cantilever beam and the best model for AVC is presented. The same inferences / observations presented in (a)-(h) in Section 5.1.1 are also valid here for the SISO models of the smart Timoshenko beams with embedded PZT's. Here, for the sake of convenience, only the responses of the model 1 such as the sensor output, control input and the switching function are shown here in Figs. 5.25 and 5.26 respectively. Similarly, the results are observed for the other SISO models also.

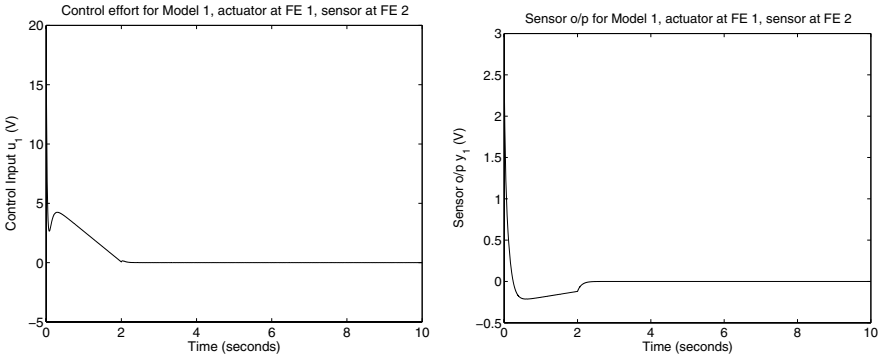

(a) (b)

Fig. 5.25. Plot of sensor o/p and control effort for the embedded Timoshenko beam as a SISO system with surface mounted PZT (model 1)

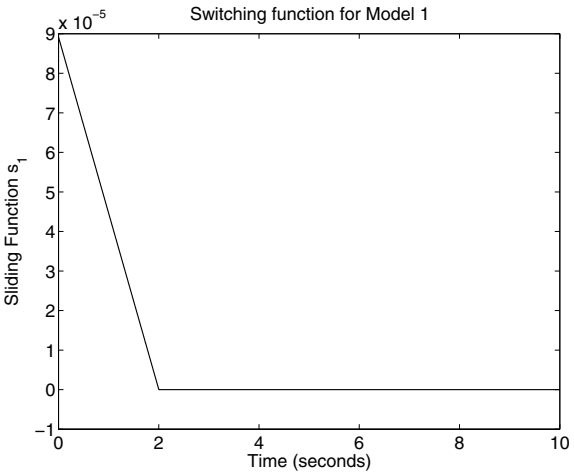

Fig. 5.26. Switching f/n $s(k)$ for Model 1, actuator at FE 1, sensor at FE 2

5.2.6 Controller Design for the Smart Beam as a Multivariable System with Embedded PZT's

The control technique discussed in Section 5.2 is used to design a MROF based DSM controller to suppress the first 2 vibration modes of a cantilever beam through smart structure concept for the multivariable space model of the smart embedded beam given in section 2.2.3:4. The MIMO model is obtained by sandwiching the actuators in between the aluminum layers at FE positions 2, 4 and sensors at FE positions 6, 8, thereby giving rise to a multivariable system as shown in Fig. 2.13. The MIMO state space model of the smart beam is given by Eqs. (2.247) and (2.248) with its numerical values given in (2.250) for three vibratory modes. The performance of this MIMO model is evaluated for AVC by carrying out the simulations and observing the various responses.

The DSM controller is designed on the similar lines as explained in the previously discussed control designs for MIMO systems. The responses such as the sensor output, control input and the switching function are shown here in the Figs. 5.27 - 5.29. The values of δ_d and δ_e are determined to be $\delta_d = 10^{-8}\begin{bmatrix}0.37 & 0.45\end{bmatrix}^T$ and $\delta_e = 10^{-7}\begin{bmatrix}0.5670 & 0.0523\end{bmatrix}^T$. From the simulation results it is observed that the multivariable control is better than the SISO control as there is multiple interactions of the input and output. Also, a multi input test provides better energy distribution and even better actuation forces and the control effort required is less compared to the SISO embedded case. Many of the inferences drawn in the conclusion part of the MIMO based smart systems are also valid here.

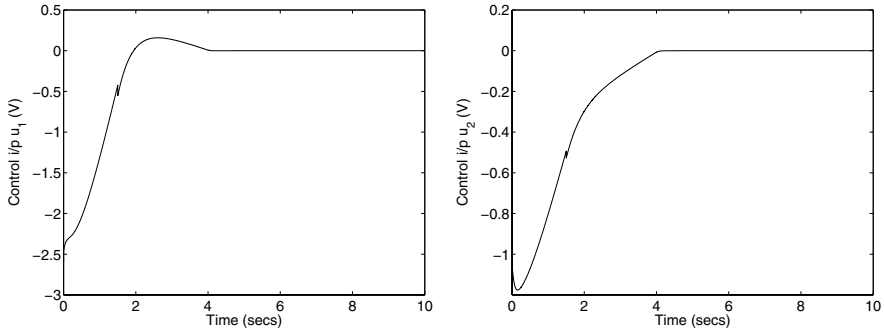

(a) (b)

Fig. 5.27. Plot of control efforts for the embedded Timoshenko beam (MIMO case)

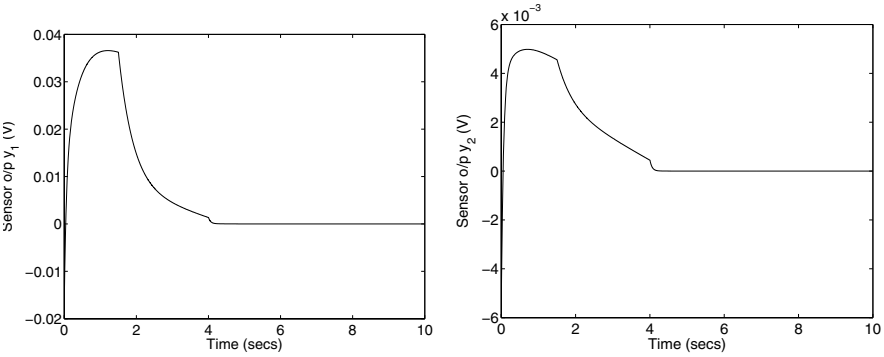

(a) (b)

Fig. 5.28. Plot of sensor outputs for the embedded Timoshenko beam (MIMO case)

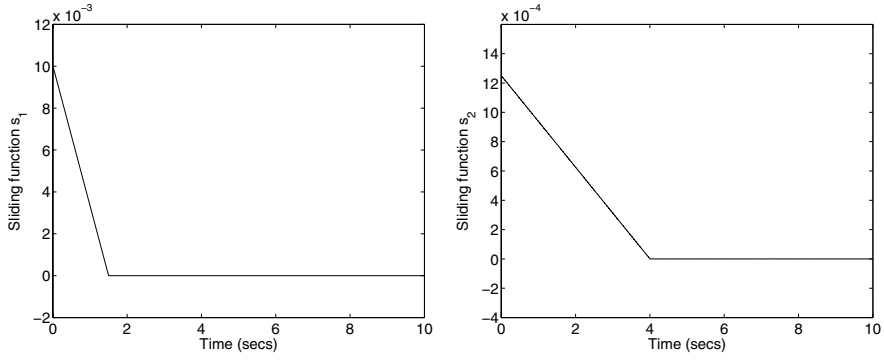

(a) (b)

Fig. 5.29. Plot of switching functions for the embedded Timoshenko beam (MIMO case)

5.3 Conclusions

Discrete sliding mode controllers are designed successfully to control the first few vibratory modes of a smart cantilever beam modelled using 2 type of beam theories, viz., Euler-Bernoulli beam theory and Timoshenko beam theory. New AVC schemes to control the flexural vibrations of SISO and MIMO smart models were presented. Different sensor / actuator locations bonded to the master structure (cantilever beam) either as surface mounted piezos or as embededd type piezos were considered, thus giving rise to many state space models of the smart structure beam. For the SISO case, it was observed that the control effort required to damp out the vibrations gets reduced when the piezo pair is moved from the free end towards the root of the structure.

The role of sensor / actuator position in the controller design is analyzed. The optimum sensor / actuator location is identified as the position near the fixed end. Better performances of the plant are obtained when the piezo pair is at the root (fixed end) rather than at the free end. Multivariable control of a smart structure is inferred to be better compared to the SISO control as there will be multiple interactions of the input and the output which will cause the vibrations in the system to be damped out quickly than the latter. A multi-input multi-output test provides better energy distribution and even better actuation forces. Also, the control efforts require are lesser compared to the SISO cases. In general, POF and FOS control schemes which were discussed in Chapters 3 and 4 are not robust, whereas the MROF based DSMC technique can be robust with respect to a class of uncertainty. Thus, MROF based DSMC has more practical values in comparison to the other controllers.

Two approaches of control strategies for smart structures were discussed. The first one is the the Discrete Quasi Sliding Mode Control (DQSMC) strategy using output samples and the second one, the Multirate Output Feedback (MROF) based Discrete Sliding Mode Control (DSMC) strategy based on bartoszewicz's law. The former control strategy makes use of the switching function in the control and hence exhibits some chattering, whereas the latter control strategy does not use the switching in the control and hence eliminates chattering. Here, the switching function and the control input is obtained directly in terms of immediate past control value and the past output samples.

In both the cases of MROF techniques, the states of the system are needed neither for switching function evaluation nor for the feedback purpose. The two DSMC algorithms are computationally simple, guarantee better robustness, faster convergence and improved steady state accuracy of the system. The two techniques are more practical because of output being used rather than states (as in many cases all the system states are not available for measurement). Thus, these techniques are very useful from the implementation point of view.

6

Implementation of Control Techniques for Smart Structures

In this Chapter, we present the experimental results of periodic output feedback and fast output sampling feedback controllers to control the structural vibrations of a flexible aluminum cantilever beam using collocated piezoelectric actuators and sensors for the fundamental mode. A digital control system consisting of MATLAB®, SIMULINK® modeling software, Real Time Workshop (RTW)® and dSPACE® 1104 controller is used for the system identification and vibration control purposes. The simulation and experimental results obtained for the experimental beam show the effectiveness of the designed controller.

6.1 Experimental Set-Up Details

The experimental set-up consists of a long flexible aluminum beam in the cantilever configuration with a pair of piezoelectric transducers mounted closer to the fixed end of the beam (i.e., nearby the first finite element) as shown in Fig. 6.1. The beam (high grade aircraft aluminum) is fixed firmly at one end with the help of two metallic clamps as vice. The vice is selected to have large enough inertia so that the vibrations of the vice do not affect the system dynamics when the beam is in the vibration mode.

Two piezoelectric patches are bonded to the master structure at a distance of 10.2 mm from the root of the beam (i.e., starting 1.2 cm from the end of fitting) as surface mounted sensors and actuators, one above the beam and one below the beam as a collocated pair. The bottom PZT acts as the sensor, whereas the top PZT acts as the control actuator. The physical properties of the experimental flexible aluminum cantilever beam and that of the piezoelectric material used are given in Table 6.1. These parameters are obtained from the manufacturers specification sheets and from the materials data handbook.

The piezoelectric patches are purchased from Sparkler Ceramics. Pvt. Ltd., Pune, India and are of SP-5H NAVY type. To excite the beam at its natural frequency, i.e., to apply an external disturbance $\mathbf{f}_{ext}$ to the beam, a third piezoelectric patch is used at the extreme end of the beam (i.e., at the fourth finite element position) as shown in Fig. 6.6. This patch is bonded onto the surface of the beam at the free end at a distance of 238.8 mm from the root hub. The piezoelectrics patches are

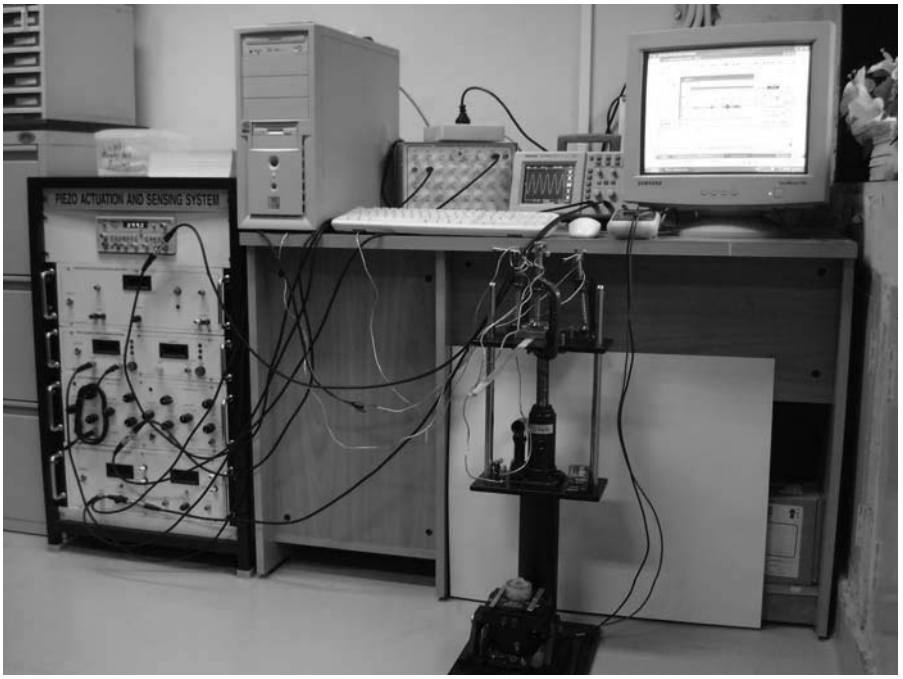

Fig. 6.1. Photographic view of the experimental set-up

Table 6.1. Properties of the experimental beam and the piezo patches

Physical parameters	**Aluminum cantilever beam**	**Piezoelectric sensor / actuator**
Length	$L_b = 0.315$ m	$l_p = 0.0762$ m
Width	$b = 0.0127$ m	$b = 0.0127$ m
Thickness	$t_b = 1$ mm	$t_a = t_s = 0.5$mm
Density	$\rho_b = 2700\ Kg/m^3$	$\rho_p = 7500\ Kg/m^3$
Young's Modulus	$E_b = 71\ GPa$	$E_p = 47.62\ GPa$
Damping Constants used in $\mathbf{C}^*$	$\alpha = 0.0836$, $\beta = 0.0005287$	
Piezoelectric Strain Constant		$d_{31} = -247 \times 10^{-12} m/V$
Piezoelectric Stress Constant		$g_{31} = -9 \times 10^{-3}\ VmN^{-1}$

bonded to the master structure using an adhesive named as 'M-bond araldite kit'. Electrodes are attached to the piezoelectric patches over its surface with fixed-on adherent silver of solderable quality lead by soldering.

Thus, this makes the delicate piezoelectric patches much easier to work with and is also easier to integrate into the structure. The controller patches were bonded on one side of the beam, while the disturbance patches were bonded on the other side of the beam as it was shown in the previous Chapters that the best model for AVC would be when the piezos are placed at nearby the fixed end as is the best location for controlling the fundamental bending mode (dominant mode). A signal generator or an audio oscillator tuned to the first mode natural frequency is used to provide the sinusoidal disturbing signal to the disturbing actuator at the free end.

The sinusoidal signal acts as the excitation input to the structure, which induces continuous vibrations in the beam. The connecting wires from the beam structure (comprising of the beam, sensor, control actuator and the disturbing actuator) to the signal generator are well shielded with a PVC covering in order to avoid the stray magnetic fields, noises, cross-talk and from radio interference. Now, the beam will be vibrating with the particular natural frequency. The output of the sensor y is given as input to the piezo sensing system which consists of a charge to voltage converting unit along with a signal conditioning amplifier and having a variable gain setting of 1, 2 and 5, i.e., the output of the piezo sensing unit will be multiplied by that amount.

The output of the piezo sensing unit is given as input to the filtering unit which filters out all the noise contents. Knobs are provided on the filtering unit with lower cut off and upper cut off frequencies to allow only that particular range of frequencies. The conditioned piezosensor signal (amplified) is given as analog input to the dSPACE1104 hardware controller board through the connector box and the analog to digital (ADC) port of the dSPACE controller board. The control algorithm is implemented using simulink software and RTW is used to generate C code from the developed simulink model.

The C code is then converted to target specific code by real time interface (RTI) and target language compiler (TLC) supported by dSPACE1104. This code is then deployed on to the rapid prototype hardware system to run the Hardware In-the-Loop Simulation (HILS), i.e., the developed control algorithms are downloaded on to the DS1104 PPC controller board using the RTI. The control signal u which is generated from the simulink model output is interfaced to the piezo actuation system through the configurable digital to analog (DAC) output port and the connector box of the dSPACE 1104 system by using multi-stranded shielded cable wires. The output of the piezo actuation system is given as the input control signal to the control actuator on the flexible aluminum beam.

Knobs are provided on the piezo actuation system to increase or decrease the control voltage to the actuator. The actuator input to the control actuator is limited to $\pm$ 200 V which is the maximum voltage that can be applied to the piezoelectric materials. Note that all the connecting wires from the smart structure to the signal conditioning measurement devices and oscilloscopes are good shielded multi-stranded connecting wires. A dual channel Tektronix oscilloscope is also used to store and measure the input and output signals of the smart structure. The signal generator, vibration inducing amplifier, piezo sensing unit, filter bank unit, piezo actuation unit are housed in a single unit, manufactured from Spranktronics Ltd., Bangalore, India.

6.2 Introduction to the dSPACE 1104 Controller Hardware

Feedback control of vibrations of the smart structure is implemented via a dSPACE DS1104 digital controller board based rapid prototyping system made by dSPACE Technologies, Padderborn, Germany. The control board sits inside a PC, which also houses both the dSPACE driver software and the analysis / simulation software tools that are required (in our case control desk software). Using the PCI slot, the controller card communicates to the outside world. This system is able to run complex control algorithms at high sampling rates. The dSPACE system builds a discrete realization of the synthesized controller directly from the simulink environment using Euler numerical integration method.

The i/o chips (ADC, DAC, muxADC, muxDAC) are used as the communication ports for the i/o signals such as sensor output signal and the control signal. The control signal from the DAC port is used for controlling some of the state variables of the plant, say the sensor voltage or the tip displacement, position, etc.,. All the ADC and DAC chips are bipolar with a voltage range of $\pm$ 10 V. Care has to be taken to see that the maximum voltage to these chips should not be exceeded, else the card gets damaged. To safeguard the controller card from high voltages, a connector box is used which prevents voltages $\geq$10 V. A high voltage power amplifier (piezo actuation system) is used to amplify the signal sent to the actuator. A 1 GHz Intel Pentium 4 PC is used for the data acquisition, analysis, modeling and control of the plant. Thus, a SISO control system environment is set up in the laboratory for the experimental evaluation of the smart structure.

6.3 System Identification of the Smart Structure

In order to design a good controller for a process, a good process model is often required. A controller designed on the basis of a good process model often works better than the one designed without a model. Unfortunately, model development from first principles is a difficult and an expensive task requiring participation of experts in numerous fields of engineering. This is also a time consuming and tedious process. In this computerized age, a lot of plant data is generally available, and hence this plant data can be used to generate the model of the process. Thus, the system identification can be defined as the process of developing a mathematical model of a physical system using the obtained experimental data [130].

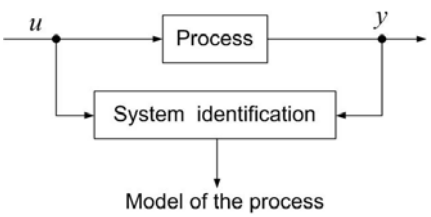

Fig. 6.2. System identification - a schematic

Once appropriate input, output and the noise measurements are made, we proceed to obtain the model. There are 2 steps in this process, viz., identification of an appropriate model structure and estimation of values of parameters that pertain to the above model structure. The information used in the system identification consists of the input and output data and an assumption about the error. The schematic of the system identification is shown in the Fig. 6.2. The process of identifying a physical system can be classified into 3 types, viz.,

(a) Modal parameter identification,
(b) Structural model parameter identification and the
(c) Control model identification.

In (a), the dynamics of the structures is characterized by the modal parameters such as the natural frequencies, damping ratios and the mode shapes. In (b), using the identified modal parameters, additional processes can be performed to obtain structural model parameters such as the mass, damping and the stiffness matrices. In (c), the control model identification finds a parametric model to represent a system in order to design a controller. In the context of the monograph, the identification technique employed by us refers to the control-model identification.

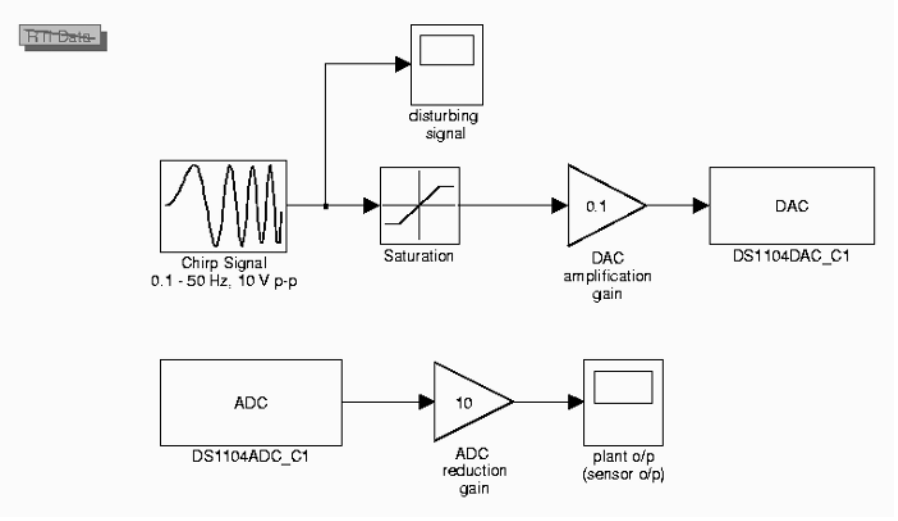

Fig. 6.3. Simulink diagram for disturbance TF identification

The approach of determining the transfer function using the mathematical modeling (from first principles) and using the finite element analysis is quite complex and a tedious process. The finite element models are sometimes not feasible for control purposes because the order should be high for achieving the desired accuracy. However, the system identification technique based upon the experimentation offers a rather simplistic approach for getting the transfer function of the system. Further, the state space model of the beam can also be arrived at. Based upon the input applied to the system, the output signals from the system are analyzed in order to get a model which will be required for designing a controller.

The identification procedure of the plant considered in the experimentation is as follows. To identify the dynamics of the beam, the beam needs to be stimulated via the disturbing actuator. Exciting force $F(t) = sin(\omega_1 t) = sin(2\pi f_1 t)$ exerted at the corner point of the beam was chosen according to the first natural frequency of interest. Since the disturbance is a sine function, its s-plane poles are complex conjugate numbers $\lambda_1 = \pm j\ \omega_1$ and f_1 is the frequency of the first mode. In the work considered, first mode transfer function is identified by the input and output data from the smart structure using the well known prediction Output Error (OE) identification method from the ident tool box in MATLAB.

The disturbance transfer function is obtained as follows. To excite the structure, the simulink model shown in the Fig. 6.3 is considered. Using the described experimental set up, the piezo disturbing actuator is excited by a sweep sinusoidal chirp signal of frequency varying from 0.01 Hz to 50 Hz in a sweep time of around 100 secs through the dSPACE, DAC port and the piezo actuation system. The input signal to stimulate the structure is selected as the signal which has wide-band characteristics containing the natural frequencies of the beam. Regarding the identification experiment, the sampling time is selected as small as possible in order not to lose the information. The disturbing actuator signal from the DAC is amplified by the power amplifier of the piezo actuation system and then given to it. Because of this disturbance, the beam starts vibrating and the sensor voltage is produced.

The sensor voltage from the sensor is signal conditioned using the piezo sensing system, amplified and then taken into the dSPACE environment through the ADC port as shown in Fig. 6.3. A substantial amount of data is collected for around 100 secs for model parametrization as shown in Fig. 6.4. The data collected is analyzed and is used for evaluation as well as for validation of the model. Fig. 6.4 shows the chirp excitation input and the sensor output captured from the dSPACE control desk for obtaining the disturbance transfer function (TF). The chirp input data and the sensor output data are taken from the dSPACE environment into the MATLAB environment and using the system identification tool box (ident.), a tenth order discrete transfer function model is obtained with a maximum fit of 95 %.

This tenth order discrete transfer function as identified above is then converted to a 10^{th} order continuous time transfer function model using the d2c command in Matlab. The 10^{th} order state space model is obtained from the CT transfer function model. As the order of the identified state space model is very high, it is reduced to a lower order model using the balanced realization and modred techniques in Matlab so that the reduced order state space model has only the first mode natural frequency. Using this identified state space model, the E matrix is obtained, which is the disturbance matrix. This disturbance matrix E couples the external disturbance to the system.

Similarly, on the above lines, the plant transfer function is obtained by giving a chirp signal as input to the control actuator and observing the sensor output on the dSPACE control desk. These input and output waveforms are shown in the Fig. 6.5. This input and output data is then taken to the MATLAB environment and using the ident. toolbox, a reduced order state space model is identified with a proper fit of 98.86 % (Fig. 6.5). Using this reduced order state space model, the A, B, C and D matrices are obtained.

Thus, the identified state space model of the beam by conducting the experiment can be written in compact form as

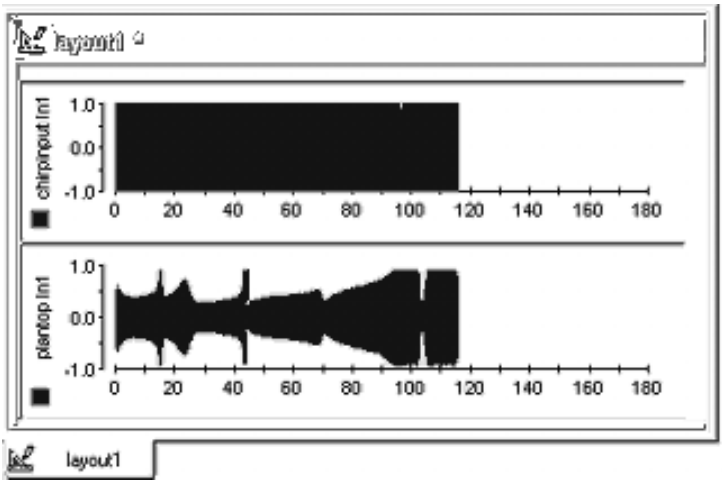

Fig. 6.4. Captured chirp input and output sensor signal of the smart structure for the disturbance transfer function identification using the dSPACE control desk

$$\dot{\mathbf{x}}(t) = A\mathbf{x}(t) + B\mathbf{u}(t) + Er(t), \quad y(t) = C^T\mathbf{x}(t) + D\mathbf{u}(t). \tag{6.1}$$

with

$$A = \begin{bmatrix} 96.3093 & 102.0090 \\ -101.4007 & -96.9075 \end{bmatrix}, \quad B = \begin{bmatrix} -0.0708 \\ 0.0409 \end{bmatrix}, \quad C^T = [\,1 \quad 0\,],$$

$$D = 0, \quad E = \begin{bmatrix} -0.0069 \\ 0.0028 \end{bmatrix}, \tag{6.2}$$

for the first mode. From the above 2 simple experiments, two transfer functions (disturbance TF and the plant TF) was established from which the unknown parameters of the smart structure are estimated using the output error based identification method, which is proven to be more universal and feasible than analytical and numerical models for the same.

Test for measurement of damping coefficient ξ, structural constants α and β :

To experimentally obtain the damping coefficient of the modes at which the controller should target, a simple test was performed. The beam was excited manually by tapping at its free end by the hand and the data was recorded in the dSPACE control desk. This data is then taken into the MATLAB environment to plot the damped sinusoidal response. The peaks of the overshoots are observed. The damping coefficient ξ is calculated by considering the first n pulses (say, $n = 20$ cycles) using the formula

$$\xi = \frac{1}{2\ \pi\ n} ln \frac{A_1}{A_n}, \tag{6.3}$$

where A_1 and A_n are the amplitudes of the first peak and the n^{th} peak of the response at t interval of time. The damping coefficient for the first mode was found to be 0.0096.

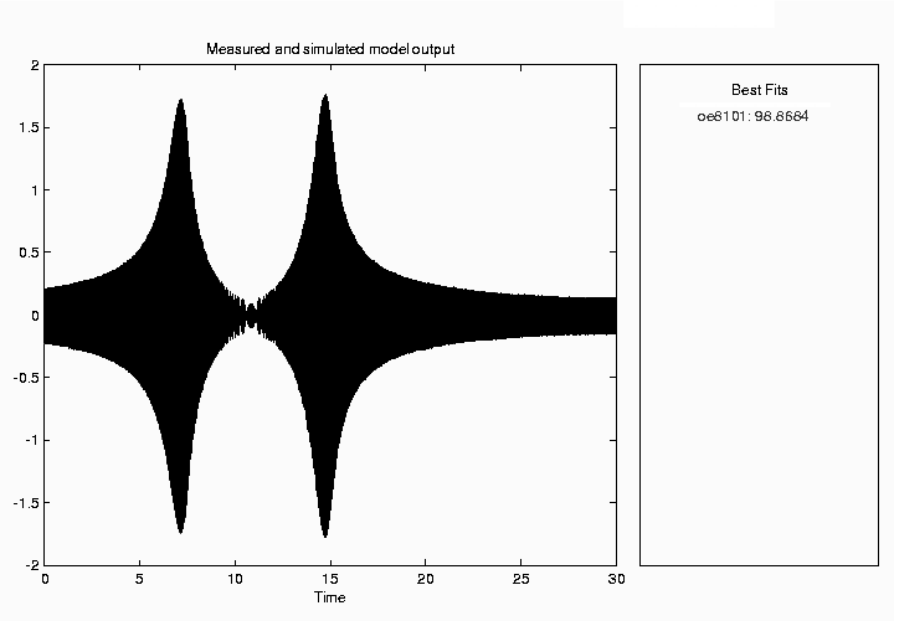

Fig. 6.5. Identified, measured plant output data obtained from the ident. tool box

To find the natural frequencies experimentally, a sinusoidal signal is given as input to the actuator and the sensor output is observed on the oscilloscope. The frequency of the sinusoidal signal from the signal generator is gradually increased from 1 Hz (say) till a particular value. By carefully observing the senor outputs on the oscilloscope, we can observe that the sensor voltage goes on increasing till the first mode and at the first mode frequency, the sensor output is maximum and if the frequency of the sinusoidal signal is increased further, the sensor output voltage decreases. The first frequency at which the sensor voltage is maximum is the first natural frequency. Like this, the second mode natural frequency is also found out. The frequencies found out by this method for the first 2 modes was 5.0595 Hz and 31.25 Hz respectively.

The structural constants α and β are determined from 2 given damping ratios that correspond to the two unequal natural frequencies of vibration using the relation $\alpha + \beta\omega_i^2 = 2\omega_i\xi$ to have the values as 0.0836 and 0.0005287. These constants are used in the finite element analysis of the beam for generating the state space model from first principles. The first mode natural frequency computed from the simple test, from the first principles (analytical) and from the identified state space model are given in Table 6.2 and were approximately the same.

6.4 Controller Design and Implementation

The design of the POF and FOS controllers using the first principles model (FE model) was carried out and also verified using the experimentally identified state

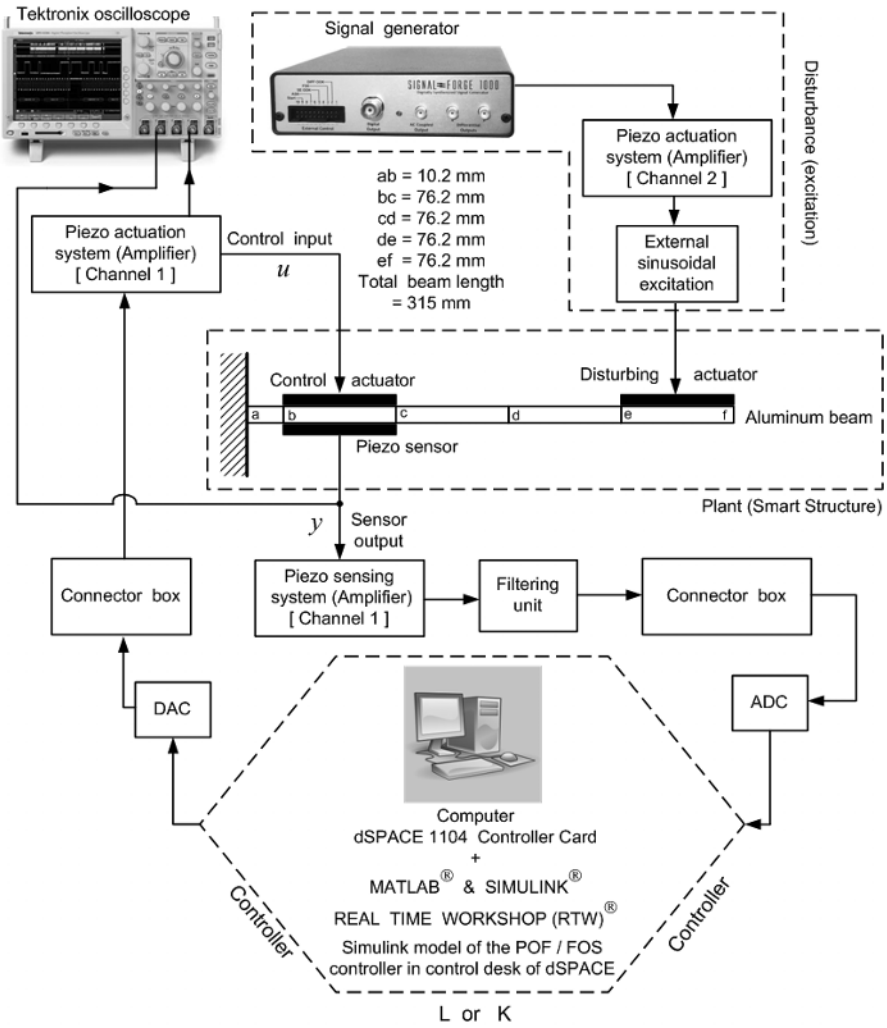

Fig. 6.6. Schematic diagram of the experimental set up of the vibration control system

Table 6.2. Comparison of the experimental and analytical results of the mode frequencies

Mode	f_1 (Hz.)		
	Experimental	Analytical	State space method (identification)
1	4.95	5.1	5.0595

space model. In both the cases, the first mode natural frequency obtained was the same.

6.4.1 Controller Design Using Simulations

In this Section, POF and FOS simulation results from the experimentally identified state space model are presented. POF and FOS controllers are designed in order to reduce the amplitude of vibrations in the smart structure during the resonance conditions with the identified model. With the controller put in the feedback loop with the plant, we must ensure that it will further shift the closed loop poles of the system to the left in the complex plane. This will guarantee that the CL system is highly damped and therefore less sensitive to external disturbances no matter where they act on the system. In this Section, we develop the control strategy for the SISO representation of the experimentally identified smart structure model given in the Eq. (6.2) using the POF control law given in Section 3.1 and using the FOS feedback control law discussed in the Section 4.1 with 1 actuator input and 1 sensor output.

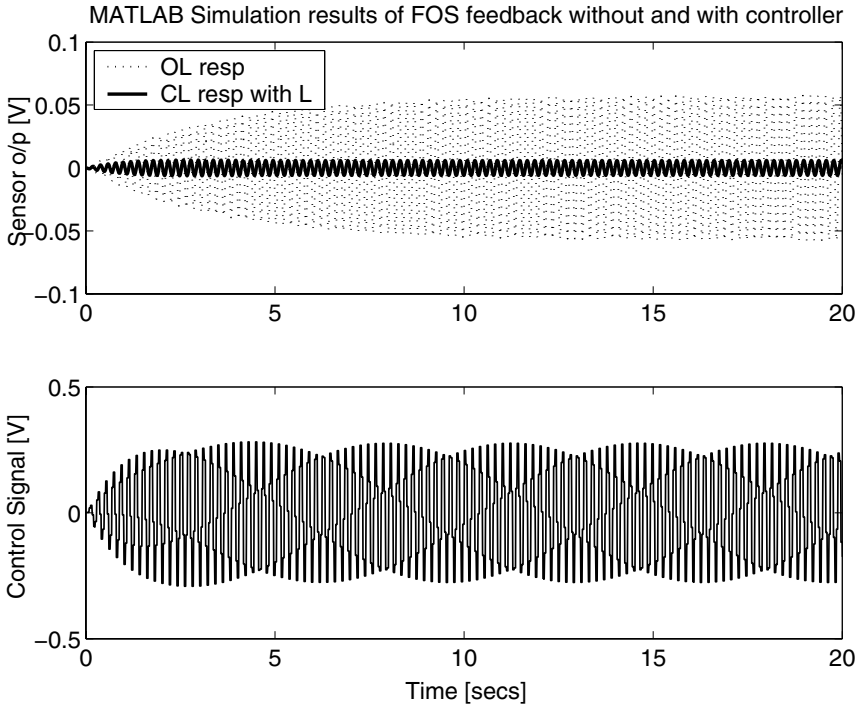

Fig. 6.7. FOS simulation results of the experimental beam

First, the sampling interval τ is taken as 0.04 secs and the number of sub-intervals N was taken as 4. A sinusoidal disturbance at first mode natural frequency of 5.0595 Hz is applied at the free end of the beam to the disturbing actuator using

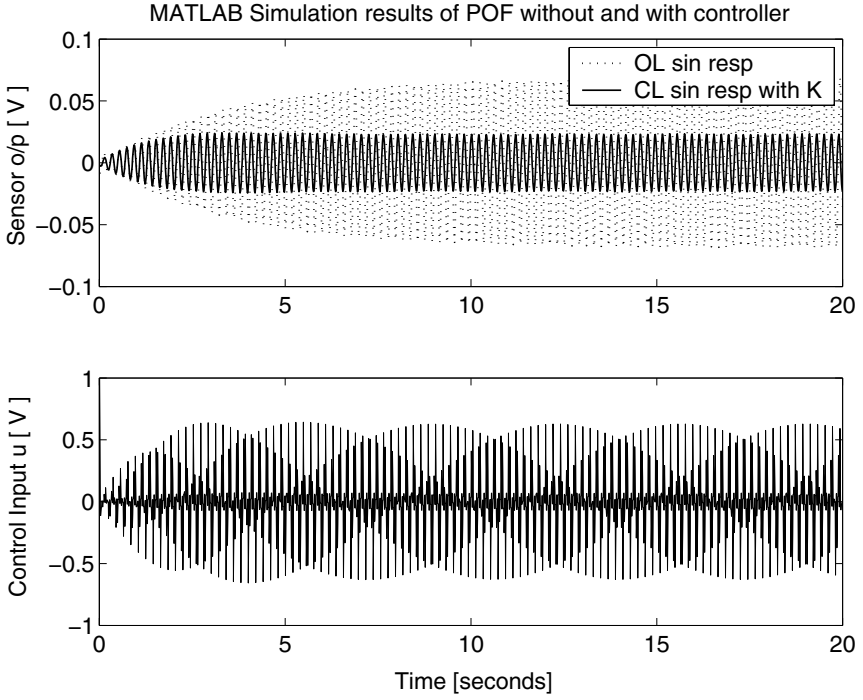

Fig. 6.8. POF simulation results of the experimental beam

a signal generator, thus subjecting it to continuous vibrations. The OL responses of the discrete system are observed. The discrete models are obtained by sampling the system in (6.2) at a rate of $\frac{1}{\tau}$ and $\frac{1}{\Delta}$ respectively giving rise to $(\Phi_\tau, \Gamma_\tau, C)$-tau system and (Φ, Γ, C)-delta system as

$$\Phi_\tau = \begin{bmatrix} 3.1607 & 3.0298 \\ -3.0118 & -2.5782 \end{bmatrix}, \quad \Gamma_\tau = \begin{bmatrix} -0.0040 \\ 0.0035 \end{bmatrix}, \quad C^T = \begin{bmatrix} 1 & 0 \end{bmatrix}, \tag{6.4}$$

$$\Phi = \begin{bmatrix} 1.8941 & 1.0000 \\ -0.9940 & 0.0000 \end{bmatrix}, \quad \Gamma = 10^{-4} \begin{bmatrix} -0.0008 \\ 0.0006 \end{bmatrix}, \quad C^T = \begin{bmatrix} 1 & 0 \end{bmatrix}. \tag{6.5}$$

The controllability index of the discrete systems is 2.

For FOS control, the stabilizing SFB gains are obtained for the tau system such that the eigenvalues of $(\Phi_\tau + \Gamma_\tau F)$ lie inside the unit circle and the response of the system has a good settling time. The SFB gain for the model is obtained as

$$F = \begin{bmatrix} -39.5016 & -51.7903 \end{bmatrix}. \tag{6.6}$$

The OL sinusoidal responses of the system with the SFB gain F is observed and shown in Figs. 6.7 (dotted line).

For POF control, the stabilizing output injection gain is obtained for the tau system such that the eigenvalues of $\left(\mathbf{\Phi}^N + GC\right)$ are placed inside the unit circle at appropriate locations and the response of the system has a good settling time. The output injection gain obtained is as

$$G = \begin{bmatrix} -0.0596 \\ -0.8285 \end{bmatrix}. \tag{6.7}$$

The OL sinusoidal responses of the beam with the output injection gain G is observed and shown in Fig. 6.8 (dotted line).

For FOS control, the FOS feedback gain matrix $\mathbf{L}$ for the smart system is obtained by solving $\mathbf{LC} \approx F$ using the LMI optimization method given by the Eqs. (4.17) and (4.20), i.e., F is realized by the FOS feedback gain by solving the linear equation $\mathbf{LC} \approx F$ subject to the LMI constraints ρ_1, ρ_2 and ρ_3. The FOS feedback gain matrix for the SISO model of the smart beam is given by

$$\mathbf{L} = [\ -8.5560 \quad -6.5908 \quad 3.7283 \quad 0.2600\ ]. \tag{6.8}$$

With the designed FOS controller put in the loop, the CL sinusoidal response of the smart system is observed and shown in Fig. 6.7 (thick line). Also, the variation of the control signal with time for is observed and graphically displayed in the Fig. 6.7.

For POF control, the POF gain matrix $\mathbf{K}$ for the smart system is obtained by solving $\mathbf{\Gamma K} \approx G$ using the LMI optimization method. The POF gain matrix for the SISO model of the smart beam is given by

$$\mathbf{K}^T = [\ 38.3225 \quad 18.7228 \quad -4.1842 \quad -4.2749\ ]. \tag{6.9}$$

With the designed POF controller put in the loop, the CL sinusoidal response (sensor output) of the system is observed and shown in Fig. 6.8 (thick line). Also, the variation of the control signal with time is observed and graphically displayed in the same figure.

6.4.2 Experimental Evaluation of the Simulated Results

The experimental set-up to demonstrate the suppression of AVC of smart structures is shown in the Fig. 6.6. The FOS and POF control algorithm is realized using simulink and implemented in real time on dSPACE 1104 system using RTW and dSPACE real time interface tools, i.e., the algorithm is downloaded from simulink onto the dSPACE 1104 DSP board . The simulink diagram for controller implementations is shown in the Figs. 6.9 and 6.10 for POF and FOS respectively.

In the simulink diagram shown, an analog plant input voltage to the A/D channel of the dSPACE board is scaled by a factor of $\frac{1}{10}$. Moreover, before a signal is sent to the D/A channel of the dSPACE board, it is multiplied by a factor of 10. Therefore, the gain of 10 (ADC reduction gain) and 0.1 (DAC amplification gain) corresponds to working with the actual voltages in the controller in between the A/D and D/A chips. The FOS or POF controller gains designed in the previous Section is used for the experimental evaluation here.

To make the beam vibrate, a sinusoidal disturbance at first mode natural frequency of the beam (10 V peak-peak) is applied to it. The sensor output obtained which is very low is given as input to the piezo sensing unit and after proper signal conditioning is given as input to the FOS or POF controller through the ADC port of the dSPACE and MATLAB / SIMULINK via the connector box. Now, the conditioned sensor output signal is sampled at a rate of $\frac{1}{\Delta} = 0.01$ secs for FOS (or $\frac{1}{\tau} = 0.04$ secs for POF) and the applied to the multirate stacker (which consists of the FOS or POF controller gains) as shown in the FOS simulink diagram in Fig. 6.10 (or POF simulink diagram in Fig. 6.9) from which the control signal is generated.

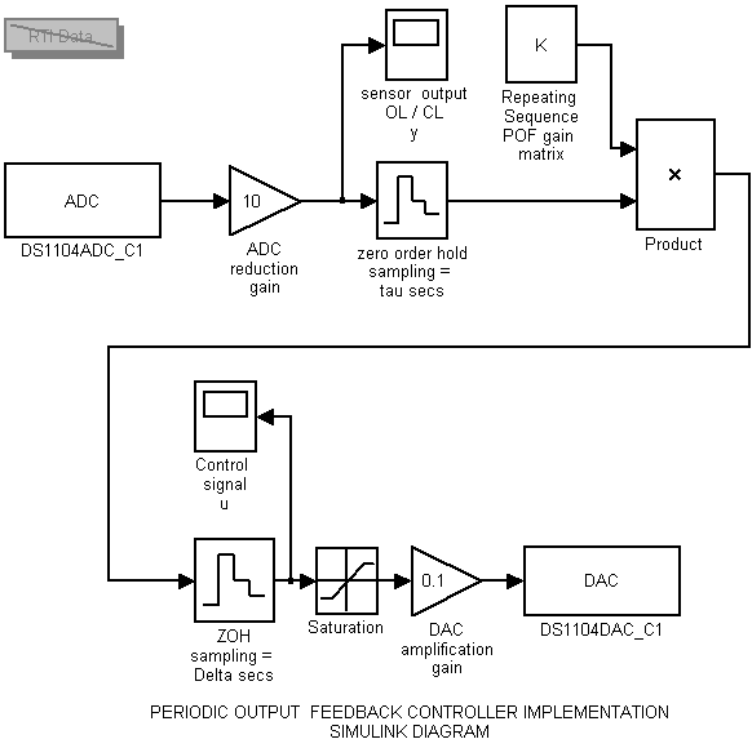

Fig. 6.9. POF controller SIMULINK implementation diagram in real time

The control signal is then updated, sampled at a interval of $\tau = 0.04$ secs for FOS (or $\frac{1}{\Delta} = 0.01$ secs for POF) and then applied to the control actuator through the DAC port of dSPACE system via the connector box and the piezo-actuation system. When the sensor signal is fed to the dSPACE control desk through the ADC port and the model is built using RTW, the real time workshop generates the C code from the developed simulink model. This C code is then converted to target specific code by RTI and TLC supported by dSPACE1104. This code is then deployed on to the rapid prototype hardware system to run HILS by generating the required control signal for the plant.

This control signal interacts with the vibrations created by the sinusoidal disturbance and using destructive interference brings down the overall amplitude of the beam vibrations, thus safeguarding the structure from wear and tear and increasing its longevity. The vibration suppression is achieved by generating the actuation signal 180° out of phase with the disturbance signal. Results were found by running the system first without the controller and then with the controller to show the control effect. The experimental results of the FOS and POF controller evaluations, i.e., the excitation signal, control signal, OL and CL sinusoidal responses with the MROF gains are shown in Figs. 6.11 and 6.12 for POF and FOS respectively.

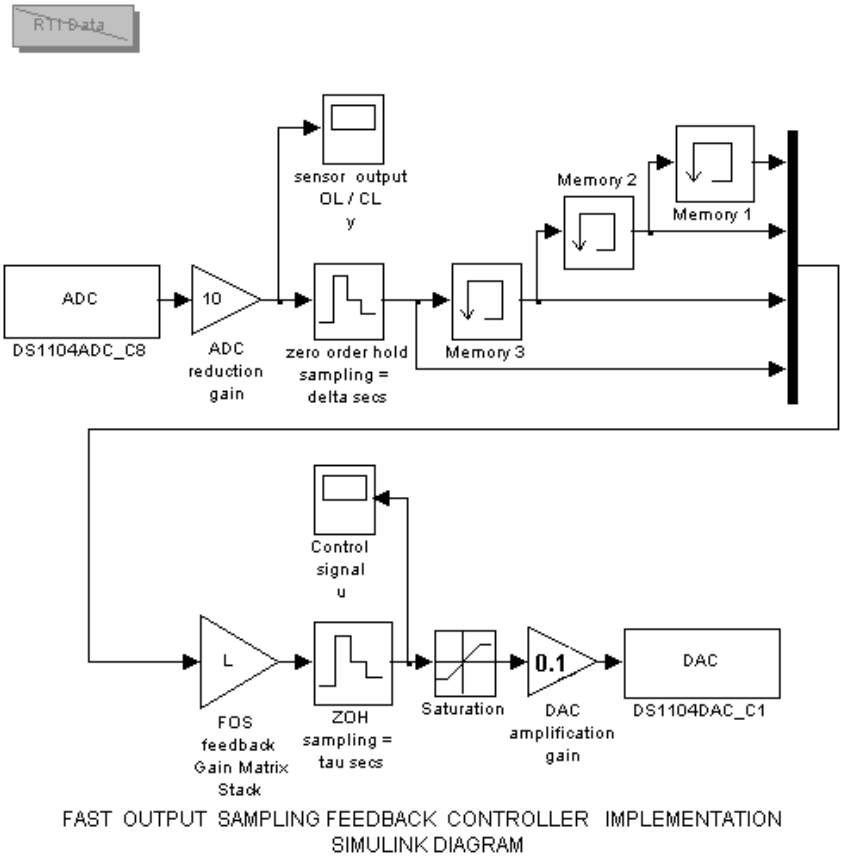

Fig. 6.10. FOS f/b controller SIMULINK implementation diagram in real time

6.4.3 Procedural Rules for Observing the OL/CL Responses in the Experiment

The following 17 rules gives a small idea about how the experimental investigation is to be carried out for the AVC of an flexible beam using the dSPACE card.

(a) Start Matlab, Simulink and dSPACE control desk.
(b) Build the FOS or POF controller in simulink environment with properly initializing the parameters for the experimental evaluation.
(c) Make the connection set up for the experiment as shown in the Fig. 6.6.
(d) To start with, the control signal to the control actuator is in OFF condition.
(e) Prepare the experiment in the control desk.
(f) Connect some data acquisition instruments such as plotters to observe the waveforms in the control desk and initialize the platform (refresh).

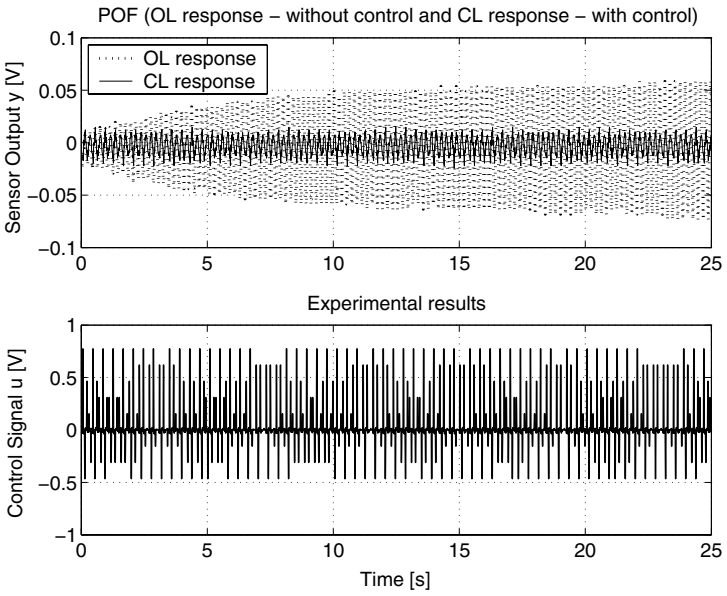

Fig. 6.11. Experimental results of POF control : OL (uncontrolled), CL sinusoidal response (controlled) and control effort at first natural frequency

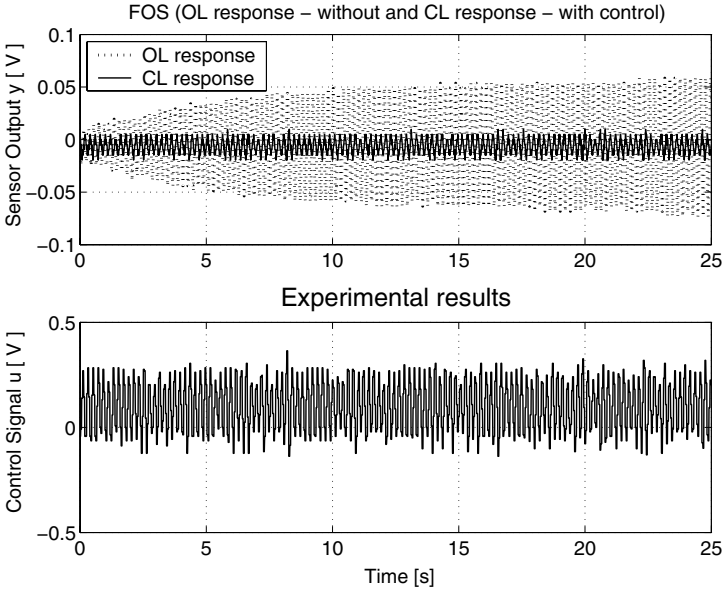

Fig. 6.12. Experimental results of FOS f/b control : OL (uncontrolled), CL sinusoidal response (controlled) and control effort at first natural frequency

(g) Excite the beam from the signal generator with the first mode natural frequency via the piezo actuation system.
(h) Build and download the model using the RTW.
(i) If the simulink model is properly designed, the C-codes will be properly downloaded and will be running on the processor and dSPACE configuration says okay, else debug the control algorithm till the errors are rectified.
(j) Once the code is running on the controller card, connect the variables you want to capture in the control desk such as the sensor output and the control signal. Select the edit capture settings context menu command of the data acquisition instruments to show the capture settings window and clear the auto repeat checkbox. This ensures that the captured data is not overwritten after the plot is complete.
(k) Start the control desk's animation mode.
(l) Switch the simstate to RUN and the data will be traced from the first sampling step.
(m) Observe the plant output, i.e., the sensor output on the control desk. This gives the OL response of the beam (control off).
(n) Switch on the controller, say after a certain time and immediately, the transverse vibrations of the beam will be reduced, i.e., the amplitude of the OL response gets drastically reduced, which is the CL response of the beam (with control). This can be seen on the control desk as well as physically with the beam.
(o) The OL data and the CL response data can be stored in the form of a .mat file format in the capture settings window and used for post-processing of the experimental data, to study the behavioral dynamics and for plotting purposes.
(p) Control desk of dSPACE is used to capture data and the relevant screen shots. The main trick is to begin the capture of the data points from $t = 0.0$ secs. This is done by initializing the simstate with RUN, so that the simulation is started immediately after the download.
(q) Once the experiment is over, proceed in the reverse before shutting off the entire experimental setup.

6.5 Conclusions

Experimental evaluation of the AVC suppression of flexible aluminum beam using piezos as surface mounted sensors and actuators at the root and disturbing actuator at the free end using dSPACE 1104 PPC hardware control system is presented in this Chapter. Two control laws were implemented and experimentally evaluated. POF and FOS controllers were also designed off-line starting from first principles and the results obtained were the same as obtained from the identified state space model and later evaluated from the experiments. The first mode frequency derived from the analytical means was also experimentally verified which was approximately the same. The experimental results of the smart structure demonstrates very good closed loop resemblance with the simulation results and thus exhibits the simplicity of the MROF controllers in real-time implementations and their control effectiveness.

From the experimental results, it was observed that the vibration reduction was approximately 85 % with the introduction of the FOS controller and 75 % with the POF controller during the resonance conditions. It was observed that the MROF gain plays a very important role in the reduction of the amplitude of vibrations. Due

to the location of only one sensor, all the modes could not be detected simultaneously and only the first mode was picked up by the sensor and controlled. Finally, to conclude, it can be inferred that FOS control is better than POF control, because the control effort to curb down the vibrations is less as the sensor output is sampled at a faster rate than the control input and hence the vibrations are suppressed to a larger extent than POF control. The simulation results was found to be in close match with the experimental results.

A

Appendix

(I). Mass and Stiffness Matrices for the Embedded Beam:

The stiffness matrix coefficients for $\left[K^b\right]$ the sandwich beam element is obtained using the Eq. (2.218) as [30], [42], [43] [44]

$$K_{11} = \frac{A\,A_{11}}{l_b}, \qquad K_{12} = K_{21} = \frac{A\,B_{11}}{l_b}, \qquad K_{13} = K_{31} = 0,$$

$$K_{14} = K_{41} = -\frac{A\,A_{11}}{l_b}, \qquad K_{15} = K_{51} = -\frac{A\,B_{11}}{l_b},$$

$$K_{16} = K_{61} = 0, \qquad K_{24} = K_{42} = -\frac{A\,B_{11}}{l_b}, \qquad K_{34} = K_{43} = 0,$$

$$K_{22} = -\frac{1}{10}\frac{Al_b(D_{11}l_b^3 - 10B_{11}\gamma l_b^2 + 60A_{55}l_b + 60\eta^2 A_{11}l_b + 120\gamma B_{11}\eta)}{(12\eta - l_b^2)^2},$$

$$K_{23} = K_{32} = \frac{6}{5}\,\frac{A}{l_b}\,\frac{D_{11}l_b^4 + 10A_{55}l_b^2 + 10\gamma^2 l_b^2 A_{11} - 20l_b^2 D_{11}\eta + 120D_{11}\eta^2}{(12\eta - l_b^2)^2},$$

$$K_{25} = K_{52} = -\frac{6}{5}\,\frac{A}{l_b}\,\frac{D_{11}l_b^4 + 10A_{55}l_b^2 + 10\gamma^2 l_b^2 A_{11} - 20l_b^2 D_{11}\eta + 120D_{11}\eta^2}{(12\eta - l_b^2)^2},$$

$$K_{26} = K_{62} = \frac{1}{10}\,\frac{Al_b(-D_{11}l_b^3 - 10B_{11}\gamma l_b^2 - 60A_{55}l_b - 60\eta^2 A_{11}l_b + 120\gamma B_{11}\eta)}{(12\eta - l_b^2)^2},$$

$$K_{33} = \frac{\begin{array}{c}A\,(2\,l_b^6\,D_{11} - 30l_b^4\,D_{11}\,\eta + 180\,l_b^2\,D_{11}\,\eta^2 - 15\,l_b^5\,\gamma\,B_{11} + 2160\,A_{55}\,\eta^2 \\ + 60\,A_{55}\,l_b^4 - 360\,A_{55}\,l_b^2 + 180\,\gamma\,l_b^3\,B_{11}\,\eta + 45\,\gamma^2\,l_b^4\,A_{11})\end{array}}{15\,l_b\,(12\,\eta - l_b^2)^2}$$

$$K_{35} = K_{53} = \frac{1}{10}\,\frac{Al_b(D_{11}l_b^3 - 10B_{11}\gamma l_b^2 + 60A_{55}l_b + 60\gamma^2 A_{11}l_b + 120\gamma B_{11}\eta)}{(12\eta - l_b^2)^2},$$

$$K_{36} = K_{63} = \frac{\begin{array}{c}-A(l_b^6 D_{11} - 60A_{55}l_b^4 - 90\gamma^2 l_b^4 A_{11} - 60l_b^4\, D_{11}\eta + 360l_b^2\, D_{11}\eta^2 + \\ 4320A_{55}\eta^2 - 720A_{55}\eta l_b^2)\end{array}}{30\, l_b\, (12\,\eta\, -\, l_b^2)^2}$$

$$K_{44} = \frac{A\, A_{11}}{l_b}, \qquad K_{45} = K_{54} = \frac{A\, B_{11}}{l_b}, \qquad K_{46} = K_{64} = 0,$$

$$K_{55} = \frac{6}{5}\,\frac{A}{l_b}\,\frac{D_{11}l_b^4 + 10A_{55}l_b^2 + 10\gamma^2 l_b^2 A_{11} - 20l_b^2 D_{11}\eta + 120D_{11}\eta^2}{(12\eta - l_b^2)^2},$$

$$K_{56} = K_{65} = -\frac{1}{10}\,\frac{Al_b(-D_{11}l_b^3 - 10B_{11}\gamma l_b^2 - 60A_{55}l_b - 60\gamma^2 A_{11}l_b + 120\gamma B_{11}\eta)}{(12\eta - l_b^2)^2},$$

$$K_{66} = \frac{\begin{array}{c}A\,(2\,l_b^6\, D_{11}\, - 30l_b^4\, D_{11}\,\eta\, +\, 180\,l_b^2\, D_{11}\,\eta^2\, + 15\,l_b^5\,\gamma\, B_{11}\, +\, 2160\, A_{55}\,\eta^2 \\ +\, 60\, A_{55}\, l_b^4\, -\, 360\, A_{55}\, l_b^2 - 180\,\gamma\, l_b^3\, B_{11}\,\eta\, +\, 45\,\gamma^2\, l_b^4\, A_{11})\end{array}}{15\, l_b\, (12\,\eta\, -\, l_b^2)^2}.$$

The mass matrix coefficients for $\left[M^b\right]$ the sandwich beam element is obtained using the Eq. (2.215) as [30], [42], [43] [44]

$$M_{11} = \frac{1}{3}l_b I_1, \qquad M_{12} = M_{21} = \frac{1}{2}\frac{\gamma l_b^2 I_1}{(12\,\eta\, -\, l_b^2)},$$

$$M_{13} = M_{31} = -\frac{1}{4}\frac{\gamma l_b^3 I_1}{(12\,\eta\, -\, l_b^2)}, M_{14} = M_{41} = \frac{1}{6}l_b I_1,$$

$$M_{15} = M_{51} = -\frac{1}{2}\frac{\gamma l_b^2 I_1}{(12\,\eta\, -\, l_b^2)}, \qquad M_{16} = M_{61} = -\frac{1}{4}\frac{\gamma l_b^3 I_1}{(12\,\eta\, -\, l_b^2)},$$

$$M_{22} = \frac{1}{35}\,\frac{\begin{array}{c}l_b(-294\, I_3\eta l_b^2 + 35\, I_2 l_b^3 + 1680\, I_3\eta^2 + \\ 13\, I_3 l_b^4 - 420\, I_2\eta l_b + 42\, I_1 l_b^2 + 42\,\gamma^2 I_1 l_b^2)\end{array}}{(12\eta - l_b^2)^2}$$

$$M_{23} = M_{32} = \frac{\begin{array}{c}-l_b\,(11\, I_3 l_b^5 - 10080\, I_2\,\eta^2 + 1260\, I_3\eta^2 l_b - 231\, I_3 l_b^3\eta \\ +126\,\gamma^2\, I_1 l_b^3 + 1260\, l_b I_1\eta + 840\, I_2\eta l_b^2 + 21\, I_1 l_b^3)\end{array}}{210\,(12\,\eta\, -\, l_b^2)^2},$$

$$M_{24} = M_{42} = \frac{1}{2}\frac{\gamma l_b^2 I_1}{(12\,\eta\, -\, l_b^2)}, M_{44} = \frac{1}{3}l_b I_1,$$

$$M_{25} = M_{52} = \frac{3}{70} \frac{\begin{array}{c} l_b\,(3\,I_3 l_b^4 - 28\,\gamma^2 I_1 l_b^2 - 28\,I_1 l_b^2 \\ -84\,I_3 \eta l_b^2 + 560\,I_3 \eta^2) \end{array}}{(12\,\eta\,-\,l_b^2)^2},$$

$$M_{26} = M_{62} = \frac{\begin{array}{c} l_b\,(13\,I_3 l_b^5 + 10080\,I_2\,\eta^2 + 2520\,I_3 \eta^2 l_b - 378\,I_3 l_b^3 \eta \\ -252\,\gamma^2\,I_1 l_b^3 - 2520\,l_b I_1 \eta - 840\,I_2 \eta l_b^2 - 42\,I_1 l_b^3) \end{array}}{420\,(12\,\eta\,-\,l_b^2)^2},$$

$$M_{33} = \frac{\begin{array}{c} l_b(252\,I_3 \eta^2 l_b^2 - 42 I_3 l_b^4 \eta + 63\,\gamma^2\,I_1 l_b^4 - 420\,I_1 \eta l_b^2 \\ -2520\,I_2 \eta^2 l_b + 210\,I_2 \eta l_b^3 + 10080\,I_1\,\eta^2 + 28\,I_1 l_b^4 + 2\,I_1 l_b^6) \end{array}}{210\,(12\,\eta\,-\,l_b^2)^2},$$

$$M_{34} = M_{43} = -\frac{1}{4} \frac{\gamma l_b^3 I_1}{(12\,\eta\,-\,l_b^2)},$$

$$M_{35} = M_{53} = \frac{\begin{array}{c} l_b\,(13\,I_3 l_b^5 - 10080\,I_2\,\eta^2 + 2520\,I_3 \eta^2 l_b - 378\,I_3 l_b^3 \eta \\ -252\,\gamma^2\,I_1 l_b^3 - 2520\,l_b I_1 \eta + 840\,I_2 \eta l_b^2 - 42\,I_1 l_b^3) \end{array}}{420\,(12\,\eta\,-\,l_b^2)^2},$$

$$M_{36} = M_{63} = \frac{\begin{array}{c} -l_b(504\,I_3 \eta^2 l_b^2 - 84 I_3 l_b^4 \eta - 126\,\gamma^2\,I_1 l_b^4 \\ -840\,I_1 \eta l_b^2 - 10080\,I_1\,\eta^2 + 14\,I_1 l_b^4 + 3\,I_3 l_b^6) \end{array}}{420\,(12\,\eta\,-\,l_b^2)^2},$$

$$M_{45} = M_{54} = -\frac{1}{2} \frac{\gamma l_b^2 I_1}{(12\,\eta\,-\,l_b^2)}, \qquad M_{46} = M_{64} = -\frac{1}{4} \frac{\gamma l_b^3 I_1}{(12\,\eta\,-\,l_b^2)},$$

$$M_{55} = \frac{1}{35} \frac{\begin{array}{c} l_b\,(13\,I_3 l_b^4 - 35\,I_2 l_b^3 + 42\,\gamma^2 I_1 l_b^2 \\ +42,I_1 l_b^2 - 294\,I_3 \eta l_b^2 + 420\,I_2 \eta l_b + 1680\,I_3 \eta^2) \end{array}}{(12\,\eta\,-\,l_b^2)^2},$$

$$M_{56} = M_{65} = \frac{\begin{array}{c} l_b\,(11\,I_3 l_b^5 - 231\,I_3\,l_b^3\,\eta + 126\,\gamma^2\,I_1 l_b^3 - 840\,I_2 \eta l_b^2 + 21\,I_1 l_b^3 \\ +1260\,l_b I_1 \eta + 1260\,I_3 \eta^2 l_b + 10080\,I_2 \eta^2) \end{array}}{210\,(12\,\eta\,-\,l_b^2)^2},$$

$$M_{66} = \frac{\begin{array}{c} l_b(252\,I_3 \eta^2 l_b^2 - 42 I_3 l_b^4 \eta + 63\,\gamma^2\,I_1 l_b^4 - 420\,I_1 \eta l_b^2 \\ +2520\,I_2 \eta^2 l_b - 210\,I_2 \eta l_b^3 + 10080\,I_1\,\eta^2 + 28\,I_1 l_b^4 + 2\,I_3 l_b^6) \end{array}}{210\,(12\,\eta\,-\,l_b^2)^2},$$

(II). Material Constants:

The material constants are calculated using the formulas

$$Q_{11} = \frac{E_{11}}{1 - \nu_{12}\nu_{12}}, \quad Q_{22} = \frac{E_{22}}{1 - \nu_{12}\nu_{12}}, \quad Q_{12} = \frac{\nu_{12}\;E_{11}}{1 - \nu_{12}\nu_{12}},$$

$$\frac{\nu_{12}}{E_{11}} = \frac{\nu_{21}}{E_{22}}, \quad Q_{66} = G_{12},$$

where G is the shear modulus.

(III). Shape Function of the Embedded Beam:

$$N_1 = 1 - \frac{x}{l_b}, \qquad N_2 = \frac{6\gamma}{12\eta - l_b^2}x - \frac{6\gamma}{l_b(12\eta - l_b^2)}x^2,$$

$$N_3 = -\frac{6\gamma}{12\eta - l_b^2}x + \frac{6\gamma}{l_b(12\eta - l_b^2)}x^2, \qquad N_4 = \frac{x}{l_b},$$

$$N_5 = \frac{3\gamma l_b}{12\eta - l_b^2}x + \frac{3\gamma}{l_b(12\eta - l_b^2)}x^2, \qquad N_6 = -\frac{3\gamma l_b}{12\eta - l_b^2}x + \frac{3\gamma}{l_b(12\eta - l_b^2)}x^2,$$

$$N_7 = 1 - \frac{12\eta}{l_b(12\eta - l_b^2)}x + \frac{3}{12\eta - l_b^2}x^2 - \frac{2}{l_b(12\eta - l_b^2)}x^2,$$

$$N_8 = \left(\frac{6\eta}{12\eta - l_b^2} - 1\right)x - \frac{x^2}{2l_b} - \frac{3}{2}\frac{l_b}{12\eta - l_b^2}x^2 + \frac{1}{12\eta - l_b^2}x^3,$$

$$N_9 = \frac{12\eta}{l_b(12\eta - l_b^2)}x - \frac{3}{12\eta - l_b^2}x^2 + \frac{2}{l_b(12\eta - l_b^2)}x^3,$$

$$N_{10} = \frac{6\eta}{12\eta - l_b^2}x - \frac{x^2}{2l_b} - \frac{3}{2}\frac{l_b}{12\eta - l_b^2}x^2 + \frac{1}{12\eta - l_b^2}x^3,$$

$$N_{11} = -\frac{6}{12\eta - l_b^2}x + \frac{6}{l_b(12\eta - l_b^2)}x^2, \qquad N_{12} = 1 - \frac{x}{l_b} + \frac{3l_b}{12\eta - l_b^2}x - \frac{3}{12\eta - l_b^2}x^2,$$

$$N_{13} = -\frac{6}{12\eta - l_b^2}x - \frac{6}{l_b(12\eta - l_b^2)}x^2, \qquad N_{14} = \frac{x}{l_b} + \frac{3l_b}{12\eta - l_b^2}x - \frac{3}{12\eta - l_b^2}x^2$$

and

$$\gamma = \frac{B_{11}}{A_{11}}, \qquad \text{and} \qquad \eta = \frac{D_{11}}{A_{55}}\left(\frac{\gamma B_{11}}{D_{11}} - 1\right)$$

are the constants, which are, being expressed in terms of bending and shear stiffness coefficients. Here, l_b is the length of the beam element.

(IV). Spatial Derivatives of the Shape Functions of EB Beam:

$$[\mathbf{n_1}] = \begin{bmatrix} f_1'(x) \\ f_2'(x) \\ f_3'(x) \\ f_4'(x) \end{bmatrix} = \begin{bmatrix} -\frac{6}{l_b^2} + \frac{12x}{l_b^3} \\ -\frac{4}{l_b} + \frac{6x}{l_b^2} \\ \frac{6}{l_b^2} - \frac{12x}{l_b^3} \\ -\frac{2}{l_b} + \frac{6x}{l_b^2} \end{bmatrix}, \quad [\mathbf{n_2}] = \begin{bmatrix} f_1''(x) \\ f_2''(x) \\ f_3''(x) \\ f_4''(x) \end{bmatrix} = \begin{bmatrix} -\frac{6x}{l_b^2} + \frac{6x^2}{l_b^3} \\ 1 - \frac{4x}{l_b} + \frac{3x^2}{l_b^2} \\ \frac{6x}{l_b^2} - \frac{6x^2}{l_b^3} \\ -\frac{2x}{l_b} + \frac{3x^2}{l_b^2} \end{bmatrix}, \quad [\mathbf{n_3}] = [\mathbf{n}]$$

(V). Smart Cantilever Beam Divided into 3, 4, 5 FE:

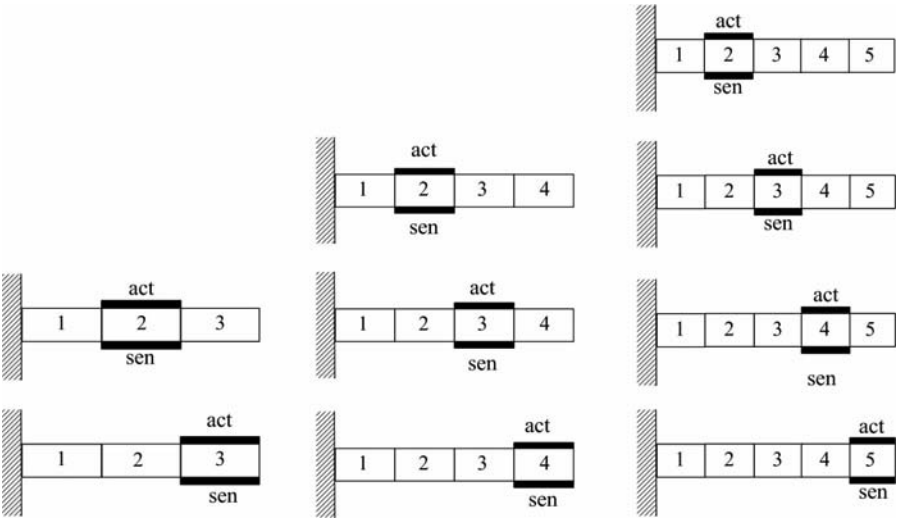

Fig. A.1. Flexible beam divided into 3 types of systems, viz., system 1 : 3 FE (PZT at FE 2, 3), system 2 : 4 FE (PZT at FE 2, 3, 4), system 3 : 5 FE (PZT at FE 2, 3, 4, 5)

(VI). Concept of FEM Technique of Assembling the Individual Elemental Matrices:

The 4 elemental mass matrices (local mass matrices) of the smart beam as shown in Fig. 2.2 is given by

$$M_1 = \begin{bmatrix} m_{a1} & m_{a2} & m_{a3} & m_{a4} \\ m_{a5} & m_{a6} & m_{a7} & m_{a8} \\ m_{a9} & m_{a10} & m_{a11} & m_{a12} \\ m_{a13} & m_{a14} & m_{a15} & m_{a16} \end{bmatrix}, \quad M_2 = \begin{bmatrix} m_{b1} & m_{b2} & m_{b3} & m_{b4} \\ m_{b5} & m_{b6} & m_{b7} & m_{b8} \\ m_{b9} & m_{b10} & m_{b11} & m_{b12} \\ m_{b13} & m_{b14} & m_{b15} & m_{b16} \end{bmatrix},$$

$$M_3 = \begin{bmatrix} m_{c1} & m_{c2} & m_{c3} & m_{c4} \\ m_{c5} & m_{c6} & m_{c7} & m_{c8} \\ m_{c9} & m_{c10} & m_{c11} & m_{c12} \\ m_{c13} & m_{c14} & m_{c15} & m_{c16} \end{bmatrix}, \quad M_4 = \begin{bmatrix} m_{d1} & m_{d2} & m_{d3} & m_{d4} \\ m_{d5} & m_{d6} & m_{d7} & m_{d8} \\ m_{d9} & m_{d10} & m_{d11} & m_{d12} \\ m_{d13} & m_{d14} & m_{d15} & m_{d16} \end{bmatrix},$$

which can be written as

$$M_1 = \begin{bmatrix} a_1 & b_1 \\ c_1 & d_1 \end{bmatrix}, \quad M_2 = \begin{bmatrix} a_2 & b_2 \\ c_2 & d_2 \end{bmatrix}, \quad M_3 = \begin{bmatrix} a_3 & b_3 \\ c_3 & d_3 \end{bmatrix}, \quad M_4 = \begin{bmatrix} a_4 & b_4 \\ c_4 & d_4 \end{bmatrix},$$

The global mass matrix $\mathbf{M}$, i.e., the mass matrix of the entire beam is obtained by assembling the individual mass matrices M_1 to M_4. First, $\bar{\mathbf{M}}$ is obtained as

$$\bar{\mathbf{M}} = \begin{bmatrix} a_1 & b_1 & 0 & 0 & 0 \\ c_1 & d_1 + a_2 & b_2 & 0 & 0 \\ 0 & c_2 & d_2 + a_3 & b_3 & 0 \\ 0 & 0 & c_3 & d_3 + a_4 & b_4 \\ 0 & 0 & 0 & c_4 & d_4 \end{bmatrix}_{10\times 10}.$$

Then, by neglecting the DOF's w_1 and θ_1 at the fixed end and by row and column shifting procedure, we get the the global or the assembled mass matrix of the 4 FE beam as

$$\mathbf{M} = \begin{bmatrix} d_1 + a_2 & b_2 & 0 & 0 \\ c_2 & d_2 + a_3 & b_3 & 0 \\ 0 & c_3 & d_3 + a_4 & b_4 \\ 0 & 0 & c_4 & d_4 \end{bmatrix}_{8\times 8}.$$

Similarly, we obtain the global stiffness matrix $\mathbf{K}$ for the beam shown in Fig. 2.2.

The modal matrix T is obtained as follows. Say,

$$\bar{\mathbf{T}} = \mathbf{M}^{-1}\mathbf{K} = \begin{bmatrix} t11 & t12 & t13 & t14 & t15 & t16 & t17 & t18 \\ t21 & t22 & t23 & t24 & t25 & t26 & t27 & t28 \\ t31 & t32 & t33 & t34 & t35 & t36 & t37 & t38 \\ t41 & t42 & t43 & t44 & t45 & t46 & t47 & t48 \\ t51 & t52 & t53 & t54 & t55 & t56 & t57 & t58 \\ t61 & t62 & t63 & t64 & t65 & t66 & t67 & t68 \\ t71 & t72 & t73 & t74 & t75 & t76 & t77 & t78 \\ t81 & t82 & t83 & t84 & t85 & t86 & t87 & t88 \end{bmatrix}.$$

Here, the matrices $\bar{\mathbf{T}}$, $\mathbf{M}$ and $\mathbf{K}$ are of sizes (8×8). $\mathbf{T}$ is the modal matrix which contains the eigen vectors representing the first two modes. To obtain the modal matrix from $\bar{\mathbf{T}}$, select only the last 2 columns which corresponds to the first two vibratory modes. Hence, we get the modal matrix for the first two vibratory modes as

$$\mathbf{T} = \mathbf{M}^{-1}\mathbf{K} = \begin{bmatrix} t17 & t18 \\ t27 & t28 \\ t37 & t38 \\ t47 & t48 \\ t57 & t58 \\ t67 & t68 \\ t77 & t78 \\ t87 & t88 \end{bmatrix}_{(8\times 2)}.$$

References

1. Gandhi M.V. and Thompson B.S., "Smart Materials and Smart Structures," *Chapman and Hall*, London, 1992.
2. Inderjit Chopra, "Review of state of art of smart structures and integrated systems," *AIAA Journal*, Vol. 40, No. 11, pp. 2145-2187, 2002.
3. Culshaw B., "Smart structures : A concept or a reality," *Journal of Systems and Control Engg.*, Vol. 26, No. 206, pp. 1-8, 1992.
4. Hermen S., "Analysis of beams containing piezoelectric sensors and actuators," *J. Smart Materials and Structures*, Vol. 3, No. 4, pp. 439-447, 1994.
5. Ramesh C., Umapathy M., Dhanalakshmi K. and Manjunath T.C., "Design of variable structure control for seismically excited vibration using electro-rheological fluids," *Third International Conf. on Smart Materials, Structures and Systems, ISSS-SPIE-2002*, I.I.Sc., Bangalore, India, Vol. 70, No. SA-430, pp. 234–241, Dec. 2002.
6. Rao S. and Sunar M., "Piezoelectricity and its uses in disturbance sensing and control of flexible structures : A survey," *Applied Mechanics Rev.*, Vol. 17, No. 2, pp. 113-119, 1994.
7. Baily T. and Hubbard J.E.Jr. , "Distributed piezoelectric polymer active vibration control of a cantilever beam," *Journal of Guidance, Dynamics and Control*, Vol. 8, No. 5, pp. 605-611, 1985.
8. Hanagud S., Obal M.W. and Callise A.J., "Optimal vibration control by the use of piezoelectric sensors and actuators," *J. Contr. Guidance*, Vol. 15, No. 5, pp. 1199-1206, 1992.
9. Fanson J.L. and Caughey T.K., "Positive position feedback control for structures," *AIAA J.*, Vol. 18, No. 4, pp. 717-723, 1990.
10. Mark Balas J., "Feedback control of flexible structures," *IEEE Trans. Auto. Contr.*, Vol. AC-23, No. 4, pp. 673-679, 1978.
11. Burdess J.S. and Fawcett J.N., "Experimental evaluation of piezoelectric actuator for the control of vibrations in a cantilever beam," *J. Syst. Control. Engg.*, Vol. 206, No. 12, pp. 99-106, 1992.
12. Brennan M.J., Bonito J.G., Elliot S.J., David A. and Pinnington R.J., "Experimental investigation of different actuator technologies for active vibration control," *Smart Materials and Structures*, Vol. 8, No. 3, pp. 145-153, 1999.

13. Yang S.M. and Lee Y.J., "Optimization of non-collocated sensor / actuator location and feedback gain in control systems," *Smart Materials and Structures J.*, Vol. 8, pp. 96-102, 1993.
14. Crawley E.F. and Luis J.De., "Use of piezoelectric actuators as elements of intelligent structures," *AIAA J.*, Vol. 25, pp. 1373-1385, 1987.
15. Woo Seok Hwang and Hyun Chul Park, "Finite element modeling of piezoelectric sensors and actuators," *AIAA Journal J.*, Vol. 31, No. 5, pp. 930-937, 1993.
16. Bona B., Indri M. and Tornamble A., "Flexible piezoelectric structures approximate motion equations and control algorithms," *IEEE Auto. Contr.*, Vol. AC-42, No. 1, pp. 94-101, 1997.
17. Schiehlen W. and Schonerstedt H., "Controller design for the active vibration damping of beam structure," *Proc. Smart Mechanical Systems Adaptronics SAE International*, USA, pp. 137-146, 1998.
18. Seung-Bok Choi and Chae-Cheon Cheong and Chul-Hea Lee, "Position tracking control of a smart flexible structure featuring a piezofilm actuator," *Journal of Guidance and Control*, Vol. 19, No. 6, pp. 1364-1369, 1996.
19. Forouza Pourki, "Distributed controllers for flexible structures using piezoelectric actuators / sensors," *Proc. 32nd IEEE CDC Conf.*, Texas, USA, pp. 1367-1369, Dec. 1993.
20. Bandyopadhyay B. and Axay Mehta, "Vibration control of smart strucutres using second order sliding mode control," *Proc. IEEE-International Conf. Industrial Technology-CCA-2005*, Toronto, Canada, pp. 1691-1696, Aug. 2005.
21. Shiang Lee W., "System identification and control of smart structures using neural networks," *Automatica*, Vol. 38, Nos. 4-8, pp. 269–276, 1996.
22. Gosavi S.V. and Kelkar A.V., "Modeling, identification, and passivity-based robust control of piezo-actuated flexible beam," *Journal of Vibration and Acoustics*, Vol. 129, pp. 260-271, apr. 2004.
23. Tokhi M.O., "Self tuning active vibration control in flexible beam structures," *Journal of Systems and Control Engineering - Proceedings of the Institute of Mechanical Engineers*, Vol. 208, pp. 263-277, 1994.
24. Moita J.S.M., Coreia I.F.P., Soares C.M.M. and Soares C.A.M., "Active control of adaptive laminated structures with bonded piezoelectric sensors and actuators," *Computers and Structures*, Vol. 82, pp. 1349-1358, 2004.
25. Ulrich Gabbert, Tamara Nestorovic Trajkov, Heinz Kppel, "Modeling, control and simulation of piezoelectric smart structures using finite element method and optimal lq control," *Facta Universitatis Series : Mechanics, Automatic Control and Robotics*, Vol. 12, No. 3, pp. 417-430, 2002.
26. Young-Hun Lim, Senthil Gopinathan V., Vasundara Varadhan V. and Vijay Varadan K., "Finite element simulation of smart structures using an optimal output feedback controller for vibration and noise control," *Int. Journal of Smart Materials and Structures*, Vol. 8, No. 8, pp. 324-337, 1999.
27. Vukovich G. and Koma A.Y., "Vibration suppression of flexible beams with bonded piezo-transducers using wave-absorbing controllers," *Journal of Guidance, Control and Dynamcis*, Vol. 29, pp. 347-354, 2000.
28. Anjanappa M. and Bi. J., "Magnetostrictive mini actuators for smart structures for smart structure applications," *Int. J. Smart Materials and Structures*, Vol. 3, No. 4, pp. 383-390, 1994.

29. Aldraihem O.J., Wetherhold T. and Singh T., "Distributed control of laminated beams : Timoshenko vs. Euler-Bernoulli theory," *Journal of Intelligent Materials Systems and Structures*, Vol. 8, No. 5, pp. 149-157, 1997.
30. Abramovich H., "Deflection control of laminated composite beam with piezoceramic layers-Closed form solutions," *Composite Structures*, Vol. 43, No. 3, pp. 217-131, 1998.
31. Chandrashekara K. and Varadarajan S., "Adaptive shape control of composite beams with piezoelectric actuators," *Intelligent Materials Systems and Structures*, Vol. 8, pp. 112-124, 1997.
32. Sun C.T. and Zhang X.D., "Use of thickness-shear mode in adaptive sandwich structures," *Smart Materials and Structures Journal*, Vol. 3, No. 4, pp. 202-206, 1995.
33. Aldraihem O.J. and Khedir Ahmed A., "Smart beams with extension and thickness-shear piezoelectric actuators," *J. Smart Materials and Structures*, Vol. 9, No. 1, pp. 1-9, 2000.
34. Doschner C. and Enzmann M., "On model based controller design for smart structure," *Proc. Smart Mechanical Systems Adaptronics SAE International*, USA, 157-166.
35. Robin Scott, Michael Brown and Martin Levesley, "Robust multivariable control of a double beam cantilever smart structure," *J. Smart Materials and Structures*, Vol. 13, pp. 731–743, 2003.
36. Zhang X.D. and Sun C.T., "Formulation of an adaptive sandwich beam," *Smart Materials and Structures Journal*, Vol. 5, No. 6, pp. 814–823, 1996.
37. Donthireddy P. and Chandrashekhara K., "Modeling and shape control of composite beam with embedded piezoelectric actuators," *System and Control Letters*, Vol. 35, No. 2, pp. 237–244, 1996.
38. Murali G. and Pajunen G.A., "Model reference control of vibrations in flexible smart structures," *34th IEEE Conference on Decision and Control*, New Orleans, USA, pp. 3551-3556, Dec. 1995.
39. Thomas J. and Abbas B.A.H., "Finite element methods for dynamic analysis of Timoshenko beam," *J. of Sound and Vibration*, Vol. 41, pp. 291-299, 1975.
40. Benjeddou A., Trindade M.A. and Ohayon R., "New shear actuated smart structure beam finite element," *Journal of Guidance, Dynamics and Control*, Vol. 37, pp. 378-383, 1999.
41. Raja S., Prathap G. and Sinha P.K., "Active vibration control of composite sandwich beams with piezoelectric extension-bending and shear actuators," *J. Smart Materials and Structures*, Vol. 11, No. 1, pp. 63-71, 2002.
42. Friedman Z. and Kosmataka J.B., "An improved two-node Timoshenko beam finite element," *Computers and Structures*, Vol. 47, No. 3, pp. 473–481, 1993.
43. Azulay L.E. and Abramovich H., "Piezoelectric actuation and sensing mechanisms : Closed form solutions," *Composite Structures*, Vol. 64, pp. 443-453, 2004.
44. Haim Waisman and Haim Abramovich, "Active stiffening of laminated composite beams using piezoelectric actuators," *Composite Structures*, Vol. 58, No. 3, pp. 109–120, 2002.
45. Abramovich H. and Lishvits A., "Free vibrations of non-symmetric cross-ply laminated composite beams," *Journal of Sound and Vibration*, Vol. 176, No. 5, pp. 597–612, 1994.
46. Seshu P., "A Textbook of Finite Element Analysis," *Prentice Hall of India*, New Delhi, 2004.

47. Levine W.S. and Athans M., "On the determine of the optimal constant output feedback gains for linear multivariable systems," *IEEE Trans. Auto. Contr.*, Vol. AC-15, No. 1, pp. 44-48, 1970.
48. Syrmos V.L., Abdallah P., Dorato P. and Grigoriadis K., "Static output feedback : A survey," *Automatica*, Vol. 33, No. 2, pp. 125–137, 1997.
49. Yong Yan C., Lam J. and Sun Y.X., "Static output feedback stabilization : An LMI Approach," *Automatica*, Vol. 34, No. 12, pp. 1641-1645, 1998.
50. Geromel J.C., De Souza C.C. and Skeleton R.E., "LMI numerical solution for output feedback stabilization," *Proc. American Control Conference*, USA, pp. 40–44, 1994.
51. Werner H. and Furuta K., "Simultaneous stabilization based on output measurements," *Kybernetika*, Vol. 31, No. 4, pp. 395-411, 1995.
52. Werner H., "Multimodal robust control by fast output sampling - An LMI approach," *Automatica*, Vol. 34, No. 12, pp. 1625-1630, 1998.
53. Chammas A.B. and Leondes C.T., "Pole placement by piecewise constant output feedback," *Int. J. Contr.*, Vol. 29, pp. 31-38, 1979.
54. Chammas A.B. and Leondes C.T., "On the design of LTI systems by periodic output feedback, Part-II, Output feedback controllability," *Int. J. Contr.*, Vol. 27, pp. 895-903, 1978.
55. Werner H., "Robust multivariable control of a turbo-generator by periodic output feedback," *American Control Conference*, New Mexico, USA, pp. 1979-1983, 1997.
56. Janardhanan S., Bandyopadhyay B. and Manjunath T.C., "Fast output sampling based output feedback sliding mode control law for uncertain systems," *Proc. Third Intl. Conf. on System Identification and Control Problems, SICPRO-2004*, Moscow, Russia, Paper No. 23010, pp. 1300–1312, Jan. 2004.
57. Werner H., "Robust control of a laboratory flight simulator by non-dynamic multirate output feedback," *Proc. IEEE Conf. Decision and Control*, pp. 1575-1580, 1996.
58. Marshall S.A., "An approximate method for reducing the order of a linear system," pp. 642-643, 1966.
59. Chidambara M.R. and Davison E.J., "A method for simplifying linear dynamical systems," *IEEE Trans. Auto. Contr.*, Vol. AC-12, pp. 119–121, 1967.
60. Mahapatra G.B., "A note on selecting a low-order system by Davison's model simplification technique," *IEEE Trans. Auto. Contr.*, Vol. AC-22, No. 4, pp. 677-678, 1977.
61. Lamba S.S. and Vittal Rao S., "On the suboptimal control via the simplified model of Davison," *IEEE Trans. Auto. Contr.*, Vol. AC-19, pp. 448-450, 1974.
62. Davison E.J., "A method for simplifying linear dynamical systems," *IEEE Trans. Auto. Contr.*, Vol. AC-11, pp. 93–101, 1966.
63. Utkin V.I., "Variable structure systems with sliding modes," *IEEE. Trans. Auto. Contr.*, Vol. AC-22, pp. 212-222, 1977.
64. Axay Mehta, Bandyopadhyay B. and Manjunath T.C., "On second order sliding mode control : An application to variable length pendulum system," *First National Conf. Communication, Controls and Bio-informatics NCCCB - 06*, Kota, Rajasthan, India, Paper No. C-5, Mar. 8-10, 2006.
65. Hung J.Y. and Gao W. and Hung J.C., "Variable structure control : A survey," *IEEE Trans. Industrial Electronics*, Vol. 40, No. 1, pp. 2-21, 1993.
66. Young K.D., Utkin V.I. and Ozunger U., "A control engineer's guide to sliding mode control," *IEEE Trans. Auto. Contr.*, Vol. AC-7, No. 3, pp. 328-342, 1999.

67. Sarpturk S.Z., Istefanopulos Y. and Kaynak O., "On the stability of discrete-time sliding mode systems," *IEEE Trans. Auto. Contr.*, Vol. AC-32, pp. 930-931, 1987.
68. Furuta K, "Sliding mode control of a discrete system," *System and Control Letters*, Vol. 14, pp. 145-152, 1990.
69. Gao W., Wang Y. and Homaifa A., "Discrete-time variable structure control systems," *IEEE Trans. Ind. Electron.*, Vol. 42, No. 2, pp. 117-122, 1995.
70. Bandyopadhyay B., Thakkar V., Saaj C.M. and Janardhanan S., "Algorithm for computing sliding mode control and switching surfaces from output samples," *Proc. of the 8th IEEE VSS workshop*, Spain, No. 4, sep. 2004.
71. Bartoszewicz A., "Discrete-time quasi-sliding-mode control strategies," *IEEE Trans. Ind. Electron.*, Vol. 45, No. 1, pp. 633-637, 1998.
72. Manjunath T.C. and Bandyopadhyay B., "Vibration control of a smart flexible cantilever beam using periodic output feedback control technique," *Proc. Fourth Asian Control Conference ASCC-2002*, Singapore, Paper No. 53-1679, pp. 1302–1307, Sep. 2002.
73. Manjunath T.C. and Bandyopadhyay B., "Smart control of cantilever structures using output feedback, A Special issue on Modelling, Simulation and Decision Support" , Vol. 7, Nos. 4-5, pp. 51-68, Jul. 2006.
74. Manjunath T.C. and Bandyopadhyay B., "Modeling and fast output sampling feedback control of a smart Timoshenko cantilever beam," *International Journal of Smart Structures and Systems*, Vol. 1, No. 3, pp. 283–308, Sep. 2005.
75. Manjunath T.C. and Bandyopadhyay B., "Vibration suppression of Timoshenko beams with embedded piezoelectrics using POF," *International Journal of Intelligent Technology*, Vol. 1, No. 1, pp. 21–30, Jan. 2006.
76. Manjunath T.C. and Bandyopadhyay B., "Modeling and FOS feedback based control of SISO intelligent structures with embedded shear sensors and actuators," *International Journal of Intelligent Technology*, Vol. 1, No. 1, pp. 1–20, Jan. 2006.
77. Manjunath T.C. and Bandyopadhyay B., "Multivariable control of a smart structure using periodic output feedback control technique," *Proc. of the Seventh Int. Conf. on Control, Automation, Robotics and Computer Vision, ICARCV-02*, Singapore, Paper No. 2002P1283, pp. 1481–1486, Dec. 2-5, 2002.
78. Manjunath T.C. and Bandyopadhyay B., "Multivariable control of smart Timoshenko beam structures using periodic output feedback technique," *International Journal of Signal Processing*, Vol. 3, No. 2, pp. 74–90, apr. 2006.
79. Manjunath T.C. and Bandyopadhyay B., "Controller design for Euler-Bernoulli smart structures using robust decentralized FOS via reduced order modeling," *International Journal of Intelligent Technology*, Vol. 1, No. 2, pp. 111–130, Jun. 2006.
80. Manjunath T.C. and Bandyopadhyay B., "Controller design for Euler-Bernoulli smart structures using robust decentralized periodic output feedback via reduced order modeling," *International Journal of Signal Processing*, Vol. 3, No. 3, pp. 205–221, Jul. 2006.
81. Manjunath T.C. and Bandyopadhyay B., "Fault tolerant control of flexible smart structures using robust decentralized periodic output sampling feedback technique," *Proc. SPIE's, 11th Annual Symposium / Conference on Smart Structures and Materials / NDE Joint Conference*, San Diego, California, USA, Paper No. SS04-SS08-44, pp. 1-12, Mar. 14-18, 2004.

82. Manjunath T.C. and Bandyopadhyay B., "Fault tolerant control of flexible smart structures using robust decentralized periodic output sampling feedback technique," *Int. Journal of Smart Materials and Structures*, Vol. 14, No. 4, pp. 624–636, Aug. 1999.
83. Manjunath T.C. and Bandyopadhyay B., "Fault tolerant control of flexible smart structures using robust decentralized fast output sampling feedback technique," *Proc. of the Fifth Asian Control Conference, ASCC-05*, Melbourne, Australia, Paper No. 265, pp. 1677-1685, Jul. 20–23, 2004.
84. Manjunath T.C. and Bandyopadhyay B., "Fault tolerant control of flexible smart structures using robust decentralized fast output sampling feedback technique," *to be published in Asian Journal of Control in* Vol. 9, No. 3, Sep. 2007.
85. Manjunath T.C. and Bandyopadhyay B., "Design of multivariable POF controller for smart flexible composite beam using embedded shear sensors and actuators," *to appear in Int. Journal of Simulation, System Science and Technology, A Special issue*, Vol. 7, No. 6-7, Sep-Oct. 2006.
86. Umapathy M. and Bandyopadhyay B., "Control of flexible beam through smart structure concept using periodic output feedback," *System Science Journal*, Vol. 26, No. 1, pp. 23-46, 2000.
87. Manjunath T.C. and Bandyopadhyay B., "Vibration control of a smart flexible cantilever beam using periodic output feedback," *Asian Journal of Control*, Vol. 6, No. 1, pp. 74–87, Mar. 2004.
88. Umapathy M., Bandyopadhyay B. and Unbehauen H., "Design of output feedback compensator for smart structure model via reduced order model," *System Science Journal*, Vol. 28, No. 4, pp. 61-84, May-Jun. 2005.
89. Umapathy M., Bandyopadhyay B. and Unbehauen H., "Design of output feedback compensator for discrete time system via reduced order model," *IETE Journal of Research*, Vol. 51, no. 3, pp. 201-207, 2002.
90. Umapathy M. and Bandyopadhyay B., "Design of fast output sampling feedback control for smart structure model," *SPIE 9th Annual Symposium / Conf. on Smart Structures and Materials / NDE Joint Conf.* , San Diego, California, USA, Vol. 4693, pp. 222-233, 2002.
91. Manjunath T.C., Bandyopadhyay B., Seshu P. and Umapathy M., "Active vibration control of smart structures using fast output sampling feedback technique," *Proc. Fourth ISSS Int. Conf. on Smart Materials, Structures and Systems ISSS-05*, I.I.Sc., Bangalore, Karnataka, India, Vol. 1, No. ISSS-2005 / SA-11, pp. SA 84-SA 91, Jul. 28–30, 2005.
92. Manjunath T.C. and Bandyopadhyay B., "Control of vibrations in flexible smart structures using fast output sampling feedback technique," *International Journal of Computational Intelligence*, Vol. 3, No. 2, pp. 127–141, Apr. 2006.
93. Manjunath T.C. and Bandyopadhyay B., "Multivariable control of a smart structure cantilever beam using fast output sampling feedback," *Proc. Third International Conference on System Identification and Control Problems SICPRO-04*, Institute of Control Sciences, Moscow, Russia, Paper No. 23016, pp. 1300-1312, Jan. 28-30, 2004.
94. Manjunath T.C., Bandyopadhyay B. and Janardhanan S., "Multirate output feedback based sliding mode controller design for active vibration control of SISO smart structures," *Proc. 29th National Systems Conference NSC-2005*, IIT Bombay, Mumbai, India, Paper No. 54, Dec. 2005.

95. Saurabh Jain, Manjunath T.C. and Bandyopadhyay B., "Active vibration control of glass-epoxy composite beam using output feedback," *Accepted for publication in IEEE Int. Conf. Industrial Technology, ICIT-2006 to be held in Dec. 2006*, Mumbai, India.
96. Manjunath T.C. and Bandyopadhyay B and Janardhanan S, "Vibration control of smart structures using multirate output feedback sliding mode control law," *Proc. 1st National Conference on Control and Dynamical Systems NCCDS 05*, IIT Bombay, Mumbai, India, Paper No. 61, pp. , Jan. 2005.
97. Manjunath T.C., Bandyopadhyay B., Seshu P. and Umapathy M., "Discrete output feedback sliding mode control of flexible Euler-Bernoulli based smart structures," *Proc. Fourth ISSS International Conference on Smart Materials, Structures and Systems ISSS-05*, I.I.Sc., Bangalore, Karnataka, India, Vol. 1, Paper No. ISSS-2005 / SA-22, pp. SA 163–SA170, Jul. 28–30, 2005.
98. Umapathy M., "Modeling and control of smart structures," *Ph.D. Thesis*, Systems and Control Engg., IIT Bombay, India, 2001.
99. Francis Lee and Ivan Morse and Rollnad Hinkle, "Mechanical Engineering Vibrations," *CBS Publishers*, New Delhi, India.
100. IEEE standards on piezoelectricity, *ANSI / IEEE Std. 176-1987, E-ISBN : 0-7381-2411-7*, 29 Jan. 1988.
101. Seung-Hwan Kim, Seung-Bok Choi, Sung-Ryong Hong and Moon-Sik Han M.S., "Vibration control of a flexible structure using a hybrid mount," *International Journal of Mechanical Sciences*, Vol. 46, No. 1, pp. 143-157, 2004.
102. Mahmoud M.S. and Singh G.M., "Large scale systems modeling," *Pergamon Press*, Oxford, 1981.
103. Moshe Eisenberger and Haim Abramovich, "Shape control of non-symmetric piezolaminated composite beams," *Computers and Structures*, Vol. 38, Nos. 1-4, pp. 565-571, 1977.
104. Shi G. and Lam K.Y., "Finite element vibration analysis of composite beams based on higher order beam theory," *Journal of Sound and Vibration*, Vol. 219, No. 4, pp. 707–721, 1999.
105. Shi G., Lam K.Y. and Tay T.E., "On efficient finite element modeling of composite beams and plates using higher order theories and an accurate composite beam element," *Compoiste Structures*, Vol. 41, pp. 159-165, 1998.
106. Cowper G.R., "The shear coefficient in Timoshenko's beam theory," *ASME J. App. Mech.*, Vol. 33, pp. 335–340, 1966.
107. Tessler A. and Dong S.B., "On a hierarchy of conforming Timoshenko beam elements," *Computers and Structures*, Vol. 14, No. 3-4, pp. 335-344, 1981.
108. Paolo Gaudenzi, "Exact higher order solutions for a simple adaptive structure," *International Journal of Solids and Structures*, Vol. 35, Nos. 26-27, pp. 3595–3610, 1998.
109. Robbins D.H. and Reddy J.N., "Analysis of a piezo-electrically actuate beams using a layer-wise displacement theory," *Computers and Structures*, Vol. 41, No. 2, pp. 265–279, 1991.
110. Murthy M.V.V.S., Roy Mahapatra D., Badrinarayana K. and Gopalakrishnan S., "a refined higher order finite element for asymmetric composite beams," *Composite structures*, Vol. 67, No. 1, pp. 27–35, 2005.
111. Zhongdong Wang, Su-huan Chen and Wanzhi Han, "the static shape control for intelligent structures," *Finite Elements in Analysis and Deisgn*, Vol. 26, pp. 303–314, 1997.

112. Manjunath T.C. and Bandyopadhyay B., "Mathematical modeling of SISO based Timoshenko structures - A case study," *International Journal of Mathematics Sciences*, Vol. 1, No. 1, pp. 1–19, Jan. 2007.
113. Vinson J.R. and Sierakowski R.L., "The behavior of structures composed of composite materials," *Martinus Nijhoff*, The Netherlands 1986.
114. Narayanan S. and Balamurugan V., "Finite element modeling of piezolaminated smart structures for active vibration control with distributed sensors and actuators," *Journal of Sound and Vibration*, Vol. 262, pp. 529–562, 2003.
115. Paulo Gaudenzi, "Exact higher order solutions for a simple adaptive structure," *Int. J. Solids and Structures*, Vol. 35, Nos. 26-27, pp. 3595–3610, 1998.
116. Fuh Gwo Y. and Robert Miller E., "A new finite element for laminated composite beams," *Computers and Structures*, Vol. 31, No. 5, pp. 737–745, 1989.
117. Banarjee J.R., "Free vibrations of sandwiched beams using the dynamic stiffness method," *Computers and Structures*, Vol. 81, pp. 1915–1922, 2003.
118. Louis R.C., Edward C.S. and Brian M., "Induced shear piezoelectric actuators for rotor blade trailing edge flaps," *J. Smart Materials and Structures*, Vol. 11, pp. 24-35, 2002.
119. Zapfe J.A. and Lesieutre G.A., "Discrete layer beam finite element for the dynamic analysis of composite sandwiched beams with integral damping layers," *Computers and Structures*, Vol. 70, No. 1, pp. 647-666, 1999.
120. Chammas A.B. and Leondes C.T., "On the design of LTI systems by periodic output feedback, Part-I, Discrete Time pole assignment," *Int. J. Contr.*, Vol. 27, pp. 885-894, 1978.
121. Gahnet P.A., Nemirovski, Laub A.J. and Chilali M., "LMI Tool Box for Matlab," *The Math works Inc.*, Natick MA, 1995.
122. Kleinman D.L., Fortmann T. and Athans M., "On the design of linear systems with pieceise constant feedback gains," *IEEE Trans. Auto. Contr.*, Vol. AC-13, pp. 345-361, 1968.
123. Gopal M., "Digital control and state variable methods - conventional and neuro fuzzy control systems," *Tata McGraw Hill*, India, pp. 88-89, 2003.
124. Rajeev G., Bandyopadhyay B. and Kulkarni A.M., "Robust decentralized POF technique based power system stablizer for multi-machine power system," *IEE Proc. on Control Theory and Applications*, Vol. 152, No. 1, pp. 3-8, 2005.
125. Aoki M., "Control of large scale dynamic systems by aggregation," *IEEE Trans. Auto. Contr.*, Vol. AC-13, pp. 246-253, 1968.
126. Herbert Werner and Tilo Meister, "Robust control of a laboratory aircraft model via fast output sampling," *Control Engg. Practice*, Vol. 7, No. 3, pp. 305–313, 1999.
127. Chakravithini M.S., Bandyopadhyay B. and Unbehauen H., "A new algorithm for discrete time sliding mode control using FOS feedback," *IEEE Trans. Ind. Electron.*, Vol. 49, No. 3, pp. 518-523, 2002.
128. Bandyopadhyay B. and Saaj C.M., "Discrete sliding mode control by non-dynamic multirate output feedback," *Proc. Seventh Intl. Workshop on Variable Structure Systems*, pp. 145-151, 2002.
129. Bartoszewicz A., "Remarks on discrete-time variable structure systems," *IEEE Transactions on Industrial Electronics*, Vol. 43, No. 1, pp. 235–238, 1996.
130. Okugawa M. and Sasaki M., "System identification and controller design of a self-sensing piezoelectric cantilever structure," *Jounal of Intelligent Materials Systems and Structures*, Vol. 13, pp. 241-252, 2002.

Index

Lecture Notes in Control and Information Sciences

Edited by M. Thoma and M. Morari

Further volumes of this series can be found on our homepage:
springer.com

Vol. 349: Teutsch, H.
Modal Array Signal Processing: Principles and Applications of Acoustic Wavefield Decomposition
253 p. 2007 [978-3-540-40893-2]

Vol. 348: Rogers, E.T.A.; Galkowski, K.; Owens, D.H.
Control Systems Theory and Applications for Linear Repetitive Processes
482 p. 2007 [978-3-540-42663-9]

Vol. 347: Assawinchaichote, W.; Nguang, S.K.; Shi, P.
Fuzzy Control and Filter Design for Uncertain Fuzzy Systems
178 p. 2006 [978-3-540-37011-6]

Vol. 346: Tarbouriech, S.; García, G.; Glattfelder, A.H. (Eds.)
Advanced Strategies in Control Systems with Input and Output Constraints
430 p. 2006 [978-3-540-37009-3]

Vol. 345: Huang, D.-S.; Li, K.; Irwin, G.W. (Eds.)
Intelligent Computing in Signal Processing and Pattern Recognition (ICIC 2006)
1179 p. 2006 [978-3-540-37257-8]

Vol. 344: Huang, D.-S.; Li, K.; Irwin, G.W. (Eds.)
Intelligent Control and Automation (ICIC 2006)
1121 p. 2006 [978-3-540-37255-4]

Vol. 343: Jalali, A.A.; Sims, C.S.; Famouri, P.
Reduced Order Systems
170 p. 2006 [978-3-540-34358-5]

Vol. 342: Hasegawa, Y.; Suzuki, T.
Realization Theory and Design of Digital Images
275 p. 2006 [978-3-540-36115-2]

Vol. 341: Commault, C.; Marchand, N. (Eds.)
Positive Systems
448 p. 2006 [978-3-540-34771-2]

Vol. 340: Diehl, M.; Mombaur, K. (Eds.)
Fast Motions in Biomechanics and Robotics
500 p. 2006 [978-3-540-36118-3]

Vol. 339: Alamir, M.
Stabilization of Nonlinear Systems Using Receding-horizon Control Schemes
325 p. 2006 [978-1-84628-470-0]

Vol. 338: Tokarzewski, J.
Finite Zeros in Discrete Time Control Systems
325 p. 2006 [978-3-540-33464-4]

Vol. 337: Blom, H.; Lygeros, J. (Eds.)
Stochastic Hybrid Systems
395 p. 2006 [978-3-540-33466-8]

Vol. 336: Pettersen, K.Y.; Gravdahl, J.T.; Nijmeijer, H. (Eds.)
Group Coordination and Cooperative Control
310 p. 2006 [978-3-540-33468-2]

Vol. 335: Kozłowski, K. (Ed.)
Robot Motion and Control
424 p. 2006 [978-1-84628-404-5]

Vol. 334: Edwards, C.; Fossas Colet, E.; Fridman, L. (Eds.)
Advances in Variable Structure and Sliding Mode Control
504 p. 2006 [978-3-540-32800-1]

Vol. 333: Banavar, R.N.; Sankaranarayanan, V.
Switched Finite Time Control of a Class of Underactuated Systems
99 p. 2006 [978-3-540-32799-8]

Vol. 332: Xu, S.; Lam, J.
Robust Control and Filtering of Singular Systems
234 p. 2006 [978-3-540-32797-4]

Vol. 331: Antsaklis, P.J.; Tabuada, P. (Eds.)
Networked Embedded Sensing and Control
367 p. 2006 [978-3-540-32794-3]

Vol. 330: Koumoutsakos, P.; Mezic, I. (Eds.)
Control of Fluid Flow
200 p. 2006 [978-3-540-25140-8]

Vol. 329: Francis, B.A.; Smith, M.C.; Willems, J.C. (Eds.)
Control of Uncertain Systems: Modelling, Approximation, and Design
429 p. 2006 [978-3-540-31754-8]

Vol. 328: Loría, A.; Lamnabhi-Lagarrigue, F.; Panteley, E. (Eds.)
Advanced Topics in Control Systems Theory
305 p. 2006 [978-1-84628-313-0]

Vol. 327: Fournier, J.-D.; Grimm, J.; Leblond, J.; Partington, J.R. (Eds.)
Harmonic Analysis and Rational Approximation
301 p. 2006 [978-3-540-30922-2]

Vol. 326: Wang, H.-S.; Yung, C.-F.; Chang, F.-R.
H_∞ Control for Nonlinear Descriptor Systems
164 p. 2006 [978-1-84628-289-8]

Vol. 325: Amato, F.
Robust Control of Linear Systems Subject to Uncertain Time-Varying Parameters
180 p. 2006 [978-3-540-23950-5]

Vol. 324: Christofides, P.; El-Farra, N.
Control of Nonlinear and Hybrid Process Systems
446 p. 2005 [978-3-540-28456-7]

Vol. 323: Bandyopadhyay, B.; Janardhanan, S.
Discrete-time Sliding Mode Control
147 p. 2005 [978-3-540-28140-5]

Vol. 322: Meurer, T.; Graichen, K.; Gilles, E.D. (Eds.)
Control and Observer Design for Nonlinear Finite and Infinite Dimensional Systems
422 p. 2005 [978-3-540-27938-9]

Vol. 321: Dayawansa, W.P.; Lindquist, A.; Zhou, Y. (Eds.)
New Directions and Applications in Control Theory
400 p. 2005 [978-3-540-23953-6]

Vol. 320: Steffen, T.
Control Reconfiguration of Dynamical Systems
290 p. 2005 [978-3-540-25730-1]

Vol. 319: Hofbaur, M.W.
Hybrid Estimation of Complex Systems
148 p. 2005 [978-3-540-25727-1]

Vol. 318: Gershon, E.; Shaked, U.; Yaesh, I.
H_∞ Control and Estimation of State-muliplicative Linear Systems
256 p. 2005 [978-1-85233-997-5]

Vol. 317: Ma, C.; Wonham, M.
Nonblocking Supervisory Control of State Tree Structures
208 p. 2005 [978-3-540-25069-2]

Vol. 316: Patel, R.V.; Shadpey, F.
Control of Redundant Robot Manipulators
224 p. 2005 [978-3-540-25071-5]

Vol. 315: Herbordt, W.
Sound Capture for Human/Machine Interfaces: Practical Aspects of Microphone Array Signal Processing
286 p. 2005 [978-3-540-23954-3]

Vol. 314: Gil', M.I.
Explicit Stability Conditions for Continuous Systems
193 p. 2005 [978-3-540-23984-0]

Vol. 313: Li, Z.; Soh, Y.; Wen, C.
Switched and Impulsive Systems
277 p. 2005 [978-3-540-23952-9]

Vol. 312: Henrion, D.; Garulli, A. (Eds.)
Positive Polynomials in Control
313 p. 2005 [978-3-540-23948-2]

Vol. 311: Lamnabhi-Lagarrigue, F.; Loría, A.; Panteley, E. (Eds.)
Advanced Topics in Control Systems Theory
294 p. 2005 [978-1-85233-923-4]

Vol. 310: Janczak, A.
Identification of Nonlinear Systems Using Neural Networks and Polynomial Models
197 p. 2005 [978-3-540-23185-1]

Vol. 309: Kumar, V.; Leonard, N.; Morse, A.S. (Eds.)
Cooperative Control
301 p. 2005 [978-3-540-22861-5]

Vol. 308: Tarbouriech, S.; Abdallah, C.T.; Chiasson, J. (Eds.)
Advances in Communication Control Networks
358 p. 2005 [978-3-540-22819-6]

Vol. 307: Kwon, S.J.; Chung, W.K.
Perturbation Compensator based Robust Tracking Control and State Estimation of Mechanical Systems
158 p. 2004 [978-3-540-22077-0]

Vol. 306: Bien, Z.Z.; Stefanov, D. (Eds.)
Advances in Rehabilitation
472 p. 2004 [978-3-540-21986-6]

Vol. 305: Nebylov, A.
Ensuring Control Accuracy
256 p. 2004 [978-3-540-21876-0]

Vol. 304: Margaris, N.I.
Theory of the Non-linear Analog Phase Locked Loop
303 p. 2004 [978-3-540-21339-0]

Vol. 303: Mahmoud, M.S.
Resilient Control of Uncertain Dynamical Systems
278 p. 2004 [978-3-540-21351-2]

Vol. 302: Filatov, N.M.; Unbehauen, H.
Adaptive Dual Control: Theory and Applications
237 p. 2004 [978-3-540-21373-4]

Vol. 301: de Queiroz, M.; Malisoff, M.; Wolenski, P. (Eds.)
Optimal Control, Stabilization and Nonsmooth Analysis
373 p. 2004 [978-3-540-21330-7]

Vol. 300: Nakamura, M.; Goto, S.; Kyura, N.; Zhang, T.
Mechatronic Servo System Control
Problems in Industries and their Theoretical Solutions
212 p. 2004 [978-3-540-21096-2]

Vol. 299: Tarn, T.-J.; Chen, S.-B.; Zhou, C. (Eds.)
Robotic Welding, Intelligence and Automation
214 p. 2004 [978-3-540-20804-4]

Vol. 298: Choi, Y.; Chung, W.K.
PID Trajectory Tracking Control for Mechanical Systems
127 p. 2004 [978-3-540-20567-8]

Vol. 297: Damm, T.
Rational Matrix Equations in Stochastic Control
219 p. 2004 [978-3-540-20516-6]

Vol. 296: Matsuo, T.; Hasegawa, Y.
Realization Theory of Discrete-Time Dynamical Systems
235 p. 2003 [978-3-540-40675-4]

Vol. 295: Kang, W.; Xiao, M.; Borges, C. (Eds)
New Trends in Nonlinear Dynamics and Control, and their Applications
365 p. 2003 [978-3-540-10474-0]

Vol. 294: Benvenuti, L.; De Santis, A.; Farina, L. (Eds)
Positive Systems: Theory and Applications (POSTA 2003)
414 p. 2003 [978-3-540-40342-5]

Vol. 293: Chen, G.; Hill, D.J.
Bifurcation Control
320 p. 2003 [978-3-540-40341-8]

Vol. 292: Chen, G.; Yu, X.
Chaos Control
380 p. 2003 [978-3-540-40405-7]

Vol. 291: Xu, J.-X.; Tan, Y.
Linear and Nonlinear Iterative Learning Control
189 p. 2003 [978-3-540-40173-5]